Flávia Ariany Belato Costa

A coevolução dos animais e do oxigênio no Neoproterozóico

The coevolution of animals and oxygen in the Neoproterozoic

São Paulo

2024

Flávia Ariany Belato Costa

A coevolução dos animais e do oxigênio no Neoproterozóico

The coevolution of animals and oxygen in the Neoproterozoic

Tese apresentada ao Instituto de Biociências da Universidade de São Paulo, para a obtenção do Título de Doutora em Ciências Biológicas, na Área de Zoologia.

Orientador: Prof. Dr. André Carrara Morandini
Coorientadora: Dr.ª Elisa Maria Costa e Silva de Paiva

São Paulo

2024

Ficha Catalográfica

Belato Costa, Flávia Ariany
A coevolução dos animais e do oxigênio no Neoproterozóico / Belato Costa Flávia Ariany ; orientador Carrara Morandini André ; coorientadora Costa e Silva de Paiva Elisa Maria -- São Paulo, 2024.
191 p.

Tese (Doutorado) -- Instituto de Biociências da Universidade de São Paulo. Ciências Biológicas (Zoologia).

1. Hipóxia. 2. Metazoa. 3. Evolução Molecular. 4. Origem dos Animais. 5. Neoproterozóico. I. Carrara Morandini, André, orient. II. Costa e Silva de Paiva, Elisa Maria, coorient. Título.

Bibliotecária responsável pela catalogação:
Elisabete da Cruz Neves - CRB - 8/6228

Comissão Julgadora:

_____	_____
Prof. Dr. André Carrara Morandini	Prof. Dr.
Orientador – Presidente da Banca	
_____	_____
Prof. Dr.	Prof. Dr.

Dedicatória

À minha mãe, que sempre acreditou que eu era capaz.

Epígrafe

“I would rather have questions that can't be answered than answers that can't be questioned.”

Richard P. Feynman

Agradecimentos

Devo muito da minha trajetória acadêmica (e pessoal) à orientação, amizade e parceria da Elisa, por isso agradeço primeiramente a ela, por estar ao meu lado nessa jornada de mais de 11 anos na Biologia. Elisa, obrigada por todos esses anos de amizade, companheirismo, incentivo, orientação e parceria nas horas boas e ruins. Com certeza eu não teria chegado até aqui sem você do meu lado.

Agradeço também ao Prof. André Morandini, por ter aceitado a tarefa da minha orientação nesse doutorado, por ter me dado apoio nos momentos difíceis que enfrentei no exterior, e por toda orientação prática, burocrática e científica ao longo desses anos. André, obrigada por fazer parte da minha trajetória acadêmica.

Agradeço ao Prof. Federico Brown por ter aceitado me ceder um espaço em seu laboratório para frequentar como aluna, para montar os experimentos e utilizar seus equipamentos. Agradeço a ajuda com ideias e sugestões para o projeto nos vários *lab meetings*, e por me permitir conviver com seus alunos por todos esses anos.

Agradeço ao Prof. Márcio Reis Custódio pela valiosa ajuda com as "gambiarras" necessárias na fase inicial dos experimentos, pelas orientações na escolha e manutenção das esponjas em seu laboratório, pelas dicas de coleta e por ceder espaço em seu laboratório para os experimentos.

Sou grata ainda aos membros do projeto temático ao qual meu doutorado está vinculado. Agradeço ao Prof. Ricardo Trindade, que chefia o projeto, por ter custeado a maior parte dos gastos com o sequenciamento. Agradeço ao Prof. Douglas Galante por ter montado o misturador de gases, e ao seu aluno Evandro, pela ajuda com os cilindros e válvulas reguladoras. Agradeço muito a ajuda do Rodrigo Oliveira Abans (*in memoriam*), pelo trabalho essencial no design inicial das câmaras, e todos os protótipos antes do modelo final. Agradeço também aos demais membros envolvidos no projeto temático, a Prof. Juliana de Moraes Leme, e o técnico Iran de Godoi.

Minha jornada na academia não teria sido a mesma sem a convivência e a amizade dos membros do laboratório de Evo-Devo. Meu agradecimento especial para a Luiza Saad, que compartilhou comigo esse trajeto cheio de frustrações e descobertas, e se tornou uma amiga querida. Agradeço também aos membros antigos e atuais do laboratório pela parceria ao longo dos anos: Sheina, Oscar, David, Laurel, Ruan, Sergio e Carlos. Agradeço ainda a oportunidade e confiança em poder coorientar, ajudar e/ou participar dos trabalhos de iniciação de científica dos alunos que passaram pelo projeto Neoprot: Bruno, Guilherme, Thabata, Pablo, Marco e Pedro. Também não posso me esquecer de agradecer a amizade do Thyago e da Lucia, que mesmo com altos e baixos, acompanham minha trajetória desde antes de eu vir para São Paulo.

Estabeleci muitas conexões e parcerias de trabalho ao longo dessa jornada de quase cinco anos de doutorado, o que proporcionou crescimento e experiência profissional e pessoal. Agradeço ao Dr. Ken Halanych pelos ótimos comentários, sugestões e críticas aos manuscritos de bioinformática. Sou grata ao Dr. Christopher Coates pela ajuda, correções e sugestões nos trabalhos de bioinformática e evolução de proteínas. E um agradecimento especial à Dra. Beatriz Mello que é especialista em datação molecular, e contribuiu muito para a realização das análises e aprimoramento dos artigos.

Sou grata a todos os funcionários do Instituo de Biociências da USP, em especial os do departamento de Zoologia. Todos os professores, coordenadores do programa, secretários, seguranças, equipe da limpeza, técnicos e demais funcionários que lidam com a burocracia. Gostaria de agradecer em especial a ajuda dos técnicos Manuel, Beatriz e Tatiana, que me auxiliaram na parte de bancada do projeto.

Tive a oportunidade de realizar um estágio de pesquisa no Canadá que me trouxe muitos aprendizados pessoais e acadêmicos. Sou grata a Dra. Sally Leys por me aceitar em seu laboratório, por me dar *insights* quanto à análise dos dados e por me apresentar ao Dr. Warren Gallin e à Dra. Ana Riesgo. Os dois me ajudaram muito na elaboração inicial de *pipelines*, e na montagem e anotação dos transcriptomas, e por isso sou muito agradecida.

Todo o meu doutorado só foi possível por eu ter recebido suporte financeiro das agências de fomento FAPESP e CNPq. Agradeço profundamente o financiamento recebido em forma de bolsa, reserva técnica e demais verbas por meio das bolsas com os seguintes números de processo: 142159/2019-0 (CNPq), 2019/18051-7 (FAPESP) e 2021/14115-0 (BEPE – FAPESP), além do projeto temático ao qual meu doutorado está vinculado 2016/06114-6 (FAPESP).

Agradeço à minha família pelo apoio incondicional. À minha mãe, por estar presente e acreditar em mim. Eu te amo, você é a maior responsável por eu chegar aonde cheguei. Obrigada pelo amor e pelos sacrifícios que você fez e faz até hoje por mim. Agradeço ao meu pai (*in memoriam*), que deu suporte financeiro para meu irmão e eu até onde lhe foi possível e viável. Sua maior herança deixada para mim foi a paixão por ler, descobrir e aprender, e isso eu levarei comigo para sempre. Agradeço à minha segunda família, meus sogros e minha cunhada, por me acolherem em sua casa no momento em que precisei de abrigo. Por fim, agradeço ao meu companheiro de vida, melhor amigo e esposo, Ricardo. Sou infinitamente grata por todo seu amor, por me aguentar nos dias bons e ruins, por segurar a barra enquanto eu estive no exterior, por me apoiar cegamente nas minhas escolhas, por dividir os sonhos comigo e me ajudar como pôde a concluir esse doutorado. Eu não teria chegado até aqui sem todo o suporte que recebi.

Índice

Introdução Geral

1. A história evolutiva do oxigênio no planeta Terra: do GOE ao NOE

Evidências geoquímicas e paleontológicas indicam que a vida na Terra tenha surgido há ~ 3,7–3,2 bilhões de anos (giga-ano = Ga), no Éon Arqueano (4,0–2,5 Ga) (Pearce et al., 2018). Traços do isótopo estável de carbono ^{13}C, que é comumente utilizado para inferir atividade biológica, foram encontrados em rochas de > 3,7 Ga, na Groenlândia (Rosing, 1999; Ohtomo et al., 2014), onde também foram encontradas formações rochosas de 3,7 Ga, controversamente interpretadas como estromatólitos – rochas formadas pela atividade de micro-organismos em meio aquático (Nutman et al., 2016). Porém, a evidência mais direta da existência de vida na Terra vem da presença de fósseis, e os micro fósseis mais antigos que possuem indicativos críticos de autenticidade biológica (e.g., lúmen celular e paredes celulares carbonáceas) datam de ~3,4–3,2 Ga (Wacey, 2009; Javaux et al., 2010; Wacey et al., 2011; Schirrmeister et al., 2016). A despeito da controvérsia em relação à datação exata do surgimento da vida, é sabido que a Terra primitiva foi caracterizada pela ausência de oxigênio molecular (O_2) na atmosfera e nos oceanos (Holland, 2006; Kump, 2008; Planavsky et al., 2014).

Acredita-se que as concentrações de O_2 aumentaram pela primeira vez ($>10^{-4}$ –10^{-2} % P.A.L. – *Present Atmospheric Levels*) durante o chamado Grande Evento de Oxidação (G.O.E. – *Great Oxidation Event*), cerca de 2,5 – 2,3 Ga atrás, no Éon Proterozóico (2,5–0,54 Ga; Farquhar et al., 2000; Holland, 2002; Sessions et al., 2009; Planavsky et al., 2014). Esse aumento é atribuído ao acúmulo do O_2 gerado pelas cianobactérias que realizavam fotossíntese oxigênica, as quais surgiram há ~ 2,95–2,7 Ga (Canfield,

2005; Buick, 2008; Sessions et al., 2009; Planavsky et al., 2014). Porém, os oceanos primordiais continham imensas quantidades de metais dissolvidos em seus estados reduzidos, o que é corroborado pela existência de B.I.F.s (*Banded Iron Formations*) em rochas arqueanas (Kump e Holland, 1992; Johnson et al., 2008). Por conta disso, em um primeiro momento, o O_2 que começou a ser gerado pela fotossíntese era totalmente consumido na oxidação desses metais, e somente quando os reservatórios oceânicos de metais reduzidos se esgotaram, as concentrações de O_2 livre começaram a aumentar (Canfield, 2005; Kasting e Howard, 2006; Decker e van Holde, 2011). Esse aumento nos níveis de O_2 atmosféricos resultou na formação da camada de ozônio (O_3), o que trouxe benefícios aos organismos primordiais (Kasting e Catling, 2003). O ozônio é capaz de filtrar os raios ultravioleta com comprimento de onda entre 200 e 300 nanômetros, responsáveis por quebrar as ligações do DNA e das proteínas nas células, gerando uma proteção para a superfície da água contra a radiação prejudicial à vida (Kasting e Catling, 2003). Isso permitiu que os organismos fotossintetizantes começassem a povoar as camadas superiores dos oceanos, onde a luz solar era mais abundante, o que pode ter contribuído para uma explosão na produção de O_2 (Canfield, 2005; Holland, 2006; Decker e van Holde, 2011).

Marcadores geoquímicos demonstram que os níveis de O_2 no Proterozóico eram muito mais variáveis e heterogêneos do que se pensava anteriormente (Sperling et al., 2014; Tang et al., 2016; Diamond e Lyons, 2018; Doyle et al., 2018; Li et al., 2018a, 2018b; Planavsky et al., 2018; He et al., 2019). O aumento dos níveis de O_2 no Proterozóico não foi constante, mesmo após uma aparente estabilidade ter sido alcançada ao fim do G.O.E., marcadores geoquímicos sugerem um retorno a condições de hipóxia entre ~ 2,0–1,8 Ga (Canfield, 2005; Poulton e Canfield, 2011; Reinhard et al., 2016; 2017; Tostevin e Mills, 2020). A teoria do “Oceano

de Canfield" postula que condições anóxicas e euxínicas (anóxico, com sulfeto livre) se mantiveram estáveis nos oceanos profundos durante a maior parte do Proterozóico, e apenas no final do período Ediacarano (635–538 milhões de anos, Ma) ocorreu um aumento relativamente unidirecional dos níveis de O_2 (Canfield, 1998). Décadas antes do trabalho seminal de Canfield, os trabalhos de Nursall (1959) e Berkner e Marshall (1965) já traziam a ideia de que houve um aumento nos níveis de O_2 (~ 1% P.A.L.) ao final do Ediacarano.

As evidências de uma oxigenação parcial de águas mais profundas durante o final do Neoproterozóico (Canfield et al., 2007, 2008) deram suporte ao estabelecimento da hipótese de um Evento de Oxigenação do Neoproterozóico (N.O.E.; Och e Shields-Zhou, 2012). Entretanto, reinterpretações recentes de diferentes marcadores geoquímicos sugerem que o N.O.E. poderia ser descrito mais precisamente não como um único evento, e sim como janelas de oxigenação do Neoproterozóico (N.O.W.s – *Neoproterozoic Oxygenation Windows*; Tostevin e Mills, 2020). Os N.O.W.s seriam caracterizados por pulsos dinâmicos de oxigenação oceânica que ocorreram ao longo de um período de crescimento gradual dos níveis de O_2, e mudanças para um cenário estável só foram alcançadas no Paleozóico (Tostevin e Mills, 2020). Os trabalhos de Sahoo et al. (2016) e Wood et al. (2019) também já haviam proposto que enquanto o ambiente marinho se manteve majoritariamente anóxico durante o Neoproterozóico, ao menos quatro Eventos de Oxigenação Oceânica (O.O.E.s – *Oceanic Oxygenation Events*) teriam acontecido entre o final do Criogeniano e o final do Ediacarano (~640–538 Ma).

Embora os níveis de O_2 da metade final do Proterozóico (800 – 500 Ma) ainda sejam muito debatidos, as estimativas de oxigenação para esse período são consideradas tradicionalmente como sendo entre cerca de 1 e 10 % P.A.L. (*Present Atmospheric Level*; Holland, 2006; Kump, 2008). As

muitas tentativas de modelar a oxigenação do Proterozóico concluem que a distribuição do O_2 oceânico era complexa e irregular (Reinhard et al., 2016; Wood et al., 2019; Tostevin e Mills, 2020). Assim, a busca por uma narrativa congruente acerca da história do O_2 ainda se mostra um grande desafio que necessita da integração de diversas áreas do conhecimento.

2. A história evolutiva dos animais no Neoproterozóico

Os fatores que podem ter influenciado o surgimento dos animais na Era Neoproterozóica têm sido alvo de debates há décadas (Nursall, 1959; Mills e Canfield, 2014). Durante o Neoproterozóico (1.000–538 Ma) a biosfera experimentou uma de suas etapas evolutivas mais fundamentais, com o surgimento das formas de vida complexas, novos planos corporais e complexas relações ecológicas (Canfield et al., 2007; Dzik, 2007; Sperling et al., 2015; Cordani et al., 2020; Wood et al., 2020). Esses eventos biológicos foram acompanhados por flutuações nas condições redox dos oceanos; eventos climáticos extremos, como ao menos duas glaciações em escala global, chamadas Marinoana e Sturtiana; e grandes mudanças na configuração dos continentes, como a formação e o rompimento do supercontinente Rodinia (Canfield et al., 2007; Pierrehumbert et al., 2011; Sperling et al., 2014; 2015; Pu et al., 2016; Wood et al., 2020). Nesse contexto, as ligações entre as inovações biológicas e as mudanças ambientais geralmente estão implícitas, mas sabemos pouco sobre como esses diferentes eventos se relacionam entre si, e principalmente como essas mudanças influenciaram e foram influenciadas pelo surgimento e a diversificação dos primeiros metazoários.

Existem ainda muitas questões não respondidas acerca de quais são os pré-requisitos ambientais mínimos necessários para o surgimento, a manutenção da vida animal e seu sucesso ecológico (Mills e Canfield, 2014; Mills et al., 2014; 2018). Além disso, considerando a distância

temporal entre o surgimento dos animais no Neoproterozóico e sua grande diversificação no Cambriano, a origem e os vários eventos de diversificação metazoária devem ser encarados como eventos distintos, o que significa que ambos ou apenas um deles podem ter sido independentes do O_2 (Cole et al., 2020; Hammarlund et al., no prelo). Embora ainda seja debatida a validade de fósseis mais antigos (*e.g.*, biomarcadores orgânicos e fósseis corporais de esponjas do Criogeniano, > 635 Ma; Love et al., 2009; Brain et al., 2012; Antcliffe et al., 2014; Yin et al., 2015), o registro fóssil animal mais antigo aceito atualmente tem datação do final do Ediacarano, ~ 571 Ma (Narbonne, 2005; Pu et al., 2016; Droser et al., 2017; Wood et al., 2019). Vale mencionar que recentemente foram descobertos fósseis de ~ 890 Ma interpretados como micro esponjas (Turner, 2021), representando assim o possível registro fóssil mais antigo de um metazoário. Porém, como fósseis animais > 600 Ma geralmente são controversos (dos Reis et al., 2015), validações adicionais serão necessárias para confirmar essa descoberta.

Apesar dos primeiros registros fósseis animais aceitos terem datação do final do Ediacarano, a maioria das estimativas de relógio molecular concorda que o último ancestral comum de todos os animais existentes surgiu há ~850 Ma, no período Toniano, o que é corroborado pela descoberta do fóssil de ~890 Ma (Erwin et al., 2011; dos Reis et al., 2015; Dohrmann e Wörheide, 2017; Turner, 2021). Usando diferentes pontos de calibração e conjuntos de dados moleculares, as datações estimadas para o surgimento e a diversificação dos animais variam muito, desde ~ 1.298 a 615 Ma (Douzery et al., 2004; Hedges et al., 2004; Peterson et al., 2004; Cartwright e Collins, 2007; Erwin et al., 2011; Parfrey et al., 2011; dos Reis et al., 2015; Dohrmann e Wörheide, 2017). No entanto, a maioria dessas estimativas concorda que o surgimento dos animais ocorreu muito antes da evidência mais antiga dos pulsos de oxigenação oceânica do

Neoproterozóico (~ 640 – 540 Ma; Sahoo et al., 2012; Lenton e Daines, 2017; Zhang et al., 2018; Wood et al., 2019; Tostevin e Mills, 2020). Portanto, os níveis de O_2 podem ter sido um aspecto evolutivo limitante, e poderiam ter imposto restrições energéticas na diversidade, abundância e fisiologia dos primeiros animais (Fenchel e Finlay, 1995; Reinhard et al., 2016; Cole et al., 2020). Dessa forma, o entendimento de em qual período geológico os primeiros metazoários surgiram, e como era a fisiologia respiratória deles, se mostra de caráter essencial para esclarecer quais fatores ambientais, genéticos, ecológicos e/ou evolutivos influenciaram a origem e a diversificação inicial da vida animal na Terra (dos Reis et al., 2015; Cole et al., 2020).

Sabe-se que todos os animais viventes atualmente conhecidos são organismos aeróbicos. Isso significa que, por pelo menos uma parte de seus ciclos de vida (Mentel et al., 2016; Cole et al., 2020), eles são dependentes da utilização do O_2 como o principal aceptor final de elétrons no metabolismo oxidativo, para a produção de energia em forma de ATP (adenosina trifosfato; Catling et al., 2005; Brochier-Armanet et al., 2009). Além de ser essencial na respiração celular, estudos demonstram que o O_2 também tem um papel crucial na via bioquímica da síntese de colágeno (Prockop et al., 1963). O colágeno é uma proteína exclusiva dos animais, e serve como componente primário da matriz extracelular metazoária, que é uma das sinapomorfias do grupo (Shoulders e Raines, 2009). Por conta dessa relação intrínseca com o O_2, o aumento da disponibilidade de O_2 nos oceanos durante o Neoproterozóico foi considerado, por diversos autores ao longo de décadas, a principal razão para a evolução animal nesse período, em um modelo causa-consequência (Nursall, 1959; Berkner e Marshall, 1965; Cloud, 1968; 1969; Canfield et al., 2008).

A "hipótese de controle do O_2" descrita por Knoll (1992) afirmou que o aumento dos níveis de O_2 no planeta Terra teria criado o ambiente

permissivo crítico para a evolução animal. Por este motivo, o aumento da disponibilidade do O_2 é frequentemente referido na literatura como um gatilho para a evolução e diversificação animal (Mills e Canfield, 2014). Esse tipo de discussão assume a premissa de que os primeiros metazoários eram aeróbicos obrigatórios. No entanto, sabe-se que muitos animais modernos podem viver sem O_2 por longos períodos, ou por pelo menos alguns estágios de seu ciclo de vida (Fenchel e Finlay, 1995; Mentel e Martin, 2008; Müller et al., 2012; Mentel et al., 2016; Mills et al., 2014; 2018).

Entretanto, considerando as evidências crescentes de que os primeiros animais surgiram em ambientes pouco oxigenados, permanece a dúvida em relação à fisiologia respiratória e aos mecanismos moleculares utilizados por eles para viver nesses ambientes. Embora todos os animais necessitem de O_2 para sobreviver, suas demandas energéticas não são as mesmas (Leys e Kahn, 2018). Esponjas e ctenóforos, que são os dois clados candidatos a serem grupo irmão de todos os filos animais (Pisani et al., 2015; Whelan et al., 2015; Halanych, 2016; King e Rokas, 2017), podem viver sob baixas concentrações de O_2 (Purcell et al., 2001; Levin, 2003; Thuesen et al., 2005; Mosch et al., 2012). Além disso, estimativas teóricas acerca da demanda energética dos primeiros metazoários são baixas, variando de 0,4 – 1% P.A.L. (Runnegar, 1982; Mills et al., 2014; Mills e Canfield, 2014; Sperling et al., 2013; 2015).

Apoiando essa hipótese, a literatura atual sugere que os primeiros animais eram pequenos, de corpo mole, pobres em colágeno e restringiam seu uso de O_2 a funções fisiológicas de alta prioridade (Mills et al., 2014; Mills e Canfield, 2014; Cole et al., 2020). Estudos experimentais já demonstraram que esponjas sobrevivem e mantém a transcrição inalterada após exposição a < 0,25 % P.A.L. (Mills et al, 2014; 2018). Essas evidências apontam que possivelmente os primeiros animais não estavam

sob estresse por falta de O_2, ou possuíam outros mecanismos ainda desconhecidos para lidar com a hipóxia (Mills et al., 2018).

Além disso, o ambiente fisiológico celular possui concentrações de O_2 variando de 2 – 9%, estado chamado de normóxia, que é bem abaixo no nível atmosférico, o qual é em torno de 21% de O_2 (Ivanovic, 2009). Vale ressaltar também que o ambiente celular das células tronco embrionárias, assim como das células não diferenciadas varia entre 0,5 – 5% de O_2 (Covello et al., 2006; Simon e Keith, 2008). Dessa forma, condições de hipóxia no ambiente fisiológico celular podem ser um dos fatores que regulam a manutenção do estado não diferenciado das células durante o desenvolvimento dos animais, o que também poderia estar relacionado ao estado de determinação celular basal e do metabolismo primitivo dos primeiros agregados celulares dos metazoários primordiais (Simon e Keith, 2008).

3. Como os animais modernos lidam com o oxigênio?

3.1. O metabolismo aeróbico em normóxia

Por serem organismos aeróbicos, os animais usam o O_2 molecular como receptor final de elétrons (Lehninger, 1949). Entretanto, a evolução favoreceu o metabolismo aeróbico, não apenas porque o O_2 tornou-se disponível, mas também pelo fato dele ser muito mais eficiente na captação da energia vinda da degradação das moléculas combustíveis, como a glicose (Von Stockar e Marison, 1993; Vazquez et al., 2010). A respiração celular é definida como a oxidação de moléculas combustíveis para produzir energia, e compreende basicamente três etapas: a glicólise, o ciclo do ácido cítrico, conhecido também como Ciclo de Krebs, e a fosforilação oxidativa (Babcock e Wikström, 1992; Songer e Mintzes, 1994).

A glicólise ocorre no citoplasma das células e converte a glicose em ácido pirúvico, onde cada molécula de glicose fornece duas moléculas de ATP e NADH ao ser oxidada (Chandel, 2021). O ácido pirúvico entra na

mitocôndria e é oxidado formando a enzima acetilcoenzima A (Acetil-CoA), e uma molécula de NADH (Fothergill-Gilmore e Michels, 1993). Essa degradação da Acetil-CoA, que ocorre através de uma série de reações na matriz mitocondrial é o chamado Ciclo de Krebs, que pode ser produzido a partir de aminoácidos, ácidos graxos e de glicose, o que faz desse ciclo o ponto chave de integração do metabolismo aeróbico (Nelson et al., 2013; Akram, 2014). No ciclo de Krebs – que tem como produtos finais CO_2, ATP, NADH e FADH – a oxidação da Acetil-CoA resulta na redução das coenzimas NAD+ e FAD, que são então oxidadas na cadeia respiratória, fornecendo elétrons ricos em energia (Nelson et al., 2013; Akram, 2014).

As enzimas NADH e FADH servem como moléculas transportadoras de energia, e são utilizadas pela cadeia transportadora de elétrons no bombeamento de prótons para o espaço intermembranas (Chance e Williams, 1955), resultando na força motriz que é utilizada pela ATP sintase, na fosforilação oxidativa (Nelson et al., 2013; Akram, 2014). A energia em forma de ATP gerada pelo metabolismo aeróbico constitui cerca de dois terços da energia produzida pelos organismos, e é comumente relacionada ao aumento dos níveis de O_2 e à complexidade dos organismos, em especial os metazoários (Hedges et al., 2004; Raymond e Segrè, 2006; Koch e Britton, 2008, Lane e Martin, 2010; Mills e Canfield, 2014). No entanto, estudos evolutivos que questionam o surgimento e as relações evolutivas das proteínas e enzimas envolvidas nas reações do metabolismo aeróbico são limitados e escassos (Dean e Golding, 1997; Nekrutenko et al., 1998; Yasutake et al., 2003).

Uma dessas enzimas, a Isocitrato Desidrogenase (IDH – *isocitrate dehydrogenase*), possui papel essencial na regulação da taxa de rotatividade do ciclo de Krebs, e consequentemente atua de forma crítica no metabolismo aeróbico (Nelson et al., 2013). A IDH catalisa a oxidação,

muitas vezes irreversível, do isocitrato em alfa-cetoglutarato (e CO_2), concomitante à redução da coenzima NAD em NADH, controlando o equilíbrio redox mitocondrial, atuando na defesa celular contra danos induzidos pelo estresse oxidativo (Jo et al., 2001; Mailloux et al., 2007; Nunes-Nesi et al., 2013).

Ao longo da evolução da vida, a regulação da proteína IDH tornou-se mais complexa, e as IDHs se diversificaram muito em termos de número de subunidades, tamanho da proteína e coenzima de ligação (Taylor et al., 2008). Os fungos e algas verdes possuem uma IDH com duas subunidades: a IDH1, que está ligada à regulação alostérica da enzima; e a IDH2, responsável pela catálise do substrato (Cupp e McAlister-Henn, 1991; Martínez-Rivas e Vega, 1998). Os metazoários possuem uma IDH com três subunidades: α, β e γ (Ramachandran e Colman, 1980). A subunidade α é estruturalmente semelhante à IDH2 dos fungos, sugerindo provavelmente que ela também possui uma função catalítica. As subunidades β e γ se assemelham à estrutura da subunidade IDH1 dos fungos, sugerindo que elas também possuem função reguladora (Kim et al., 1995; Nichols et al., 1995).

Como os animais dependem da respiração celular, estudos de datação molecular de proteínas relacionadas ao metabolismo oxidativo podem auxiliar a estimar o tempo de divergência dessas vias moleculares essenciais aos animais. O papel crucial da IDH no metabolismo aeróbico (Mailloux et al., 2007) torna sua história evolutiva uma valiosa fonte de conhecimento para estudar a evolução dos primeiros animais e seus ancestrais eucariotos. Estudos recentes demonstram que ao menos 22 famílias de enzimas que produzem ou utilizam o O_2 surgiram em torno de 3.1 Ga, muito antes do G.O.E. (~2.5 – 2.3 Ga; Jabłońska e Tawfik, 2021). Fato que poderia ser explicado pela possível existência de oásis de O_2

ocupados por organismos que realizavam fotossíntese oxigenada (Ślesak et al., 2012; Olson et al., 2013).

Também é argumentado que independentemente do ambiente, o O_2 estava presente nas células desde o início da vida. Estudos teorizam que espécies reativas de oxigênio (ROS) produzidas abioticamente poderiam ter sido a fonte primordial de O_2 molecular (Sperling e Stockey, 2018; Jabłońska e Tawfik, 2021). Esses resultados indicam que, ao contrário do que é pensado por muitos autores, o aumento dos níveis de O_2 atmosférico pode não ter sido um gatilho (ou o único gatilho) para as novidades evolutivas da Terra primitiva, tornando a história evolutiva das enzimas do metabolismo aeróbico uma intrigante fonte de informações sobre os animais primordiais (Olson et al., 2013; Jabłońska e Tawfik, 2021).

3.2. O metabolismo aeróbico em hipóxia: o papel da via HIF

Em condições de hipóxia, a maioria dos animais possui uma via evolutivamente conservada para manter a homeostase fisiológica do O_2. Essa via desencadeia mudanças adaptativas na expressão de genes que auxiliam o organismo a manter um nível estável de O_2 em suas células, a qual é mediada pelo fator de transcrição conhecido como fator induzido por hipóxia 1 (HIF1 – *Hypoxia-inducible factor* 1; Semenza, 2007; Kaelin e Ratcliffe, 2008; Loenarz, 2011). A molécula da HIF consiste em duas subunidades: a HIF1α, que tem seu acúmulo e degradação regulados pelo O_2, e a HIF1β (ARNT – *Aryl Hydrocarbon Receptor Nuclear Translocator*), que é expressa constitutivamente. Ambas as subunidades são compostas por dois domínios *basic helix–loop–helix* (bHLH) e *Per-ARNT-Sim* (PAS), os quais permitem a dimerização das subunidades quando as concentrações de O_2 celular estão baixas (Semenza, 2007; Kaelin e Ratcliffe, 2008).

Em normóxia, a HIF1α é continuamente sintetizada e degradada através de um mecanismo celular complexo. Duas proteínas, chamadas prolil hidroxilase (PHD – *prolyl hydroxylase*) e fator inibidor de HIF1 (FIH1 – *factor inhibiting HIF1*), hidroxilam prolinas específicas presentes na HIF1α (chamadas de domínio de degradação dependente de O_2, ODDD – *oxygen-dependent degradation domain*; Hon et al., 2002; Peet e Linke, 2006). A proteína *von Hippel-Lindau* (VHL) reconhece os grupamentos hidroxila na HIF1α e promove a sua ubiquitinação e degradação mediada pelo proteossomo (Min et al., 2002; Semenza, 2007; Kaelin e Ratcliffe, 2008). Em hipóxia, esses processos são inibidos devido à inativação das hidroxilases, levando a uma rápida estabilização da HIF1α, que é protegida da degradação, acumula-se no citoplasma e liga-se à HIF1β, formando o heterodímero ativo. O complexo transloca-se para o núcleo e regula positivamente a transcrição de centenas de genes associados à conservação do O_2, hematopoiese, função mitocondrial, metabolismo energético e transporte de O_2 (Semenza, 2007; Kaelin e Ratcliffe, 2008).

Mills e colaboradores (2018) demonstraram que tanto esponjas quanto ctenóforos não possuem componentes-chave da via HIF, indicando que esses animais não têm uma via HIF funcional. Esses resultados sugerem ainda que o último ancestral comum animal provavelmente também não tinha a via funcional e, possivelmente, poderia manter o metabolismo aeróbico e a transcrição inalterada sob os baixos níveis de O_2 de seu ambiente (Mills et al., 2018). Considerando o papel crucial do O_2 na vida animal, a história evolutiva da HIFα, uma proteína considerada um regulador-mestre da homeostase do O_2 (Semenza, 2007), também pode ser uma ótima fonte de conhecimento acerca do surgimento e da diversificação dos animais.

4. Como os primeiros animais lidavam com o oxigênio?

4.1. O uso de abordagens experimentais

Sabe-se que algumas linhagens animais são capazes de lidar com períodos prolongados de hipóxia, e até mesmo anóxia sazonal, como esponjas, ctenóforos, cnidários, poliquetas, crustáceos e bivalves (Reiswig e Miller, 1998; Bell e Barnes, 2000; Purcell et al., 2001; Sussarellu et al., 2010; Mosch et al., 2012; Müller et al., 2012; Troch et al., 2013; Parris et al., 2014; Grego et al., 2014; Lucey et al., 2020; Grimes et al., 2020). Entretanto, os processos moleculares envolvidos na resposta à hipóxia ainda estão sendo investigados. Sussarellu et al. (2010) submeteram ostras a 20 dias de hipóxia (2 mg O_2/L) e observaram que a maioria dos genes super expressos estão envolvidos na defesa antioxidante ou são da cadeia respiratória, sugerindo estresse oxidativo e resposta antecipada à recuperação da condição de normóxia. Grimes et al. (2021) avaliaram as variações na expressão gênica de poliquetas após exposição prolongada e intermitente a diferentes intensidades de hipóxia (4–1 mg O_2/L). Foi visto que componentes da via HIF possuem resposta modulada à hipóxia, dependendo da intensidade do estresse oxidativo. Mills et al. (2018) avaliaram que a esponja *Tethya wilhelma* mantém expressão gênica normal após quatro dias de exposição à hipóxia (0,25–2% P.A.L.). Eles também observaram que após uma hora de exposição à anóxia, a esponja apresentou expressão diferencial de genes envolvidos em funções metabólicas como proteínas de ligação ao heme e ubiquitinas, indicando um possível estresse oxidativo nessas condições.

Considerando os diferentes aspectos ambientais do Neoproterozóico, pouco se sabe sobre os mecanismos moleculares dos animais que estavam adaptados para viver naqueles ambientes. Entender como os animais modernos respondem em nível molecular à hipóxia e anóxia pode ajudar a esclarecer aspectos da fisiologia dos primeiros animais. Para isso, análogos modernos dos primeiros metazoários foram usados como modelos para inferir a fisiologia de seus ancestrais. Empregando câmaras de simulação

que recriam as condições oceânicas de baixo O_2 do Neoproterozóico, foram realizados testes com o objetivo de comparar as diferenças na expressão gênica de animais submetidos aos experimentos com aqueles mantidos em situação controle. A correlação dos genes e vias metabólicas diferencialmente expressos com dados paleoambientais da Era Neoproterozóica se mostrou uma técnica eficaz na geração de informação acerca da fisiologia dos primeiros metazoários.

5. Justificativa e objetivos

A presente tese de doutorado teve por objetivo principal entender como era a fisiologia dos animais primordiais que surgiram no Neoproterozóico. Para tal, foram empregadas abordagens bioinformáticas e experimentais. Na abordagem essencialmente bioinformática, o objetivo foi estudar a fisiologia dos primeiros animais por meio da análise evolutiva e datação molecular de proteínas envolvidas no metabolismo do O_2. Compreender a evolução de proteínas ligadas a processos oxidativos é uma etapa essencial na correlação entre o surgimento dos primeiros animais e os fatores ambientais do Neoproterozóico. Como os animais dependem da oxidação de moléculas orgânicas para sobreviver, a evolução de proteínas relacionadas ao metabolismo oxidativo pode ser usada para rastrear o surgimento dessas vias nesses organismos. O objetivo final dos estudos bioinformáticos foi correlacionar a datação obtida para cada gene e, consequentemente, o aparecimento dessas vias metabólicas, com dados paleoambientais gerando novas informações sobre aspectos fisiológicos dos metazoários primordiais.

Já na abordagem essencialmente experimental, foram utilizados animais modernos como modelos para inferir aspectos da fisiologia dos seus ancestrais. Através de testes que simularam as condições oceânicas do Neoproterozóico, as variações na expressão gênica dos indivíduos testados foram quantificadas e comparadas. Para isso, foi construído um

sistema de Câmaras de Simulação das condições de oxigenação oceânica estimadas para o Neoproterozóico, e a demoesponja *Hymeniacidon heliophila* foi utilizada como análogo moderno dos metazoários primordiais. As esponjas foram escolhidas pois são consideradas um dos primeiros clados animais a divergir e que, com base no registro fóssil, permanecem relativamente inalteradas em relação a sua morfologia e hábitos de filtração (Suarez e Leys, 2022). Com base na comparação dos perfis de expressão gênica dos indivíduos testados foram feitas inferências acerca da fisiologia respiratória dos animais que viveram no Neoproterozóico.

A tese aqui apresentada engloba todos os resultados obtidos ao longo do meu período como aluna de doutorado no Programa de Pós-Graduação em Zoologia do Instituto de Biociências da Universidade de São Paulo, e durante um estágio de pesquisa de três meses no laboratório da Dra. Sally P. Leys na University of Alberta, no Canadá. Os resultados estão organizados em três capítulos, escritos em formato de artigos, que tiveram como objetivo principal entender a fisiologia dos metazoários primordiais. Integrando estudos bioinformáticos de datação molecular com experimentos de simulação e análise da expressão gênica diferencial, minha intenção foi alcançar novos horizontes nas áreas de evolução e diversificação inicial dos animais.

Os primeiros dois capítulos, já publicados, trazem estudos de datação molecular da enzima IDH e da HIFα (Bezerra et al., 2021; Belato et al., 2023). Para estabelecer a história evolutiva e o tempo de divergência das duas proteínas, foram empregados métodos de reconstrução filogenética e datação molecular assumindo relógio molecular relaxado. Os resultados aqui obtidos demonstraram que eventos de duplicação gênica ocorreram tanto na história evolutiva da IDH quanto na da HIFα. Esses dados corroboram a hipótese de que uma grande parte do *toolkit*

gênico necessário para o desenvolvimento animal evoluiu em seus ancestrais eucarióticos (Sebé-Pedrós et al., 2011, 2012; de Mendoza et al., 2013). Os resultados gerados a partir das análises de datação do surgimento da HIFα e da IDH suportam a hipótese de uma diversificação dos eucariotos antes do período Toniano, bem como um surgimento pré-Criogeniano dos animais em condições de hipóxia.

O terceiro capítulo traz os resultados dos experimentos de simulação das condições oceânicas do Neoproterozóico onde as esponjas foram submetidas às condições de anóxia e hipóxia, além de um controle oxigenado. Os dados gerados neste capítulo indicam que tanto a condição oxigenada quanto a anóxia desencadeiam as mesmas respostas fisiológicas e moleculares de estresse, sugerindo que as esponjas estão mais bem adaptadas à hipóxia. Os resultados também sugerem que apesar dos primeiros metazoários não possuírem a via HIF como mecanismo de detecção dos níveis de O_2 molecular, eles provavelmente utilizavam outros meios para essa função, como o metabolismo do sulfeto. Em condição de estresse oxidativo, foi observada a expressão diferencial de genes relacionados à glicólise e à reorganização do sistema aquífero, sugerindo um possível papel ancestral desses mecanismos nos metazoários ancestrais. Os resultados obtidos aqui revelam possíveis adaptações fisiológicas que podem ter sido vantajosas aos primeiros animais, corroborando a hipótese de que eles possuíam mecanismos moleculares adaptados para viver em ambientes com baixos níveis de O_2 (Mills et al., 2018).

Referências Bibliográficas

Akram, M. (2014). Citric acid cycle and role of its intermediates in metabolism. *Cell biochemistry and biophysics*, *68*(3), 475–478.

Antcliffe, J. B., Callow, R. H. T., & Brasier, M. D. (2014). Giving the early fossil record of sponges a squeeze. *Biological Reviews*, *89*(4), 972–1004.

Babcock, G. T., & Wikström, M. (1992). Oxygen activation and the conservation of energy in cell respiration. *Nature*, *356*(6367), 301–309.

Belato, F. A., Mello, B., Coates, C. J., Halanych, K. M., Brown, F. D., Morandini, A. C., de Moraes Leme, J., Trindade, R. I. F., & Costa-Paiva, E. M. (2023). Divergence time estimates for the hypoxia-inducible factor-1 alpha (HIF1α) reveal an ancient emergence of animals in low-oxygen environments. *Geobiology*, *22*(1), 1–14.

Bell, J. J., & Barnes, D. K. A. (2000). A sponge diversity centre within a marine `island'. In M. B. Jones, J. M. N. Azevedo, A. I. Neto, A. C. Costa, & A. M. F. Martins (Eds.), *Island, Ocean and Deep-Sea Biology* (pp. 55–64). Springer Netherlands.

Berkner, L. V., & Marshall, L. C. (1965). On the Origin and Rise of Oxygen Concentration in the Earth's Atmosphere. *Journal of the Atmospheric Sciences*, *22*(3), 225–261.

Bezerra, B. S., Belato, F. A., Mello, B., Brown, F., Coates, C. J., de Moraes Leme, J., Trindade, R. I. F., & Costa-Paiva, E. M. (2021). Evolution of a key enzyme of aerobic metabolism reveals Proterozoic functional subunit duplication events and an ancient origin of animals. *Scientific Reports*, *11*(1), 1–11.

Brain, C. K., Prave, A. R., Hoffmann, K.-H., Fallick, A. E., Botha, A., Herd, D. A., Sturrock, C., Young, I., Condon, D. J., & Allison, S. G. (2012). The first animals: ca. 760-million-year-old sponge-like fossils from Namibia. *South African Journal of Science*, *108*(1), 1–8.

Brochier-Armanet, C., Talla, E., & Gribaldo, S. (2009). The multiple evolutionary histories of dioxygen reductases: Implications for the origin and evolution of aerobic respiration. *Molecular Biology and Evolution*, *26*(2), 285–297.

Buick, R. (2008). When did oxygenic photosynthesis evolve? *Philosophical Transactions of the Royal Society B: Biological Sciences*, *363*(1504), 2731–2743.

Canfield, D. E. (1998). A new model for Proterozoic ocean chemistry. *Nature*, *396*(6710), 450–453.

Canfield, D. E. (2005). The early history of atmospheric oxygen: Homage to Robert M. Garrels. *Annual Review of Earth and Planetary Sciences*, *33*(1), 1–36.

Canfield, D. E., Poulton, S. W., Knoll, A. H., Narbonne, G. M., Ross, G., Goldberg, T., & Strauss, H. (2008). Ferruginous Conditions Dominated Later Neoproterozoic Deep-Water Chemistry. *Science*, *321*(5891), 949–952.

Canfield, D. E., Poulton, S. W., & Narbonne, G. M. (2007). Late-Neoproterozoic Deep-Ocean Oxygenation and the Rise of Animal Life. *Science*, *315*(5808), 92–95.

Cartwright, P., & Collins, A. (2007). Fossils and phylogenies: integrating multiple lines of evidence to investigate the origin of early major metazoan lineages. *Integrative and Comparative Biology*, *47*(5), 744–751.

Catling, D. C., Glein, C. R., Zahnle, K. J., & McKay, C. P. (2005). Why O 2 Is Required by Complex Life on Habitable Planets and the Concept of Planetary "Oxygenation Time." *Astrobiology*, *5*(3), 415–438.

Chance, B., & Williams, G. R. (1955). Respiratory enzymes in oxidative phosphorylation: II. Difference spectra. *Journal of Biological Chemistry*, *217*(1), 395–407.

Chandel, N. S. (2021). Glycolysis. *Cold Spring Harbor Perspectives in Biology*, *13*(5), 1–12.

Cloud, P. E. (1968). Atmospheric and Hydrospheric Evolution on the Primitive Earth. *Science, 160*(3829), 729–736.

Cloud, P. E. (1969). Pre-Paleozoic Sediments and Their Significance for Organic Geochemistry. In Mangum, C. P. (Ed.), *Organic Geochemistry* (pp. 727–736). Springer Berlin Heidelberg.

Cole, D. B., Mills, D. B., Erwin, D. H., Sperling, E. A., Porter, S. M., Reinhard, C. T., & Planavsky, N. J. (2020). On the co-evolution of surface oxygen levels and animals. *Geobiology*, *18*(3), 260–281.

Cordani, U. G., Fairchild, T. R., Ganade, C. E., Babinski, M., & Leme, J. de M. (2020). Dawn of metazoans: to what extent was this influenced by the onset of "modern-type plate tectonics"? *Brazilian Journal of Geology, 50*(2), 1–15.

Covello, K. L., Kehler, J., Yu, H., Gordan, J. D., Arsham, A. M., Hu, C. J., Labosky, P., Simon, M., Keith, B. (2006). HIF–2α regulates Oct–4: effects of hypoxia on stem cell function, embryonic development, and tumor growth. *Genes and Development*, *20*(5), 557–570.

Cupp, J. R., & McAlister-Henn, L. (1991). NAD(+)-dependent isocitrate dehydrogenase. Cloning, nucleotide sequence, and disruption of the IDH2 gene from Saccharomyces cerevisiae. *Journal of Biological Chemistry*, *266*(33), 22199–22205.

de Mendoza, A., Sebé-Pedrós, A., Sestak, M. S., Matejcic, M., Torruella, G., Domazet-Loso, T., & Ruiz-Trillo, I. (2013). Transcription factor evolution in eukaryotes and the assembly of the regulatory toolkit in multicellular lineages. *Proceedings of the National Academy of Sciences*, *110*(50), E4858–E4866.

Dean, A. M., & Golding, G. B. (1997). Protein engineering reveals ancient adaptive replacements in isocitrate dehydrogenase. *Proceedings of the National Academy of Sciences*, *94*(7), 3104–3109.

Decker, H., & van Holde, K. E. (2011). *Oxygen and the Evolution of Life*. Springer Berlin Heidelberg.

Diamond, C. W., & Lyons, T. W. (2018). Mid-Proterozoic redox evolution and the possibility of transient oxygenation events. *Emerging Topics in Life Sciences*, *2*(2), 235–245.

Dohrmann, M., & Wörheide, G. (2017). Dating early animal evolution using phylogenomic data. *Scientific Reports*, *7*(1), 1–6.

dos Reis, M., Thawornwattana, Y., Angelis, K., Telford, M. J., Donoghue, P. C. J., & Yang, Z. (2015). Uncertainty in the Timing of Origin of Animals and the Limits of Precision in Molecular Timescales. *Current Biology*, *25*(22), 2939–2950.

Douzery, E. J. P., Snell, E. A., Bapteste, E., Delsuc, F., & Philippe, H. (2004). The timing of eukaryotic evolution: Does a relaxed molecular clock reconcile proteins and fossils? *Proceedings of the National Academy of Sciences, 101*(43), 15386–15391.

Doyle, K. A., Poulton, S. W., Newton, R. J., Podkovyrov, V. N., & Bekker, A. (2018). Shallow water anoxia in the Mesoproterozoic ocean: Evidence from the Bashkir Meganticlinorium, Southern Urals. *Precambrian Research*, *317*, 196–210.

Droser, M. L., Tarhan, L. G., & Gehling, J. G. (2017). The Rise of Animals in a Changing Environment: Global Ecological Innovation in the Late Ediacaran. *Annual Review of Earth and Planetary Sciences*, *45*(July), 593–617.

Dzik, J. (2007). The Verdun Syndrome: simultaneous origin of protective armour and infaunal shelters at the Precambrian–Cambrian transition. *Geological Society, London, Special Publications*, *286*(1), 405–414.

Erwin, D. H., Laflamme, M., Tweedt, S. M., Sperling, E. A., Pisani, D., & Peterson, K. J. (2011). The Cambrian conundrum: Early divergence and later ecological success in the early history of animals. *Science*, *334*(6059), 1091–1097.

Farquhar, J., Bao, H., & Thiemens, M. (2000). Atmospheric Influence of Earth's Earliest Sulfur Cycle. *Science*, *289*(5480), 756–758.

Fenchel, T., & Finlay, B. J. (1995). *Ecology and Evolution in Anoxic Worlds*. Oxford University Press.

Fothergill-Gilmore, L. A., & Michels, P. A. (1993). Evolution of glycolysis. *Progress in biophysics and molecular biology*, *59*(2), 105–235.

Grego, M., Riedel, B., Stachowitsch, M., & De Troch, M. (2014). Meiofauna winners and losers of coastal hypoxia: Case study harpacticoid copepods. *Biogeosciences*, *11*(2), 281–292.

Grimes, C. J., Capps, C., Petersen, L. H., & Schulze, A. (2020). Oxygen consumption during and post-hypoxia exposure in bearded fireworms (Annelida: Amphinomidae). *Journal of Comparative Physiology B*, *190*(6), 681–689.

Grimes, C. J., Petersen, L. H., & Schulze, A. (2021). Differential gene expression indicates modulated responses to chronic and intermittent hypoxia in corallivorous fireworms (*Hermodice carunculata*). *Scientific Reports*, *11*(1), 1–13.

Halanych, K. M. (2016). How our view of animal phylogeny was reshaped by molecular approaches: lessons learned. *Organisms Diversity and Evolution*, *16*(2), 319–328.

Hammarlund, E., Bukkuri, A., Norling, M., Posth, N., Carroll, C., Baratchart, E., Amend, S., Gatenby, R., Pienta, K., Brown, J., Peters, S., & Hancke, K. (*in press*). Benthic daily oxygen variability and stress as drivers for animal diversification in the Cambrian. *Nature Ecology and Evolution.*

He, T., Zhu, M., Mills, B. J. W., Wynn, P. M., Zhuravlev, A. Y., Tostevin, R., Pogge von Strandmann, P. A. E., Yang, A., Poulton, S. W., & Shields, G. A. (2019). Possible links between extreme oxygen perturbations and the Cambrian radiation of animals. *Nature Geoscience*, *12*(6), 468–474.

Hedges, S. B., Blair, J. E., Venturi, M. L., & Shoe, J. L. (2004). A molecular timescale of eukaryote evolution and the rise of complex multicellular life. *BMC Evolutionary Biology*, *4*(1), 1–9.

Holland, H. D. (2002). Volcanic gases, black smokers, and the great oxidation event. *Geochimica et Cosmochimica Acta*, *66*(21), 3811–3826.

Holland, H. D. (2006). The oxygenation of the atmosphere and oceans. *Philosophical Transactions of the Royal Society B: Biological Sciences*, *361*(1470), 903–915.

Hon, W. C., Wilson, M. I., Harlos, K., Claridge, T. D. W., Schofield, C. J., Pugh, C. W., Maxwell, P. H., Ratcliffe, P. J., Stuart, D. I., & Jones, E. Y. (2002). Structural basis for the recognition of hydroxyproline in HIF-1α by pVHL. *Nature*, *417*(6892), 975–978.

Ivanovic, Z. (2009). Hypoxia or in situ normoxia: The stem cell paradigm. *Journal of Cellular Physiology*, *219*(2), 271–275.

Jabłońska, J., & Tawfik, D. S. (2021). The evolution of oxygen-utilizing enzymes suggests early biosphere oxygenation. *Nature Ecology & Evolution*, *5*(4), 442–448.

Javaux, E. J., Marshall, C. P., & Bekker, A. (2010). Organic-walled microfossils in 3.2-billion-year-old shallow-marine siliciclastic deposits. *Nature*, *463*(7283), 934–938.

Jo, S. H., Son, M. K., Koh, H. J., Lee, S. M., Song, I. H., Kim, Y. O., Lee, Y.-S., Jeong, K.-S., Kim, W. B., Park, J.-W., Song, B. J., & Huhe, T. L. (2001). Control of mitochondrial redox balance and cellular defense against oxidative damage by mitochondrial NADP+-dependent isocitrate dehydrogenase. *Journal of Biological chemistry*, *276*(19), 16168–16176.

Johnson, C. M., Beard, B. L., Klein, C., Beukes, N. J., & Roden, E. E. (2008). Iron isotopes constrain biologic and abiologic processes in banded iron formation genesis. *Geochimica et Cosmochimica Acta*, *72*(1), 151–169.

Kaelin, W. G., & Ratcliffe, P. J. (2008). Oxygen Sensing by Metazoans: The Central Role of the HIF Hydroxylase Pathway. *Molecular Cell*, *30*(4), 393–402.

Kasting, J. F., & Catling, D. (2003). Evolution of a Habitable Planet. *Annual Review of Astronomy and Astrophysics*, *41*(1), 429–463.

Kasting, J. F., & Howard, M. T. (2006). Atmospheric composition and climate on the early Earth. *Philosophical Transactions of the Royal Society B: Biological Sciences*, *361*(1474), 1733–1742.

Kim, Y. O., Oh, I. U., Park, H. S., Jeng, J., Song, B. J., & Huh, T. L. (1995). Characterization of a cDNA clone for human NAD+-specific isocitrate dehydrogenase α-subunit and structural comparison with its isoenzymes from different species. *Biochemical Journal*, *308*(1), 63–68.

King, N., & Rokas, A. (2017). Embracing Uncertainty in Reconstructing Early Animal Evolution. *Current Biology*, *27*(19), R1081–R1088.

Knoll, A. H. (1992). The early evolution of eukaryotes: a geological perspective. *Science*, *256*(5057), 622–627.

Koch, L. G., & Britton, S. L. (2008). Aerobic metabolism underlies complexity and capacity. *The Journal of Physiology*, *586*(1), 83–95.

Kump, L. R. (2008). The rise of atmospheric oxygen. *Nature*, *451*(7176), 277–278.

Kump, L. R., & Holland, H. D. (1992). Iron in Precambrian rocks: Implications for the global oxygen budget of the ancient Earth. *Geochimica et Cosmochimica Acta*, *56*(8), 3217–3223.

Lane, N., & Martin, W. (2010). The energetics of genome complexity. *Nature*, *467*(7318), 929–934.

Lehninger, A. L. (1949). Esterification of inorganic phosphate coupled to electron transport between dihydrodiphosphopyridine nucleotide and oxygen. II. *Journal of biological chemistry*, *178*(2), 625–644.

Lenton, T. M., & Daines, S. J. (2017). Biogeochemical Transformations in the History of the Ocean. *Annual Review of Marine Science*, *9*(1), 31–58.

Levin, L. A. (2003). Oxygen Minimum Zone Benthos: Adaptation and Community Response to Hypoxia. *Oceanography and Marine Biology: An Annual Review*, *41*(1), 1–45.

Leys, S. P., & Kahn, A. S. (2018). Oxygen and the energetic requirements of the first multicellular animals. *Integrative and Comparative Biology*, *58*(4), 666–-676.

Li, C., Cheng, M., Zhu, M., & Lyons, T. W. (2018a). Heterogeneous and dynamic marine shelf oxygenation and coupled early animal evolution. *Emerging Topics in Life Sciences*, *2*(2), 279–288.

Li, Z.-Q., Zhang, L.-C., Xue, C.-J., Zheng, M.-T., Zhu, M.-T., Robbins, L. J., Slack, J. F., Planavsky, N. J., & Konhauser, K. O. (2018b). Earth's youngest banded iron formation implies ferruginous conditions in the Early Cambrian Ocean. *Scientific Reports*, *8*(1), 1–10.

Loenarz, C., Coleman, M. L., Boleininger, A., Schierwater, B., Holland, P. W. H., Ratcliffe, P. J., & Schofield, C. J. (2011). The hypoxia-inducible transcription factor pathway regulates oxygen sensing in the simplest animal, Trichoplax adhaerens. *EMBO Reports*, *12*(1), 63–70.

Love, G. D., Grosjean, E., Stalvies, C., Fike, D. A., Grotzinger, J. P., Bradley, A. S., Kelly, A. E., Bhatia, M., Meredith, W., Snape, C. E., Bowring, S. A., Condon, D. J., & Summons, R. E. (2009). Fossil steroids record the appearance of Demospongiae during the Cryogenian period. *Nature*, *457*(7230), 718–721.

Lucey, N. M., Collins, M., & Collin, R. (2020). Oxygen-mediated plasticity confers hypoxia tolerance in a corallivorous polychaete. *Ecology and Evolution*, *10*(3), 1145–1157.

Mailloux, R. J., Bériault, R., Lemire, J., Singh, R., Chénier, D. R., Hamel, R. D., & Appanna, V. D. (2007). The Tricarboxylic Acid Cycle, an Ancient Metabolic Network with a Novel Twist. *PLOS ONE*, *2*(8), 1–10.

Martínez-Rivas, J. M., & Vega, J. (1998). Purification and Characterization of NAD-Isocitrate Dehydrogenase from *Chlamydomonas reinhardtii1*. *Plant Physiology*, *118*(1), 249–255.

Mentel, M., Martin, W. (2008). Energy metabolism among eukaryotic anaerobes in light of Proterozoic ocean chemistry. *Philosophical Transactions of the Royal Society B: Biological Sciences*, *363*(1504), 2717–2729.

Mentel, M., Tielens, A. G. M., & Martin, W. F. (2016). Animals, anoxic environments, and reasons to go deep. *BMC Biology*, *14*(1), 1–3.

Mills, D. B., & Canfield, D. E. (2014). Oxygen and animal evolution: Did a rise of atmospheric oxygen "trigger" the origin of animals? *BioEssays*, *36*(12), 1145–1155.

Mills, D. B., Francis, W. R., Vargas, S., Larsen, M., Elemans, C. P., Canfield, D. E., & Wörheide, G. (2018). The last common ancestor of animals lacked the HIF pathway and respired in low-oxygen environments. *ELife*, *7*, 1–17.

Mills, D. B., Ward, L. M., Jones, C. A., Sweeten, B., Forth, M., Treusch, A. H., & Canfield, D. E. (2014). Oxygen requirements of the earliest animals. *Proceedings of the National Academy of Sciences*, *111*(11), 4168–4172.

Min, J. H., Yang, H., Ivan, M., Gertler, F., Kaelin Jr, W. G., & Pavletich, N. P. (2002). Structure of an HIF-1α-pVHL complex: hydroxyproline recognition in signaling. *Science*, *296*(5574), 1886–1889.

Mosch, T., Sommer, S., Dengler, M., Noffke, A., Bohlen, L., Pfannkuche, O., Liebetrau, V., & Wallmann, K. (2012). Factors influencing the distribution of epibenthic megafauna across the Peruvian oxygen minimum zone. *Deep Sea Research Part I: Oceanographic Research Papers*, *68*, 123–135.

Müller, M., Mentel, M., van Hellemond, J. J., Henze, K., Woehle, C., Gould, S. B., Yu, R.-Y., van der Giezen, M., Tielens, A. G. M., & Martin, W. F. (2012). Biochemistry and Evolution of Anaerobic Energy Metabolism in Eukaryotes. *Microbiology and Molecular Biology Reviews*, *76*(2), 444–495.

Narbonne, G. M. (2005). The Ediacara Biota: Neoproterozoic Origin of Animals and Their Ecosystems. *Annual Review of Earth and Planetary Sciences*, *33*(1), 421–442.

Nekrutenko, A., Hillis, D. M., Patton, J. C., Bradley, R. D., & Baker, R. J. (1998). Cytosolic isocitrate dehydrogenase in humans, mice, and voles and phylogenetic analysis of the enzyme family. *Molecular biology and evolution*, *15*(12), 1674–1684.

Nelson, D. L., Lehninger, A. L., & Cox, M. M. (2013). *Lehninger principles of biochemistry* (6th Ed). New York, H. Freeman.

Nichols, B. J., Perry, A. C. F., Hall, L., & Denton, R. M. (1995). Molecular cloning and deduced amino acid sequences of the α- and β- subunits of mammalian NAD+-isocitrate dehydrogenase. *Biochemical Journal*, *310*(3), 917–922.

Nunes-Nesi, A., Araújo, W. L., Obata, T., & Fernie, A. R. (2013). Regulation of the mitochondrial tricarboxylic acid cycle. *Current Opinion in Plant Biology*, *16*(3), 335–343.

Nursall, J. R. (1959). Oxygen as a Prerequisite to the Origin of the Metazoa. *Nature*, *183*(4669), 1170–1172.

Nutman, A. P., Bennett, V. C., Friend, C. R. L., Van Kranendonk, M. J., & Chivas, A. R. (2016). Rapid emergence of life shown by discovery of 3,700-million-year-old microbial structures. *Nature*, *537*(7621), 535–538.

Och, L. M., & Shields-Zhou, G. A. (2012). The Neoproterozoic oxygenation event: Environmental perturbations and biogeochemical cycling. *Earth-Science Reviews*, *110*(1–4), 26–57.

Ohtomo, Y., Kakegawa, T., Ishida, A., Nagase, T., & Rosing, M. T. (2014). Evidence for biogenic graphite in early Archaean Isua metasedimentary rocks. *Nature Geoscience*, *7*(1), 25–28.

Olson, S. L., Kump, L. R., & Kasting, J. F. (2013). Quantifying the areal extent and dissolved oxygen concentrations of Archean oxygen oases. *Chemical Geology*, *362*, 35–43.

Parfrey, L. W., Lahr, D. J. G., Knoll, A. H., & Katz, L. A. (2011). Estimating the timing of early eukaryotic diversification with multigene molecular clocks. *Proceedings of the National Academy of Sciences*, *108*(33), 13624–13629.

Parris, D. J., Ganesh, S., Edgcomb, V. P., DeLong, E. F., & Stewart, F. J. (2014). Microbial eukaryote diversity in the marine oxygen minimum zone off northern Chile. *Frontiers in Microbiology*, *5*(1), 1–11.

Pearce, B. K. D., Tupper, A. S., Pudritz, R. E., & Higgs, P. G. (2018). Constraining the Time Interval for the Origin of Life on Earth. *Astrobiology*, *18*(3), 343–364.

Peet, D., & Linke, S. (2006). Regulation of HIF: asparaginyl hydroxylation. In *Signalling Pathways in Acute Oxygen Sensing: Novartis Foundation Symposium 272* (pp. 37-53). Chichester, UK, John Wiley & Sons, Ltd.

Peterson, K. J., Lyons, J. B., Nowak, K. S., Takacs, C. M., Wargo, M. J., & McPeek, M. A. (2004). Estimating metazoan divergence times with a molecular clock. *Proceedings of the National Academy of Sciences*, *101*(17), 6536–6541.

Pierrehumbert, R., Abbot, D., Voigt, A., Koll, D. (2011). Climate of the Neoproterozoic. *Annual Review of Earth and Planetary Sciences*, *39*, 417–460.

Pisani, D., Pett, W., Dohrmann, M., Feuda, R., Rota-Stabelli, O., Philippe, H., Lartillot, N., & Wörheide, G. (2015). Genomic data do not support comb jellies as the sister group to all other animals. *Proceedings of the National Academy of Sciences*, *112*(50), 15402–15407.

Planavsky, N. J., Asael, D., Hofmann, A., Reinhard, C. T., Lalonde, S. V., Knudsen, A., Wang, X., Ossa Ossa, F., Pecoits, E., Smith, A. J. B., Beukes, N. J., Bekker, A., Johnson, T. M., Konhauser, K. O., Lyons, T. W., & Rouxel, O. J. (2014). Evidence for oxygenic photosynthesis half a billion years before the Great Oxidation Event. *Nature Geoscience*, *7*(4), 283–286.

Planavsky, N. J., Cole, D. B., Isson, T. T., Reinhard, C. T., Crockford, P. W., Sheldon, N. D., & Lyons, T. W. (2018). A case for low atmospheric oxygen levels during Earth's middle history. *Emerging Topics in Life Sciences*, *2*(2), 149–159.

Poulton, S. W., & Canfield, D. E. (2011). Ferruginous Conditions: A Dominant Feature of the Ocean through Earth's History. *Elements*, *7*(2), 107–112.

Prockop, D., Kaplan, A., & Udenfriend, S. (1963). Oxygen-18 studies on the conversion of proline to collagen hydroxyproline. *Archives of Biochemistry and Biophysics*, *101*(3), 499–503.

Pu, J. P., Bowring, S. A., Ramezani, J., Myrow, P., Raub, T. D., Landing, E., Mills, A., Hodgin, E., & Macdonald, F. A. (2016). Dodging snowballs: Geochronology of the Gaskiers glaciation and the first appearance of the Ediacaran biota. *Geology*, *44*(11), 955–958.

Purcell, J. E., Breitburg, D. L., Decker, M. B., Graham, W. M., Youngbluth, M. J., & Raskoff, K. A. (2001). Pelagic cnidarians and ctenophores in low dissolved oxygen environments: A review. In N. N. Rabalais & R. E. Turner (Eds.), *Coastal Hypoxia: Consequences for Living Resources and Ecosystems* (pp. 77–100). American Geophysical Union.

Ramachandran, N., & Colman, R. F. (1980). Chemical characterization of distinct subunits of pig heart DPN-specific isocitrate dehydrogenase. *Journal of Biological Chemistry*, *255*(18), 8859–8864.

Raymond, J., & Segrè, D. (2006). The effect of oxygen on biochemical networks and the evolution of complex life. *Science*, *311*(5768), 1764–1767.

Reinhard, C. T., Planavsky, N. J., Gill, B. C., Ozaki, K., Robbins, L. J., Lyons, T. W., Fischer, W. W., Wang, C., Cole, D. B., & Konhauser, K. O. (2017). Evolution of the global phosphorus cycle. *Nature*, *541*(7637), 386–389.

Reinhard, C. T., Planavsky, N. J., Olson, S. L., Lyons, T. W., & Erwin, D. H. (2016). Earth's oxygen cycle and the evolution of animal life. *Proceedings of the National Academy of Sciences*, *113*(32), 8933–8938.

Reiswig, H. M., & Miller, T. L. (1998). Freshwater Sponge Gemmules Survive Months of Anoxia. *Invertebrate Biology*, *117*(1), 1–8.

Rosing, M. T. (1999). 13C-Depleted Carbon Microparticles in >3700-Ma Sea-Floor Sedimentary Rocks from West Greenland. *Science*, *283*(5402), 674–676.

Runnegar, B. (1982). Oxygen requirements, biology and phylogenetic significance of the late Precambrian worm Dickinsonia, and the evolution of the burrowing habit. *Alcheringa: An Australasian Journal of Palaeontology*, *6*(3), 223–239.

Sahoo, S. K., Planavsky, N. J., Jiang, G., Kendall, B., Owens, J. D., Wang, X., Shi, X., Anbar, A. D., & Lyons, T. W. (2016). Oceanic oxygenation events in the anoxic Ediacaran ocean. *Geobiology*, *14*(5), 457–468.

Sahoo, S. K., Planavsky, N. J., Kendall, B., Wang, X., Shi, X., Scott, C., Anbar, A. D., Lyons, T. W., & Jiang, G. (2012). Ocean oxygenation in the wake of the Marinoan glaciation. *Nature*, *489*(7417), 546–549.

Schirrmeister, B. E., Sanchez-Baracaldo, P., & Wacey, D. (2016). Cyanobacterial evolution during the Precambrian. *International Journal of Astrobiology*, *15*(3), 187–204.

Sebé-Pedrós, A., de Mendoza, A., Lang, B. F., Degnan, B. M., & Ruiz-Trillo, I. (2011). Unexpected Repertoire of Metazoan Transcription Factors in the Unicellular Holozoan *Capsaspora owczarzaki*. *Molecular Biology and Evolution*, *28*(3), 1241–1254.

Sebé-Pedrós, A., Zheng, Y., Ruiz-Trillo, I., & Pan, D. (2012). Premetazoan Origin of the Hippo Signaling Pathway. *Cell Reports*, *1*(1), 13–20.

Semenza, G. L. (2007). Life with oxygen. *Science*, *318*(5847), 62–64.

Sessions, A. L., Doughty, D. M., Welander, P. V, Summons, R. E., & Newman, D. K. (2009). The Continuing Puzzle of the Great Oxidation Event. *Current Biology*, *19*(14), R567–R574.

Shoulders, M. D., & Raines, R. T. (2009). Collagen Structure and Stability. *Annual Review of Biochemistry*, *78*(1), 929–958.

Simon, M. C., Keith, B. (2008). The role of oxygen availability in embryonic development and stem cell function. *Nature Reviews Molecular Cell Biology*, *9*(4), 285–296.

Ślesak, I., Ślesak, H., & Kruk, J. (2012). Oxygen and Hydrogen Peroxide in the Early Evolution of Life on Earth: In silico Comparative Analysis of Biochemical Pathways. *Astrobiology*, *12*(8), 775–784.

Songer, C. J., & Mintzes, J. J. (1994). Understanding cellular respiration: An analysis of conceptual change in college biology. *Journal of Research in Science Teaching*, *31*(6), 621–637.

Sperling, E. A., Halverson, G. P., Knoll, A. H., Macdonald, F. A., & Johnston, D. T. (2013). A basin redox transect at the dawn of animal life. *Earth and Planetary Science Letters*, *371*, 143–155.

Sperling, E. A., Rooney, A. D., Hays, L., Sergeev, V. N., Vorob'eva, N. G., Sergeeva, N. D., Selby, D., Johnston, D. T., & Knoll, A. H. (2014). Redox heterogeneity of subsurface waters in the Mesoproterozoic ocean. *Geobiology*, *12*(5), 373–386.

Sperling, E. A., & Stockey, R. G. (2018). The Temporal and Environmental Context of Early Animal Evolution: Considering All the Ingredients of an "Explosion." *Integrative and Comparative Biology*, *58*(4), 605–622.

Sperling, E. A., Wolock, C. J., Morgan, A. S., Gill, B. C., Kunzmann, M., Halverson, G. P., Macdonald, F. A., Knoll, A. H., & Johnston, D. T. (2015). Statistical analysis of iron geochemical data suggests limited late Proterozoic oxygenation. *Nature*, *523*(7561), 451–454.

Suarez, P. A., & Leys, S. P. (2022). The sponge pump as a morphological character in the fossil record. *Paleobiology*, *48*(3), 1–16.

Sussarellu, R., Fabioux, C., Le Moullac, G., Fleury, E., & Moraga, D. (2010). Transcriptomic response of the Pacific oyster *Crassostrea gigas* to hypoxia. *Marine Genomics*, *3*(3), 133–143.

Tang, D., Shi, X., Wang, X., & Jiang, G. (2016). Extremely low oxygen concentration in mid-Proterozoic shallow seawaters. *Precambrian Research*, *276*, 145–157.

Taylor, A. B., Hu, G., Hart, P. J., & McAlister-Henn, L. (2008). Allosteric Motions in Structures of Yeast NAD+-specific Isocitrate Dehydrogenase. *Journal of Biological Chemistry*, *283*(16), 10872–10880.

Thuesen, E. V, Rutherford, L. D., & Brommer, P. L. (2005). The role of aerobic metabolism and intragel oxygen in hypoxia tolerance of three ctenophores: *Pleurobrachia bachei*, *Bolinopsis infundibulum* and *Mnemiopsis leidyi*. *Journal of the Marine Biological Association of the United Kingdom*, *85*(3), 627–633.

Tostevin, R., & Mills, B. J. W. (2020). Reconciling proxy records and models of Earth's oxygenation during the Neoproterozoic and Palaeozoic. *Interface Focus*, *10*(4), 1–13.

Troch, M., Roelofs, M., Riedel, B., & Grego, M. (2013). Structural and functional responses of harpacticoid copepods to anoxia in the Northern Adriatic: an experimental approach. *Biogeosciences*, *10*(6), 4259–4272.

Turner, E. C. (2021). Possible poriferan body fossils in early Neoproterozoic microbial reefs. *Nature*, *596*(7870), 87–91.

Vazquez, A., Liu, J., Zhou, Y., & Oltvai, Z. N. (2010). Catabolic efficiency of aerobic glycolysis: the Warburg effect revisited. *BMC systems biology*, *4*(1), 1–9.

Von Stockar, U., & Marison, I. W. (1993). The definition of energetic growth efficiencies for aerobic and anaerobic microbial growth and their determination by calorimetry and by other means. *Thermochimica acta*, *229*, 157–172.

Wacey, D. (2009). *Early Life on Earth: A Practical Guide*. Springer Netherlands.

Wacey, D., Kilburn, M. R., Saunders, M., Cliff, J., & Brasier, M. D. (2011). Microfossils of sulphur-metabolizing cells in 3.4-billion-year-old rocks of Western Australia. *Nature Geoscience*, *4*(10), 698–702.

Whelan, N. V., Kocot, K. M., Moroz, L. L., & Halanych, K. M. (2015). Error, signal, and the placement of Ctenophora sister to all other animals. *Proceedings of the National Academy of Sciences*, *112*(18), 5773–5778.

Wood, R., Donoghue, P. C. J., Lenton, T. M., Liu, A. G., & Poulton, S. W. (2020). The origin and rise of complex life: progress requires interdisciplinary integration and hypothesis testing. *Interface Focus*, *10*(4), 1–10.

Wood, R., Liu, A. G., Bowyer, F., Wilby, P. R., Dunn, F. S., Kenchington, C. G., Cuthill, J. F. H., Mitchell, E. G., & Penny, A. (2019). Integrated records of environmental change and evolution challenge the Cambrian Explosion. *Nature Ecology and Evolution*, *3*(4), 528–538.

Yasutake, Y., Watanabe, S., Yao, M., Takada, Y., Fukunaga, N., & Tanaka, I. (2003). Crystal structure of the monomeric isocitrate dehydrogenase in the presence of NADP+: insight into the cofactor recognition, catalysis, and evolution. *Journal of Biological Chemistry*, *278*(38), 36897–36904.

Yin, Z., Zhu, M., Davidson, E. H., Bottjer, D. J., Zhao, F., & Tafforeau, P. (2015). Sponge grade body fossil with cellular resolution dating 60 Myr before the Cambrian. *Proceedings of the National Academy of Sciences*, *112*(12), E1453–E1460.

Zhang, F., Xiao, S., Kendall, B., Romaniello, S. J., Cui, H., Meyer, M., Gilleaudeau, G. J., Kaufman, A. J., & Anbar, A. D. (2018). Extensive marine anoxia during the terminal Ediacaran Period. *Science Advances*, *4*(6), 1–11.

Capítulo 1

O capítulo a seguir foi publicado no periódico *Scientific Reports* e está disponível em: https://doi.org/10.1038/s41598-021-95094-4

Referência: Bezerra, B. S., **Belato, F. A.**, Mello, B., Brown, F., Coates, C. J., de Moraes Leme, J., Trindade, R. I. F., & Costa-Paiva, E. M. (2021). Evolution of a key enzyme of aerobic metabolism reveals Proterozoic functional subunit duplication events and an ancient origin of animals. *Scientific Reports*, *11*(1), 1-11.

Evolution of a key enzyme of aerobic metabolism reveals Proterozoic functional subunit duplication events and an ancient origin of animals

Bruno Santos Bezerra[1], **Flávia Ariany Belato[1]**, Beatriz Mello[2], Federico Brown[1], Christopher J. Coates[3], Juliana de Moraes Leme[4], Ricardo I. F. Trindade[5] & Elisa Maria Costa-Paiva[1,5*]

1.Institute of Biosciences, Department of Zoology, University of Sao Paulo, Brazil

2.Biology Institute, Genetics Department, Federal University of Rio de Janeiro, Brazil

3.Department of Biosciences, Faculty of Science and Engineering, Swansea University, United Kingdom

4.Geoscience Institute, University of Sao Paulo, Brazil

5.Institute of Astronomy, Geophysics and Atmospheric Sciences, University of Sao Paulo, Brazil

Corresponding author: elisam.costapaiva@gmail.com

Abstract

The biological toolkits for aerobic respiration were critical for the rise and diversification of early animals. Aerobic life forms generate ATP through the oxidation of organic molecules in a process known as Krebs' Cycle, where the enzyme isocitrate dehydrogenase (IDH) regulates the cycle's turnover rate. Evolutionary reconstructions and molecular dating of proteins related to oxidative metabolism, such as IDH, can therefore

provide an estimate of when the diversification of major taxa occurred, and their coevolution with the oxidative state of oceans and atmosphere. To establish the evolutionary history and divergence time of NAD-dependent IDH, we examined transcriptomic data from 195 eukaryotes (mostly animals). We demonstrate that two duplication events occurred in the evolutionary history of NAD-IDH, one in the ancestor of eukaryotes approximately at 1,967 Ma, and another at 1,629 Ma, both in the Paleoproterozoic Era. Moreover, NAD-IDH regulatory subunits β and γ are exclusive to metazoans, arising in the Mesoproterozoic. Our results therefore support the concept of an ‘‘earlier-than-Tonian’’ diversification of eukaryotes and the pre-Cryogenian emergence of a metazoan IDH enzyme.

Keywords: aerobic metabolism, gene tree, isocitrate dehydrogenase, eukaryotes, gene duplication, molecular dating

Introduction

All living aerobic organisms need energy for their maintenance and growth – yielding ATP through the oxidation of organic molecules and using oxygen as the terminal electron acceptor (Nelson *et al*., 2013). The Tricarboxylic Acid (TCA) Cycle, also known as the Citric Acid Cycle or Krebs’ Cycle (Nunes-Nesi *et al*., 2013) undertakes sequential oxidation. Considered a molecular furnace, the TCA does not simply play a role in ATP generation through catabolism of macromolecules, but it is inextricably linked to cellular functionality and homeostasis. The TCA (1) plays a unique role as an NAD and NADP coenzyme reducer for ATP production in the respiratory chain, (2) acts as a core metabolic integration point for catabolic processes of different macromolecules including carbohydrates, lipids, and proteins, and (3) produces intermediate

components of anabolic processes, e.g., citrate that is used for lipogenesis (Nelson *et al*., 2013; Nunes-Nesi *et al*., 2013). The turnover of the TCA cycle and the accumulation of citrate is influenced by the enzyme isocitrate dehydrogenase (IDH), which catalyzes the often-irreversible oxidation decarboxylation of isocitrate to alpha-ketoglutarate (and CO2), concurrent to coenzyme (NAD+, NADP) reduction (Nelson *et al*., 2013).

Across the evolution of life, IDH regulation became more complex and the proteins diversified in terms of subunit number, size, or coenzyme binding (Taylor *et al*., 2008). The TCA cycle in eukaryotes uses the hetero-oligomeric NAD-IDH that exclusively locates into the mitochondrial matrix, whereas prokaryotes use mostly the homodimeric enzyme NADP-IDH (Hurley *et al*., 1989). Eukaryotes also have homodimeric NADP-IDHs that do not function in the TCA cycle, but aid lipid metabolism and counter oxidative damage in the cytosol and mitochondria (Sun *et al*., 2019). Overall, eukaryotic NAD-IDH and NADP-IDH show more complex allosteric regulation processes than the prokaryotic phosphorylation-mediated regulation of NADP-IDH (Martínez-Rivas & Vega, 1998; Mailloux *et al*., 2007; Taylor *et al*., 2008; Sun *et al*., 2019). Such differences in the eukaryotic and prokaryotic NADP-IDH allostery seem to have originated from two different mutation events in the NAD-dependent ancestor (Dean & Golding, 1997). Eukaryotic NADP-IDHs regulate their activity by substrate induced conformational changes in the allosteric site in the presence of the substrate (Mailloux *et al*., 2007; Sun *et al*., 2019). Conversely, prokaryotic NADP-IDHs loose activity when phosphate groups are added to specific serine residues in the presence of acetate, alpha-ketoglutarate, and NADPH (Hurley *et al*., 1989). Generally, the eukaryotic IDHs have more complex regulation processes than single-step phosphorylation/de-phosphorylation switches (Taylor *et al*., 2008).

Among lineages, we find distinct numbers of IDH subunits that have evolved to act as heteromeric protein assemblies. Fungal and green algal IDHs are formed by two different subunits: IDH1 associated with allosteric regulation of the enzyme, and IDH2 responsible for substrate catalysis (Cupp & McAlister-Henn, 1991; Martínez-Rivas & Vega, 1998). IDH1 is also the name used for the cytosolic NADP-isocitrate dehydrogenase, whereas IDH2 is used for mitochondrial NADP-IDH (widely studied in humans). In the present study, we refer to IDH1 and IDH2 as the two subunits of the fungal NAD-dependent IDH. Metazoans, a lineage of opisthokonts (taxon composed by holozoans, including animals and fungi), present an exclusively octameric IDH with three different subunits: α, β and γ in a stoichiometric ratio 2:1:1 (Ramachandran & Colman, 1980). The α subunit from mammals is structurally similar to the fungal IDH2 subunit, indicating that it has a catalytic function, whereas the β and γ subunits resemble the structure of the fungal IDH1 subunit, which serves as evidence of its regulatory function (Kim *et al*., 1995; Nichols *et al*., 1995).

Regarding animals, the need for oxygen is almost exclusively associated with aerobic respiration. Previous investigators have suggested a causal link between the diversification of animals and the rise of atmospheric dioxygen levels in the late Neoproterozoic (1.000–541 Ma) (Nursal, 1959; Canfield *et al*., 2007). In fact, recent studies suggest that the earliest animals were likely small, soft-bodied, and collagen-poor – evolving under low oxygen levels that restricted their use of oxygen to high-priority physiological functions (Mills & Canfield, 2014; Mills *et al*., 2014), including basal cellular aerobic respiration. Moreover, much of the molecular toolkit required for animal development originated deep in eukaryote evolutionary history during low oxygen periods (Sebé-Pedrós *et al*., 2011).

The evolutionary history of animals could be traced by considering single and multicellular eukaryotes as well as animal phylogenies, and the divergence times among their major lineages. Even for the metazoan lineage, which is one of the best-studied eukaryotic lineages, a consensus does not exist regarding its basal relationships (e.g., ctenophore vs porifera controversy). Moreover, reconstructions of the last common ancestor for animals are contentious (Pisani *et al*., 2015; Whelan *et al*., 2015; Giribet, 2016; Halanych, 2016), partly because early putative animal fossil records are problematic (Budd & Jensen, 2000; Budd, 2008). While molecular dating for crown Metazoa range between 1,298 - 615 Ma, the earliest metazoan fossils date to the late Ediacaran ~580 Ma (Hedges *et al*., 2004; Peterson *et al*., 2004; dos Reis *et al*., 2015). Fossils older than 600 Ma remain controversial and are limited to a few small sponges (Brain *et al*., 2012; Antcliffe *et al*., 2014; Cordani *et al*., 2020). Regarding eukaryotes, molecular clock estimates for their last common ancestor span ~1 billion years (Berney & Pawlowski, 2006; Chernikova *et al*., 2011; Parfrey *et al*., 2011. Eme *et al*., 2014). Some differences can be attributed to the use of the fossil Bangiomorpha pubescens – a presumed bangiophyte red alga – as a calibration point. Time estimates obtained without employing B. pubescens as a calibration point are 200–300 Ma younger than those that do (Porter, 2020). Recently, the development of refined molecular clock methodologies has helped to reduce the disparities among molecular dating and the fossil evidence used to estimate clade age minima (dos Reis *et al*., 2015; Dohrmann & Wörheide, 2017).

To elucidate the evolutionary processes that led to the diversification of major taxa during the geological history of the Earth, molecular estimates of divergence times are now used as a standard technique to infer chronograms (Mello, 2018) and have improved dramatically in recent years for deep time studies (Misof *et al*., 2014;

Irisarri *et al*., 2017; Delsuc *et al*., 2018; Wolfe *et al*., 2019). The method consists of estimating the age of internal nodes based on the rates of nucleotide or amino acid substitutions among lineage sequences (Mello, 2018). Understanding species phylogeny is a prerequisite for studying protein function and adaptations at the molecular level. In fact, the proteins of an organism share the same phylogenetic history, and changes in protein sequences can be used to date the origin of various physiological adaptations (Burmester, 2002). Therefore, molecular dating of specific genes can provide new insights into well-established topics, such as the diversification of eukaryotes and animals (dos Reis *et al*., 2015; Zhang *et al*., 2019). Although most deep time studies use hundreds of genes in order to estimate divergence times of species lineages (dos Reis *et al*., 2015; Dohrmann & Wörheide, 2017), molecular dating of particular proteins can recover the evolutionary history of these proteins against a background of the evolution of major taxa that are intrinsically linked to these proteins. Molecular dating of deep divergences may be challenging, mostly because of issues such as sequence saturation, which can affect analyses by biasing the estimated genetic distances (Wilke *et al*., 2009; Schwartz & Mueller, 2010; Zheng *et al*., 2011; Magallón *et al*., 2013). However, estimated divergence times based on amino acid sequences that are more conserved compared to nucleotides sequences can alleviate the problem of saturation.

Because animals depend on the oxidation of organic molecules for cellular respiration, the evolution of proteins related to oxidative metabolism can allow us to trace their emergence time (Decker & van Holde, 2011). The crucial role of NAD-IDH for cellular respiration and Krebs' Cycle (Mailloux *et al*., 2007) makes its evolutionary history a compelling source of information to study the evolution of early animals and eukaryotes. Previous works have presented the phylogenetic relationships of the IDH protein family in Prokaryotes and Eukaryotes

(Dean & Golding, 1997), however the evolutionary history of NAD-IDHs in animals, as well as molecular dating estimates of protein divergence, are still unclear. Previously, authors described lineage-specific duplication events that gave rise to three IDH subunits (α, β and γ) in metazoans only (Ramachandran & Colman, 1980), and these events can be used to estimate the time of animal diversification (dos Reis *et al*., 2015). We present the evolutionary history of eukaryotic NAD-IDHs and molecular dating estimates for the emergence of animal IDH and subsequent duplication events.

Methods

Sequence retrieval. The dataset consisted of 195 protein sequences obtained from the National Centre for Biotechnological Information (NCBI) database (Supplementary Table S1; Supplementary Figure S2). Considering that the accuracy of a phylogeny protocol is strongly dependent on the taxonomic sampling, number of sequences and the sequence length, we bolstered our dataset by searching for as many sequences from all metazoan phyla available at NCBI. Sequences functionally annotated as "isocitrate dehydrogenase" in the protein database were retrieved with the following criteria used to filter the appropriate sequences: 1) for taxa with more than 15 sequences available in NCBI, those sequences that were denoted as "Putative", "Hypothetical", "Low-quality", and "partial" were removed; 2) sequences with fewer than 350 amino acid residues were also removed. To confirm the protein domain identity of the sequences, a local search using HMMER 3.3 was performed using the Pfam database with an e-value cutoff of $1e^{-5}$ (Potter *et al*., 2018). Sequences remaining after those validation steps were incorporated into the final dataset for analysis.

Alignments and phylogenetic reconstructions. In order to infer homology between the sequences, we aligned the dataset using MAFFT software (Katoh & Standley, 2013) with the accurate algorithm "G-INS-i". To obtain a biologically correct alignment, we performed a visual inspection and a manual curation to remove spuriously aligned sequences, based on similarity to the protein alignment as a whole. In order to eliminate poorly aligned regions, the alignment was trimmed using the software trimAl (Capella-Gutierrez *et al*., 2009) with a 75% gap threshold. To eliminate redundancy from the dataset, sequences with 100% similarity to each other after trimming were removed. The resulted alignment was used for downstream analysis.

Phylogenetic reconstructions rely on the assumption of empirical models of substitution and are therefore dependent on the correct choice of those models. Thus, the best-fit model of protein evolution for the dataset was selected using ModelFinder, implemented in the IQ-TREE software (Kalyaanamoorthy *et al*., 2017), which uses Akaike and Bayesian Information Criteria methods. IQ-TREE was also used to perform a maximum likelihood inference (Nguyen *et al*., 2015). The branch supports and the robustness of the analyses were obtained by using an ultrafast bootstrap approximation with 1,000 replicates (Hoang *et al*., 2018). Moreover, we also performed Bayesian inference with MrBayes 3.2.1 (Ronquist & Huelsenbeck, 2003) using two independent runs, each with four Metropolis-coupled chains for 107 generations, sampling from the posterior distribution every 500 generations. To confirm whether chains achieved stationary and to determine an appropriate burn-in, we evaluated trace plots of all MrBayes parameter outputs in Tracer v1.6 (Rambaut *et al*., 2014). The first 25% of samples were discarded as burn-in and a majority rule consensus tree was generated. The software FigTree 1.4.3 (Rambaut, 2007) was used to summarize and root the resulting

phylogenetic trees using two sequences of isocitrate dehydrogenase from bacteria as an outgroup. Because of the evolutionary depth of our dataset, the phylogenetic reconstruction was also performed with a mixture model, which alleviates the issues related to saturation and long branch attraction by accommodating site-specific features of protein evolution (Lartillot & Philippe, 2004; Lartillot *et al*., 2007). This was done in PhyloBayes (Lartillot & Philippe, 2004) by using the CAT-GTR model with a gamma distribution (Γ4) of site-rate heterogeneity and multiple chains to check for convergence.

Divergence time estimates were obtained using the software BEAST 2.4.7 (Bouckaert *et al*., 2014) with the uncorrelated lognormal relaxed clock (Drummond *et al*., 2006) using the LG substitution model (Whelan & Goldman, 2001), and a birth-death tree prior with default settings. To calibrate divergence times, only speciation nodes were considered because calibration information derived from fossil data provides information regarding the split times between biological lineages (i.e., speciation events). Therefore, divergences classified as speciation nodes that reflected robust biological clades and were free of duplication events were chosen for calibration. These were the crown nodes of Pancrustacea and Gnathostomata. For both taxa, the aforementioned requirements were met three times (i.e., speciation nodes that included only Pancrustacea or Gnathostomata NAD-IDH sequences were recovered three times in the estimated phylogeny). Because of that, six speciation nodes were calibrated with uniform distributions with lower and upper boundaries based on estimates from Benton *et al*. (2015) and dos Reis *et al*. (2015). We used time ranges of 514–531.22 Ma and 420.7 to 468.4 Ma to calibrate the tMRCA (time to the Most Recent Common Ancestor) of pancrustaceans and gnathostomes, respectively. Our calibration points were determined using coherent criteria according to Parham et al. (2012).

It is worth mentioning that calibrated nodes were constrained to monophyletic, while other phylogenetic relationships were estimated in BEAST. MCMC (Markov Chain Monte Carlo) models were run for 200 million generations with a sampling frequency of 10,000 and a discarded burn-in period of 10% (20 million generations). To access convergence of chains, two independent MCMC runs were performed. In both runs, effective sample size values were higher than 200 after discarding the burn-in period. We also estimated divergence times in PhyloBayes by using the UGAM relaxed clock model and the phylogeny estimated previously in PhyloBayes by running multiple chains to check for convergence. To reduce computational burden, the CAT-Poisson mixture model was used with a gamma distribution (Γ4) of site-rate heterogeneity. As in BEAST, calibrations were provided as uniform distributions. Because PhyloBayes requires a root calibration, we used a loose gamma distribution (mean = 1520, SD = 240) to calibrate the divergence between Euglenozoa and the remaining eukaryotes, which was based on estimated times retrieved from the TimeTree database (Kumar *et al*., 2017).

Results

Evolutionary history. Our final empirical dataset comprised 193 IDH sequences from eukaryotes and two IDH sequences from bacteria, used here as the outgroup (Supplementary Table S1; Supplementary Figure S2). Following alignment and trimming, the dataset included 353 residues (alignment file available at 10.6084/m9.figshare.13158116). Bayesian inference and maximum likelihood analyses recovered the same topology for the main eukaryotic lineages with high support values, and also poorly resolved nodes that are often observed in gene genealogies (DeSalle, 2015; Figure 1; IQ-tree tree file available at 10.6084/m9.figshare.13158101 and MrBayes tree file available at 10.6084/m9.figshare.13158110).

Phylogenetic reconstruction performed with a mixture model, presented high concordance with Bayesian and maximum likelihood phylogenies based on regular substitution models (PhyloBayes tree file available at 10.6084/m9.figshare.14633157). In order to check if our heterogeneous taxonomic ensemble could bias the phylogenetic reconstructions, we tested the effect of taxonomic sampling by running a maximum likelihood analysis with only one representative for each taxon per subunit. The topology recovered was congruent with those obtained for our complete dataset.

Gene genealogy clearly evidenced multiple duplication events of eukaryotic NAD-IDH subunits that resulted in the three metazoan subunits, α, β and γ. IDHα was already present in the ancestor of metazoans, whereas IDHβ and IDHγ duplicated and diverged within the metazoan lineage (arrows, Figure 1). IDHβ+IDHγ were sister groups to an unnamed IDH group – including Fungi, Capsaspora, and Choanoflagellate IDHs – forming a monophyletic opisthokonta clade. The opisthokonta IDHs showed a sister group relationship to another ciliate specific IDH that comprises the molecule in animals and the two subunits present in other opisthokonts (Figure 1). This ciliate specific IDH likely originated from an earlier duplication event that pre-dated the opisthokonta ancestor.

The topology of the NAD-IDH gene tree corroborated the consensus of recent phylogenomic studies of Eukarya (Adl *et al*., 2019; Burki *et al*., 2020). We found two highly supported clades (PP. =1; BP = 100%): one comprised exclusively of IDH sequences from euglenozoans (Discoba) and the second contained all remaining sequences. The latter clade was formed by two sister-groups and displayed the first duplication event present in the eukaryotic NAD-IDH evolutionary history. These two well-supported clades were clade I containing catalytic subunits IDH2 and animal subunit α (Figure 1; pink clade; PP = 1; BP = 100%) and clade II

containing regulatory subunits IDH1 and animal subunits β + γ (Figure 1; blue and green clades; PP > 0.9; BP > 95%).

The clade containing the catalytic NAD-IDH subunits (Figure 1; pink clade) revealed the divergence between a clade comprising the ciliate IDH sequences (Figure 1; PP. = 1; BP = 100%) and another composed of Amorphea (Opisthokonta + Amoebozoa) IDH sequences (Figure 1; PP. > 0,5; BP > 80%). The latter is further divided into two sister-groups: amoebozoans (Figure 1; PP. = 1; BP = 100%) and opisthokonts IDHs (Figure 1; PP = 1; BP = 100%). The opisthokont clade is further subdivided into a single IDH2 fungal sequence and a holozoan clade (Figure 1; PP = 1; BP = 100%). In the holozoan clade, we found two IDH sequences, one from a Capsaspora species and one from a choanoflagellate species, which was the sister clade to the metazoans (Figure 1; PP = 1; BP = 100%). The genealogy of the catalytic subunit(s) recapitulated the recent phylogenetic relationships recovered for these organisms, suggesting a common evolutionary history of the gene and the events of lineage divergence in the opisthokonts.

Clade II – composed of the regulatory subunits – showed evidence for a second eukaryotic gene duplication event that gave rise to animal subunits β and γ (Figure 1; blue and green clades; PP = 1.0; BP =100%). Prior to this duplication event, another separation of two gene lineages occurred: one formed by a ciliate specific gene clade, and another formed by IDH1 genes of choanoflagellates, capsasporans, and fungi (Figure 1; PP > 0,9; BP > 80%). The second duplication event in the clade was associated exclusively with metazoan IDH sequences (Figure 1; blue and green clades; PP > 0,9; BP > 95%). All metazoan lineages used in this study were represented in both the β subunit (Figure 1; blue clade; PP > 0.9; BP > 95%) and γ subunit (Figure 1; green clade; PP = 1,0; BP = 100%) clades.

Molecular dating. The topology estimated by BEAST differed from the maximum-likelihood and Bayesian inferences. For instance, the euglenozoans NAD-IDH sequences formed a monophyletic clade within the catalytic subunit clade and only after the first eukaryotic duplication event. Moreover, a significant difference was observed in the position of choanoflagellate sequences in relation to animal subunits β and γ. In our former analysis (Figure 1), IDH1 sequences of choanoflagellate, capsasporans, and fungi were the sister-group to animal subunits β and γ, prior to the second duplication event. In contrast, the BEAST analyses showed that the single choanoflagellate gene sequence appeared as a sister-group to animal subunit γ. With the exception of very deep divergences, node ages and credibility intervals estimated based on a mixture model in PhyloBayes generally matched the ones inferred by BEAST for the major clades (Supplementary Figure S3 and PhyloBayes timescale file available at 10.6084/m9.figshare.14633271). Because of this, we centered our results and discussion around BEAST timescale.

The age estimated for the first duplication event of eukaryotic NAD-IDH giving rise to catalytic subunits (IDH2 and α) and regulatory subunits (IDH1, β and γ) was approximately 1,967 Ma (1,641–2,329 Ma) in the Paleoproterozoic (Figure 2). Regarding the catalytic subunit, the split between the euglenozoan subunit and other eukaryotes occurred at ~1,494 Ma (1,186–1,838 Ma). The split of amoebozoan subunits and opisthokont catalytic subunit was dated at ~1,224 Ma (1,016–1,447 Ma), whereas amoebozoan catalytic NAD-IDH was dated at ~816 Ma (538–1,120 Ma) (Figure 2). The estimated divergence date between choanoflagellates and capsasporan NAD-IDH and animal α NAD-IDH occurred at approximately 943 Ma (807–1,089 Ma). Finally, the emergence of subunit α for animal NAD-IDH was dated at ~866 Ma (753–991 Ma), in the Neoproterozoic (Figure 2).

The gene lineage that gave rise to eukaryotic regulatory subunits IDH1 and metazoan regulatory subunits β and γ diverged at approximately 1,747 Ma (1,431–2,023 Ma), before the second eukaryotic gene duplication event. This divergence gave rise to a fungal and capsasporan IDH1 clade dated at ~1,254 Ma (854–1,651 Ma) and a metazoan IDHβ + IDHγ clade dated ~1,629 Ma (1,334–1,884 Ma). The latter clade, composed of metazoan subunits β and γ, located the second gene duplication event. The origin of subunit β was estimated at ~1,249 Ma (1,020–1,490 Ma), while the subunit γ was dated at ~1,531 Ma (1,221–1,769 Ma). Although the subunit β is exclusive to animals, this analysis recovered a choanoflagellate IDH sequence as a sister group to animal subunit γ. Thus, the estimated age for the origin of animal subunit γ (without considering the choanoflagellate IDH sequence) was approximately 1,319 Ma (1,100–1,558 Ma; Figure 2).

Discussion

We interrogated the emergence of metazoan NAD-IDH lineages in an attempt to resolve the relationships and evolutionary history of this protein among eukaryotic NAD-IDHs. Our results demonstrate that two gene duplication events occurred in the evolutionary history of NAD-IDH, one in the ancestor of eukaryotes approximately at ~1,967 Ma, and another at ~1,629 Ma (both in the Paleoproterozoic Era). Additionally, we reveal that NAD-IDH regulatory subunits β and γ are exclusive to metazoans and arose in the Mesoproterozoic. Previous studies have investigated the relationships between IDHs, focusing on NAD-IDH and NADP-IDH types (Dean & Golding, 1997; Wang et al., 2015). Although the first members of NAD-IDHs were likely to be present in the eukaryotic ancestor, the quaternary structure of these enzymes remain unresolved. Early IDHs may have functioned as a homodimer as observed in living prokaryotes (Hurley

et al., 1989), an octameric structure as observed in extant eukaryotes (Taylor *et al*., 2008), or as intermediate heterodimers. Previous evolutionary analyses indicated eubacterial IDHs first evolved from an NAD-dependent precursor about 3.5 Ga (Dean & Golding, 1997). In the evolutionary history of this protein, our findings suggest that there was a tendency to increase regulatory complexity in eukaryotes, which concurs with other studies (Taylor *et al*., 2008) (Figure 3). In bacteria, the regulation of IDH is achieved by simple phosphorylation events (Hurley *et al*., 1989), whereas eukaryotic IDHs contain at least two different subunits that show allosteric regulation by distinct factors (Taylor *et al*., 2008). Animals are the only eukaryotic group with three different subunits; more binding motifs that can trigger protein activity have been identified (e.g., ATP and Ca2+) (Nichols *et al*., 1993; Qi *et al*., 2008).

The ancestor of eukaryotic NAD-IDH arose ~1,967 Ma (1,641–2,329 Ma) in the Paleoproterozoic. At that time, Earth was colonized mainly by microbial lifeforms, and representative species of only a few microbial clades are preserved in the fossil record. Moreover, the interpretation of these early eukaryote fossils is challenging because their key distinguishing characteristics, such as organelles and nuclei, do not preserve well (Wood *et al*., 2020). Our findings for the emergence of eukaryotic NAD-IDH during the Paleoproterozoic is in agreement with contemporary molecular clock estimates for eukaryotes emergence (Parfrey *et al*., 2011; Eme *et al*., 2014) and for the canonical view that stem and crown-group eukaryotes may have emerged early in the Proterozoic, keeping low diversity levels in restricted environments until a late Mesoproterozoic diversification (Brocks, 2018; Jarrett *et al*., 2019; Nguyen *et al*., 2019). Previous studies suggested that the last common eukaryotic ancestor lived between 1,866–1,679 Ma (Parfrey *et al*., 2011; Betts *et al*., 2018), which is consistent with the earliest unambiguous

microfossils interpreted as eukaryotic microfossils found in latest Paleoproterozoic rocks (ca. 1,650 Ma; Javaux *et al*., 2003; Knoll, 2014; Miao *et al*., 2019). Additionally, the early development of the eukaryotic molecular toolkit originating from a stem–line of descent – a propagating series of pluripotent cellular entities – at approximately 2,000 Ma continues to gather support in the literature (Caetano-Anollés *et al*., 2014). Using molecular clock estimates of protein folds, the emergence of eukaryotes in the Paleoproterozoic is also corroborated (Wang *et al*., 2011; Caetano-Anollés, 2017). Nevertheless, recent evidence suggest a late Mesoproterozoic origin of the eukaryotic crown group based mainly on eukaryotic sterols, which are presumed to have been present in the eukaryotic crown-ancestor and is absent from rock records until the early Neoproterozoic (Porter, 2020). Although our results may support a deep Paleoproterozoic origin of eukaryotes with a late Mesoproterozoic origin of the crown group, they do not support a late emergence of aerobic respiration (ca. 800 Ma as suggested by Porter, 2020).

The catalytic NAD-IDH subunit arose ca. 1,967 Ma in the Paleoproterozoic as a result of the first gene duplication event in eukaryotes. This duplication event generated two NAD-IDHs, a subunit with catalytic function and another with regulatory function. According to our results, animal catalytic subunit α is closer to the fungal catalytic IDH2 sequences than to the other metazoan subunits β and γ, suggesting an orthologous relationship among animal α and fungal IDH2 (Kim *et al*., 1995; Nichols *et al*., 1995). The emergence of the opisthokont NAD-IDH catalytic subunit during the Mesoproterozoic (ca. 1,224 Ma) corroborates recent paleontological studies from rocks dated at 1,700–800 Ma and suggests a higher eukaryotic diversity during this earlier interval than previously known (Baludikay *et al*., 2016; Agić *et al*., 2017; Beghin *et al*., 2017; Loron *et al*., 2019). The emergence of the amoebozoan NAD-IDH

catalytic subunit was estimated to have occurred as recently as ~816 Ma in the Neoproterozoic, i.e., almost 700 Ma later than previous molecular dating estimates (Parfrey *et al*., 2011). Amoebozoa is the eukaryotic supergroup sister to Obazoa, the group containing animals, fungi, and several microbial eukaryotic lineages (Figure 3 – Kang *et al*., 2017; Lahr *et al*., 2019).

The emergence of the NAD-IDH regulatory subunit was dated at ~1,747 Ma, giving rise to two distinct gene lineages: a fungi + capsasporan NAD-IDH and a metazoan NAD-IDH β + γ. The emergence of the fungi/capsasporan NAD-IDH regulatory subunit occurred in the Mesoproterozoic and was dated at ~1,254 Ma, corroborating previous estimates for the last common ancestor of extant Opisthokonta from 1,389–1,240 Ma (Parfrey *et al*., 2011). The regulatory subunit IDH1 in fungi is closely related to subunits β and γ in animals, indicating that a second duplication event occurred. This result corroborates a previously identified physiochemical properties between fungi and mammalian NAD-IDH sequences, such as, comparable molecular weights of subunits and active site architecture (Nichols *et al*., 1993, 1995).

The NAD-IDH regulatory subunit originated from a gene duplication event in the Paleoproterozoic (ca. 1,967 Ma). However, the emergence of the lineage that gave rise to metazoan subunits β + γ occurred later in the Mesoproterozoic (ca. 1,629 Ma). Dates of emergence of animal-specific NAD-IDH subunit β (~1,249 Ma) and NAD-IDH subunit γ (~1,532 Ma) provide support for an earlier emergence of metazoans compared to previous estimates that date their origin to ~800 Ma (Mills *et al*., 2018; Sperling & Stockey, 2018). If animal divergence began in the Mesoproterozoic or even later in the Neoproterozoic, as suggested by recent molecular estimates (Cartwright & Collins, 2007; dos Reis *et al*., 2015; Dohrmann & Wörheide, 2017), hypoxic conditions should have

prevailed in most environmental settings for more than half of animal evolutionary history (Hammarlund, 2020). An alternative scenario could be the existence of oxygenic niches present at the microscale since the rise of oxidative photosynthesis about 3.0 Ga (Crowe *et al*., 2013; Hammarlund, 2020). In spite of the strong debate surrounding those conditions (Planavsky *et al*., 2016; Zhang *et al*., 2016; Diamond *et al*., 2018; Zhang *et al*., 2019), the fact is that hypoxic niches may have prevailed for most of Earth's history. Thus, a long-lasting hypoxic period of animal evolution may have resulted in particular adaptations to meet the metabolic demands of oxygen, which could explain an evolutionary trend towards an increase of complexity in the NAD-IDH molecule. Beyond IDHs, tracing the presence/absence and evolutionary history of oxygen reductases (e.g., complex IV and cytochrome bd) would offer further insight into the prototypical pathways of aerobic metabolism in early metazoans when oxygen availability was a limiting factor.

Overall, our results support the hypothesis of an ''earlier-than-Tonian'' diversification of eukaryotes, as well as a pre-Cryogenian emergence of metazoans under low-oxygen conditions. This implies there has been an evolutionary trend towards increasing complexity in the regulatory subunit of animal NAD-IDH, which includes a complex of three subunits (one catalytic and two regulatory subunits). Our study also highlights the importance of molecular dating estimates of protein families for enhancing our understanding of evolution in deep time.

Data Availability

The datasets generated and analyzed during the current study are available in the FigShare repository. IQ-tree tree file available at 10.6084/m9.figshare.13158101, MrBayes tree file available at 10.6084/m9.figshare.13158110 and alignment file available at

10.6084/m9.figshare.13158116. PhyloBayes tree file available at 10.6084/m9.figshare.14633157 and PhyloBayes timescale file available at 10.6084/m9.figshare.14633271.

Acknowledgments

The study was supported by FAPESP, by thematic project (Proc. 2016/06114-6), coordinated by R.I.T. A fellowship to E.M.C-P. was provided by FAPESP (Fundação de Amparo à Pesquisa do Estado de São Paulo, Brazil – 2018/20268–1). F.A.B. was supported by CNPq and FAPESP (Proc. 2019/18051-7). C.J.C.'s contributions are facilitated by start-up funds from the College of Science, Swansea University.

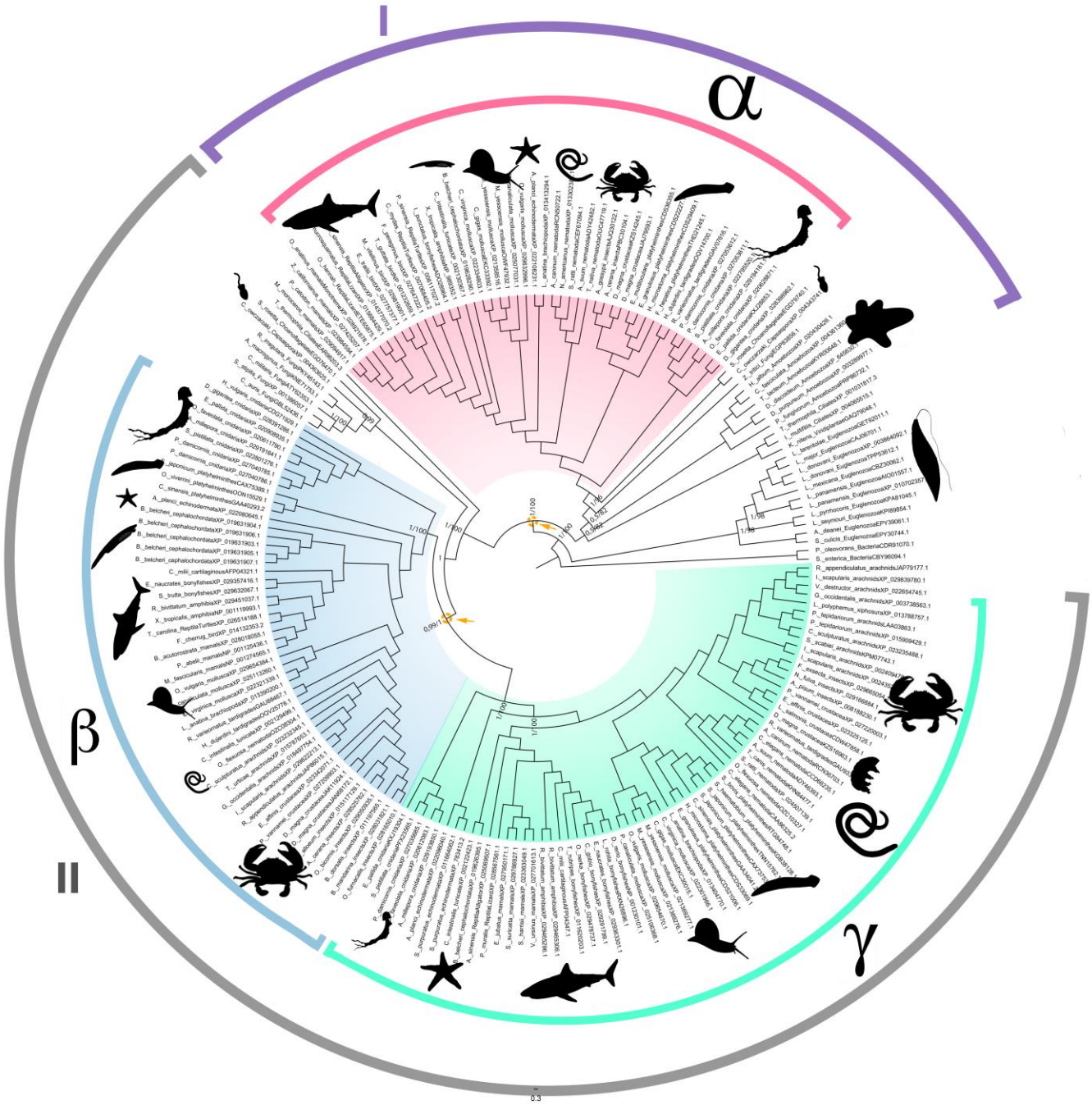

Figure 1 - NAD-isocitrate dehydrogenase gene tree rooted with two bacterial sequences. Clade I is composed of eukaryotic catalytic subunits, and Clade II consists of eukaryotic regulatory subunits. The pink clade refers to metazoan catalytic subunit α, the blue clade refers to metazoan regulatory subunit β, and the green clade is the metazoan regulatory subunit γ. Arrows indicate gene duplication events that led to the evolution of NAD-IDH functional subunits. The number after the taxon name indicates the genetic identifier (GenBank) for each gene. Posterior probabilities and bootstrap support values are indicated for discussed nodes (PP/BP).

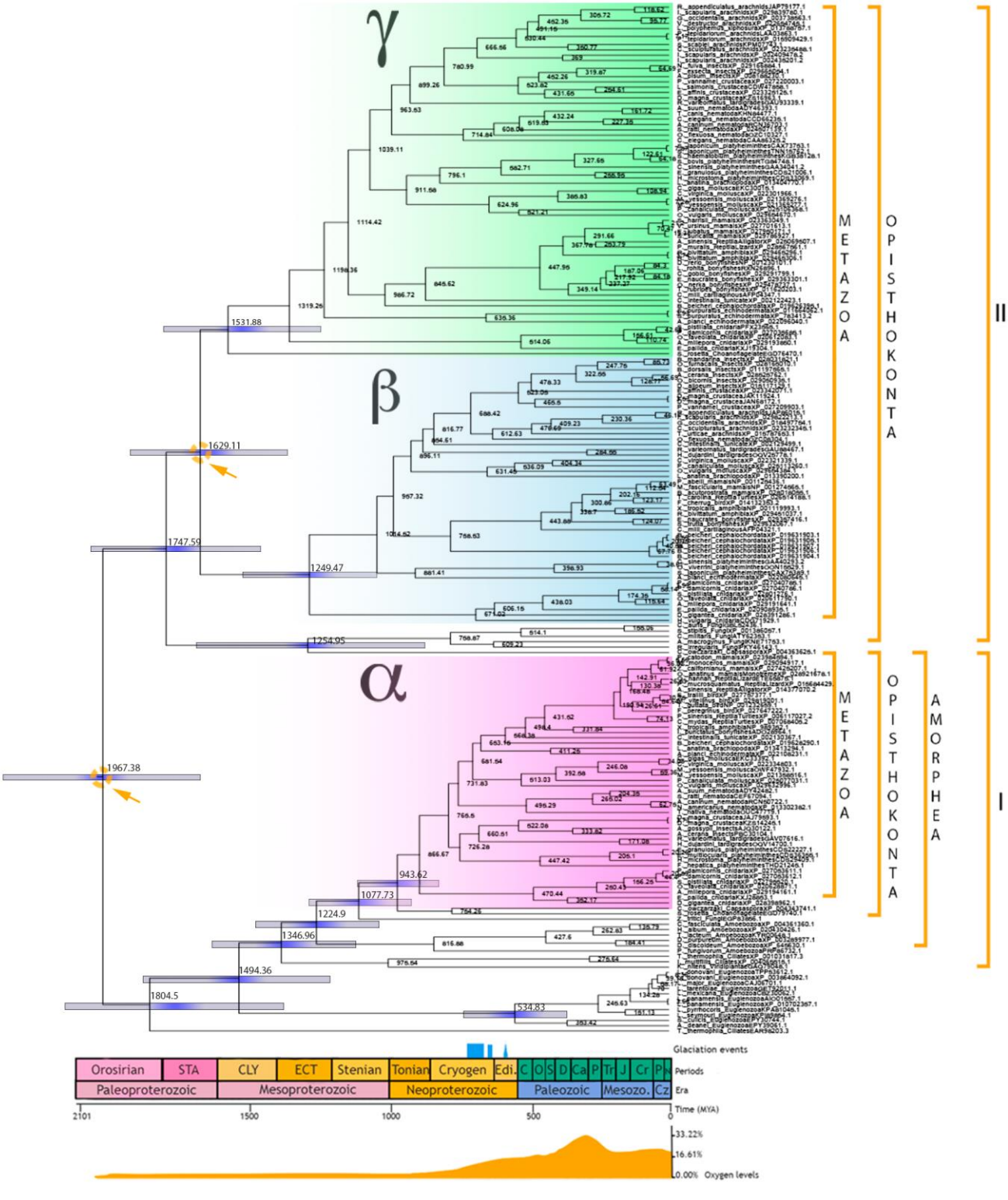

Figure 2 - Timetree of NAD-isocitrate dehydrogenases. Clades I and II contain eukaryotic catalytic and regulatory subunits, respectively. The pink clade refers to metazoan catalytic subunit α, the blue clade refers to metazoan regulatory subunit β, and the green clade is the metazoan regulatory subunit γ. Node ages are plotted and node bars are displaying 95% HDP. STA, Statherian; CLY, Calymmian; ECT, Ectasian; Ediac, Ediacaran; C, Cambrian; O, Ordovician; S, Silurian; D, Devonian; Carb, Carboniferous, P, Permian; Tr, Triassic; J, Jurassic; K, Cretaceous; Pg, Paleogene; Ng, Neogene; Cz, Cenozoic; Ma, Million years ago. Glaciation events and atmospheric oxygen level estimates are indicated. The number after the taxon name indicates the genetic identifier (GenBank) for each gene.

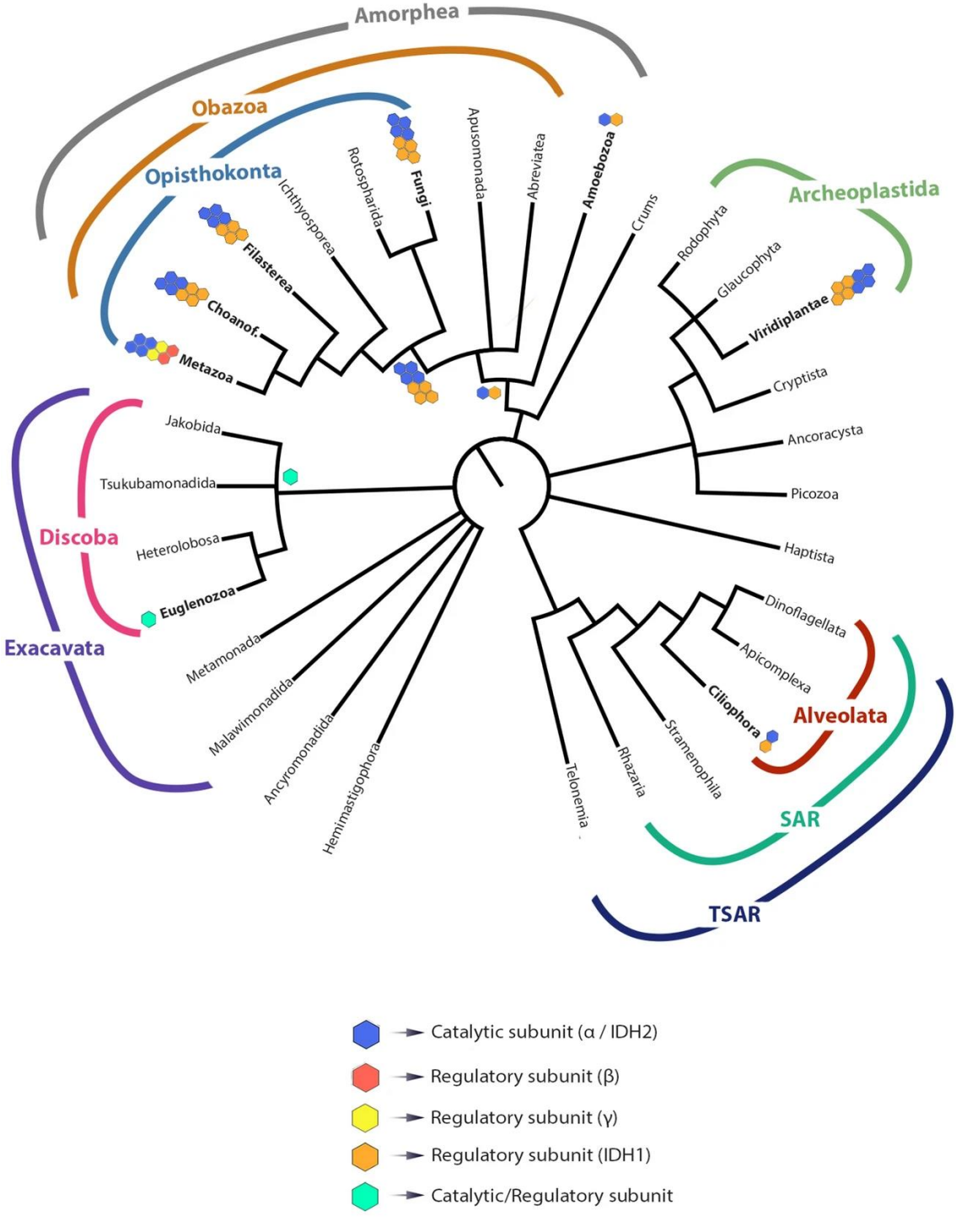

Figure 3 - Hypothesized relationships among eukaryotes derived from recent phylogenomic studies [32, 49, 50]. Names in bold represent analyzed taxa. Colored hexagons represent NAD-IDH subunits: (A) Blue hexagons represent catalytic subunit α or IDH1; (B) Red hexagons represent metazoan regulatory subunit β; (C) Yellow hexagons represent metazoan regulatory subunit γ; (D) Orange hexagons represent eukaryotic regulatory subunit IDH1; and (E) Green hexagons represent the euglenozoan catalytic/regulatory subunit. The way the hexagons are organized represent the quaternary protein structure: octamers in fungi, filasterean, choanoflagellates, metazoans, and viridiplants or unknow in ciliates, amoebozoans, and euglenozoans. Question marks indicate absence of information about function and/or structure.

References

Adl, S. M., Bass, D., Lane, C. E., Lukeš, J., Schoch, C. L., Smirnov, A., Agatha, S., Berney, C., Brown, M. W., Burki, F., Cárdenas, P., Čepička, I., Chistyakova, L., del Campo, J., Dunthorn, M., Edvardsen, B., Eglit, Y., Guillou, L., Hampl, V., Heiss, A. A., Hoppenrath, M., James, T. Y., Karnkowska, A., Karpov, S., Kim, E., Kolisko, M., Kudryavtsev, A., Lahr, D. J. G., Lara, E., Le Gall, L., Lynn, D. H., Mann, D. G., Massana, R., Mitchell, E. A. D., Morrow, C., Park, J. S., Pawlowski, J., W., Powell, M. J., Richter, D. J., Rueckert, S., Shadwick, L., Shimano, S., Spiegel, F. W., Torruella, G., Youssef, N., Zlatogursky, V., & Zhang, Q. (2019). Revisions to the classification, nomenclature, and diversity of eukaryotes. *Journal of Eukaryotic Microbiology*, *66*(1), 4–119.

Agić, H., Moczydłowska, M., & Yin, L. (2017). Diversity of organic–walled microfossils from the early Mesoproterozoic Ruyang Group, North China Craton–A window into the early eukaryote evolution. *Precambrian Research*, *297*, 101–130.

Antcliffe, J. B., Callow, R. H., & Brasier, M. D. (2014). Giving the early fossil record of sponges a squeeze. *Biological Reviews*, *89*(4), 972–1004.

Baludikay, B. K., Storme, J. Y., François, C., Baudet, D., & Javaux, E. J. (2016). A diverse and exquisitely preserved organic–walled microfossil assemblage from the Meso–Neoproterozoic Mbuji–Mayi Supergroup (Democratic Republic of Congo) and implications for Proterozoic biostratigraphy. *Precambrian research*, *281*, 166–184.

Beghin, J., Storme, J. Y., Blanpied, C., Gueneli, N., Brocks, J. J., Poulton, S. W., & Javaux, E. J. (2017). Microfossils from the late mesoproterozoic–early neoproterozoic atar/el Mreïti group, Taoudeni basin, Mauritania, northwestern Africa. *Precambrian research*, *291*, 63–82.

Benton, M. J., Donoghue, P. C., Asher, R. J., Friedman, M., Near, T. J., & Vinther, J. (2015). Constraints on the timescale of animal evolutionary history. *Palaeontologia Electronica*, *18*(1), 1–106.

Berney, C., & Pawlowski, J. (2006). A molecular time–scale for eukaryote evolution recalibrated with the continuous microfossil record. *Proceedings of the Royal Society B: Biological Sciences*, *273*(1596), 1867–1872.

Betts, H. C., Puttick, M. N., Clark, J. W., Williams, T. A., Donoghue, P. C., & Pisani, D. (2018). Integrated genomic and fossil evidence illuminates life's early evolution and eukaryote origin. *Nature ecology & evolution*, *2*(10), 1556–1562.

Bouckaert, R., Heled, J., Kühnert, D., Vaughan, T., Wu, C. H., Xie, D., Suchard, M. A., Rambaut, A., & Drummond, A. J. (2014). BEAST 2: a software platform for Bayesian evolutionary analysis. *PLoS computational biology*, *10*(4), 1–6.

Brain, C. B., Prave, A. R., Herd, D. A., Allison, S. G., Hoffmann, K. H., Fallick, A. E., Botha, A., Sturrock, C., Young, I., & Condon, D. J. (2012). The first animals: ca. 760–million–year–old sponge–like fossils from Namibia. *South African Journal of Science*, *108*(1), 1–8.

Brocks, J. J. (2018). The transition from a cyanobacterial to algal world and the emergence of animals. *Emerging Topics in Life Sciences*, *2*(2), 181–190.

Budd, G. E. (2008). The earliest fossil record of the animals and its significance. *Philosophical Transactions of the Royal Society B: Biological Sciences*, *363*(1496), 1425–1434.

Budd, G. E., & Jensen, S. (2000). A critical reappraisal of the fossil record of the bilaterian phyla. *Biological Reviews*, *75*(2), 253–295.

Burki, F., Roger, A. J., Brown, M. W., & Simpson, A. G. (2020). The new tree of eukaryotes. *Trends in ecology & evolution*, *35*(1), 43–55.
Burmester, T. (2002). Origin and evolution of arthropod hemocyanins and related proteins. *Journal of Comparative Physiology B*, *172*, 95–107.
Caetano–Anollés, G. (2017). RubisCO and the Search for Biomolecular Culprits of Planetary Change. *Bioessays*, *39*(11), 1–3.
Caetano–Anollés, G., Mittenthal, J. E., Caetano–Anollés, D., & Kim, K. M. (2014). A calibrated chronology of biochemistry reveals a stem line of descent responsible for planetary biodiversity. *Frontiers in Genetics*, *5*, 1–6.
Canfield, D. E., Poulton, S. W., & Narbonne, G. M. (2007). Late–Neoproterozoic deep–ocean oxygenation and the rise of animal life. *Science*, *315*(5808), 92–95.
Capella–Gutiérrez, S., Silla–Martínez, J. M., & Gabaldón, T. (2009). trimAl: a tool for automated alignment trimming in large–scale phylogenetic analyses. *Bioinformatics*, *25*(15), 1972–1973.
Cartwright, P., & Collins, A. (2007). Fossils and phylogenies: integrating multiple lines of evidence to investigate the origin of early major metazoan lineages. *Integrative and Comparative Biology*, *47*(5), 744–751.
Chernikova, D., Motamedi, S., Csürös, M., Koonin, E. V., & Rogozin, I. B. (2011). A late origin of the extant eukaryotic diversity: divergence time estimates using rare genomic changes. *Biology direct*, *6*, 1–18.
Cordani, U. G., Fairchild, T. R., Ganade, C. E., Babinski, M., & Leme, J. D. M. (2020). Dawn of metazoans: to what extent was this influenced by the onset of "modern–type plate tectonics"?. *Brazilian Journal of Geology*, *50*, 1–15.
Crowe, S. A., Døssing, L. N., Beukes, N. J., Bau, M., Kruger, S. J., Frei, R., & Canfield, D. E. (2013). Atmospheric oxygenation three billion years ago. *Nature*, *501*(7468), 535–538.
Cupp, J. R., & McAlister–Henn, L. (1991). NAD (+)–dependent isocitrate dehydrogenase. Cloning, nucleotide sequence, and disruption of the IDH2 gene from Saccharomyces cerevisiae. *Journal of Biological Chemistry*, *266*(33), 22199–22205.
Dean, A. M., & Golding, G. B. (1997). Protein engineering reveals ancient adaptive replacements in isocitrate dehydrogenase. *Proceedings of the National Academy of Sciences*, *94*(7), 3104–3109.
Decker, H., & Van Holde, K. E. (2011). *Oxygen and the Evolution of Life*. Berlin Heidelberg: Springer Science & Business Media.
Delsuc, F., Philippe, H., Tsagkogeorga, G., Simion, P., Tilak, M. K., Turon, X., López–Legentil, S., Piette, J., Lemaire, P., & Douzery, E. J. (2018). A phylogenomic framework and timescale for comparative studies of tunicates. *Bmc Biology*, *16*, 1–14.
DeSalle, R. (2015). Can single protein and protein family phylogenies be resolved better. *J Phylogenetics Evol Biol*, *3*, 1–5
Diamond, C. W., Planavsky, N. J., Wang, C., & Lyons, T. W. (2018). What the~ 1.4 Ga Xiamaling Formation can and cannot tell us about the mid-Proterozoic ocean. *Geobiology*, *16*(3), 219–236.
Dohrmann, M., & Wörheide, G. (2017). Dating early animal evolution using phylogenomic data. *Scientific reports*, *7*(1), 1–6.
dos Reis, M., Thawornwattana, Y., Angelis, K., Telford, M. J., Donoghue, P. C., & Yang, Z. (2015). Uncertainty in the timing of origin of animals and the limits of precision in molecular timescales. *Current biology*, *25*(22), 2939–2950.

Drummond, A. J., Ho, S. Y. W., Phillips, M. J., & Rambaut, A. (2006). Relaxed phylogenetics and dating with confidence. *PLoS biology*, *4*(5), 1–12.

Eme, L., Sharpe, S. C., Brown, M. W., & Roger, A. J. (2014). On the age of eukaryotes: evaluating evidence from fossils and molecular clocks. *Cold Spring Harbor Perspectives in Biology*, *6*(8), 1–18.

Giribet, G. (2016). New animal phylogeny: future challenges for animal phylogeny in the age of phylogenomics. *Organisms Diversity & Evolution*, *16*, 419–426.

Halanych, K. M. (2016). How our view of animal phylogeny was reshaped by molecular approaches: lessons learned. *Organisms Diversity & Evolution*, *16*, 319–328.

Hammarlund, E. U. (2020). Harnessing hypoxia as an evolutionary driver of complex multicellularity. *Interface Focus*, *10*(4), 1–11.

Hedges, S. B., Blair, J. E., Venturi, M. L., & Shoe, J. L. (2004). A molecular timescale of eukaryote evolution and the rise of complex multicellular life. *BMC evolutionary biology*, *4*(1), 1–9.

Hoang, D. T., Chernomor, O., Von Haeseler, A., Minh, B. Q., & Vinh, L. S. (2018). UFBoot2: improving the ultrafast bootstrap approximation. *Molecular biology and evolution*, *35*(2), 518–522.

Hurley, J. H., Thorsness, P. E., Ramalingam, V., Helmers, N. H., Koshland Jr, D. E., & Stroud, R. M. (1989). Structure of a bacterial enzyme regulated by phosphorylation, isocitrate dehydrogenase. *Proceedings of the National Academy of Sciences*, *86*(22), 8635–8639.

Irisarri, I., Baurain, D., Brinkmann, H., Delsuc, F., Sire, J. Y., Kupfer, A., Petersen, J., Meyer, A., Vences, M., & Philippe, H. (2017). Phylotranscriptomic consolidation of the jawed vertebrate timetree. *Nature ecology & evolution*, *1*(9), 1370–1378.

Jarrett, A. J., Cox, G. M., Brocks, J. J., Grosjean, E., Boreham, C. J., & Edwards, D. S. (2019). Microbial assemblage and palaeoenvironmental reconstruction of the 1.38 Ga Velkerri Formation, McArthur Basin, northern Australia. *Geobiology*, *17*(4), 360–380.

Javaux, E. J., Knoll, A. H., & Walter, M. (2003). Recognizing and interpreting the fossils of early eukaryotes. *Origins of Life and Evolution of the Biosphere*, *33*, 75–94.

Kalyaanamoorthy, S., Minh, B. Q., Wong, T. K., Von Haeseler, A., & Jermiin, L. S. (2017). ModelFinder: fast model selection for accurate phylogenetic estimates. *Nature methods*, *14*(6), 587–589.

Kang, S., Tice, A. K., Spiegel, F. W., Silberman, J. D., Pánek, T., Čepička, I., Kostka, M., Kosakyan, A., Alcântara, D. M. C., Roger, A. J., Shadwick, L. L., Smirnov, A., Kudryavtsev, A., Lahr, D. J. G., & Brown, M. W. (2017). Between a pod and a hard test: the deep evolution of amoebae. *Molecular biology and evolution*, *34*(9), 2258–2270.

Katoh, K., & Standley, D. M. (2013). MAFFT multiple sequence alignment software version 7: improvements in performance and usability. *Molecular biology and evolution*, *30*(4), 772–780.

Kim, Y. O., Oh, I. U., Park, H. S., Jeng, J. I. I. N. G. J. A. U., Song, B. J., & Huh, T. L. (1995). Characterization of a cDNA clone for human NAD+–specific isocitrate dehydrogenase α–subunit and structural comparison with its isoenzymes from different species. *Biochemical Journal*, *308*(1), 63–68.

Knoll, A. H. (2014). Paleobiological perspectives on early eukaryotic evolution. *Cold Spring Harbor Perspectives in Biology*, *6*(1), 1–16.

Kumar, S., Stecher, G., Suleski, M., & Hedges, S. B. (2017). TimeTree: a resource for timelines, timetrees, and divergence times. *Molecular biology and evolution*, *34*(7), 1812–1819.

Lahr, D. J., Kosakyan, A., Lara, E., Mitchell, E. A., Morais, L., Porfirio–Sousa, A. L., Ribeiro, G. M., Tice., A. K., Pánek, T., Kang, S., & Brown, M. W. (2019). Phylogenomics and morphological reconstruction of Arcellinida testate amoebae highlight diversity of microbial eukaryotes in the Neoproterozoic. *Current Biology*, *29*(6), 991–1001.

Lartillot, N., & Philippe, H. (2004). A Bayesian mixture model for across–site heterogeneities in the amino–acid replacement process. *Molecular biology and evolution*, *21*(6), 1095–1109.

Lartillot, N., Brinkmann, H., & Philippe, H. (2007). Suppression of long–branch attraction artefacts in the animal phylogeny using a site–heterogeneous model. *BMC evolutionary biology*, *7*(1), 1–14.

Loron, C. C., Rainbird, R. H., Turner, E. C., Greenman, J. W., & Javaux, E. J. (2019). Organic–walled microfossils from the late Mesoproterozoic to early Neoproterozoic lower Shaler Supergroup (Arctic Canada): diversity and biostratigraphic significance. *Precambrian Research*, *321*, 349–374.

Magallón, S., Hilu, K. W., & Quandt, D. (2013). Land plant evolutionary timeline: gene effects are secondary to fossil constraints in relaxed clock estimation of age and substitution rates. *American Journal of Botany*, *100*(3), 556–573.

Mailloux, R. J., Beriault, R., Lemire, J., Singh, R., Chenier, D. R., Hamel, R. D., & Appanna, V. D. (2007). The tricarboxylic acid cycle, an ancient metabolic network with a novel twist. *PloS one*, *2*(8), 1–10.

Martinez–Rivas, J. M., & Vega, J. (1998). Purification and characterization of NAD–isocitrate dehydrogenase from *Chlamydomonas reinhardtii*. *Plant physiology*, *118*(1), 249–255.

Mello, B. (2018). Estimating timetrees with MEGA and the TimeTree resource. *Molecular biology and evolution*, *35*(9), 2334–2342.

Miao, L., Moczydłowska, M., Zhu, S., & Zhu, M. (2019). New record of organic–walled, morphologically distinct microfossils from the late Paleoproterozoic Changcheng Group in the Yanshan Range, North China. *Precambrian Research*, *321*, 172–198.

Mills, D. B., & Canfield, D. E. (2014). Oxygen and animal evolution: Did a rise of atmospheric oxygen "trigger" the origin of animals?. *BioEssays*, *36*(12), 1145–1155.

Mills, D. B., Francis, W. R., Vargas, S., Larsen, M., Elemans, C. P., Canfield, D. E., & Wörheide, G. (2018). The last common ancestor of animals lacked the HIF pathway and respired in low–oxygen environments. *Elife*, *7*, 1–17.

Mills, D. B., Ward, L. M., Jones, C., Sweeten, B., Forth, M., Treusch, A. H., & Canfield, D. E. (2014). Oxygen requirements of the earliest animals. *Proceedings of the National Academy of Sciences*, *111*(11), 4168–4172.

Misof, B., Liu, S., Meusemann, K., Peters, R. S., Donath, A., Mayer, C., Frandsen, P. B., Ware, J., Flouri, T., Beutel, R. G., Niehuis, O., Petersen, M., Izquierdo–Carrasco, F., Wappler, T., Rust, J., Aberer, A. J., Aspock, U., Aspock, H., Bartel, D., Blanke, A., Berger, S., Bohm, A., Buckley, T. R., Calcott, B., Chen, J., Friedrich, F., Fukui, M., Fujita, M., Greve, C., Grobe, P., Gu, S., Huang, Y., Jermiin, L. S., Kawahara, A. Y., Krogmann, L., Kubiak, M., Lanfear, R., Letsch, H., Li, Y., Li, Z., Li, J., Lu, H., Machida, R., Mashimo, Y., Kapli, P., McKenna, D. D., Meng, G., Nakagaki, Y,, Navarrete–Heredia, J. L., Ott, M., Ou, Y., Pass,

G., Podsiadlowski, L., Pohl, H., Reumont, B.M. von, Schutte, K., Sekiya, K., Shimizu, S., Slipinski, A., Stamatakis, A., Song, W., Su, X., Szucsich, N. U., Tan, M., Tan, X., Tang, M., Tang, J., Timelthaler, G., Tomizuka, S., Trautwein, M., Tong, X., Uchifune, T., Walzl, M. G., Wiegmann, B. M., Wilbrandt, J., Wipfler, B., Wong, T. K. F., Wu, Q., Wu, G., Xie, Y., Yang, S., Yang, Q., Yeates, D. K., Yoshizawa, K., Zhang, Q., Zhang, R., Zhang, W., Zhang, Y., Zhao, J., Zhou, C., Zhou, L., Ziesmann, T., Zou, S., Li, Y., Xu, X., Zhang, Y., Yang, H., Wang, J., Wang, J., Kjer, K. M., & Zhou, X. (2014). Phylogenomics resolves the timing and pattern of insect evolution. *Science*, *346*(6210), 763–767.

Nelson, D. L., Lehninger, A. L., & Cox, M. M. (2013). *Lehninger principles of biochemistry* (6th Ed). New York, H. Freeman.

Nguyen, K., Love, G. D., Zumberge, J. A., Kelly, A. E., Owens, J. D., Rohrssen, M. K., Bates, S. M., Cai, C., & Lyons, T. W. (2019). Absence of biomarker evidence for early eukaryotic life from the Mesoproterozoic Roper Group: Searching across a marine redox gradient in mid-Proterozoic habitability. *Geobiology*, *17*(3), 247–260.

Nguyen, L. T., Schmidt, H. A., Von Haeseler, A., & Minh, B. Q. (2015). IQ–TREE: a fast and effective stochastic algorithm for estimating maximum–likelihood phylogenies. *Molecular biology and evolution*, *32*(1), 268–274.

Nichols, B. J., Hall, L., Perry, A. C. F., & Denton, R. M. (1993). Molecular cloning and deduced amino acid sequences of the γ–subunits of rat and monkey NAD+–isocitrate dehydrogenases. *Biochemical Journal*, *295*(2), 347–350.

Nichols, B. J., Perry, A. C., Hall, L., & Denton, R. M. (1995). Molecular cloning and deduced amino acid sequences of the α–and β–subunits of mammalian NAD+–isocitrate dehydrogenase. *Biochemical Journal*, *310*(3), 917–922.

Nunes–Nesi, A., Araújo, W. L., Obata, T., & Fernie, A. R. (2013). Regulation of the mitochondrial tricarboxylic acid cycle. *Current opinion in plant biology*, *16*(3), 335–343.

Nursall, J. R. (1959). Oxygen as a prerequisite to the origin of the Metazoa. *Nature*, *183*(4669), 1170–1172.

Parfrey, L. W., Lahr, D. J., Knoll, A. H., & Katz, L. A. (2011). Estimating the timing of early eukaryotic diversification with multigene molecular clocks. *Proceedings of the National Academy of Sciences*, *108*(33), 13624–13629.

Parham, J. F., Donoghue, P. C., Bell, C. J., Calway, T. D., Head, J. J., Holroyd, P. A., Inoue, J. G., Irmis, R. B., Joyce, W. G., Ksepka, D. T., Patané, J. S. L., Smith, N. D., Tarver, J. E., van Tuinen, M., Yang, Z., Angielczyk, K. D., Greenwood, J. M., Hipsley, C. A., Jacobs, L., Makovicky, P. J., Müller, J., Smith, K. T., Theodor, J. M., Warnock, R. C. M., & Benton, M. J. (2012). Best practices for justifying fossil calibrations. *Systematic Biology*, *61*(2), 346–359.

Peterson, K. J., Lyons, J. B., Nowak, K. S., Takacs, C. M., Wargo, M. J., & McPeek, M. A. (2004). Estimating metazoan divergence times with a molecular clock. *Proceedings of the National Academy of Sciences*, *101*(17), 6536–6541.

Pisani, D., Pett, W., Dohrmann, M., Feuda, R., Rota–Stabelli, O., Philippe, H., Lartillot, N., & Wörheide, G. (2015). Genomic data do not support comb jellies as the sister group to all other animals. *Proceedings of the National Academy of Sciences*, *112*(50), 15402–15407.

Planavsky, N. J., Cole, D. B., Reinhard, C. T., Diamond, C., Love, G. D., Luo, G., Zhang, S., Konhauser, K. O., & Lyons, T. W. (2016). No evidence for high atmospheric oxygen levels 1,400 million years ago. *Proceedings of the National Academy of Sciences*, *113*(19), E2550–E2551.

Porter, S. M. (2020). Insights into eukaryogenesis from the fossil record. *Interface Focus*, *10*(4), 1–9.

Potter, S. C., Luciani, A., Eddy, S. R., Park, Y., Lopez, R., & Finn, R. D. (2018). HMMER web server: 2018 update. *Nucleic acids research*, *46*(W1), W200–W204.

Qi, F., Chen, X., & Beard, D. A. (2008). Detailed kinetics and regulation of mammalian NAD–linked isocitrate dehydrogenase. *Biochimica et Biophysica Acta (BBA)–Proteins and Proteomics*, *1784*(11), 1641–1651.

Ramachandran, N., & Colman, R. F. (1980). Chemical characterization of distinct subunits of pig heart DPN–specific isocitrate dehydrogenase. *Journal of Biological Chemistry*, *255*(18), 8859–8864.

Rambaut, A. (2009). FigTree. Tree figure drawing tool. Available at http://tree.bio.ed.ac.uk/software/figtree/.

Rambaut, A., Suchard, M. A., Xie, D., & Drummond, A. J. (2014). Tracer v1. 6. Available at http://beast.community/tracer.

Ronquist, F., & Huelsenbeck, J. P. (2003). MrBayes 3: Bayesian phylogenetic inference under mixed models. *Bioinformatics*, *19*(12), 1572–1574.

Schwartz, R. S., & Mueller, R. L. (2010). Branch length estimation and divergence dating: estimates of error in Bayesian and maximum likelihood frameworks. *BMC Evolutionary Biology*, *10*(1), 1–21.

Sebé–Pedrós, A., de Mendoza, A., Lang, B. F., Degnan, B. M., & Ruiz–Trillo, I. (2011). Unexpected repertoire of metazoan transcription factors in the unicellular holozoan *Capsaspora owczarzaki*. *Molecular biology and evolution*, *28*(3), 1241–1254.

Sperling, E. A., & Stockey, R. G. (2018). The temporal and environmental context of early animal evolution: Considering all the ingredients of an "explosion". *Integrative and Comparative Biology*, *58*(4), 605–622.

Sun, P., Ma, T., Zhang, T., Zhu, H., Zhang, J., Liu, Y., & Ding, J. (2019). Molecular basis for the function of the αβ heterodimer of human NAD–dependent isocitrate dehydrogenase. *Journal of Biological Chemistry*, *294*(44), 16214–16227.

Taylor, A. B., Hu, G., Hart, P. J., & McAlister–Henn, L. (2008). Allosteric motions in structures of yeast NAD+–specific isocitrate dehydrogenase. *Journal of Biological Chemistry*, *283*(16), 10872–10880.

Wang, M., Jiang, Y. Y., Kim, K. M., Qu, G., Ji, H. F., Mittenthal, J. E., Zhang, H. Y., & Caetano–Anollés, G. (2011). A universal molecular clock of protein folds and its power in tracing the early history of aerobic metabolism and planet oxygenation. *Molecular biology and evolution*, *28*(1), 567–582.

Wang, P., Lv, C., & Zhu, G. (2015). Novel type II and monomeric NAD+ specific isocitrate dehydrogenases: phylogenetic affinity, enzymatic characterization and evolutionary implication. *Scientific reports*, *5*(1), 1–11.

Whelan, N. V., Kocot, K. M., Moroz, L. L., & Halanych, K. M. (2015). Error, signal, and the placement of Ctenophora sister to all other animals. *Proceedings of the National Academy of Sciences*, *112*(18), 5773–5778.

Whelan, S., & Goldman, N. (2001). A general empirical model of protein evolution derived from multiple protein families using a maximum–likelihood approach. *Molecular biology and evolution*, *18*(5), 691–699.

Wilke, T., Schultheiß, R., & Albrecht, C. (2009). As time goes by: a simple fool's guide to molecular clock approaches in invertebrates. *American Malacological Bulletin*, *27*(1/2), 25–45.

Wolfe, J. M., Breinholt, J. W., Crandall, K. A., Lemmon, A. R., Lemmon, E. M., Timm, L. E., Siddall, M. E., & Bracken–Grissom, H. D. (2019). A phylogenomic framework, evolutionary timeline and genomic resources for comparative studies of decapod crustaceans. *Proceedings of the Royal Society B*, *286*(1901), 1–10.

Wood, R., Donoghue, P. C., Lenton, T. M., Liu, A. G., & Poulton, S. W. (2020). The origin and rise of complex life: progress requires interdisciplinary integration and hypothesis testing. *Interface Focus*, *10*(4), 1–10.

Zhang, S., Wang, X., Wang, H., Bjerrum, C. J., Hammarlund, E. U., Dahl, T. W., & Canfield, D. E. (2016). Reply to Planavsky et al.: Strong evidence for high atmospheric oxygen levels 1,400 million years ago. *Proceedings of the National Academy of Sciences*, *113*(19), E2552–E2553.

Zhang, S., Wang, X., Wang, H., Bjerrum, C. J., Hammarlund, E. U., Haxen, E. R., Wen, H., Ye, Y., & Canfield, D. E. (2019). Paleoenvironmental proxies and what the Xiamaling Formation tells us about the mid-Proterozoic ocean. *Geobiology*, *17*(3), 225–246.

Zhang, T., Yuan, D., Xie, J., Lei, Y., Li, J., Fang, G., Tian, L., Liu, J., Cui, Y., Zhang, M., Xiao, Y., Xu., Y., Zhang, J., Zhu, M., Zhan, S., & Li, S. (2019). Evolution of the cholesterol biosynthesis pathway in animals. *Molecular Biology and Evolution*, *36*(11), 2548–2556.

Zheng, Y., Peng, R., Kuro–o, M., & Zeng, X. (2011). Exploring patterns and extent of bias in estimating divergence time from mitochondrial DNA sequence data in a particular lineage: a case study of salamanders (Order Caudata). *Molecular Biology and Evolution*, *28*(9), 2521–2535.

Supplementary Table S1 – List of all taxa analyzed in this study, including sequence name, species name, taxonomic group and GenBank accession number.

Sequence Name	Species	Taxonomic Group	Accession number
A._planci_echinodermataXP_022080645.1	*Acanthaster planci*	Echinodermata	XP_022080645.1
A._planci_echinodermataXP_022096040.1	*Acanthaster planci*	Echinodermata	XP_022096040.1
A._planci_echinodermataXP_022108231.1	*Acanthaster planci*	Echinodermata	XP_022108231.1
A._millepora_cnidariaXP_029191641.1	*Acropora millepora*	Cnidaria	XP_029191641.1
A._millepora_cnidariaXP_029193850.1	*Acropora millepora*	Cnidaria	XP_029193850.1
A._millepora_cnidariaXP_029194161.1	*Acropora millepora*	Cnidaria	XP_029194161.1
A._pisum_insectsXP_008188230.1	*Acyrthosiphon pisum*	Arthropoda	XP_008188230.1
A._sinensis_ReptilaAlligatorXP_014377070.2	*Alligator sinensis*	Vertebrata	XP_014377070.2
A._sinensis_ReptilaAlligatorXP_025069507.1	*Alligator sinensis*	Vertebrata	XP_025069507.1
A._macrogynus_FungiKNE71753.1	*Allomyces macrogynus*	Fungi	KNE71753.1
A._caninum_nematodaRCN36703.1	*Ancylostoma caninum*	Nematoda	RCN36703.1
A._caninum_nematodaRCN50722.1	*Ancylostoma caninum*	Nematoda	RCN50722.1
A._deanei_EuglenozoaEPY39061.1	*Angomonas deanei*	Euglenozoa	EPY39061.1
A._gossypii_insectsAJQ30122.1	*Aphis gossypii*	Arthropoda	AJQ30122.1
A._cerana_insectsXP_028525762.1	*Apis cerana*	Arthropoda	XP_028525762.1
A._cerana_insectsPBC30104.1	*Apis cerana cerana*	Arthropoda	PBC30104.1
A._suum_nematodaADY42482.1	*Ascaris suum*	Nematoda	ADY42482.1
A._suum_nematodaADY46393.1	*Ascaris suum*	Nematoda	ADY46393.1
B._dorsalis_insectsXP_011197565.1	*Bactrocera dorsalis*	Arthropoda	XP_011197565.1
B._scammoni_mamalsXP_028018055.1	*Balaenoptera acutorostrata scammoni*	Vertebrata	XP_028018055.1
B._mandarina_insectsXP_028031821.1	*Bombyx mandarina*	Arthropoda	XP_028031821.1
B._belcheri_cephalochordataXP_019626395.1	*Branchiostoma belcheri*	Cephalochordata	XP_019626395.1
B._belcheri_cephalochordataXP_019628290.1	*Branchiostoma belcheri*	Cephalochordata	XP_019628290.1
B._belcheri_cephalochordataXP_019631903.1	*Branchiostoma belcheri*	Cephalochordata	XP_019631903.1
B._belcheri_cephalochordataXP_019631904.1	*Branchiostoma belcheri*	Cephalochordata	XP_019631904.1
B._belcheri_cephalochordataXP_019631905.1	*Branchiostoma belcheri*	Cephalochordata	XP_019631905.1
B._belcheri_cephalochordataXP_019631906.1	*Branchiostoma belcheri*	Cephalochordata	XP_019631906.1

B._belcheri_cephalochordataXP_019631907.1	*Branchiostoma belcheri*	Cephalochordata	XP_019631907.1
C._elegans_nematodaCAA86325.2	*Caenorhabditis elegans*	Nematoda	CAA86325.2
C._elegans_nematodaCCD66235.1	*Caenorhabditis elegans*	Nematoda	CCD66235.1
C._milii_cartilaginousAFP04321.1	*Callorhinchus milii*	Vertebrata	AFP04321.1
C._milii_cartilaginousAFP04347.1	*Callorhinchus milii*	Vertebrata	AFP04347.1
C._auris_FungiGBL52436.1	*Candida auris*	Fungi	GBL52436.1
C._owczarzaki_CapsasporaXP_004343741.1	*Capsaspora owczarzaki*	Filasterea	XP_004343741.1
C._owczarzaki_CapsasporaXP_004363625.1	*Capsaspora owczarzaki*	Filasterea	XP_004363625.1
C._fasciculata_AmoebozoaXP_004361360.1	*Cavenderia fasciculata*	Amoebozoa	XP_004361360.1
C._sculpturatus_arachnidsXP_023232345.1	*Centruroides sculpturatus*	Arthropoda	XP_023232345.1
C._sculpturatus_arachnidsXP_023235488.1	*Centruroides sculpturatus*	Arthropoda	XP_023235488.1
C._mydas_ReptilaTurtlesXP_007068405.2	*Chelonia mydas*	Vertebrata	XP_007068405.2
C._intestinalis_tunicateXP_002122423.1	*Ciona intestinalis*	Urochordata	XP_002122423.1
C._intestinalis_tunicateXP_002129499.1	*Ciona intestinalis*	Urochordata	XP_002129499.1
C._intestinalis_tunicateXP_002130367.1	*Ciona intestinalis*	Urochordata	XP_002130367.1
C._sinensis_platyhelminthesGAA34041.2	*Clonorchis sinensis*	Platyhelminthes	GAA34041.2
C._sinensis_platyhelminthesGAA40293.2	*Clonorchis sinensis*	Platyhelminthes	GAA40293.2
C._militaris_FungiATY62353.1	*Cordyceps militaris*	Fungi	ATY62353.1
C._gobio_bonyfishesXP_029291799.1	*Cottoperca gobio*	Vertebrata	XP_029291799.1
C._gigas_molluscaEKC30015.1	*Crassostrea gigas*	Mollusca	EKC30015.1
C._gigas_molluscaEKC33392.1	*Crassostrea gigas*	Mollusca	EKC33392.1
C._virginica_molluscaXP_022301966.1	*Crassostrea virginica*	Mollusca	XP_022301966.1
C._virginica_molluscaXP_022321339.1	*Crassostrea virginica*	Mollusca	XP_022321339.1
C._virginica_molluscaXP_022334803.1	*Crassostrea virginica*	Mollusca	XP_022334803.1
D._rerio_bonyfishesNP_001230101.1	*Danio rerio*	Vertebrata	NP_001230101.1
D._magna_crustaceaJAJ79593.1	*Daphnia magna*	Arthropoda	JAJ79593.1
D._magna_crustaceaJAK11924.1	*Daphnia magna*	Arthropoda	JAK11924.1
D._magna_crustaceaJAN68172.1	*Daphnia magna*	Arthropoda	JAN68172.1
D._magna_crustaceaKZS14245.1	*Daphnia magna*	Arthropoda	KZS14245.1
D._magna_crustaceaKZS16963.1	*Daphnia magna*	Arthropoda	KZS16963.1
D._gigantea_cnidariaXP_028391286.1	*Dendronephthya gigantea*	Cnidaria	XP_028391286.1

D._gigantea_cnidariaXP_028398962.1	*Dendronephthya gigantea*	Cnidaria	XP_028398962.1
D._alloeum_insectsXP_015117129.1	*Diachasma alloeum*	Arthropoda	XP_015117129.1
D._discoideum_AmoebozoaXP_645630.1	*Dictyostelium discoideum*	Amoebozoa	XP_645630.1
D._purpureum_AmoebozoaXP_003289977.1	*Dictyostelium purpureum*	Amoebozoa	XP_003289977.1
E._naucrates_bonyfishesXP_029357416.1	*Echeneis naucrates*	Vertebrata	XP_029357416.1
E._naucrates_bonyfishesXP_029363301.1	*Echeneis naucrates*	Vertebrata	XP_029363301.1
E._granulosus_platyhelminthesCDS21006.1	*Echinococcus granulosus*	Platyhelminthes	CDS21006.1
E._granulosus_platyhelminthesCDS22227.1	*Echinococcus granulosus*	Platyhelminthes	CDS22227.1
E._multilocularis_platyhelminthesCDS36355.1	*Echinococcus multilocularis*	Platyhelminthes	CDS36355.1
E._traillii_birdXP_027757377.1	*Empidonax traillii*	Vertebrata	XP_027757377.1
E._jubatus_mamalsXP_027950171.1	*Eumetopias jubatus*	Vertebrata	XP_027950171.1
E._affinis_crustaceaXP_023325125.1	*Eurytemora affinis*	Arthropoda	XP_023325125.1
E._affinis_crustaceaXP_023342071.1	*Eurytemora affinis*	Arthropoda	XP_023342071.1
E._pallida_cnidariaKXJ19304.1	*Exaiptasia pallida*	Cnidaria	KXJ19304.1
E._pallida_cnidariaKXJ28853.1	*Exaiptasia pallida*	Cnidaria	KXJ28853.1
E._pallida_cnidariaXP_020908935.1	*Exaiptasia pallida*	Cnidaria	XP_020908935.1
F._cherrug_birdXP_014132353.2	*Falco cherrug*	Vertebrata	XP_014132353.2
F._peregrinus_birdXP_027647222.1	*Falco peregrinus*	Vertebrata	XP_027647222.1
F._hepatica_platyhelminthesTHD21245.1	*Fasciola hepatica*	Platyhelminthes	THD21245.1
F._exsecta_insectsXP_029665054.1	*Formica exsecta*	Arthropoda	XP_029665054.1
G._occidentalis_arachnidsXP_003738563.1	*Galendromus occidentalis*	Arthropoda	XP_003738563.1
G._occidentalis_arachnidsXP_018497754.1	*Galendromus occidentalis*	Arthropoda	XP_018497754.1
H._album_AmoebozoaXP_020430426.1	*Heterostelium album*	Amoebozoa	XP_020430426.1
H._vulgaris_cnidariaCDG71929.1	*Hydra vulgaris*	Cnidaria	CDG71929.1
H._microstoma_platyhelminthesCDS29409.1	*Hymenolepis microstoma*	Platyhelminthes	CDS29409.1
H._microstoma_platyhelminthesCDS33069.1	*Hymenolepis microstoma*	Platyhelminthes	CDS33069.1
H._dujardini_tardigradesOQV14700.1	*Hypsibius dujardini*	Tardigrada	OQV14700.1
H._dujardini_tardigradesOQV25778.1	*Hypsibius dujardini*	Tardigrada	OQV25778.1
I._multifiliis_CiliatesXP_004065515.1	*Ichthyophthirius multifiliis*	Ciliophora	XP_004065515.1

I._punctatus_bonyfishesADO28964.1	*Ictalurus punctatus*	Vertebrata	ADO28964.1
I._scapularis_arachnidsXP_002409478.2	*Ixodes scapularis*	Arthropoda	XP_002409478.2
I._scapularis_arachnidsXP_002435201.2	*Ixodes scapularis*	Arthropoda	XP_002435201.2
I._scapularis_arachnidsXP_029822213.1	*Ixodes scapularis*	Arthropoda	XP_029822213.1
I._scapularis_arachnidsXP_029839780.1	*Ixodes scapularis*	Arthropoda	XP_029839780.1
K._nitens_ViridiplantaeGAQ79048.1	*Klebsormidium nitens*	Viridiplantae	GAQ79048.1
L._rohita_bonyfishesRXN26896.1	*Labeo rohita*	Vertebrata	RXN26896.1
L._donovani_EuglenozoaTPP53612.1	*Leishmania donovani*	Euglenozoa	TPP53612.1
L._donovani_EuglenozoaXP_003864092.1	*Leishmania donovani*	Euglenozoa	XP_003864092.1
L._major_EuglenozoaCAJ06701.1	*Leishmania* major strain Friedlin	Euglenozoa	CAJ06701.1
L._mexicana_EuglenozoaCBZ30062.1	*Leishmania mexicana*	Euglenozoa	CBZ30062.1
L._panamensis_EuglenozoaAIO01557.1	*Leishmania panamensis*	Euglenozoa	AIO01557.1
L._panamensis_EuglenozoaXP_010702357.1	*Leishmania panamensis*	Euglenozoa	XP_010702357.1
L._tarentolae_EuglenozoaGET92011.1	*Leishmania tarentolae*	Euglenozoa	GET92011.1
L._salmonis_crustaceaCDW47858.1	*Lepeophtheirus salmonis*	Arthropoda	CDW47858.1
L._pyrrhocoris_EuglenozoaKPA81045.1	*Leptomonas pyrrhocoris*	Euglenozoa	KPA81045.1
L._seymouri_EuglenozoaKPI89854.1	*Leptomonas seymouri*	Euglenozoa	KPI89854.1
L._polyphemus_xiphosuraXP_013788757.1	*Limulus polyphemus*	Arthropoda	XP_013788757.1
L._anatina_brachiopodaXP_013390200.1	*Lingula anatina*	Brachiopoda	XP_013390200.1
L._anatina_brachiopodaXP_013404770.1	*Lingula anatina*	Brachiopoda	XP_013404770.1
L._anatina_brachiopodaXP_013413294.1	*Lingula anatina*	Brachiopoda	XP_013413294.1
M._fascicularis_mamalsNP_001274565.1	*Macaca fascicularis*	Vertebrata	NP_001274565.1
M._vitellinus_birdXP_029819001.1	*Manacus vitellinus*	Vertebrata	XP_029819001.1
M._yessoensis_molluscaOWF47932.1	*Mizuhopecten yessoensis*	Mollusca	OWF47932.1
M._yessoensis_molluscaXP_021358516.1	*Mizuhopecten yessoensis*	Mollusca	XP_021358516.1
M._yessoensis_molluscaXP_021369276.1	*Mizuhopecten yessoensis*	Mollusca	XP_021369276.1
M._yessoensis_molluscaXP_021369277.1	*Mizuhopecten yessoensis*	Mollusca	XP_021369277.1
M._monoceros_mamalsXP_029094917.1	*Monodon monoceros*	Vertebrata	XP_029094917.1
N._americanus_nematodaXP_013302382.1	*Necator americanus*	Nematoda	XP_013302382.1
N._fulva_insectsXP_029166884.1	*Nylanderia fulva*	Arthropoda	XP_029166884.1
O._vulgaris_molluscaXP_029632996.1	*Octopus vulgaris*	Mollusca	XP_029632996.1

O._vulgaris_molluscaXP_029654384.1	*Octopus vulgaris*	Mollusca	XP_029654384.1
O._vulgaris_molluscaXP_029654670.1	*Octopus vulgaris*	Mollusca	XP_029654670.1
O._flexuosa_nematodaOZC08304.1	*Onchocerca flexuosa*	Nematoda	OZC08304.1
O._flexuosa_nematodaOZC10327.1	*Onchocerca flexuosa*	Nematoda	OZC10327.1
O._nerka_bonyfishesXP_029478737.1	*Oncorhynchus nerka*	Vertebrata	XP_029478737.1
O._hannah_ReptilaLizardETE65875.1	*Ophiophagus hannah*	Vertebrata	ETE65875.1
O._viverrini_platyhelminthesOON15529.1	*Opisthorchis viverrini*	Platyhelminthes	OON15529.1
O._faveolata_cnidariaXP_020611790.1	*Orbicella faveolata*	Cnidaria	XP_020611790.1
O._faveolata_cnidariaXP_020612083.1	*Orbicella faveolata*	Cnidaria	XP_020612083.1
O._faveolata_cnidariaXP_020628871.1	*Orbicella faveolata*	Cnidaria	XP_020628871.1
O._anatinus_mamalsMonotremeXP_028921678.1	*Ornithorhynchus anatinus*	Vertebrata	XP_028921678.1
O._bicornis_insectsXP_029050935.1	*Osmia bicornis bicornis*	Arthropoda	XP_029050935.1
O._furnacalis_insectsXP_028165010.1	*Ostrinia furnacalis*	Arthropoda	XP_028165010.1
P._tepidariorum_arachnidsLAA03863.1	*Parasteatoda tepidariorum*	Arthropoda	LAA03863.1
P._tepidariorum_arachnidsXP_015909429.1	*Parasteatoda tepidariorum*	Arthropoda	XP_015909429.1
P._sinensis_ReptilaTurtlesXP_006117027.2	*Pelodiscus sinensis*	Vertebrata	XP_006117027.2
P._vannamei_crustaceaXP_027209903.1	*Penaeus vannamei*	Arthropoda	XP_027209903.1
P._vannamei_crustaceaXP_027220003.1	*Penaeus vannamei*	Arthropoda	XP_027220003.1
P._catodon_mamalsXP_023984594.1	*Physeter catodon*	Vertebrata	XP_023984594.1
P._fungivorum_AmoebozoaPRP86732.1	*Planoprotostelium fungivorum*	Amoebozoa	PRP86732.1
P._damicornis_cnidariaXP_027035685.1	*Pocillopora damicornis*	Cnidaria	XP_027035685.1
P._damicornis_cnidariaXP_027040785.1	*Pocillopora damicornis*	Cnidaria	XP_027040785.1
P._damicornis_cnidariaXP_027040786.1	*Pocillopora damicornis*	Cnidaria	XP_027040786.1
P._damicornis_cnidariaXP_027053611.1	*Pocillopora damicornis*	Cnidaria	XP_027053611.1
P._damicornis_cnidariaXP_027053612.1	*Pocillopora damicornis*	Cnidaria	XP_027053612.1
P._muralis_ReptilaLizardXP_028567561.1	*Podarcis muralis*	Vertebrata	XP_028567561.1
P._canaliculata_molluscaXP_025077031.1	*Pomacea canaliculata*	Mollusca	XP_025077031.1
P._canaliculata_molluscaXP_025106368.1	*Pomacea canaliculata*	Mollusca	XP_025106368.1
P._canaliculata_molluscaXP_025113260.1	*Pomacea canaliculata*	Mollusca	XP_025113260.1
P._abelii_mamalsNP_001125436.1	*Pongo abelii*	Vertebrata	NP_001125436.1

P._mucrosquamatus_ReptilaLizardXP_015684429.1	*Protobothrops mucrosquamatus*	Vertebrata	XP_015684429.1
P._oleovorans_BacteriaCDR91070.1	*Pseudomonas oleovorans*	Bacteria	CDR91070.1
R._varieornatus_tardigradesGAU88467.1	*Ramazzottius varieornatus*	Tardigrada	GAU88467.1
R._varieornatus_tardigradesGAU93339.1	*Ramazzottius varieornatus*	Tardigrada	GAU93339.1
R._varieornatus_tardigradesGAV07616.1	*Ramazzottius varieornatus*	Tardigrada	GAV07616.1
R._bivittatum_amphibiaXP_029451037.1	*Rhinatrema bivittatum*	Vertebrata	XP_029451037.1
R._bivittatum_amphibiaXP_029465296.1	*Rhinatrema bivittatum*	Vertebrata	XP_029465296.1
R._bivittatum_amphibiaXP_029465306.1	*Rhinatrema bivittatum*	Vertebrata	XP_029465306.1
R._appendiculatus_arachnidsJAP79177.1	*Rhipicephalus appendiculatus*	Arthropoda	JAP79177.1
R._appendiculatus_arachnidsJAP86015.1	*Rhipicephalus appendiculatus*	Arthropoda	JAP86015.1
R._irregularis_FungiPKY46143.1	*Rhizophagus irregularis*	Fungi	PKY46143.1
S._trutta_bonyfishesXP_029632067.1	*Salmo trutta*	Vertebrata	XP_029632067.1
S._enterica_BacteriaCBY96094.1	*Salmonella enterica* subsp. *enterica* serovar Weltevreden	Bacteria	CBY96094.1
S._rosetta_ChoanoflagelateEGD76470.1	*Salpingoeca rosetta*	Choanoflagellata	EGD76470.1
S._rosetta_ChoanoflagelateEGD79740.1	*Salpingoeca rosetta*	Choanoflagellata	EGD79740.1
S._harrisii_mamalsXP_023363049.1	*Sarcophilus harrisii*	Vertebrata	XP_023363049.1
S._scabiei_arachnidsKPM07743.1	*Sarcoptes scabiei*	Arthropoda	KPM07743.1
S._stipitis_FungiXP_001386057.1	*Scheffersomyces stipitis*	Fungi	XP_001386057.1
S._bovis_platyhelminthesRTG84748.1	*Schistosoma bovis*	Platyhelminthes	RTG84748.1
S._haematobium_platyhelminthesKGB38128.1	*Schistosoma haematobium*	Platyhelminthes	KGB38128.1
S._japonicum_platyhelminthesCAX73753.1	*Schistosoma japonicum*	Platyhelminthes	CAX73753.1
S._japonicum_platyhelminthesCAX75389.1	*Schistosoma japonicum*	Platyhelminthes	CAX75389.1
S._japonicum_platyhelminthesTNN15762.1	*Schistosoma japonicum*	Platyhelminthes	TNN15762.1
S._culicis_EuglenozoaEPY30744.1	*Strigomonas culicis*	Euglenozoa	EPY30744.1
S._purpuratus_echinodermataXP_783413.2	*Strongylocentrotus purpuratus*	Echinodermata	XP_783413.2
S._purpuratus_echinodermataXP_011664062.1	*Strongylocentrotus purpuratus*	Echinodermata	XP_011664062.1

S._ratti_nematodaCEF67094.1	*Strongyloides ratti*	Nematoda	CEF67094.1
S._ratti_nematodaXP_024507139.1	*Strongyloides ratti*	Nematoda	XP_024507139.1
S._pistillata_cnidariaPFX23565.1	*Stylophora pistillata*	Cnidaria	PFX23565.1
S._pistillata_cnidariaXP_022795520.1	*Stylophora pistillata*	Cnidaria	XP_022795520.1
S._pistillata_cnidariaXP_022801276.1	*Stylophora pistillata*	Cnidaria	XP_022801276.1
S._suricatta_mamalsXP_029786927.1	*Suricata suricatta*	Vertebrata	XP_029786927.1
T._guttata_birdNP_001232659.1	*Taeniopygia guttata*	Vertebrata	NP_001232659.1
T._rubripes_bonyfishesXP_011620203.1	*Takifugu rubripes*	Vertebrata	XP_011620203.1
T._triunguis_ReptilaTurtlesXP_026514188.1	*Terrapene carolina triunguis*	Vertebrata	XP_026514188.1
T._thermophila_CiliatesEAR98203.3	*Tetrahymena thermophila*	Ciliophora	EAR98203.3
T._thermophila_CiliatesXP_001031817.3	*Tetrahymena thermophila*	Ciliophora	XP_001031817.3
T._urticae_arachnidsXP_015787653.1	*Tetranychus urticae*	Arthropoda	XP_015787653.1
T._lacteum_AmoebozoaKYR00648.1	*Tieghemostelium lacteum*	Amoebozoa	KYR00648.1
T._canis_nematodaKHN84477.1	*Toxocara canis*	Nematoda	KHN84477.1
T._nativa_nematodaOUC47719.1	*Trichinella nativa*	Nematoda	OUC47719.1
V._destructor_arachnidsXP_022654745.1	*Varroa destructor*	Arthropoda	XP_022654745.1
V._ursinus_mamalsXP_027701613.1	*Vombatus ursinus*	Vertebrata	XP_027701613.1
X._tropicalis_amphibiaNP_989352.1	*Xenopus tropicalis*	Vertebrata	NP_989352.1
X._tropicalis_amphibiaNP_001119993.1	*Xenopus tropicalis*	Vertebrata	NP_001119993.1
Z._californianus_mamalsXP_027425207.1	*Zalophus californianus*	Vertebrata	XP_027425207.1
Z._tritici_FungiEGP83856.1	*Zymoseptoria tritici*	Fungi	EGP83856.1

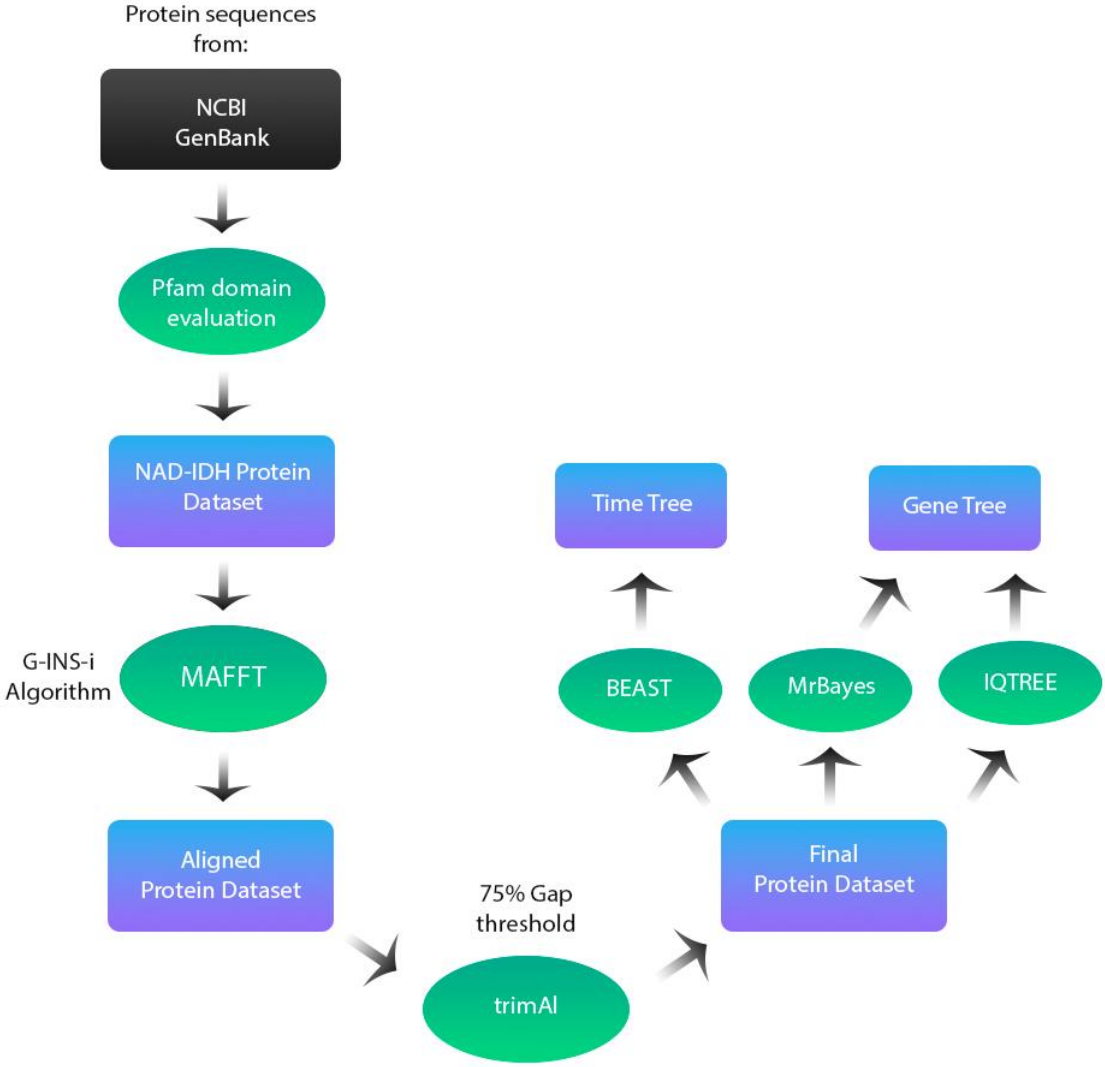

Supplementary Figure S2 – Bioinformatic pipeline. Ovals represent software or scripts, and rounded rectangles represent input/output files. The dataset was formed using 195 previously published NAD-IDH sequences distributed as: 193 eukaryotic sequences and two bacterial.

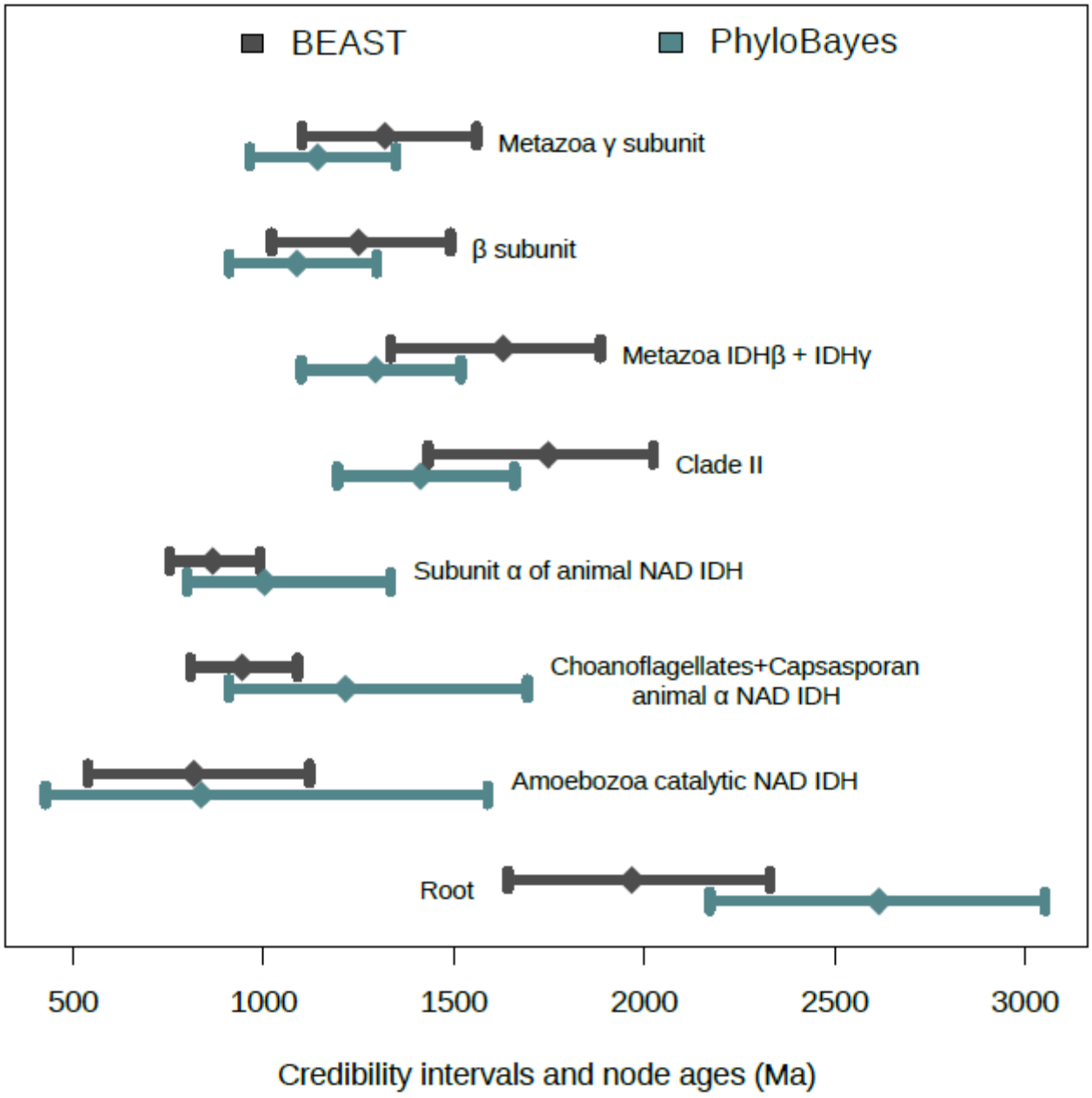

Supplementary Figure S3 – Credidibility intervals and node ages estimated based on a mixture model in PhyloBayes and ones inferred by BEAST.

Capítulo 2

O capítulo a seguir foi publicado no periódico *Geobiology* e está disponível em: https://doi.org/10.1111/gbi.12577

Referência: **Belato, F. A.**, Mello, B., Coates, C. J., Halanych, K. M., Brown, F. D., Morandini, A. C., de Moraes Leme, J., Trindade, R. I. F., & Costa-Paiva, E. M. (2023). Divergence time estimates for the hypoxia-inducible factor-1 alpha (HIF1α) reveal an ancient emergence of animals in low-oxygen environments. *Geobiology, 22*(1), 1–14.

Divergence time estimates for the hypoxia-inducible factor-1 alpha (HIF1α) reveal an ancient emergence of animals in low-oxygen environments

Flávia A. Belato[1], Beatriz Mello[2], Christopher J. Coates[3], Kenneth M. Halanych[4], Federico D. Brown[1], André C. Morandini[1], Juliana de Moraes Leme[5], Ricardo I. F. Trindade[6] & Elisa Maria Costa-Paiva[1,6*]

1. Institute of Biosciences, Department of Zoology, University of Sao Paulo, Brazil
2. Biology Institute, Genetics Department, Federal University of Rio de Janeiro, Brazil
3. Zoology, Ryan Institute, School of Natural Sciences, University of Galway, Galway, Ireland
4. Center for Marine Science, University of North Carolina Wilmington, USA.
5. Geoscience Institute, University of Sao Paulo, Brazil
6. Institute of Astronomy, Geophysics and Atmospheric Sciences, University of Sao Paulo, Brazil

Corresponding author: flavia.ariany@live.com

Abstract

Unveiling the tempo and mode of animal evolution is necessary to understand the links between environmental changes and biological innovation. Although the earliest unambiguous metazoan fossils date to the late Ediacaran period, molecular-clock estimates agree that the last common ancestor (LCA) of all extant animals emerged ~850 Ma, in the

Tonian period, before the oldest evidence for widespread ocean oxygenation at ~635–560 Ma in the Ediacaran period. Metazoans are aerobic organisms, i.e., they are dependent on oxygen to survive. In low-oxygen conditions, most animals have an evolutionarily conserved pathway for maintaining oxygen homeostasis that triggers physiological changes in gene expression via the hypoxia-inducible factor (HIFa). However, here we confirm the absence of the characteristic HIFa protein domain responsible for the oxygen sensing of HIFa in sponges and ctenophores, indicating the LCA of metazoans lacked the functional protein domain as well, and so could have maintained their transcription levels unaltered under the very low-oxygen concentrations of their environments. Using Bayesian relaxed molecular-clock dating, we inferred that the ancestral gene lineage responsible for HIFa arose in the Mesoproterozoic Era, ~1,273 Ma (Credibility Interval 957–1,621 Ma), consistent with the idea that important genetic machinery associated with animals evolved much earlier than the LCA of animals. Our data suggest at least two duplication events in the evolutionary history of HIFa, which generated three vertebrate paralogs, products of the two successive whole-genome duplications that occurred in the vertebrate LCA. Overall, our results support the hypothesis of a pre-Tonian emergence of metazoans under low-oxygen conditions, and an increase of oxygen response elements during animal evolution.

Introduction

Defining when metazoans first emerged is crucial to understanding the processes of early animal life. Although pre-Cambrian fossil records of animals remain scarce and controversial (e.g., debated organic biomarkers of sponges from the Cryogenian period (>635 Ma) and Tonian period, >890 Ma (Love *et al.*, 2009; Brain *et al.*, 2012; Antcliffe *et al.*,

2014; Yin *et al.*, 2015; Turner, 2021). The currently accepted earliest fossil record of an undisputed animal is from the late Ediacaran period ~571 Ma (Narbonne, 2005; Pu *et al.*, 2016; Droser *et al.*, 2017; Wood *et al.*, 2019). In contrast, most molecular clock estimates agree that the last common ancestor of all extant animals emerged ~850 Ma in the Tonian period, before the onset of long-term global glaciations (~720–635 Ma) (Erwin *et al.*, 2011; dos Reis *et al.*, 2015; Cunningham *et al.*, 2017; Dohrmann & Wörheide, 2017). Estimates for the timing of animal diversification, using different calibration points and molecular datasets, range from 1,298 to 615 Ma (Douzery *et al.*, 2004; Hedges *et al.*, 2004; Peterson *et al.*, 2004; Cartwright & Collins, 2007; Erwin *et al.*, 2011; Parfrey *et al.*, 2011; dos Reis *et al.*, 2015; Dohrmann & Wörheide, 2017). Nevertheless, almost all these molecular estimates place the emergence of animals long before the oldest evidence for ocean oxygenation pulses at ~635–560 Ma in the Ediacaran period (Sahoo *et al.*, 2012; Lenton & Daines, 2017; Zhang *et al.*, 2018; Wood *et al.*, 2019; Tostevin & Mills, 2020).

As strictly aerobic organisms, metazoans are dependent on oxygen as the main electron acceptor during oxidative metabolism for energy production (Semenza, 2007; Kaelin & Ratcliffe, 2008). Recent studies on the geochemistry of the ancient Earth suggest that Cryogenian to Ediacaran oceans had no more than 1–10% of modern atmospheric oxygen saturation (Lyons *et al.*, 2014; Lenton & Daines, 2017; Lenton, 2020; Liu *et al.*, 2021; Mills *et al.*, 2022), environmental low-oxygen levels could have limited metazoans by placing energetic constraints on the diversity, abundance, and physiology of early animals (Fenchel & Finlay, 1995; Reinhard *et al.*, 2016; Cole *et al.*, 2020). When exposed to hypoxia, most animals have an evolutionarily conserved pathway for maintaining physiological oxygen homeostasis that triggers adaptive changes in gene expression. This pathway is mediated by the transcription factor hypoxia-inducible factor 1

(HIF-1) (Semenza, 2007; Kaelin & Ratcliffe, 2008; Loenarz *et al.*, 2011). HIF1 consists of two subunits: an oxygen-regulated HIF1a and a constitutively expressed HIF1b (Aryl Hydrocarbon Receptor Nuclear Translocator, ARNT). Both subunits are composed of two basic helix–loop–helix (bHLH) and Per-ARNT-Sim (PAS) domains that allow subunit dimerization when cellular oxygen concentrations are low. They promote the transcription of hundreds of genes involved in mitochondrial function, energy metabolism, oxygen binding and delivery, and hematopoiesis (Semenza, 2007; Kaelin & Ratcliffe, 2008). HIFa is continuously synthesized and degraded when oxygen supply is sufficient (normoxia; Fig. 1). Prolyl hydroxylases (PHD) target defined proline residues (called the oxygen-dependent degradation domain, ODDD, on the HIF1a subunit (Fig. 2-A; Hon *et al.*, 2002), which are recognized by the von Hippel–Lindau (VHL) protein and promote the ubiquitination mediated proteasomal degradation of HIF1a (Min *et al.*, 2002; Semenza, 2007; Kaelin & Ratcliffe, 2008). Another hydroxylase, FIH1 (factor inhibiting HIF1), prevents the transcriptional activity of any HIF1a that has not been degraded (Peet & Linke, 2006; Semenza, 2007; Kaelin & Ratcliffe, 2008). During hypoxia, PHD and FIH1 are inactivated, and therefore, HIF1a is protected from degradation, accumulates within the cell, and dimerizes with HIF1b forming a heterodimeric HIF1a/HIF1b complex (Semenza, 2007). The complex translocates to the nucleus and up-regulates genes associated with oxygen conservation (Fig. 1; Semenza, 2007; Kaelin & Ratcliffe, 2008).

Although all animals need oxygen to survive, their demands are not the same. Sponges and ctenophores, which are likely sister groups to all remaining animal phyla (Pisani *et al.*, 2015; Whelan *et al.*, 2015; Halanych, 2016; King & Rokas, 2017), can live under low oxygen concentrations (Purcell *et al.*, 2001; Levin, 2003; Thuesen *et al.*, 2005;

Mosch *et al.*, 2012). Experimental outcomes demonstrated that these early-diverging clades lack key components of the HIF pathway, implying they have very low oxygen requirements (Mills *et al.*, 2014, 2018b). The last common ancestor of metazoans may also have lacked a functional HIF pathway and maintained aerobic metabolism and normal transcription in oxygen-poor environments (Mills *et al.*, 2018b). In support of this hypothesis, recent works have proposed that early animals were likely small, soft-bodied, collagen-poor, and restricted their use of oxygen to high-priority physiological functions (Mills & Canfield, 2014; Mills *et al.*, 2014; Cole *et al.*, 2020).

Molecular dating techniques, which consist of estimating the age of internal nodes of a phylogenetic tree based on molecular sequences using mainly fossil calibrations (Ho & Duchêne, 2014; Mello, 2018), have advanced tremendously in recent years. They are now considered standard methods to infer dates of divergence essential to elucidating evolutionary processes that led to the diversification of major taxa through Earth's geological history (Ho & Duchêne, 2014; Misof *et al.*, 2014; dos Reis *et al.*, 2015; Irisarri *et al.*, 2017; Delsuc *et al.*, 2018; Wolfe *et al.*, 2019). Divergence time estimates are applied to gene trees to infer the origin of various physiological modalities. Consequently, our understanding of the tempo and mode of early animal evolution can be enhanced by molecular dating of specific genes and proteins (Shih & Matzke, 2013; Yu & Li, 2014; Bezerra *et al.*, 2021; Boden *et al.*, 2021; Costa-Paiva *et al.*, 2021).

Herein, we explored divergence estimates for HIFa genes to elucidate their evolutionary history. Oxygen is crucial for all animals, as such, investigating the evolutionary history of a protein involved crucially in oxygen homeostasis, namely HIFa (Semenza, 2007), provides an effective source of knowledge on the emergence and diversification of animals. By applying a Bayesian uncorrelated relaxed clock to a HIFa

dataset with representative sampling of all major animal lineages, our data support a pre-Tonian emergence of the ancestral gene lineage that later originated metazoan HIFa, consistent with previous molecular clock estimates for an ancient origin of animals (Dohrmann & Wörheide, 2017).

Methods

1. Data acquisition

Sequences were obtained from three different sources: 1) WormNet II transcriptomes generated by our research group, 2) NCBI database, and 3) Mills *et al*. (2018b) and Graham and Presnell (2017) (all listed in Supplementary File 1). First, we used the transcriptomes of 77 metazoan species collected as part of the WormNet II project on annelid phylogeny (Weigert *et al*., 2014). Specimens were collected by several techniques, including intertidal sampling, dredging and box cores, and preserved either in RNALater or frozen at −80 °C. RNA extraction, cDNA library preparation, and high-throughput sequencing protocols followed Kocot *et al*. (2011) and Whelan *et al*. (2015). Subsequently, total RNA was extracted using TRIzol (Invitrogen) either from whole animals or from the body walls and purified with on-column DNase digestion of the RNeasy kit (Qiagen). The SMART cDNA Library Construction Kit (Clontech) was used to reverse transcribe the single-stranded RNA templates. The Advantage 2 PCR system (Clontech) was used to synthesize double-stranded cDNA. Barcoding and library sequencing were performed with Illumina technology by The Genomic Services Lab at the Hudson Alpha Institute (Huntsville, AL). Because transcriptomic sequencing was carried out from 2012 to 2015, paired-end runs were of 100 or 125 bp in length, using either v3 or v4 chemistry on Illumina HiSeq 2000 or 2500 platforms (San Diego, CA). Finally, to facilitate sequence assembly, paired-end transcriptome data were digitally normalized to an average k-mer coverage

of 30 using the script normalize-by-median.py (Brown *et al.*, 2012). Transcriptomes were assembled using Trinity r2013-02-25 with default settings (Grabherr *et al.*, 2011).

All transcriptomes were annotated using the Trinotate annotation pipeline (http://trinotate.github.io/) (Grabherr *et al.*, 2011). This pipeline uses a BLAST-based method against the EggNOG 4.5.1 v (Huerta-Cepas *et al.*, 2016) and KEGG (Kanehisa *et al.*, 2012) databases to provide the gene ontology annotations. Gene ontology is a standardized functional classification system for genes that describe properties of genes and their products using a dynamic-updated controlled vocabulary (Gene Ontology Consortium, 2004). Software used with the Trinotate pipeline included HMMER 3.2.1 for protein domain identification (Finn *et al.*, 2011); tmHMM 2.0 for prediction of transmembrane helices of proteins (Krogh *et al.*, 2001); RNAmmer 1.2 for prediction of ribosomal RNA (Lagesen *et al.*, 2007); SignalP 4.1 to predict signal peptide cleavage sites (Petersen *et al.*, 2011); GOseq for prediction of the gene ontology (Young *et al.*, 2010); EggNOG 4.5.1 for searching orthologous groups of genes (Huerta-Cepas *et al.*, 2016).

After Trinotate annotation, retrieved transcriptome sequences were verified to select sequences functionally assigned as hypoxia-inducible factor 1-alpha (HIF1a) genes. Sequences identified as HIF1a genes were translated from RNA into amino acids using TransDecoder with default settings (https://transdecoder.github.io/). TransDecoder translation can produce multiple open reading frames (ORFs), therefore, the homology between sequences was confirmed based on structural motif presence, validating the Pfam domain (Finn *et al.*, 2016) of translated protein sequences against the EMBL-EBI protein database with an e-value cutoff of 10^{-5}. Sequences with a minimum length of 300 amino acid residues with a verified bHLH-PAS domain were retained for further analysis. Because

HIF genes are part of the larger bHLH-PAS protein family, we only selected sequences that contained this domain.

Our second source of HIF1a sequences was the National Center for Biotechnology Information (NCBI) database. We searched for protein sequences functionally annotated as hypoxia-inducible factor 1-alpha on GenBank, focusing mainly on invertebrate sequences. "Putative", "Hypothetical", "Low-quality", and "partial" sequences were excluded, as well as those with fewer than 300 amino acids. Pfam domain validation (Finn *et al.*, 2016) with an e-value cutoff of 10^{-5} was performed and the presence of the bHLH-PAS domain was verified. To expand our dataset, we obtained 89 HIFa sequences from different metazoans, including vertebrates, from Mills *et al*. (2018b) using their HIFa project dataset (https://bitbucket.org/molpalmuc/sponge-oxygen/src/master/) and Graham and Presnell (2017) (https://doi.org/10.1371/journal.pone.0179545.s001). All sequence information is detailed in Supplementary file 1.

2. Alignments and phylogenetic reconstructions

Sequences (n=218) were aligned in MAFFT using the E-INS-I algorithm (Katoh & Standley, 2013), and gap-rich regions were removed in trimAl 1.2 (Capella-Gutierrez *et al.*, 2009) using a gap threshold of 0.75. To remove spuriously aligned sequences based on similarity to the alignment, sequences were manually inspected with Geneious 11.1.2 (Kearse *et al.*, 2012). To eliminate dataset redundancy, identical sequences were removed. The resulting amino acid alignment of 136 sequences was analyzed further.

Statistical selection of the best-fit model of protein evolution was carried out using the Akaike and Bayesian Information Criteria (AIC and BIC, respectively; Darriba *et al.*, 2011) with ModelFinder in IQ-Tree

software (Kalyaanamoorthy *et al.*, 2017). Two different phylogenetic inference methods were employed in our analysis: (1) a maximum likelihood routine in IQ-Tree (Nguyen *et al.*, 2015) with 1,000 ultrafast bootstrap replicates (UFBoot; Minh *et al.*, 2013); and (2) Bayesian inference using MrBayes 3.2.7 (Ronquist & Huelsenbeck, 2003) with two independent runs, each containing four Metropolis-coupled chains of 10^7 generations that were sampled every 500th generation to approximate posterior distributions. To confirm whether chains achieved stationarity, and to determine an appropriate burn-in, we evaluated trace plots of all MrBayes parameter outputs in Tracer v1.6 (Rambaut *et al.*, 2015). The first 25% of samples were discarded as burn-in and a majority rule consensus tree was generated using MrBayes. Bayesian posterior probabilities were used to gauge the statistical support of each bipartition. Because of the evolutionary time depth of our dataset, phylogenetic reconstruction was also performed with a mixture model in IQ-Tree to help alleviate the issues related to saturation and long-branch attraction by accommodating site-specific features of protein evolution (Lartillot & Philippe, 2004; Lartillot *et al.*, 2007). To consider heterogeneity at the site level in the Bayesian reconstruction, we ran an analysis in PhyloBayes (Larillot et al., 2009) using the CAT-GTR mixture model. The program was run twice to check for convergence of the chains, which was accessed by the maxdiff value (maxdiff was <0.1). Trees were visualized in FigTree 1.4.3 (Rambaut, 2009) and rooted using two bHLH-PAS protein sequences of the single-celled eukaryotic outgroup, *Capsaspora owczarzaki* (Suga *et al.*, 2013; Mills *et al.*, 2018b).

3. Molecular dating

BEAST 2.4.7 (Bouckaert *et al.*, 2014) was used to obtain divergence time estimates with an uncorrelated lognormal relaxed clock (Drummond

et al., 2006), the LG substitution model (Whelan & Goldman, 2001) and a birth-death tree prior with default settings. As calibration information derived from fossil data provides information regarding the split times between biological lineages (i.e., speciation events), only speciation nodes were considered to calibrate divergence times. Therefore, divergences classified as speciation nodes that reflected robust biological clades and were free of duplication events were chosen. These were the LCA of seven crown nodes: Vertebrata, Actinopterygii, Sarcopterygii (including Tetrapoda), Ambulacraria, Mollusca, Pancrustacea, and Cnidaria. For Actinopterygii and Sarcopterygii, the requirements cited above were met three times (i.e., speciation nodes that included only Actinopterygii or Sarcopterygii HIFa sequences were recovered three times each in the estimated phylogeny). Therefore, 11 speciation nodes were calibrated with uniform distributions with lower and upper boundaries based on calibration information from Benton *et al*. (2015) and dos Reis *et al*. (2015).

The date range (minimum and maximum boundaries of the uniform distributions) used to calibrate the time of the Most Recent Common Ancestor (tMRCA) for Vertebrata was 457.5–636.1 Ma, for Actinopterygii 378.19–422.4 Ma, for Sarcopterygii 408–427.9 Ma, for Ambulacraria 515.5–636.1 Ma, for Mollusca 534–549 Ma, for Pancrustacea 514–531.22 Ma, and for Cnidaria 529–636.1 Ma. All calibration points were obtained from dos Reis *et al*. (2015) and Benton *et al*. (2015) using coherent criteria accordingly with Parham *et al.* (2012). Notably, calibrated nodes were constrained to be monophyletic, while other phylogenetic relationships were estimated in BEAST. Markov Chain Monte Carlo (MCMC) was run for 200 million generations with a sampling frequency of 10,000 and a discarded burn-in period of 20 million generations (10%). To access the convergence of chains, two independent MCMC runs were performed. In

both runs, after discarding the burn-in period, effective sample sizes (ESS) values were higher than 200. The resulting timetree was plotted using the 'geoscalePhylo' function ('strap' R v.4.0.3 package; Bell & Lloyd, 2015) and modified using Inkscape v1.1.1.

To verify the robustness of the divergence times estimates generated in BEAST, we performed molecular dating analyses using different parameters in MCMCTree (Yang, 2007). MCMCTree analyses were performed using the fixed topologies obtained in BEAST and IQ-Tree. We considered independent and correlated evolutionary rates, and an additional calibration at the root, which was a soft maximum of 833 Ma, based on dos Reis et al. (2015) and Benton et al. (2015). All MCMCTree analyses were conducted under the approximate likelihood calculation method (dos Reis and Yang, 2011), with at least two chains to check for convergence.

Results

The final dataset consisted of 134 HIFa sequences (Supplementary file 1) from 115 metazoan species and two bHLH-PAS sequences (outgroup) from the unicellular eukaryotic filozoan *Capsaspora owczarzaki* (Suga *et al.*, 2013; Mills *et al.*, 2018b). After alignments and trimming, the final alignment had a maximum sequence length of 416 amino acids (Supplementary file 2, and https://figshare.com/s/54350fa8b7573951990b). Untrimmed sequences are available in Supplementary file 3 and at https://figshare.com/s/f14d22a30cb636d0bd93. The 33 sequences obtained from the WormNet II database were deposited at GenBank under accessions OQ354979–OQ355011. The best fitting standard substitution model for both Bayesian and maximum likelihood analyses according to ModelFinder was WAG (Whelan & Goldman, 2001). The best maximum

likelihood mixture model was LG+C40+F+G. Phylogenetic reconstructions performed with mixture models (IQ-Tree mixture model tree file available at https://figshare.com/s/0369cceffa0947d93ca8 and PhyloBayes mixture model tree file available at https://figshare.com/s/a6b98a40d0949dc60750) were in agreement with Bayesian and maximum likelihood phylogenies based on site-homogeneous substitution models (Supplementary files 4 and 5). All datasets, alignments, and tree files used in this work are publicly available at https://figshare.com/projects/Divergence_time_estimates_for_the_hypoxia-inducible_factor-1_alpha_HIF1_reveal_an_ancient_emergence_of_animals_in_low-oxygen_environments/164017.

All HIFa proteins have a characteristic motif with a key proline residue (preceded by an alanine) that signals the protein for degradation, this region is called the oxygen-dependent degradation domain (ODDD) (Fig. 2-A; Tarade *et al.*, 2019). The motif varies between clades, where the LA**P**Y motif in vertebrate HIFa is instead RA**P**Y in most protostomes, RA**P**Y or RA**P**F in cnidarians, and LA**P**F in placozoans (Fig. 2B-E). None of these motifs were found in the five sponge and single ctenophore homolog sequences retrieved from the transcriptomes we queried.

Bayesian and maximum likelihood inferences generated similar tree topologies with several strongly supported clades (Fig. 3; Supplementary files 4 and 5). The main difference was the Bayesian tree presented some poorly resolved nodes in Arthropoda and Mollusca (Supplementary file 4), whereas the maximum likelihood inference recovered strongly supported nodes in those clades. The position of both sponges and ctenophore in the tree suggests that sequences of sponges and ctenophore are sisters to all HIFa proteins (Fig. 3). Although all metazoan sequences formed a

monophyletic group, the absence of the characteristic HIFa domain in the five sponge and single ctenophore sequences suggests they are not true HIFa due to the absence of an ODDD motif, as previously suggested by Mills *et al.* (2018b).

HIFa sequences that clustered into monophyletic groups, representing recognized phyla, with strong statistical support were the placozoans (100%; PP=1; clade XII; Fig. 3), cnidarians (100%; PP=1; clade XI; Fig. 3), arthropods (93%; clade X; Fig. 3), phoronids (100%; PP=1; clade IX; Fig. 3), brachiopods (86%; clade VIII; Fig. 3), mollusks (96%; clade VII; Fig. 3), hemichordates (87%; PP=1; clade VI; Fig. 3), echinoderms (100%; PP=1; clade V; Fig. 3), and cephalochordates (100%; PP=1; clade IV; Fig. 3). A single nemertine sequence fell within annelids rendering Annelida non-monophyletic (Fig. 3). Notably, the *Ciona intestinalis* sequence fell in an odd position within the tree (Fig. 3). However, we chose to maintain this sequence because other works analyzed it and yielded similarly unusual results (Graham & Presnell, 2017; Mills *et al.*, 2018b). We considered the position of *C. intestinalis* as an artifact that needs further investigation (Fig. 3). Importantly, tunicate sequences have high rates of substitution (Tsagkogeorga *et al.*, 2009, 2012; Berná & Alvarez-Valin, 2014).

According to our gene genealogy obtained for the HIFa family, vertebrate HIFa arose from a series of duplication events that brought about three distinct vertebrate HIFa clades: HIF1a, HIF2a, and HIF3a (Clades I, 100%; PP=1; II, 100%; PP=1; and III, 100%; PP=1; Fig. 3). Up to five HIFa protein sequences were identified in vertebrate specimens (e.g., zebrafish *Danio rerio*), and these paralogs most likely resulted from multiple genome duplication events that occurred in the vertebrate stem lineage, and signatures of the two rounds of vertebrate genome duplication can be clearly seen in the HIFa gene tree (arrows and asterisks, Fig. 3).

Additional paralogs seen in *D. rerio* were most likely a result of the teleost-specific whole-genome duplication (Glasauer & Neuhauss, 2014).

The tree topology estimated by BEAST was mostly congruent with those obtained by IQ-Tree and MrBayes (Fig. 4, tree file available at https://figshare.com/s/72173e8c3b390ac9c55a). The posterior distributions of estimated node ages were wide, probably due to the short alignment length. Therefore, all the estimated times are reported along with their credibility intervals (CrIs). The estimated age for the LCA gene that later gave rise to the gene lineage including metazoan HIFa genes, sponge homologs, and ctenophore homologs was ~1,273 Ma (Credibility Interval (CrI) 957–1,621 Ma) in the Mesoproterozoic (Fig. 4). Cnidarian and placozoan HIFa sequences diverged from sponges and ctenophores homologs at 1,218 Ma (CrI 760–1,331 Ma). The bilaterian HIFa lineage originated at 959 Ma (CrI 801–1,122 Ma) in the Neoproterozoic Era (Fig. 4). The estimated time of the emergence of cnidarian HIFa was 594 Ma (CrI 541–636 Ma) in the Ediacaran Period. The divergence time estimated for the appearance of arthropodan HIFa occurred at 651 Ma (CrI 522–788 Ma) in the Cryogenian Period, with mollusk HIFa emerging at 541 Ma (CrI 534–548 Ma) in the Ediacaran Period. The deuterostome HIFa lineage originated at 748 Ma (CrI 652–842 Ma) in the Cryogenian Period. Two duplication events occurred in the vertebrate HIFa lineage (grey circles, Fig. 4), both in the Ediacaran Period. The first event gave rise to vertebrate HIF2a and the lineage that would originate HIF1a + HIF3a occurred at 595 Ma (CrI 550–636 Ma). Subsequently, the second duplication event at 558 Ma (CrI 500–604 Ma) led to the appearance of vertebrate HIF1a and HIF3a.

Divergence time estimates obtained in MCMCTree using distinct fixed topologies (from BEAST and IQ-Tree), substitution rate models and the inclusion of a soft maximum calibration at the tree root showed high

congruence with those obtained originally in BEAST (Supplementary file 6). Divergence dates inferred for relevant nodes such as the root, the divergence of sponge and ctenophore homologs from all other animals, and the gene duplication events in vertebrates were mostly congruent among all analyses. Estimates obtained with MCMCTree validated those retrieved by BEAST, which demonstrates the consistency of our results (regardless of the selected models).

Discussion

Our results demonstrate the ancestral gene lineage that originated the metazoan HIFa emerged at approximately 1,273 Ma (CrI 957–1,621 Ma) in the Mesoproterozoic Era (Fig. 4), earlier than the dawn of metazoans. Additionally, we unveiled two duplication events in the evolutionary history of HIFa, ~595 Ma (CrI 550–636 Ma) and ~558 Ma (CrI 500–604 Ma) (Fig. 4), generating three vertebrate HIFa paralogs. Although a functional HIFa appeared after the split of all other animals from sponges and ctenophores (Mills *et al.*, 2018b), as corroborated by our results, the molecular toolkit of HIFa was most likely present in metazoan ancestors. An important fraction of the molecular genetic toolkit required for animal development evolved much earlier in their eukaryotic unicellular ancestors (Sebé-Pedrós *et al.*, 2011, 2012; de Mendoza *et al.*, 2013). In fact, homologs of bHLH-PAS proteins were already present in the LCA of *Capsaspora*, choanoflagellates, and metazoans (Opisthokonta) between 1,389–1,240 Ma (Simionato *et al.*, 2007; Degnan *et al.*, 2009; Parfrey *et al.*, 2011; Sebé-Pedrós *et al.*, 2011, 2012), which complements with our results. During metazoan evolution, bHLH-PAS proteins were cooptated, resulting in new cellular pathways and function (Kaelin & Ratcliffe, 2008; Rytkönen *et al.*, 2011; Sebé-Pedrós *et al.*, 2011; Rodriguez-Pascual & Slatter, 2016).

A functional HIFa emerged most likely in the Mesoproterozoic Era, as showed by both BEAST (Fig. 4) and MCMCTree divergence estimates (node 8 in Supplementary file 6). HIFa proteins have their availability and therefore activity regulated by oxygen variation within the cells (Min *et al.*, 2002; Semenza, 2007; Kaelin & Ratcliffe, 2008). They are sensitive to oxygen due to their unique oxygen-dependent degradation domain (ODDD), which has a key proline residue (preceded by an alanine) that signals the HIFa protein for degradation in the presence of oxygen (Fig. 2-A; Hon et al., 2002; Tarade et al., 2019). We did not find the characteristic HIFa motif (ODDD) in ctenophore and sponge sequences, which corroborate the reports of Mills *et al.* (2018b) who suggest the organisms are not expected to respond to oxygen availability, and therefore, HIFa protein absence is expected.

Although atmospheric oxygen accumulated during the Great Oxidation Event (2.5–2.3 billion years ago (Ga; Kump, 2008), it remained at low levels throughout the Palaeoproterozoic and Mesoproterozoic Eras (2.5–1.0 Ga; Farquhar et al., 2000). Before rising to modern oxygen levels in the Neoproterozoic (1.0–0.54 Ga; Och and Shields-Zhou, 2012). Recent proxy records of atmospheric oxygen and marine redox states suggest dynamic pulses of oxygenation against a background of gradually rising oxygen levels through this Era (Neoproterozoic Oxygenation Windows – NOW; Wood *et al.*, 2019; Tostevin & Mills, 2020), instead of a single oxygenation event as proposed before (Canfield *et al.*, 2007; Sperling *et al.*, 2015). These events generated oxygen concentration levels that facilitated the metabolic needs of larger, more complex animals (Canfield *et al.*, 2007). Larger-bodied animals have higher oxygen demands, but interestingly, regions of the body where embryonic and progenitor cells occur are generally hypoxic (Hammarlund *et al.*, 2018; Nakamura *et al.*, 2021). To meet the energetic and structural demands of larger animals,

oxygen is necessary to maintain ATP production through the mitochondrial respiratory chain, and to synthesize collagen (Semenza, 2007; Sperling *et al.*, 2013; Mills & Canfield, 2014). Hypoxic periods in animal evolution – generated by changes in the carbon cycle and oceanic redox conditions of the Cryogenian–Cambrian interval (Canfield and Farquhar, 2009; Li et al., 2015; Lenton and Daines, 2017, 2018) – may have resulted in driven distinct adaptations to regulate aerobic metabolism, which is consistent with the emergence of a bilaterian HIFa ca. 959 Ma (CrI 801–1,122 Ma) in the Neoproterozoic Era (Fig. 4).

Atmospheric oxygen levels may have provided a selection force on the development of cellular oxygen-sensing pathways (Taylor & McElwain, 2010; Mills *et al.*, 2018b). Hypoxia influences gene expression, the level of epigenetic modifications in cells, and is considered to play an essential role in early embryo development, cell differentiation, stem cell renewal, and cellular reprogramming (Dunwoodie, 2009; Tsuji *et al.*, 2014; Wang *et al.*, 2016; Alderman *et al.*, 2019; Nakamura *et al.*, 2021; Song *et al.*, 2021). In plants and animals, low levels of oxygen are required to maintain the undifferentiated state of cells and influence their proliferation and cell fate (Simon & Keith, 2008; Weits *et al.*, 2019; Nakamura *et al.*, 2021), therefore, HIFa is hypothesized as essential for the evolution, and control of stem cells during the origin and evolution of metazoans (Hammarlund *et al.*, 2018; Hammarlund, 2020). Although all metazoans – except Ctenophora and Porifera – express HIF1a, PHD, and VHL (Tarade *et al.*, 2019), the presence of stem cells in low oxygen environments in the bodies of marine invertebrates is largely undocumented. Investigating whether these animal cell types have retained a symplesiomorphic state of early primordial metazoan cell types, which presumably evolved a capacity to replicate and differentiate into cells that are more complex during hypoxic periods of the Neoproterozoic, would be

the next step to advance this topic (Hammarlund *et al.*, 2018; Mills *et al.*, 2018a; Nakamura *et al.*, 2021). Sponge, cnidarian, and other marine invertebrate can de-differentiate or trans-differentiate (Gold & Jacobs, 2013; Adamska, 2018; Ferrario *et al.*, 2020), therefore, it has been hypothesized that hypoxia and HIFa are involved in the fine-tuning of stem cell plasticity and development (Hammarlund, 2020).

Up to three HIFa proteins were identified in vertebrates, with *D. rerio* having five HIFa genes (Supplementary file 1, Fig. 3). Herein, the gene genealogy of HIFa (Fig. 3 and 4) supports the existence of three HIF paralogs in extant vertebrates that are most likely products of the two successive whole-genome duplications (WGD) events from 700–450 Ma in the LCA of vertebrates (Panopoulou & Poustka, 2005; Kuraku *et al.*, 2008; Sacerdot *et al.*, 2018; Simakov *et al.*, 2020). Estimated ages for the duplication events that originated the three vertebrate paralogs, ~595 Ma (CrI 550–636 Ma) and ~558 Ma (CrI 500–604 Ma) (Fig. 4), coincide with both WGD events. The additional paralog seen in *D. rerio* may be a result of the teleost-specific WGD, 450–300 Ma (Hoegg *et al.*, 2004; Panopoulou & Poustka, 2005; Crow *et al.*, 2006; Desvignes *et al.*, 2021).

Our findings differ somewhat from Rytkönen *et al.* (2011), Graham and Presnell (2017), and Mills *et al.* (2018b), which describe HIF1a and HIF2a as more closely related to each other than HIF3a. Our phylogeny (Fig. 3) indicates the ancestral HIFa first duplicated to preHIF1/3 and HIF2a. In the second round, preHIF1/3 duplicated to HIF1a and HIF3a. Uncertainties in the evolutionary origin of genes that were duplicated in the vertebrate WGDs have already been observed in other proteins, e.g., fibrillar collagens and lysyl oxidases (Rodriguez-Pascual & Slatter, 2016), and just like HIF, they linked intimately to oxygen metabolism (Mills & Canfield, 2014; Rodriguez-Pascual & Slatter, 2016; Cole *et al.*, 2020). A fourth HIFa paralog (HIF4a) has been described, mostly for fishes (Law et

al., 2006; Rytkönen et al., 2008; Graham & Presnell, 2017). However, given the absence of a clear phylogenetically related HIF4a group in our gene tree, it can be hypothesized the HIF4a paralog was most likely pseudogenized and then lost at some point in vertebrate evolution. Such steps are common in gene duplication events, where some duplicates may undergo neofunctionalization, subfunctionalization, or gene loss (Mighell et al., 2000; Zhang, 2003).

Conclusions

Our results support the hypothesis of a pre-Tonian emergence of metazoans when low-oxygen conditions prevailed. The emergence of metazoan HIFa in the Mesoproterozoic Era implies that the molecular toolkit encoding hypoxia-response elements like HIF was already present in the ancestors of metazoans. We demonstrate that at least two duplication events took place along the evolutionary history of HIFa, generating HIF1a, HIF2a, and HIF3a in vertebrates. Those paralogs probably originated from the multiple rounds of genome duplications in the vertebrate stem lineage. Our study highlights the importance of molecular dating estimates of proteins as a powerful tool for understanding the evolution of these crucial ancient protein families which are intertwined with early major lineages.

Data Availability

The data that support the findings of this study are openly available within the article, its supplementary materials, and in Figshare at https://figshare.com/projects/Divergence_time_estimates_for_the_hypoxia-inducible_factor-1_alpha_HIF1_reveal_an_ancient_emergence_of_animals_in_low-oxygen_environments/164017.

Acknowledgments

This study was supported by FAPESP thematic project (Proc. 2016/06114-6), coordinated by R.I.T. A fellowship to E.M.C-P. was provided by FAPESP (Fundação de Amparo à Pesquisa do Estado de São Paulo, Brazil – Proc. 2018/20268-1). F.A.B. was funded by CNPq and FAPESP (Procs. 2019/18051-7 and 2021/14115-0). Use of SkyNet computational resources at Auburn University is acknowledged. This work was also funded in part by National Science Foundation (grants DEB–1036537 to K.M.H. and Scott R. Santos and OCE–1155188 to K.M.H.), and FAPESP JP grant 2015/50164-5 to F.D.B.

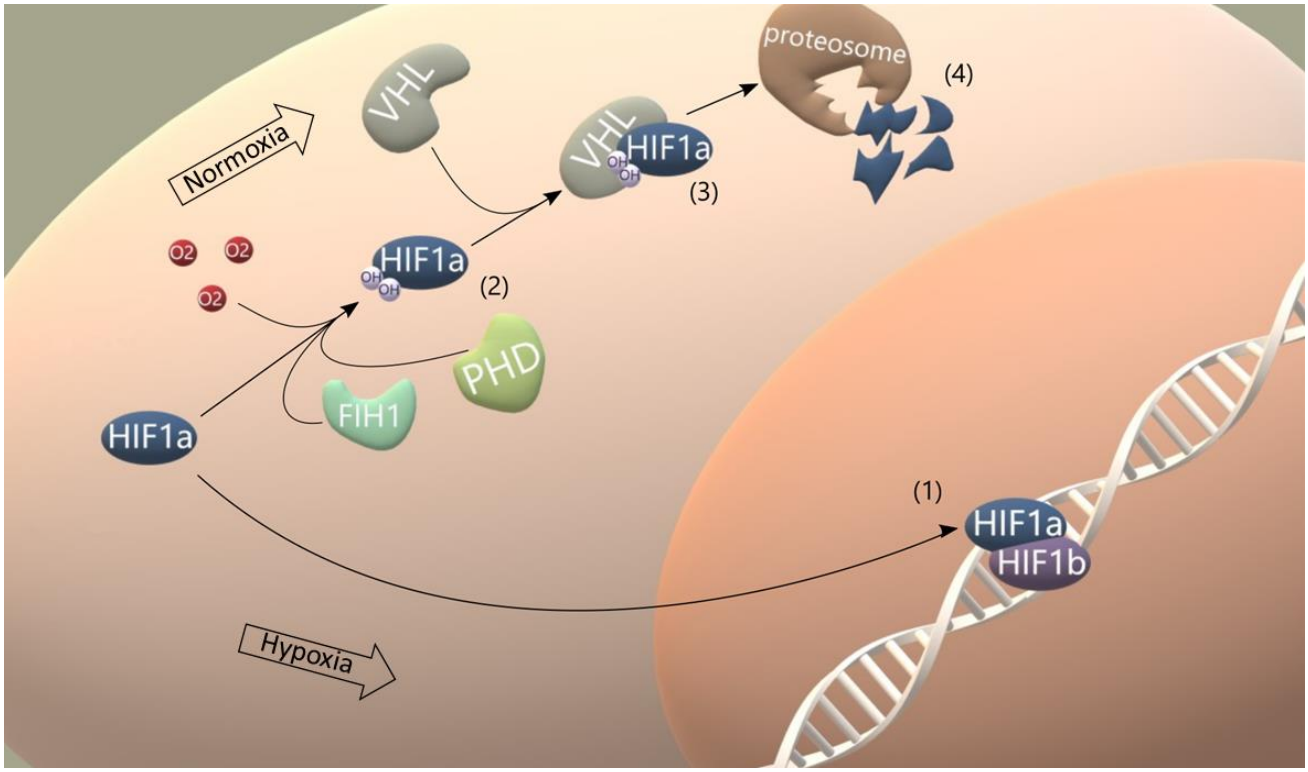

Figure 1 – The hypoxia-inducible factor pathway. When oxygen levels are sufficient oxygen is available (normoxia), HIF1a subunit is continuously synthesized and degraded. Two hydroxylases, prolyl hydroxylases (PHD) and factor inhibiting HIF1 (FIH1), hydroxylate the HIF1a subunit (2). The von Hippel–Lindau (VHL) protein recognizes the hydroxyls (3) and promotes the ubiquitination and immediate degradation of HIF1a via the proteasome (4). These processes are inhibited when oxygen is low (hypoxia) due to hydroxylase inactivation leading to a rapid stabilization of HIF1a, which is protected from degradation, accumulates within the cytoplasm, binds to HIF1b (1), forms the transcriptionally active HIF heterodimer, and enters the nucleus.

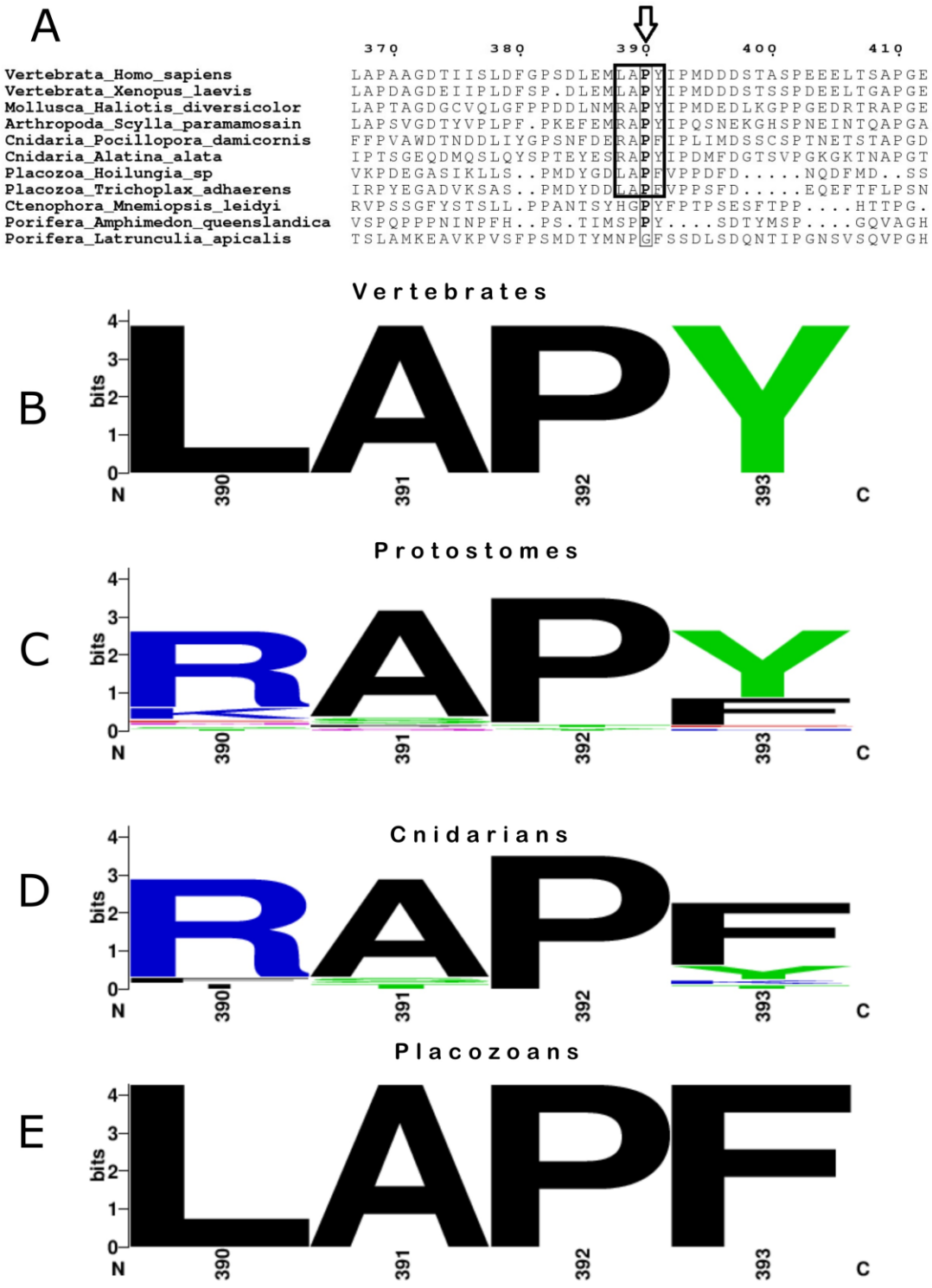

Figure 2 – Characteristic HIFa domain in metazoans. (A) Multiple amino acid sequence alignment of positions surrounding the HIFa oxygen-dependent degradation domain (ODDD) in metazoans. The domain is indicated by the black bold box. Invariant amino acid residues are marked in bold. We do not find the ODDD motif in any sponge or ctenophore sequences. (B) Sequence logo of the position weight matrix of the ODDD from our 35 vertebrate sequences. (C) Sequence logo of the position weight matrix of the ODDD from our 47 protostome sequences. (D) Sequence logo of the position weight matrix of the ODDD from our 18 cnidarian sequences. (E) Sequence logo of the position weight matrix of the ODDD from our two placozoan sequences. Sequence logos were obtained using WebLogo (Crooks et al., 2004).

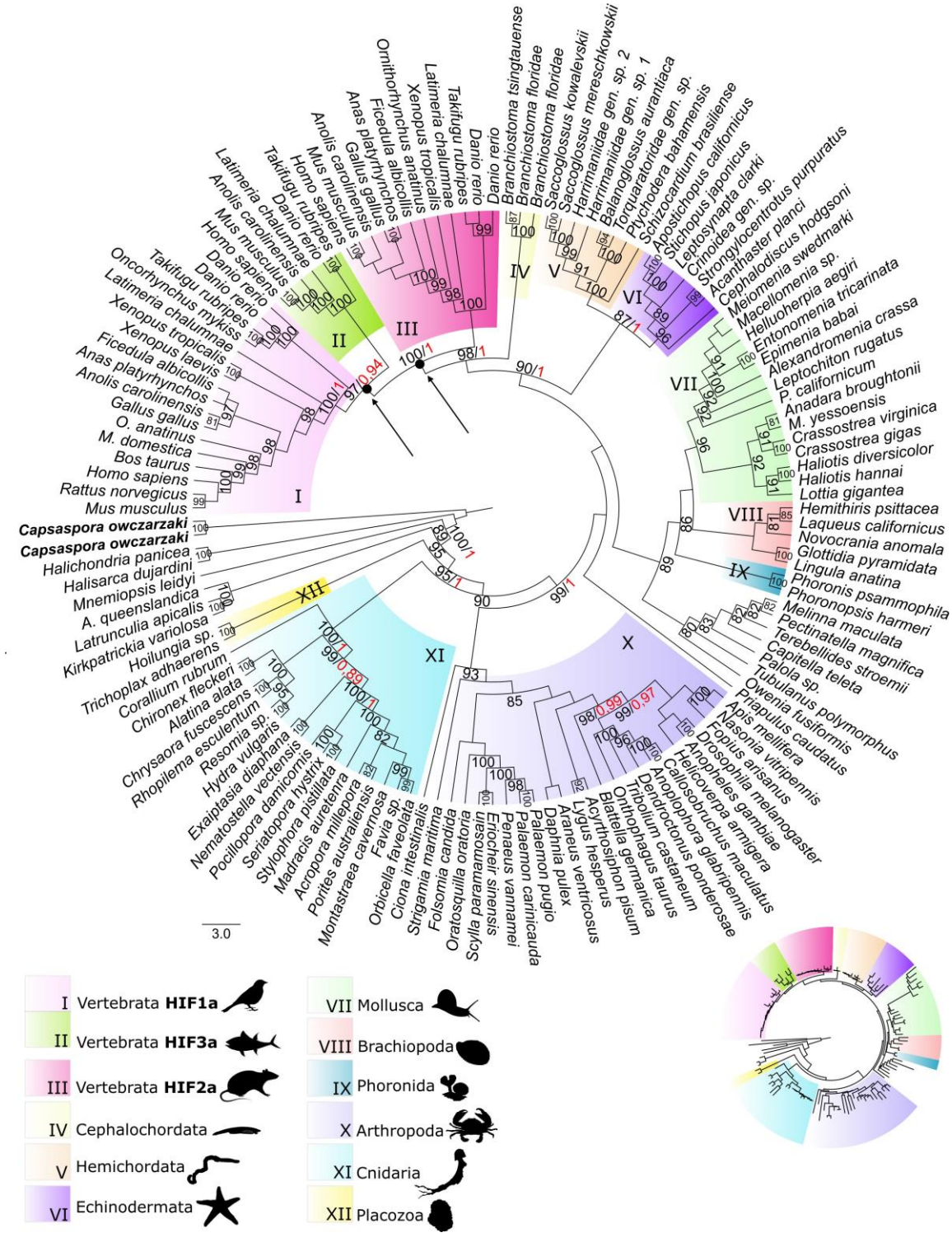

Figure 3 – HIFa gene tree rooted with two capsasporan bHLH-PAS protein sequences. Clade I contains vertebrate HIF1a sequences. Clade II is composed by vertebrate HIF3a sequences. Clade III is formed by vertebrate HIF2a sequences. Clade IV represents cephalochordate HIFa genes. Clade V is composed by hemichordate HIFa sequences. Clade VI contains echinoderm HIFa genes. Clade VII represents mollusk HIFa sequences. Clade VIII is formed by brachiopods HIFa sequences. Clade IX contains phoronids HIFa genes. Clade X represents arthropods HIFa genes. Clade XI is composed by cnidarian HIFa genes. Clade XII represents placozoan HIFa genes. Black arrows and dots indicate gene duplication events. Bootstrap support values (in black) obtained from the maximum likelihood and the Bayesian posterior probabilities values (in red) shown (BP/PP). Support values >80 or 0.8 are shown. Sequences in bold represent the two capsasporan bHLH-PAS proteins used to root the tree. Inset; small topology showing branch lengths with the same color scheme.

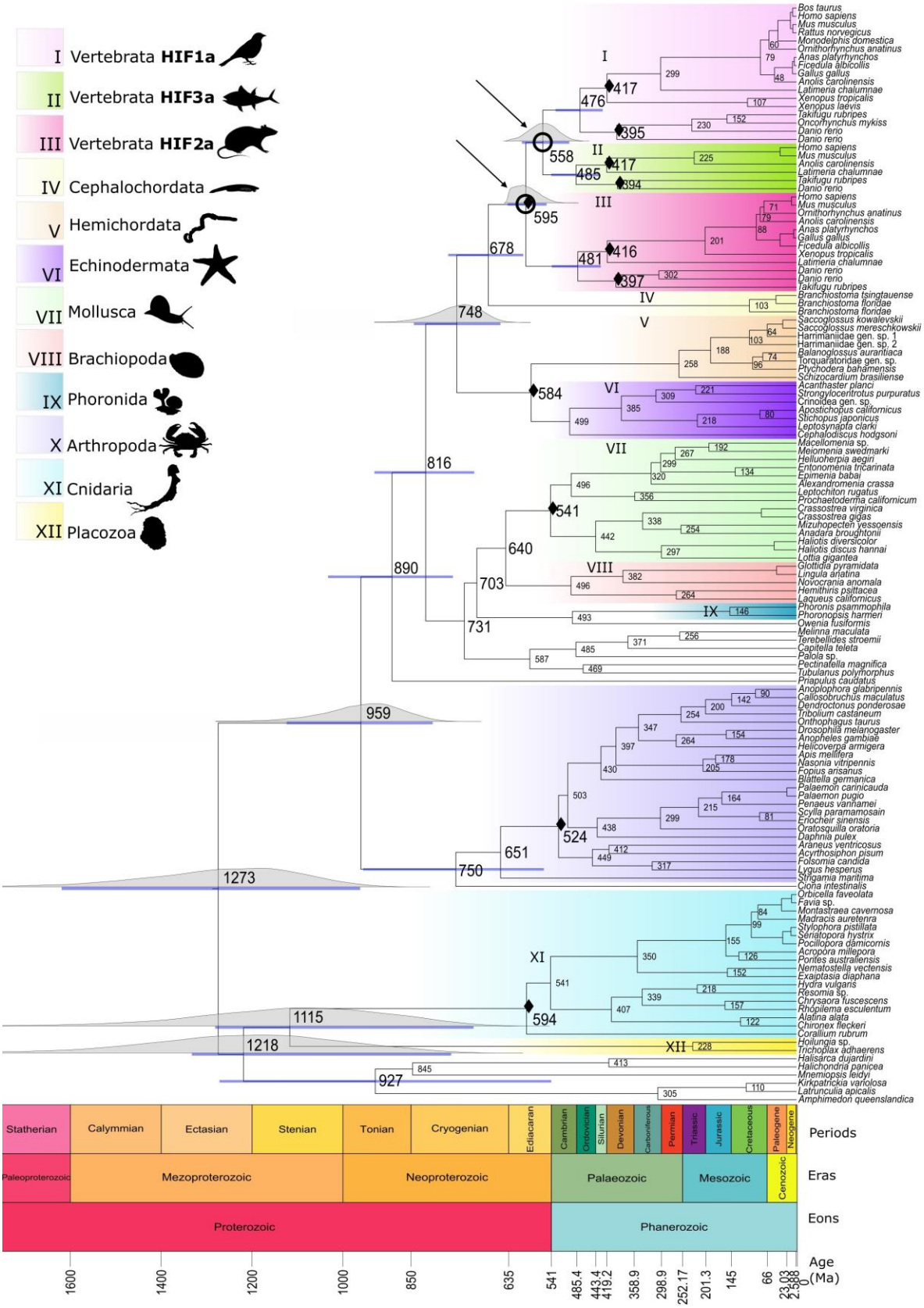

Figure 4 – Timetree of the HIFa genes. Clade I contains vertebrate HIF1a sequences; Clade II is vertebrate HIF3a sequences; Clade III is vertebrate HIF2a sequences; Clade IV represents cephalochordate HIFa sequences; Clade V is hemichordate HIFa sequences; Clade VI is echinoderm HIFa genes; Clade VII represents mollusk HIFa sequences; Clade VIII is brachiopods HIFa sequences; Clade IX contains phoronids HIFa sequences; Clade X represent arthropod HIFa; Clade XI is cnidarian HIFa sequences; Clade XII represents placozoan HIFa; Black arrows and circles indicate gene duplication events. Black diamonds indicate calibration nodes. Node ages are plotted, blue node bars are displaying 95% CrI and above them density plots highlighting the posterior distribution of node age estimates are shown for key nodes.

References

Adamska, M. (2018). Differentiation and transdifferentiation of sponge cells. In M. Kloc & J. Kubiak (Eds.). *Marine organisms as model systems in biology and medicine. Results and problems in cell differentiation*. (pp. 229–253). Cham: Springer.

Alderman, S. L., Crossley, D. A., Elsey, R. M., & Gillis, T. E. (2019). Hypoxia-induced reprogramming of the cardiac phenotype in American alligators (*Alligator mississippiensis*) revealed by quantitative proteomics. *Scientific Reports, 9*(1), 1–12.

Antcliffe, J. B., Callow, R. H. T., & Brasier, M. D. (2014). Giving the early fossil record of sponges a squeeze. *Biological Reviews, 89*(4), 972–1004.

Bell, M. A., & Lloyd, G. T. (2015). strap: an R package for plotting phylogenies against stratigraphy and assessing their stratigraphic congruence. *Palaeontology, 58*(2), 379–389.

Benton, M., Donoghue, P., Vinther, J., Asher, R., Friedman, M., & Near, T. (2015). Constraints on the timescale of animal evolutionary history. *Palaeontologia Electronica, 18*(1), 1–107.

Berná, L., & Alvarez-Valin, F. (2014). Evolutionary genomics of fast evolving tunicates. *Genome Biology and Evolution, 6*(7), 1724–1738.

Bezerra, B. S., Belato, F. A., Mello, B., Brown, F., Coates, C. J., de Moraes Leme, J., Trindade, R. I. F., & Costa-Paiva, E. M. (2021). Evolution of a key enzyme of aerobic metabolism reveals Proterozoic functional subunit duplication events and an ancient origin of animals. *Scientific Reports, 11*(1), 1–11.

Boden, J. S., Konhauser, K. O., Robbins, L. J., & Sánchez-Baracaldo, P. (2021). Timing the evolution of antioxidant enzymes in cyanobacteria. *Nature Communications, 12*(1), 1–12.

Bouckaert, R., Heled, J., Kühnert, D., Vaughan, T., Wu, C.-H., Xie, D., Suchard, M. A., Rambaut, A., & Drummond, A. J. (2014). BEAST 2: a software platform for bayesian evolutionary analysis. *PLoS Computational Biology, 10*(4), 1–6.

Brain, C. K., Prave, A. R., Hoffmann, K.-H., Fallick, A. E., Botha, A., Herd, D. A., Sturrock, C., Young, I., Condon, D. J., & Allison, S. G. (2012). The first animals: ca. 760-million-year-old sponge-like fossils from Namibia. *South African Journal of Science, 108*(1/2), 1–8.

Brown, C. T., Howe, A., Zhang, Q., Pyrkosz, A. B., & Brom, T. H. (2012). A reference-free algorithm for computational normalization of shotgun sequencing data. *arXiv preprint, 1*, 1–18. bioRxiv: 10.48550/arXiv.1203.4802.

Canfield, D. E., & Farquhar, J. (2009). Animal evolution, bioturbation, and the sulfate concentration of the oceans. *Proceedings of the National Academy of Sciences, 106*(20), 8123-8127.

Canfield, D. E., Poulton, S. W., & Narbonne, G. M. (2007). Late-Neoproterozoic deep-ocean oxygenation and the rise of animal life. *Science, 315*(5808), 92–95.

Capella-Gutierrez, S., Silla-Martinez, J. M., & Gabaldon, T. (2009). trimAl: a tool for automated alignment trimming in large-scale phylogenetic analyses. *Bioinformatics, 25*(15), 1972–1973.

Cartwright, P., & Collins, A. (2007). Fossils and phylogenies: Integrating multiple lines of evidence to investigate the origin of early major metazoan lineages. *Integrative and Comparative Biology, 47*(5), 744–751.

Cole, D. B., Mills, D. B., Erwin, D. H., Sperling, E. A., Porter, S. M., Reinhard, C. T., & Planavsky, N. J. (2020). On the co-evolution of surface oxygen levels and animals. *Geobiology, 18*(3), 260–281.

Costa-Paiva, E. M., Mello, B., Bezerra, B. S., Coates, C. J., Halanych, K. M., Brown, F., Leme, J., & Trindade, R. I. F. (2021). Molecular dating of the blood pigment hemocyanin provides new insight into the origin of animals. *Geobiology, 20*(3), 333–345.

Crooks, G. E., Hon, G., Chandonia, J., & Brenner, S. (2004). WebLogo: a sequence logo generator. *Genome research, 14*(6), 1188–1190.

Crow, K. D., Stadler, P. F., Lynch, V. J., Amemiya, C., & Wagner, G. P. (2006). The "fish-specific" Hox cluster duplication is coincident with the origin of teleosts. *Molecular Biology and Evolution, 23*(1), 121–136.

Cunningham, J. A., Liu, A. G., Bengtson, S., & Donoghue, P. C. J. (2017). The origin of animals: Can molecular clocks and the fossil record be reconciled?. *BioEssays, 39*(1), 1–12.

Darriba, D., Taboada, G. L., Doallo, R., & Posada, D. (2011). ProtTest 3: fast selection of best-fit models of protein evolution. *Bioinformatics, 27*, 1164–1165.

Degnan, B. M., Vervoort, M., Larroux, C., & Richards, G. S. (2009). Early evolution of metazoan transcription factors. *Current Opinion in Genetics & Development, 19*(6), 591–599.

Delsuc, F., Philippe, H., Tsagkogeorga, G., Simion, P., Tilak, M.-K., Turon, X., López-Legentil, S., Piette, J., Lemaire, P., & Douzery, E. J. P. (2018). A phylogenomic framework and timescale for comparative studies of tunicates. *BMC Biology, 16*, 1–14.

Desvignes, T., Sydes, J., Montfort, J., Bobe, J., & Postlethwait, J. H. (2021). Evolution after whole-genome duplication: teleost microRNAs. *Molecular Biology and Evolution, 38*(8), 3308–3331.

Dohrmann, M., & Wörheide, G. (2017). Dating early animal evolution using phylogenomic data. *Scientific Reports, 7*(1), 1–6.

Douzery, E. J., Snell, E. A., Bapteste, E., Delsuc, F., & Philippe, H. (2004). The timing of eukaryotic evolution: does a relaxed molecular clock reconcile proteins and fossils?. *Proceedings of the National Academy of Sciences, 101*(43), 15386-15391.

Droser, M. L., Tarhan, L. G., & Gehling, J. G. (2017). The Rise of Animals in a Changing Environment: Global Ecological Innovation in the Late Ediacaran. *Annual Review of Earth and Planetary Sciences, 45*, 593–617.

Drummond, A. J., Ho, S. Y. W., Phillips, M. J., & Rambaut, A. (2006). Relaxed phylogenetics and dating with confidence. *PLoS Biology, 4*(5), 1–12.

Dunwoodie, S. L. (2009). The role of hypoxia in development of the mammalian embryo. *Developmental Cell, 17*(6), 755–773.

Erwin, D. H., Laflamme, M., Tweedt, S. M., Sperling, E. A., Pisani, D., & Peterson, K. J. (2011). The Cambrian conundrum: Early divergence and later ecological success in the early history of animals. *Science, 334*(6059), 1091–1097.

Farquhar, J., Bao, H., & Thiemens, M. (2000). Atmospheric influence of Earth's earliest sulfur cycle. *Science, 289*(5480), 756-758.

Fenchel, T., & Finlay, B. J. (1995). *Ecology and evolution in anoxic worlds*. Oxford: Oxford Science Publications.

Ferrario, C., Sugni, M., Somorjai, I. M. L., & Ballarin, L. (2020). Beyond adult stem cells: Dedifferentiation as a unifying mechanism underlying regeneration in

invertebrate deuterostomes. *Frontiers in Cell and Developmental Biology, 8*, 1–25.

Finn, R. D., Clements, J., & Eddy, S. R. (2011). HMMER web server: interactive sequence similarity searching. *Nucleic Acids Research, 39*(suppl_2), W29–W37.

Finn, R. D., Coggill, P., Eberhardt, R. Y., Eddy, S. R., Mistry, J., Mitchell, A. L., Potter, S. C., Punta, M., Qureshi, M., Sangrador-Vegas, A., Salazar, G. A., Tate, J., & Bateman, A. (2016). The Pfam protein families database: towards a more sustainable future. *Nucleic Acids Research, 44*(D1), D279–D285.

Gene Ontology Consortium. (2004). The Gene Ontology (GO) database and informatics resource. *Nucleic Acids Research, 32*(Suppl. 1), D258–D261.

Glasauer, S. M. K., & Neuhauss, S. C. F. (2014). Whole-genome duplication in teleost fishes and its evolutionary consequences. *Molecular Genetics and Genomics, 289*, 1045–1060.

Gold, D. A., & Jacobs, D. K. (2013). Stem cell dynamics in Cnidaria: are there unifying principles?. *Development Genes and Evolution, 223*, 53–66.

Grabherr, M. G., Haas, B. J., Yassour, M., Levin, J. Z., Thompson, D. A., Amit, I., Adiconis, X., Fan, L., Raychowdhury, R., Zeng, Q., Chen, Z., Mauceli, E., Hacohen, N., Gnirke, A., Rhind, N., di Palma, F., Birren, B. W., Nusbaum, C., Lindblad-Toh, K., Friedman, N., Regev, A. (2011). Full-length transcriptome assembly from RNA-Seq data without a reference genome. *Nature Biotechnology, 29*(7), 644–652.

Graham, A. M., & Presnell, J. S. (2017). Hypoxia Inducible Factor (HIF) transcription factor family expansion, diversification, divergence and selection in eukaryotes. *PLoS ONE, 12*(6), 1–15.

Halanych, K. M. (2016). How our view of animal phylogeny was reshaped by molecular approaches: lessons learned. *Organisms Diversity and Evolution, 16*, 319–328.

Hammarlund, E. U. (2020). Harnessing hypoxia as an evolutionary driver of complex multicellularity. *Interface Focus, 10*(4), 1–11.

Hammarlund, E. U., von Stedingk, K., & Påhlman, S. (2018). Refined control of cell stemness allowed animal evolution in the oxic realm. *Nature Ecology & Evolution, 2*(2), 220–228.

Hedges, S. B., Blair, J. E., Venturi, M. L., & Shoe, J. L. (2004). A molecular timescale of eukaryote evolution and the rise of complex multicellular life. *BMC Evolutionary Biology, 4*(1), 1–9.

Ho, S. Y. W., & Duchêne, S. (2014). Molecular-clock methods for estimating evolutionary rates and timescales. *Molecular Ecology, 23*(24), 5947–5965.

Hoegg, S., Brinkmann, H., Taylor, J. S., & Meyer, A. (2004). Phylogenetic timing of the fish-specific genome duplication correlates with the diversification of teleost fish. *Journal of Molecular Evolution, 59*, 190–203.

Hon, W. C., Wilson, M. I., Harlos, K., Claridge, T. D. W., Schofield, C. J., Pugh, C. W., Maxwell, P. H., Ratcliffe, P. J., Stuart, D. I., & Jones, E. Y. (2002). Structural basis for the recognition of hydroxyproline in HIF-1α by pVHL. *Nature, 417*(6892), 975–978.

Huerta-Cepas, J., Szklarczyk, D., Forslund, K., Cook, H., Heller, D., Walter, M. C., Rattei, T., Mende, D. R., Sunagawa, S., Kuhn, M., Jensen, L. J., von Mering, C., & Bork, P. (2016). eggNOG 4.5: a hierarchical orthology framework with improved functional annotations for eukaryotic, prokaryotic and viral sequences. *Nucleic Acids Research, 44*(D1), D286–D293.

Irisarri, I., Baurain, D., Brinkmann, H., Delsuc, F., Sire, J.-Y., Kupfer, A., Petersen, J., Jarek, M., Meyer, A., Vences, M., & Philippe, H. (2017). Phylotranscriptomic consolidation of the jawed vertebrate timetree. *Nature Ecology & Evolution, 1*(9), 1370–1378.

Kaelin, W. G., & Ratcliffe, P. J. (2008). Oxygen sensing by metazoans: the central role of the HIF hydroxylase pathway. *Molecular Cell, 30*(4), 393–402.

Kalyaanamoorthy, S., Minh, B. Q., Wong, T. K. F., von Haeseler, A., & Jermiin, L. S. (2017). ModelFinder: fast model selection for accurate phylogenetic estimates. *Nature Methods, 14*(6), 587–589.

Kanehisa, M., Goto, S., Sato, Y., Furumichi, M., & Tanabe, M. (2012). KEGG for integration and interpretation of large-scale molecular data sets. *Nucleic Acids Research, 40*(D1), D109–D114.

Katoh, K., & Standley, D. M. (2013). MAFFT multiple sequence alignment software version 7: improvements in performance and usability. *Molecular Biology and Evolution, 30*(4), 772–780.

Kearse, M., Moir, R., Wilson, A., Stones-Havas, S., Cheung, M., Sturrock, S., Buxton, S., Cooper, A., Markowitz, S., Duran, C., Thierer, T., Ashton, B., Meintjes, P., & Drummond, A. (2012). Geneious Basic: An integrated and extendable desktop software platform for the organization and analysis of sequence data. *Bioinformatics, 28*(12), 1647–1649.

King, N., & Rokas, A. (2017). Embracing Uncertainty in Reconstructing Early Animal Evolution. *Current Biology, 27*(19), R1081–R1088.

Kocot, K. M., Cannon, J. T., Todt, C., Citarella, M. R., Kohn, A. B., Meyer, A., Santos, S. R., Schander, C., Moroz, L. L., Lieb, B., & Halanych, K. M. (2011). Phylogenomics reveals deep molluscan relationships. *Nature, 477*(7365), 452–456.

Krogh, A., Larsson, B., von Heijne, G., & Sonnhammer, E. L. L. (2001). Predicting transmembrane protein topology with a hidden markov model: application to complete genomes. *Journal of Molecular Biology, 305*(3), 567–580.

Kump, L. R. (2008). The rise of atmospheric oxygen. *Nature, 451*(7176), 277-278.

Kuraku, S., Meyer, A., & Kuratani, S. (2008). Timing of genome duplications relative to the origin of the vertebrates: did cyclostomes diverge before or after? *Molecular Biology and Evolution, 26*(1), 47–59.

Lagesen, K., Hallin, P., Rødland, E. A., Stærfeldt, H.-H., Rognes, T., & Ussery, D. W. (2007). RNAmmer: consistent and rapid annotation of ribosomal RNA genes. *Nucleic Acids Research, 35*(9), 3100–3108.

Lartillot, N., Brinkmann, H., & Philippe, H. (2007). Suppression of long-branch attraction artefacts in the animal phylogeny using a site-heterogeneous model. *BMC Evolutionary Biology, 7*(1), 1–14.

Lartillot, N., Lepage, T., & Blanquart, S. (2009). PhyloBayes 3: a Bayesian software package for phylogenetic reconstruction and molecular dating. *Bioinformatics, 25*(17), 2286-2288.

Lartillot, N., & Philippe, H. (2004). A Bayesian mixture model for across-site heterogeneities in the amino-acid replacement process. *Molecular Biology and Evolution, 21*(6), 1095–1109.

Law, S. H., Wu, R. S., Ng, P. K., Yu, R. M., & Kong, R. Y. (2006). Cloning and expression analysis of two distinct HIF-alpha isoforms – gcHIF-1alpha and gcHIF-4alpha – from the hypoxia-tolerant grass carp, *Ctenopharyngodon idellus*. *BMC Molecular Biology, 7*, 1–13.

Lenton, T. M. (2020). On the use of models in understanding the rise of complex life. *Interface Focus, 10*(4), 1–15.
Lenton, T. M., & Daines, S. J. (2017). Biogeochemical Transformations in the History of the Ocean. *Annual Review of Marine Science, 9*, 31–58.
Lenton, T. M., & Daines, S. J. (2018). The effects of marine eukaryote evolution on phosphorus, carbon and oxygen cycling across the Proterozoic–Phanerozoic transition. *Emerging Topics in Life Sciences, 2*(2), 267-278.
Levin, L. A. (2003). Oxygen minimum zone benthos: Adaptation and community response to hypoxia. *Oceanography and Marine Biology: An Annual Review, 41*, 1–45.
Li, C., Planavsky, N. J., Shi, W., Zhang, Z., Zhou, C., Cheng, M., Tarhan, L. G., Luo, G. & Xie, S. (2015). Ediacaran marine redox heterogeneity and early animal ecosystems. *Scientific Reports, 5*(1), 1-8.
Liu, P., Liu, J., Ji, A., Reinhard, C. T., Planavsky, N. J., Babikov, D., Najjar, R. G., & Kasting, J. F. (2021). Triple oxygen isotope constraints on atmospheric O2 and biological productivity during the mid-Proterozoic. *Proceedings of the National Academy of Sciences, 118*(51), 1–10.
Loenarz, C., Coleman, M. L., Boleininger, A., Schierwater, B., Holland, P. W. H., Ratcliffe, P. J., & Schofield, C. J. (2011). The hypoxia-inducible transcription factor pathway regulates oxygen sensing in the simplest animal, *Trichoplax adhaerens*. *EMBO Reports, 12*(1), 63–70.
Love, G. D., Grosjean, E., Stalvies, C., Fike, D. A., Grotzinger, J. P., Bradley, A. S., Kelly, A. E., Bhatia, M., Meredith, W., Snape, C. E., Bowring, S. A., Condon, D. J., & Summons, R. E. (2009). Fossil steroids record the appearance of Demospongiae during the Cryogenian period. *Nature, 457*(7230), 718–721.
Lyons, T. W., Reinhard, C. T., & Planavsky, N. J. (2014). The rise of oxygen in Earth's early ocean and atmosphere. *Nature, 506*(7488), 307–315.
Mello, B. (2018). Estimating timetrees with MEGA and the timetree resource. *Molecular Biology and Evolution, 35*(9), 2334–2342.
Mendoza, A. de, Sebé-Pedrós, A., Sestak, M. S., Matejcic, M., Torruella, G., Domazet-Loso, T., & Ruiz-Trillo, I. (2013). Transcription factor evolution in eukaryotes and the assembly of the regulatory toolkit in multicellular lineages. *Proceedings of the National Academy of Sciences, 110*(50), E4858–E4866.
Mighell, A. J., Smith, N. R., Robinson, P. A., & Markham, A. F. (2000). Vertebrate pseudogenes. *FEBS Letters, 468*(2-3), 109–114.
Mills, D. B., Francis, W. R., & Canfield, D. E. (2018a). Animal origins and the Tonian Earth system. *Emerging Topics in Life Sciences, 2*(2), 289–298.
Mills, D. B., Boyle, R. A., Daines, S. J., Sperling, E. A., Pisani, D., Donoghue, P. C. J., & Lenton, T. M. (2022). Eukaryogenesis and oxygen in Earth history. *Nature Ecology & Evolution, 6*(5), 520–532.
Mills, D. B., & Canfield, D. E. (2014). Oxygen and animal evolution: Did a rise of atmospheric oxygen "trigger" the origin of animals?. *BioEssays, 36*(12), 1145-1155.
Mills, D. B., Francis, W. R., Vargas, S., Larsen, M., Elemans, C. P., Canfield, D. E., & Wörheide, G. (2018b). The last common ancestor of animals lacked the HIF pathway and respired in low-oxygen environments. *ELife, 7*, 1–17.
Mills, D. B., Ward, L. M., Jones, C. A., Sweeten, B., Forth, M., Treusch, A. H., & Canfield, D. E. (2014). Oxygen requirements of the earliest animals. *Proceedings of the National Academy of Sciences, 111*(11), 4168–4172.

Min, J.-H., Yang, H., Ivan, M., Gertler, F., Kaelin, W. G., & Pavletich, N. P. (2002). Structure of an HIF-1α-pVHL complex: hydroxyproline recognition in signaling. *Science*, *296*(5574), 1886–1889.

Minh, B. Q., Nguyen, M. A. T., & von Haeseler, A. (2013). Ultrafast approximation for phylogenetic bootstrap. *Molecular Biology and Evolution*, *30*(5), 1188–1195.

Misof, B., Liu, S., Meusemann, K., Peters, R. S., Donath, A., Mayer, C., Frandsen, P. B., Ware, J., Flouri, T., Beutel, R. G., Niehuis, O., Petersen, M., Izquierdo-Carrasco, F., Wappler, T., Rust, J., Aberer, A. J., Aspock, U., Aspock, H., Bartel, D., Blanke, A., Berger, S., Bohm, A., Buckley, T. R., Calcott, B., Chen, J., Friedrich, F., Fukui, M., Fujita, M., Greve, C., Grobe, P., Gu, S., Huang, Y., Jermiin, L. S., Kawahara, A. Y., Krogmann, L., Kubiak, M., Lanfear, R., Letsch, H., Li, Y., Li, Z., Li, J., Lu, H., Machida, R., Mashimo, Y., Kapli, P., McKenna, D. D., Meng, G., Nakagaki, Y,, Navarrete-Heredia, J. L., Ott, M., Ou, Y., Pass, G., Podsiadlowski, L., Pohl, H., Reumont, B.M. von, Schutte, K., Sekiya, K., Shimizu, S., Slipinski, A., Stamatakis, A., Song, W., Su, X., Szucsich, N. U., Tan, M., Tan, X., Tang, M., Tang, J., Timelthaler, G., Tomizuka, S., Trautwein, M., Tong, X., Uchifune, T., Walzl, M. G., Wiegmann, B. M., Wilbrandt, J., Wipfler, B., Wong, T. K. F., Wu, Q., Wu, G., Xie, Y., Yang, S., Yang, Q., Yeates, D. K., Yoshizawa, K., Zhang, Q., Zhang, R., Zhang, W., Zhang, Y., Zhao, J., Zhou, C., Zhou, L., Ziesmann, T., Zou, S., Li, Y., Xu, X., Zhang, Y., Yang, H., Wang, J., Wang, J., Kjer, K. M., Zhou, X. (2014). Phylogenomics resolves the timing and pattern of insect evolution. *Science*, *346*(6210), 763–767.

Mosch, T., Sommer, S., Dengler, M., Noffke, A., Bohlen, L., Pfannkuche, O., Liebetrau, V., & Wallmann, K. (2012). Factors influencing the distribution of epibenthic megafauna across the Peruvian oxygen minimum zone. *Deep Sea Research Part I: Oceanographic Research Papers*, *68*, 123–135.

Nakamura, N., Shi, X., Darabi, R., & Li, Y. (2021). Hypoxia in cell reprogramming and the epigenetic regulations. *Frontiers in Cell and Developmental Biology*, *9*, 1–10.

Narbonne, G. M. (2005). The Ediacara Biota: Neoproterozoic Origin of Animals and Their Ecosystems. *Annual Review of Earth and Planetary Sciences*, *33*, 421–442.

Nguyen, L. T., Schmidt, H. A., Von Haeseler, A., & Minh, B. Q. (2015). IQ-TREE: a fast and effective stochastic algorithm for estimating maximum-likelihood phylogenies. *Molecular biology and evolution*, *32*(1), 268-274.

Och, L. M., & Shields-Zhou, G. A. (2012). The Neoproterozoic oxygenation event: Environmental perturbations and biogeochemical cycling. *Earth-Science Reviews*, *110*(1-4), 26-57.

Panopoulou, G., & Poustka, A. J. (2005). Timing and mechanism of ancient vertebrate genome duplications – the adventure of a hypothesis. *TRENDS in Genetics*, *21*(10), 559–567.

Parfrey, L. W., Lahr, D. J. G., Knoll, A. H., & Katz, L. A. (2011). Estimating the timing of early eukaryotic diversification with multigene molecular clocks. *Proceedings of the National Academy of Sciences*, *108*(33), 13624–13629.

Parham, J. F., Donoghue, P. C. J., Bell, C. J., Calway, T. D., Head, J. J., Holroyd, P. A., Inoue, J. G., Irmis, R. B., Joyce, W. G., Ksepka, D. T., Patané, J. S. L., Smith, N. D., Tarver, J. E., van Tuinen, M., Yang, Z., Angielczyk, K. D., Greenwood, J. M., Hipsley, C. A., Jacobs, L., Makovicky, P. J., Müller, J., Smith, K. T., Theodor, J. M., Warnock, R. C. M., Benton, M. J. (2012). Best Practices for Justifying Fossil Calibrations. *Systematic Biology*, *61*(2), 346–359.

Peet, D., & Linke, S. (2006). Regulation of HIF: asparaginyl hydroxylation. In *Signalling Pathways in Acute Oxygen Sensing: Novartis Foundation Symposium 272* (pp. 37-53). Chichester, UK: John Wiley & Sons, Ltd.

Petersen, T. N., Brunak, S., von Heijne, G., & Nielsen, H. (2011). SignalP 4.0: discriminating signal peptides from transmembrane regions. *Nature Methods, 8*(10), 785–786.

Peterson, K. J., Lyons, J. B., Nowak, K. S., Takacs, C. M., Wargo, M. J., & McPeek, M. A. (2004). Estimating metazoan divergence times with a molecular clock. *Proceedings of the National Academy of Sciences, 101*(17), 6536–6541.

Pisani, D., Pett, W., Dohrmann, M., Feuda, R., Rota-Stabelli, O., Philippe, H., Lartillot, N., & Wörheide, G. (2015). Genomic data do not support comb jellies as the sister group to all other animals. *Proceedings of the National Academy of Sciences, 112*(50), 15402–15407.

Pu, J. P., Bowring, S. A., Ramezani, J., Myrow, P., Raub, T. D., Landing, E., Mills, A., Hodgin, E., & Macdonald, F. A. (2016). Dodging snowballs: Geochronology of the Gaskiers glaciation and the first appearance of the Ediacaran biota. *Geology, 44*(11), 955–958.

Purcell, J. E., Breitburg, D. L., Decker, M. B., Graham, W. M., Youngbluth, M. J., & Raskoff, K. A. (2001). Pelagic cnidarians and ctenophores in low dissolved oxygen environments: A review. In N. N. Rabalais & R. E. Turner (Eds.), *Coastal Hypoxia: Consequences for Living Resources and Ecosystems* (pp. 77–100). American Geophyical Union.

Rambaut, A. (2009). FigTree: Tree Figure Drawing Tool. Version 1.2.2. Available: http://tree.bio.ed.ac.uk/software/figtree/. Accessed: 2022 December 18.

Rambaut, A., Suchard, M. A., Xie, D., & Drummond, A. J. (2015). Tracer. Version 1.6. Available: http://beast.community/tracer. Accessed: 2022 August 15.

Reinhard, C. T., Planavsky, N. J., Olson, S. L., Lyons, T. W., & Erwin, D. H. (2016). Earth's oxygen cycle and the evolution of animal life. *Proceedings of the National Academy of Sciences, 113*(32), 8933–8938.

Reis, M. dos, Thawornwattana, Y., Angelis, K., Telford, M. J., Donoghue, P. C. J., & Yang, Z. (2015). Uncertainty in the Timing of Origin of Animals and the Limits of Precision in Molecular Timescales. *Current Biology, 25*(22), 2939–2950.

Reis, M. dos, & Yang, Z. (2011). Approximate likelihood calculation on a phylogeny for Bayesian estimation of divergence times. *Molecular biology and evolution, 28*(7), 2161-2172.

Rodriguez-Pascual, F., & Slatter, D. A. (2016). Collagen cross-linking: Insights on the evolution of metazoan extracellular matrix. *Scientific Reports, 6*(1), 1–7.

Ronquist, F., & Huelsenbeck, J. P. (2003). MrBayes 3: Bayesian phylogenetic inference under mixed models. *Bioinformatics, 19*(12), 1572–1574.

Rytkönen, K. T., Ryynänen, H. J., Nikinmaa, M., & Primmer, C. R. (2008). Variable patterns in the molecular evolution of the hypoxia-inducible factor-1 alpha (HIF-1α) gene in teleost fishes and mammals. *Gene, 420*(1), 1–10.

Rytkönen, K. T., Williams, T. A., Renshaw, G. M., Primmer, C. R., & Nikinmaa, M. (2011). Molecular evolution of the metazoan PHD-HIF oxygen-sensing system. *Molecular Biology and Evolution, 28*(6), 1913–1926.

Sacerdot, C., Louis, A., Bon, C., Berthelot, C., & Roest Crollius, H. (2018). Chromosome evolution at the origin of the ancestral vertebrate genome. *Genome Biology, 19*(1), 1–15.

Sahoo, S. K., Planavsky, N. J., Kendall, B., Wang, X., Shi, X., Scott, C., Anbar, A. D., Lyons, T. W., & Jiang, G. (2012). Ocean oxygenation in the wake of the Marinoan glaciation. *Nature*, *489*(7417), 546–549.

Sebé-Pedrós, A., de Mendoza, A., Lang, B. F., Degnan, B. M., & Ruiz-Trillo, I. (2011). Unexpected repertoire of metazoan transcription factors in the unicellular holozoan *Capsaspora owczarzaki*. *Molecular biology and evolution*, *28*(3), 1241–1254.

Sebé-Pedrós, A., Zheng, Y., Ruiz-Trillo, I., & Pan, D. (2012). Premetazoan origin of the hippo signaling pathway. *Cell Reports*, *1*(1), 13–20.

Semenza, G. L. (2007). Life with oxygen. *Science*, *318*(5847), 62–64.

Shih, P. M., & Matzke, N. J. (2013). Primary endosymbiosis events date to the later Proterozoic with cross-calibrated phylogenetic dating of duplicated ATPase proteins. *Proceedings of the National Academy of Sciences of the United States of America*, *110*(30), 12355–12360.

Simakov, O., Marlétaz, F., Yue, J.-X., O'Connell, B., Jenkins, J., Brandt, A., Calef, R., Tung, C.-H., Huang, T.-K., Schmutz, J., Satoh, N., Yu, J.-K., Putnam, N. H., Green, R. E., & Rokhsar, D. S. (2020). Deeply conserved synteny resolves early events in vertebrate evolution. *Nature Ecology & Evolution*, *4*(6), 820–830.

Simionato, E., Ledent, V., Richards, G., Thomas-Chollier, M., Kerner, P., Coornaert, D., Degnan, B. M., & Vervoort, M. (2007). Origin and diversification of the basic helix-loop-helix gene family in metazoans: Insights from comparative genomics. *BMC Evolutionary Biology*, *7*, 1–18.

Simon, M. C., & Keith, B. (2008). The role of oxygen availability in embryonic development and stem cell function. *Nature Reviews Molecular Cell Biology*, *9*(4), 285–296.

Song, H., Chen, X., Jiao, Q., Qiu, Z., Shen, C., Zhang, G., Sun, Z., Zhang, H., & Luo, Q.-Y. (2021). HIF-1α-mediated telomerase reverse transcriptase activation inducing autophagy through mammalian target of rapamycin promotes papillary thyroid carcinoma progression during hypoxia stress. *Thyroid*, *31*(2), 233–246.

Sperling, E. A., Frieder, C. A., Raman, A. V., Girguis, P. R., Levin, L. A., & Knoll, A. H. (2013). Oxygen, ecology, and the Cambrian radiation of animals. *Proceedings of the National Academy of Sciences of the United States of America*, *110*(33), 13446–13451.

Sperling, E. A., Knoll, A. H., & Girguis, P. R. (2015). the ecological physiology of Earth's second oxygen revolution. Annual Review of Ecology, Evolution, and Systematics, 46, 215–235.

Suga, H., Chen, Z., de Mendoza, A., Sebé-Pedrós, A., Brown, M. W., Kramer, E., Carr, M., Kerner, P., Vervoort, M., Sánchez-Pons, N., Torruella, G., Derelle, R., Manning, G., Lang, B. F., Russ, C., Haas, B. J., Roger, A. J., Nusbaum, C., & Ruiz-Trillo, I. (2013). The Capsaspora genome reveals a complex unicellular prehistory of animals. *Nature Communications*, *4*(1), 1–9.

Tarade, D., Lee, J. E., & Ohh, M. (2019). Evolution of metazoan oxygen-sensing involved a conserved divergence of VHL affinity for HIF1α and HIF2α. *Nature Communications*, *10*(1), 1–12.

Taylor, C. T., & McElwain, J. C. (2010). Ancient atmospheres and the evolution of oxygen sensing via the hypoxia-inducible factor in metazoans. *Physiology*, *25*(5), 272–279.

Thuesen, E. v., Rutherford, L. D., & Brommer, P. L. (2005). The role of aerobic metabolism and intragel oxygen in hypoxia tolerance of three ctenophores:

Pleurobrachia bachei, *Bolinopsis infundibulum* and *Mnemiopsis leidyi*. *Journal of the Marine Biological Association of the United Kingdom, 85*(3), 627–633.
Tostevin, R., & Mills, B. J. W. (2020). Reconciling proxy records and models of Earth's oxygenation during the Neoproterozoic and Palaeozoic: Neoproterozoic-Palaeozoic Oxygenation. *Interface Focus, 10*(4), 1–13.
Tsagkogeorga, G., Cahais, V., & Galtier, N. (2012). The population genomics of a fast evolver: high levels of diversity, functional constraint, and molecular adaptation in the tunicate Ciona intestinalis. *Genome Biology and Evolution, 4*(8), 852–861.
Tsagkogeorga, G., Turon, X., Hopcroft, R. R., Tilak, M.-K., Feldstein, T., Shenkar, N., Loya, Y., Huchon, D., Douzery, E. J., & Delsuc, F. (2009). An updated 18S rRNA phylogeny of tunicates based on mixture and secondary structure models. *BMC Evolutionary Biology, 9*, 1–16.
Tsuji, K., Kitamura, S., & Makino, H. (2014). Hypoxia-inducible factor 1α regulates branching morphogenesis during kidney development. *Biochemical and Biophysical Research Communications, 447*(1), 108–114.
Turner, E. C. (2021). Possible poriferan body fossils in early Neoproterozoic microbial reefs. *Nature, 596*(7870), 87–91.
Wang, Y., Shi, S., Liu, H., & Meng, L. (2016). Hypoxia enhances direct reprogramming of mouse fibroblasts to cardiomyocyte-like cells. *Cellular Reprogramming, 18*(1), 1–7.
Weigert, A., Helm, C., Meyer, M., Nickel, B., Arendt, D., Hausdorf, B., Santos, S. R., Halanych, K. M., Purschke, G., Bleidorn, C., & Struck, T. H. (2014). Illuminating the base of the annelid tree using transcriptomics. *Molecular Biology and Evolution, 31*(6), 1391–1401.
Weits, D. A., Kunkowska, A. B., Kamps, N. C. W., Portz, K. M. S., Packbier, N. K., Nemec Venza, Z., Gaillochet, C., Lohmann, J. U., Pedersen, O., van Dongen, J. T., & Licausi, F. (2019). An apical hypoxic niche sets the pace of shoot meristem activity. *Nature, 569*(7758), 714–717.
Whelan, N., Kocot, K. M., Moroz, L. L., & Halanych, K. M. (2015). Error, signal, and the placement of Ctenophora sister to all other animals. *Proceedings of the National Academy of Sciences, 112*(18), 5773–5778.
Whelan, S., & Goldman, N. (2001). A general empirical model of protein evolution derived from multiple protein families using a maximum-likelihood approach. *Molecular Biology and Evolution, 18*(5), 691–699.
Wolfe, J. M., Breinholt, J. W., Crandall, K. A., Lemmon, A. R., Lemmon, E. M., Timm, L. E., Siddall, M. E., & Bracken-Grissom, H. D. (2019). A phylogenomic framework, evolutionary timeline and genomic resources for comparative studies of decapod crustaceans. *Proceedings of the Royal Society B: Biological Sciences, 286*(1901), 1–10.
Wood, R., Liu, A. G., Bowyer, F., Wilby, P. R., Dunn, F. S., Kenchington, C. G., Cuthill, J. F. H., Mitchell, E. G., & Penny, A. (2019). Integrated records of environmental change and evolution challenge the Cambrian Explosion. *Nature Ecology and Evolution, 3*(4), 528–538.
Yang, Z. (2007). PAML 4: phylogenetic analysis by maximum likelihood. *Molecular Biology and Evolution, 24*(8), 1586-1591.
Yin, Z., Zhu, M., Davidson, E. H., Bottjer, D. J., Zhao, F., & Tafforeau, P. (2015). Sponge grade body fossil with cellular resolution dating 60 Myr before the Cambrian. *Proceedings of the National Academy of Sciences, 112*(12), E1453–E1460.

Young, M. D., Wakefield, M. J., Smyth, G. K., & Oshlack, A. (2010). Gene ontology analysis for RNA-seq: accounting for selection bias. *Genome Biology, 11*(2), 1–12.

Yu, H., & Li, L. (2014). Phylogeny and molecular dating of the cerato-platanin-encoding genes. *Genetics and Molecular Biology, 37*, 423–427.

Zhang, J. (2003). Evolution by gene duplication: an update. *Trends in Ecology & Evolution, 18*(6), 292–298.

Zhang, F., Xiao, S., Kendall, B., Romaniello, S. J., Cui, H., Meyer, M., Gilleaudeau, G. J., Kaufman, A. J., & Anbar, A. D. (2018). Extensive marine anoxia during the terminal Ediacaran Period. *Science Advances, 4*(6), 1–11.

Supplementary file 1 - List of all HIFa sequences analyzed in this work, including species name, phylum, their respective accession numbers, and the database which they were retrieved from.

Species	Phylum	Accession Number	Database
Capitella teleta	Annelida	ELU17358.1	GenBank
Melinna maculata	Annelida	OQ354996	WormNet
Owenia fusiformis	Annelida	OQ354998	WormNet
Palola sp.	Annelida	OQ354999	WormNet
Terebellides stroemii	Annelida	OQ355008	WormNet
Acyrthosiphon pisum	Arthropoda	ACYPI008717	Ensembl
Apis mellifera	Arthropoda	GB44532	Ensembl
Dendroctonus ponderosae	Arthropoda	ENN78160	Ensembl
Nasonia vitripennis	Arthropoda	NV15198	Ensembl
Strigamia maritima	Arthropoda	SMAR009079-PA	Ensembl
Drosophila melanogaster	Arthropoda	FBpp0310749	Flybase
Anoplophora glabripennis	Arthropoda	XP_023312868.1	GenBank
Araneus ventricosus	Arthropoda	GBM21658.1	GenBank
Blattella germanica	Arthropoda	PSN42112.1	GenBank
Callosobruchus maculatus	Arthropoda	AFL70631.1	GenBank
Eriocheir sinensis	Arthropoda	AHH85804.1	GenBank
Folsomia candida	Arthropoda	OXA59682.1	GenBank
Fopius arisanus	Arthropoda	JAG79183.1	GenBank
Helicoverpa armigera	Arthropoda	AMH87782.1	GenBank
Lygus hesperus	Arthropoda	JAG09280.1	GenBank
Onthophagus taurus	Arthropoda	XP_022911748.1	GenBank
Oratosquilla oratoria	Arthropoda	ADH01740.1	GenBank
Palaemon carinicauda	Arthropoda	APU88435.1	GenBank
Palaemon pugio	Arthropoda	AAT72404.1	GenBank
Penaeus vannamei	Arthropoda	ACU30154.1	GenBank
Scylla paramamosain	Arthropoda	ARO76395.1	GenBank
Daphnia pulex	Arthropoda	DappuP194123	JGI
Anopheles gambiae	Arthropoda	A0A1S4GH32	UniProtKB
Tribolium castaneum	Arthropoda	D6WMG7	UniProtKB
Lingula anatina	Brachiopoda	XP_013386588.1	GenBank
Glottidia pyramidata	Brachiopoda	OQ354984	WormNet
Hemithiris psittacea	Brachiopoda	OQ354988	WormNet
Laqueus californicus	Brachiopoda	OQ354990	WormNet
Novocrania anomala	Brachiopoda	OQ354997	WormNet
Pectinatella magnifica	Bryozoa	OQ355001	WormNet
Branchiostoma belcheri tsingtauense	Cephalochordata	ADU87364.1	GenBank
Branchiostoma floridae	Cephalochordata	jgi_Brafl1_208408_e_gw.35.42.1	JGI
Branchiostoma floridae	Cephalochordata	A0A067Y838	Mills et al., 2018
Acropora millepora	Cnidaria	QCI31507.1	GenBank
Exaiptasia diaphana	Cnidaria	KXJ20783.1	GenBank

Hydra vulgaris	Cnidaria	CDG69882.1	GenBank
Nematostella vectensis	Cnidaria	AII22158.1	GenBank
Orbicella faveolata	Cnidaria	XP_020630368.1	GenBank
Pocillopora damicornis	Cnidaria	XP_027055708.1	GenBank
Stylophora pistillata	Cnidaria	ATY39324.1	GenBank
Alatina alata	Cnidaria	SRP056878	Mills et al., 2018
Chironex fleckeri	Cnidaria	Mills et al., 2018	Mills et al., 2018
Chrysaora fuscescens	Cnidaria	SRP070629	Mills et al., 2018
Corallium rubrum	Cnidaria	Mills et al., 2018	Mills et al., 2018
Favia sp.	Cnidaria	Mills et al., 2018	Mills et al., 2018
Madracis auretenra	Cnidaria	Mills et al., 2018	Mills et al., 2018
Montastraea cavernosa	Cnidaria	Mills et al., 2018	Mills et al., 2018
Porites australiensis	Cnidaria	Mills et al., 2018	Mills et al., 2018
Resomia sp.	Cnidaria	Mills et al., 2018	Mills et al., 2018
Rhopilema esculentum	Cnidaria	Mills et al., 2018	Mills et al., 2018
Seriatopora hystrix	Cnidaria	Mills et al., 2018	Mills et al., 2018
Mnemiopsis leidyi	Ctenophora	ML03195a	Mnemiopsis Genome Portal
Strongylocentrotus purpuratus	Echinodermata	SPU_001262-tr	Ensembl
Acanthaster planci	Echinodermata	XP_022097956.1	GenBank
Stichopus japonicus	Echinodermata	A0A2G8JMF8	GenBank
Apostichopus californicus	Echinodermata	OQ355000	WormNet
Crinoidea gen. sp.	Echinodermata	OQ355011	WormNet
Leptosynapta clarki	Echinodermata	OQ354993	WormNet
Capsaspora owczarzaki	Filasterea	Mills et al., 2018	Mills et al., 2018
Capsaspora owczarzaki	Filasterea	Mills et al., 2018	Mills et al., 2018
Saccoglossus kowalevskii	Hemichordata	XP_002733787.2	GenBank
Balanoglossus aurantiaca	Hemichordata	OQ354980	WormNet
Cephalodiscus hodgsoni	Hemichordata	OQ354981	WormNet
Harrimaniidae gen. sp. 2 (from Iceland)	Hemichordata	OQ354985	WormNet
Harrimaniidae gen. sp. 1 (from Norway)	Hemichordata	OQ354986	WormNet
Ptychodera bahamensis	Hemichordata	OQ355005	WormNet
Saccoglossus mereschkowskii	Hemichordata	OQ355006	WormNet
Schizocardium brasiliense	Hemichordata	OQ355007	WormNet
Torquaratoridae gen. sp.	Hemichordata	OQ355009	WormNet
Anadara broughtonii	Mollusca	A0A4D6WH33	GenBank
Crassostrea gigas	Mollusca	EKC33928	GenBank
Crassostrea virginica	Mollusca	AED87588.1	GenBank
Haliotis discus hannai	Mollusca	AWV50541.1	GenBank
Haliotis diversicolor	Mollusca	AGE97172.1	GenBank
Mizuhopecten yessoensis	Mollusca	OWF50362.1	GenBank
Lottia gigantea	Mollusca	jgi_Lotgi1_133221_e_gw1.83.92.1	JGI
Alexandromenia crassa	Mollusca	OQ354979	WormNet
Entonomenia tricarinata	Mollusca	OQ354982	WormNet

Epimenia babai	Mollusca	OQ354983	WormNet
Helluoherpia aegiri	Mollusca	OQ354987	WormNet
Leptochiton rugatus	Mollusca	OQ354992	WormNet
Macellomenia sp.	Mollusca	OQ354994	WormNet
Meiomenia swedmarki	Mollusca	OQ354995	WormNet
Prochaetoderma californicum	Mollusca	OQ355004	WormNet
Tubulanus polymorphus	Nemertea	OQ355010	WormNet
Phoronis psammophila	Phoronida	OQ355002	WormNet
Phoronopsis harmeri	Phoronida	OQ355003	WormNet
Trichoplax adhaerens	Placozoa	AFM37575.1	GenBank
Hoilungia sp.	Placozoa	Mills et al., 2018	Mills et al., 2018
Halichondria panicea	Porifera	A0A6C0SNX0	GenBank
Halisarca dujardini	Porifera	A0A6C0PMZ9	GenBank
Amphimedon queenslandica	Porifera	XP_011403285.1	NCBI
Kirkpatrickia variolosa	Porifera	OQ354989	WormNet
Latrunculia apicalis	Porifera	OQ354991	WormNet
Priapulus caudatus	Priapulida	XP_014663090.1	GenBank
Ciona intestinalis	Urochordata	NP_001071731.1	Mills et al., 2018
Anolis carolinensis	Vertebrata	ENSACAP00000016495	Ensembl
Anolis carolinensis	Vertebrata	ENSACAP00000015923	Ensembl
Anolis carolinensis	Vertebrata	ENSACAP00000004025	Ensembl
Danio rerio	Vertebrata	ENSDARP00000004329	Ensembl
Danio rerio	Vertebrata	ENSDARP00000044281	Ensembl
Danio rerio	Vertebrata	ENSDARP00000124584	Ensembl
Danio rerio	Vertebrata	ENSDARP00000074832	Ensembl
Ficedula albicollis	Vertebrata	ENSFALP00000003555	Ensembl
Ficedula albicollis	Vertebrata	ENSFALP00000013483	Ensembl
Latimeria chalumnae	Vertebrata	ENSLACP00000016026	Ensembl
Latimeria chalumnae	Vertebrata	ENSLACP00000020801	Ensembl
Latimeria chalumnae	Vertebrata	ENSLACP00000002905	Ensembl
Monodelphis domestica	Vertebrata	ENSMODP00000010901	Ensembl
Ornithorhynchus anatinus	Vertebrata	ENSOANP00000024166	Ensembl
Ornithorhynchus anatinus	Vertebrata	ENSOANP00000014474	Ensembl
Takifugu rubripes	Vertebrata	ENSTRUP00000021462	Ensembl
Takifugu rubripes	Vertebrata	ENSTRUP00000030606	Ensembl
Takifugu rubripes	Vertebrata	ENSTRUP00000013587	Ensembl
Xenopus tropicalis	Vertebrata	ENSXETP00000031610	Ensembl
Xenopus tropicalis	Vertebrata	ENSXETP00000031612	Ensembl
Danio rerio	Vertebrata	AAQ94179.1	GenBank
Bos taurus	Vertebrata	Q9XTA5	Mills et al., 2018
Gallus gallus	Vertebrata	Q9YIB9	Mills et al., 2018
Gallus gallus	Vertebrata	ASF89071.1	Mills et al., 2018
Homo sapiens	Vertebrata	Q16665	Mills et al., 2018
Homo sapiens	Vertebrata	Q9Y2N7	Mills et al., 2018
Mus musculus	Vertebrata	NP_034561.2	Mills et al., 2018
Mus musculus	Vertebrata	Mills et al., 2018	Mills et al., 2018

Mus musculus	Vertebrata	Mills et al., 2018	Mills et al., 2018
Oncorhynchus mykiss	Vertebrata	Mills et al., 2018	Mills et al., 2018
Rattus norvegicus	Vertebrata	Mills et al., 2018	Mills et al., 2018
Xenopus laevis	Vertebrata	Mills et al., 2018	Mills et al., 2018
Anas platyrhynchos	Vertebrata	XP_005030000	NCBI
Anas platyrhynchos	Vertebrata	XP_005009861	NCBI
Homo sapiens	Vertebrata	Q99814	UniProtKB

Supplementary file 2 – FASTA file of the 136 HIFa aligned and trimmed sequences used in this work. Available at: https://figshare.com/articles/dataset/Supplementary_file_2/21989165

Supplementary file 3 – FASTA file of the 136 HIFa non-aligned and untrimmed sequences used in this work. Available at: https://figshare.com/articles/dataset/Supplementary_file_3/21989207

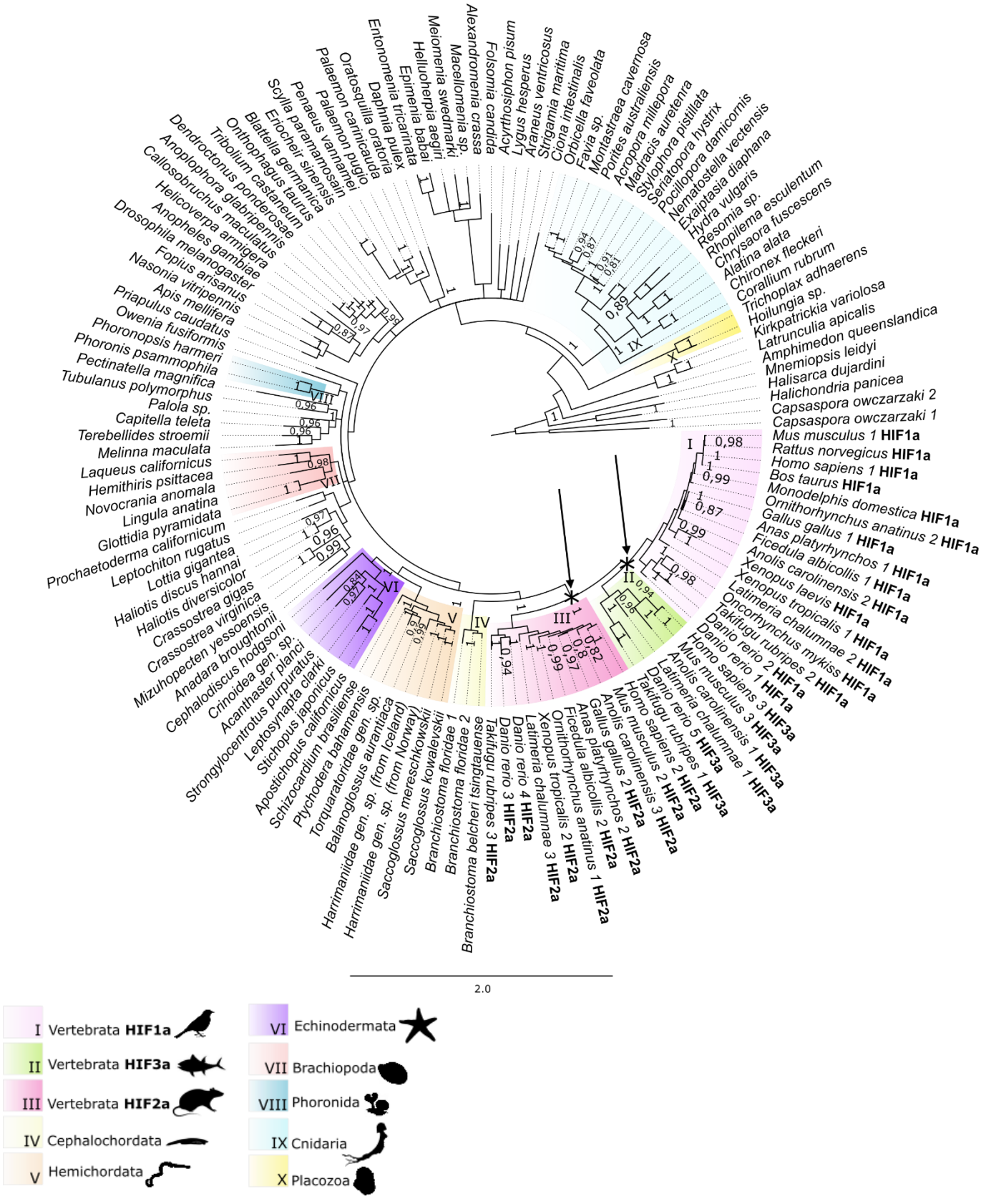

Supplementary file 4 – HIFa gene tree rooted with two capsasporan bHLH-PAS protein sequences inferred with MrBayes showing branch lengths. Clade I contains vertebrate HIF1a sequences. Clade II is composed by vertebrate HIF3a sequences. Clade III is formed by vertebrate HIF2a sequences. Clade IV represents cephalochordate HIFa genes. Clade V is composed by hemichordate HIFa sequences. Clade VI contains echinoderm HIFa genes. Clade VII represents brachiopods HIFa sequences. Clade VII contains phoronids HIFa genes. Clade VIII represents arthropods HIFa genes. Clade IX is composed by cnidarian HIFa genes. Clade X represents placozoan HIFa genes. Black arrows and asterisks indicate gene duplication events. To improve clarity, only posterior probability values >0.8 are shown.

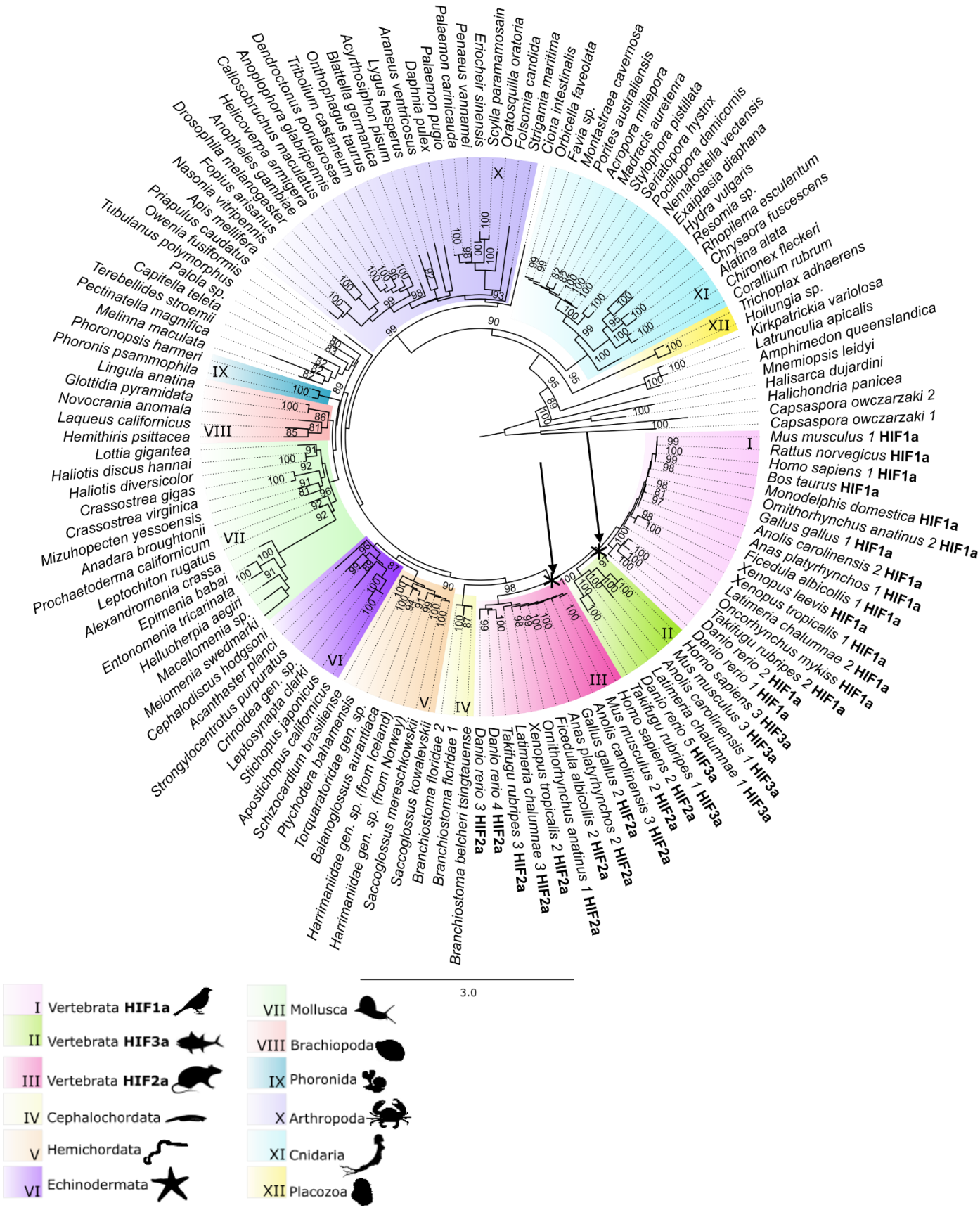

Supplementary file 5 – HIFa gene tree rooted with two capsasporan bHLH-PAS protein sequences obtained with IQ-TREE showing branch lengths. Clade I contains vertebrate HIF1a sequences. Clade II is composed by vertebrate HIF3a sequences. Clade III is formed by vertebrate HIF2a sequences. Clade IV represents cephalochordate HIFa genes. Clade V is composed by hemichordate HIFa sequences. Clade VI contains echinoderm HIFa genes. Clade VII represents mollusk HIFa sequences. Clade VIII is formed by brachiopods HIFa sequences. Clade IX contains phoronids HIFa genes. Clade X represents arthropods HIFa genes. Clade XI is composed by cnidarian HIFa genes. Clade XII represents placozoan HIFa genes. Black arrows and asterisks indicate gene duplication events. To improve clarity, only bootstrap support values >80 are shown.

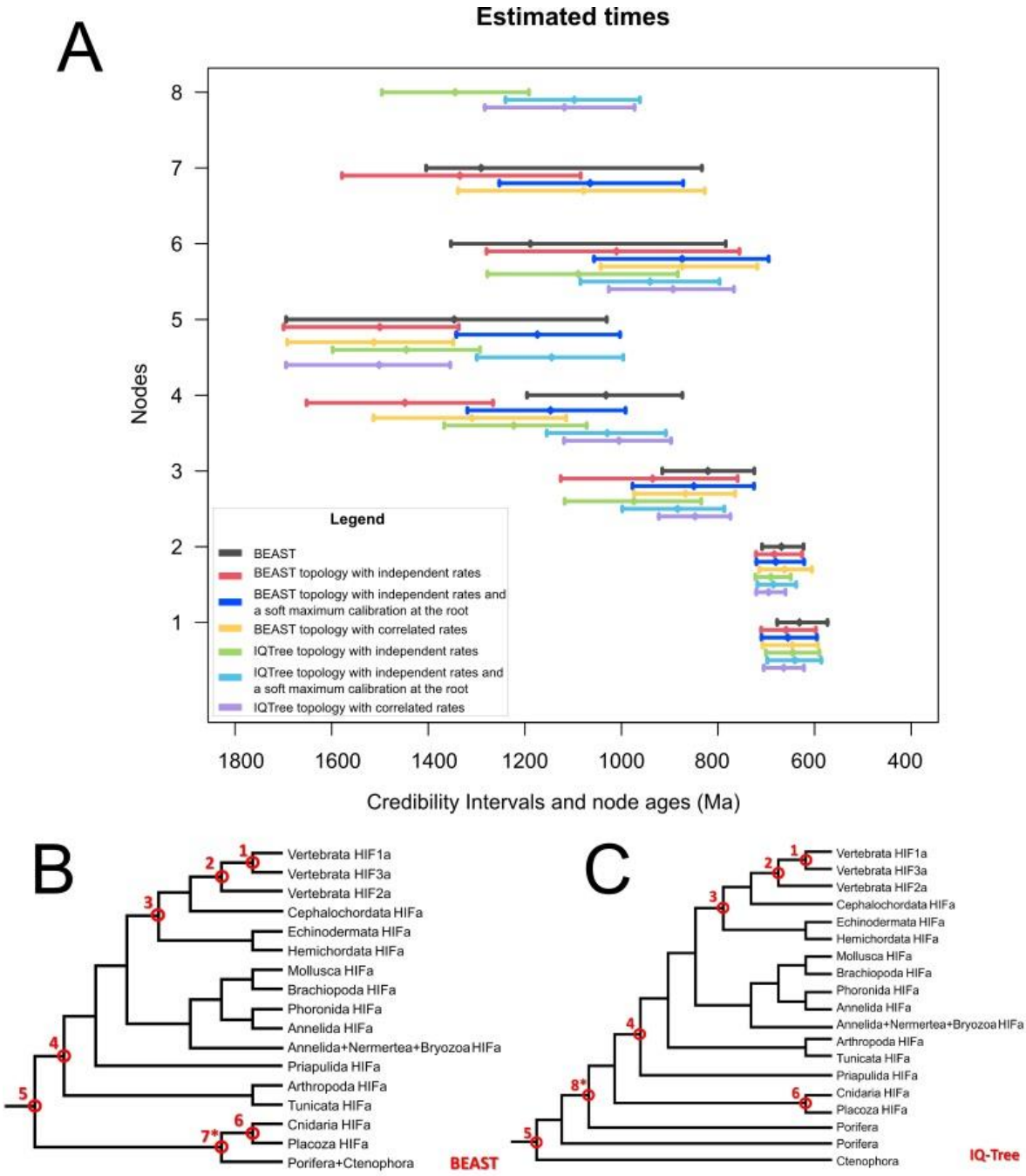

Supplementary file 6 – Comparison of divergence time estimates. (A) Range of the Credibility Intervals (CrIs) and estimated times for the nodes highlighted in panels B and C. The overlapping of the credibility intervals evidences the congruency among all analyses. Black lines represent results obtained in BEAST. Red lines represent estimates generated by MCMCTree using the fixed topology obtained in BEAST with independent rates. Dark blue lines show MCMCTree estimates retrieved using the fixed topology obtained in BEAST with independent rates and a soft maximum calibration at the root of 833 Ma based on dos Reis et al. (2015) and Benton et al. (2015). Yellow lines indicate results from MCMCTree using the BEAST fixed topology and correlated rates. Green lines represent node ages obtained by MCMCTree with the IQ-Tree fixed topology with independent rates. Light blue lines depict the results generated by MCMCTree with the IQ-Tree fixed topology, independent rates, and a soft maximum calibration at the root of 833 Ma. Lilac lines show MCMCTree estimates obtained with the IQ-Tree fixed topology with correlated rates. (B) Schematic representation of the HIFa gene tree topology obtained with BEAST. (C) HIFa gene tree topology generated by IQ-Tree. The main differences observed were due to the distinct relationships retrieved by BEAST and IQ-Tree, mainly at deeper nodes. In the IQ-Tree fixed topology, sponges and ctenophores homologs were the first to diverge from all other animal HIFs. Node 8 represents the split between Porifera+Ctenophora and the remaining Metazoa sequences, which was dated at ~1,271 Ma (CrI 1,118–1,423 Ma) by MCMCTree using an independent rate model. However, in the time tree generated by BEAST, sponges and ctenophores homologs formed a monophyletic group together with cnidarian and placozoan HIFa sequences that originated at ~1,218 Ma (CrI 760–1,331 Ma) – represented by node 7. Nodes 7 in panel B and 8 in panel C are marked with asterisks because they represent the main differences between both topologies.

Capítulo 3

Physiological and molecular responses of modern metazoans under the Neoproterozoic oceanic conditions reveal ancient adaptations to low oxygen levels

Flávia A. Belato[1*], Federico D. Brown[1], André C. Morandini[1,2], Márcio Reis Custódio[3], Ricardo I. F. Trindade[4], Sally P. Leys[5] & Elisa Maria Costa-Paiva[1,4]

1. Institute of Biosciences, Department of Zoology, University of Sao Paulo, Brazil
2. Center for Marine Biology, University of Sao Paulo, Brazil
3. Institute of Biosciences, Department of Physiology, University of Sao Paulo, Brazil
4. Institute of Astronomy, Geophysics and Atmospheric Sciences, University of Sao Paulo, Brazil
5. Department of Biological Sciences, University of Alberta, Edmonton, AB, Canada
Corresponding author: flavia.ariany@live.com

Abstract

The relationship between oxygen and the diversification of animals is a topic that has been extensively debated by scientists over the decades. All animals currently described need oxygen for at least part of their life cycle. Therefore, the transition from an anoxic to an oxygenated planet is considered as a prerequisite for the evolution of animals. However, although it is accepted that the Neoproterozoic oceans were low oxygen habitats, we know little about the respiratory physiology of early animals adapted to live in those environments. Here, we used modern analogs of early metazoans as models to infer aspects of the physiology of their early ancestors. Using simulation chambers that recreate the Neoproterozoic oxygenation oceanic conditions, we compared differences in gene expression of sponges submitted to the experiments with those maintained in control situation. We found that anoxic and oxygenated conditions

trigger the same molecular and physiological stress responses, suggesting that sponges are better adapted to hypoxia. Our results showed an overexpression of genes related to glycolysis, sulfide-removal metabolism, and remodeling of the aquiferous system under oxidative stress, implying an ancestral role of these mechanisms in ancient metazoans. Our findings reveal some of the physiological adaptations that may have granted competitive advantages to early animals during their evolution.

Introduction

The physiology of first animals that emerged in the Neoproterozoic Era is a topic of intense debate among researchers due to the challenging low oxygen levels predicted to that time. Modern molecular clock estimates place the emergence of early animals at ~850 Ma, in the Tonian period, long before the earliest evidence of Neoproterozoic oceanic oxygenation pulses at ~640–540 Ma (Erwin et al., 2011; Sahoo et al., 2012; dos Reis et al., 2015; Cunningham et al., 2017; Dohrmann and Wörheide, 2017; Lenton and Daines, 2017; Zhang et al., 2018; Wood et al., 2019; Tostevin and Mills, 2020). As all currently described metazoans are aerobic organisms, (Catling et al., 2005; Brochier-Armanet et al., 2009; Mentel et al., 2016), low oxygen levels may have been a limiting evolutionary aspect and could have imposed energetic restrictions on their diversity, abundance, and physiology (Fenchel and Finlay, 1995; Reinhard et al., 2016; Cole et al., 2020). Therefore, the physiological adaptations of early animals to hypoxia are of great interest, especially when considering the prospects that ocean oxygen levels will drop 1-7% over the next century due to climate change (Keeling et al., 2010).

In contrast to ancient dates obtained with molecular clock techniques, the oldest unequivocal animal fossil record is much younger, dating from the late Ediacaran at ~571 Ma (Narbonne, 2005; Pu et al.,

2016; Droser et al., 2017; Wood et al., 2019). Even when considering controversial older putative metazoan fossil evidence (e.g., organic biomarkers and Cryogenic putative sponge body fossils of > 635 Ma; Love et al., 2009; Brain et al., 2012; Antcliffe et al., 2014; Yin et al., 2015), there is still a time gap between molecular dating and fossil records for the emergence of animals. This disparity of the minimum Metazoa clade age obtained with different methods raised issues that fomented discussions among scientists for years. Due to the intrinsic relationship of animals with oxygen, the increase in oceanic oxygen availability in the Neoproterozoic at ~640–540 Ma was considered by many authors over decades as the trigger for animal evolution and diversification during the Ediacaran, in a cause-consequence model (Nursall, 1959; Berkner and Marshall, 1965; Cloud, 1968, 1969; Knoll and Carroll, 1999).

On the other hand, together with molecular clock evidence, theoretical estimates of early animals' oxygen demand are low, ranging from 0.4–1% of Present Atmospheric Levels (PAL; Runnegar, 1982; Sperling et al., 2013, 2015). Supporting this hypothesis, studies suggest that the first animals were likely small, soft-bodied, poor in collagen, and restricted their use of oxygen to high-priority physiological functions (Mills and Canfield, 2014; Mills et al., 2014). Therefore, the consensus in which geological period metazoans emerged is essential for understanding the correlation between the evolutionary processes that gave rise to animals with environmental changes that took place at that time (dos Reis et al., 2015; Cole et al., 2020).

Considering the strong evidence that early metazoans emerged in low oxygenated environments, their respiratory physiology and molecular mechanisms adapted to live in such conditions remain poorly understood. Studies using fossil records or theoretical estimates are useful to elucidate some aspects of their physiology. However, modern metazoans represent

the best available models to understand their early ancestors. Oxygen could represent a limiting factor if we assume the premise that early metazoans were obligate aerobics. However, many modern animals, such as sponges, ctenophores, cnidarians, annelids, and crustaceans, can live without oxygen for long periods or at least some stages of their life cycle, and some species can spend most of their life in anoxia (Reiswig and Miller, 1998; Bell and Barnes, 2000; Purcell et al., 2001; Mentel and Martin, 2008; Mosch et al., 2012; Müller et al., 2012; Troch et al., 2013; Grego et al., 2014; Mills et al., 2014; Parris et al., 2014; Lucey et al., 2020).

Furthermore, the molecular processes involved in the hypoxia/anoxia response in animals are still being investigated. Sussarellu et al. (2010) submitted the oyster *Crassostrea gigas* to 20 days of hypoxia (2 mg O_2 L^{-1}). The principal genes upregulated by hypoxic stress were involved with antioxidant defense and the respiratory chain, suggesting oxidative stress caused by hypoxia or an anticipatory response for normoxic recovery. Grimes et al. (2021) evaluated the variations in gene expression of the annelid *Hermodice carunculata* after prolonged and intermittent exposure to different hypoxia levels (4–1 mg O_2 L^{-1}). It was demonstrated that components of the Hypoxia Inducible Factor (HIF) pathway, responsible for maintaining oxygen homeostasis, have a modulated response to hypoxia, depending on the severity of hypoxic stress.

Experimental studies with modern animals focusing on unveiling the physiological aspects of early metazoans are limited. It has already been shown that the demosponge *Tethya wilhelma* survives and maintains normal transcription after exposure to four days of hypoxia (<0.25–2% PAL) (Mills et al., 2014, 2018). None of the differentially expressed genes had predicted functions related to metabolism or stress (Mills et al., 2018). After one hour in anoxia, *T. wilhelma* showed differential expression of

some metabolic genes (heme-binding proteins and ubiquitin), implying that the sponges may be stressed by these conditions (Mills et al., 2018). Leys and Kahn (2018) examined the oxygen use of ctenophores and sponges and demonstrated that both groups have very low specific respiration rates. This evidence indicates that perhaps oxygen would not have been the greatest limiter of the evolution of complex multicellular animals, and probably first animals were not under stress due to low oxygen levels or used unknown mechanisms to deal with it instead (Mills et al., 2018; Leys and Kahn, 2018).

Understanding how modern metazoans respond to hypoxia and anoxia at transcriptional level can enlighten aspects of early animals' physiology. If adaptations to low oxygen conditions are plesiomorphic, which means were inherited from early animals, then it is expected to find conserved metabolic responses in modern metazoans. As sponges are considered one of the first animal lineages to have arisen, and which from the fossil record are relatively unchanged in their morphology and filter feeding habit (Suarez and Leys, 2022), they were used here as modern analogs models. Therefore, to test our hypothesis, we submitted the demosponge *Hymeniacidon heliophila* to simulation experiments in chambers that recreate the Neoproterozoic oceanic low oxygen conditions and compared the expression levels of the whole transcriptome between our treatments. Results obtained here were discussed in the context of existing literature of experimental studies focused on unveiling the physiological aspects of early metazoans.

Methods

Sample collection

Specimens of the demosponge *Hymeniacidon heliophila* were collected on the intertidal rocks in the Araçá Bay, in São Sebastião (São

Paulo, Brazil – 23°48'56"S, 45°24'24"W). Collections were made in July, September, November, and December of 2021 and in April and July of 2022. After collection, sponges were manually cleaned of epibionts, transported to the lab, and maintained in aquaria with aerated biofiltered seawater kept at ~23°C, ~4.5 – 5 mg O_2 L^{-1} (~70%DO), and salinity of 33 PSU (Supplementary Figure 1).

Simulation chambers system

The simulation chambers (Supplementary Figure 1) consisted of a closed flow-through system that included a 3D-printed resin plate with internal tubes and four wells of 1.0 mL of volume each that were sealed with plastic O-rings, microscope slides, and metal sheets. Seawater sparged with a controlled O_2-N_2 mixture circulated from a 2.0 L reservoir plastic bottle throughout the chamber's wells within a self-contained loop via a peristaltic pump set at 3.0 mL min^{-1}. This reservoir water was sparged with the O_2-N_2 mixture set by a gas mixer, and well mixed with a magnetic stir bar to equally dissolve the gases. After the reservoir water reached the desired O_2 concentration, it was transported into the chambers by the pump through silicone tubing. The O_2 content of the bottle was measured using a multiparameter meter (HI98194, Hanna Instruments), with a probe placed inside the bottle. Water left the chamber wells through its internal pipes via overpressure and was redirected back to the reservoir bottle, thereby completing the circulation loop. The reservoir bottle was placed above a hot plate magnetic stirrer set to ~25 ºC. Dissolved O_2 concentration, pH, salinity, and temperature measurements were taken by the multiparameter meter every 2 minutes. For photographic documentation, a USB microscope connected to a notebook was placed above the chambers taking pictures of the animals every minute (Supplementary Figure 1).

Experimental procedures

For a given experimental run, four sponge fragments were cut from an individual and each one was placed inside one of the four chamber's wells (Supplementary Figure 1). Specimens were maintained in the chambers for ~24 hours with air-bubbled seawater being constantly flowed through the system (Supplementary Figure 1). This step was taken to allow trimmed fragments to recover from handling. Throughout the experiments, sponges had no external nutritional supplementation to reduce ammonia accumulation and decomposition. During trials, sponges were submitted to three oxygen conditions: hypoxia (5%DO, 0.3 – 0.4 mg O_2 L^{-1}), anoxia (0% DO, 0 mg O_2 L^{-1}), and oxygenated (100% DO, ~8 mg O_2 L^{-1}) for three time points: 1h, 6h, and 24h (Supplementary Figure 1). These time points were established following the experiments of Mills et al. (2018) and adjusted from direct observations of animals' tolerance. To generate replicates, each condition and time point tested was repeated four times. At the end of each trial, the four fragments were removed from the chambers, pooled to form one sample, flash frozen in liquid N_2, and stored at −80 °C for subsequent RNA extraction. Four pools of samples were also frozen from specimens freshly removed from the aquarium to serve as control of the aquarium condition (Supplementary Figure 1). A total of 40 samples were generated considering both the experiments and the aquarium controls.

Time-lapses, image processing, and statistical analysis

For each experimental run, images of the sponges in the chambers were obtained with an USB microscope connected to a notebook using FFmpeg (Tomar, 2006) to take pictures every minute at a resolution of 640×480 pixels. Image analysis was performed using ImageJ v.1.53 (Abràmoff et al., 2004) and sponges absolute projected area was calculated after calibrating the scale, which consisted of a transparent metric ruler placed in front of the chamber well.

For calculation of the average contraction cycle duration, projected body area graphs were analyzed using Excel. Following Nickel (2004), for each cycle, contraction duration was calculated by setting the time to zero starting from the first non-contracted state (when projected body area was maximum). Then, we counted the time taken to reach maximum contraction (when projected body area was minimum) and the time taken to return to the next non-contracted state (area maximum). The relative projected area values of each cycle were marked in relation to the antecedent maximum. In this way the influence of changes in the body size on the projected area was minimized.

For statistical analysis of the contraction cycle durations in the 24h samples, t-tests (assuming α=0.05, and equal distribution, but no equal variances) were performed on two alternative hypotheses: H_0 = no significant difference in contraction cycle durations between two conditions (e.g., anoxia vs. hypoxia); H_1 = significant difference in contraction cycle durations between two conditions. The three conditions tested were compared to each other (e.g., anoxia vs. hypoxia, anoxia vs. oxygenated, and oxygenated vs. hypoxia). Since we generated two contraction cycles datasets for each condition, to perform this analysis the datasets of each condition were combined. Therefore, t-tests were also applied between each dataset combined to make sure there was no significant difference between them (e.g., anoxia 1 vs. anoxia 2, hypoxia 1 vs. hypoxia 2, and oxygenated 1 vs. oxygenated 2).

RNA extraction and sequencing

Total RNA was extracted from the 40 sponge tissue samples using Norgen Biotek's Animal Tissue RNA Purification Kit following the manufacturer's protocol. RNA quantity and quality were measured using NanoDrop® 2000 spectrophotometer Thermo Scientific, Qubit® 2.0 Fluorometer Invitrogen, and Agilent 2100 Bioanalyzer. RNA sequencing

of the 40 samples was performed by Novogene Co. (CA, USA) with the following parameters: cDNA library preparation with mRNA poly-A enrichment using TruSeq RNA Library Prep Kit V2 (Illumina) following the manufacturer's protocol. Libraries were sequenced using 150 bp paired-end runs on Illumina HiSeq PE150 technology and an average sequencing depth of ~40 million reads per sample, generating ~12 GB of raw data per sample.

Sequence quality control, transcriptome assembly, and annotation

Removal of adapter sequences and sequence quality was confirmed using FastQC v.0.11.9 (Andrews, 2010). Ribosomal contamination was verified using SortMeRNA v.4.3.4 (Kopylova et al., 2012). However, less than 1% of contamination was found in each one of the 40 samples, so we decided not to filter the raw data due to the low levels of ribosomal contamination. The 40 samples were assembled *de novo* into a "super" reference transcriptome with all sequences using Trinity v.2.14.0 (Grabherr et al. 2011; Haas et al., 2013), with two non-standard settings: a minimum contig length of 500 bp and *in silico* read normalization. The quality and completeness of the reference transcriptome were assessed on gVolante web server (Nishimura et al., 2017) using the Benchmarking Universal Single-Copy Orthologs (BUSCO) v.5 (Simão et al., 2015), selecting the eukaryotic and metazoan BUSCO ortholog sets.

To functional annotate the transcripts, we used the Trinotate v.3.2.2 annotation pipeline (Grabherr et al., 2011; Bryant et al., 2017). Trinotate uses several different methods for automatic functional annotation, such as BLASTX and BLASTP v.2.12.0 (Altschul et al., 1990; Camacho et al., 2009) against UniProtKB/Swiss-Prot (e-value cutoff of $1e^{-3}$) for homology search. Then, proteins were predicted with TransDecoder v.5.5.0 (Haas et al., 2013) using default parameters and protein domain identification using HMMER v.3.3.2 (Finn et al., 2011) to obtain the protein PFAM domain.

Protein signal peptide was obtained using signalP v.4.1 (Petersen et al., 2011). Trinotate also leverages various annotation databases such as GO (Gene Ontology Consortium, 2004) and Kegg (Kanehisa et al., 2017). All functional annotation results derived from the different analyses were integrated into an SQLite database generating an annotation report for the transcriptome.

Differential gene expression and gene ontology (GO) enrichment analyses

To determine the set of differentially expressed genes of all samples, reads from individual replicates were aligned to the reference transcriptome assembly and estimation of transcripts abundance and expression values were performed using Bowtie2 (Langmead & Salzberg, 2012) and RSEM (Li and Dewey, 2011), respectively, within the Trinity module (Grabherr et al., 2011). Then, the count table (for the genes) was used to analyze the differential expression between the samples using the Bioconductor package edgeR (Robinson et al., 2010) within the Trinity perl wrapper script (Grabherr et al., 2011). Significantly differentially expressed genes between each of the pairwise comparisons were selected using the false discovery rate (FDR) adjusted *p*-value threshold of $1e^{-3}$ and minimum absolute (log2(a/b)) change of 2 (i.e., fourfold change), to minimize false positives. For each pairwise comparison, positive log fold changes were upregulated, and negative values were downregulated. Heatmaps were plotted using the R package pheatmap (Kolde, 2015).

The GO enrichment analysis was performed with the Bioconductor package GOseq (Young et al., 2012) using the differentially expressed genes (DEG) for each condition against the whole reference transcriptome and retained only those with a corrected *p*-value of $1e^{-3}$. Finally, REVIGO (Supek et al., 2011) was used to summarize and visualize the representative subset of GO term categories associated with those DEGs obtained with

edgeR package. To access the expression pattern of specific physiological pathways, heatmaps of genes with GO terms related to those pathways were generated using the R package pheatmap (Kolde, 2015).

Results

Survival and contraction behavior

All sponges submitted to the experiments survived the treatments, even those submitted to anoxia for 24h. Sponges survival was attested by the observation of contraction behavior. To feed, respirate, and excrete, sponges beat the flagella of choanocytes, generating water pumping through their chambers (Leys et al., 2011). Therefore, the observation of contractions was considered as evidence that the sponge was alive. The video time-lapses obtained for each one of the experiments are available at https://figshare.com/projects/Physiological_and_molecular_responses_of_modern_metazoans_under_the_Neoproterozoic_oceanic_conditions/184471. Full contraction cycles can be observed in the 24h experiments (Supplementary Figures 2-4), but contractions could also be observed in the 6h experiments (Supplementary Figures 5-7).

Although the contractions can be observed in the time-lapses (https://figshare.com/projects/Physiological_and_molecular_responses_of_modern_metazoans_under_the_Neoproterozoic_oceanic_conditions/184471), when generating the projected area graphs, some of these contractions could not be measured. As we used 2-dimensional measurements to calculate the projected body area (e.g., length and width of the body contour), when contractions occurred in 3-dimensional space (e.g., length, width, and height), they could not be properly measured. Nevertheless, the two best representatives of each 24h samples (e.g., the ones where the contraction cycles were easily visually identified) were used to calculate the average contraction cycle duration and the number of

contraction cycles over 24h (Fig. 1). The average contraction cycle duration for the anoxia 24h samples were 45.04 min and 52.88 min, with 22 and 25 contractions over 24h, respectively (Fig. 1). For the hypoxia 24h samples, the average contraction cycles lasted 123.75 min and 83.21 min, with 8 and 14 contractions, respectively. In the oxygenated condition, the average contraction cycles were of 51.13 min and 71.94 min, with 23 and 28 contractions over 24h (Fig. 1).

No significant differences (P>0.05) were found between the two contraction cycle duration datasets generated for each condition (e.g., anoxia 1 vs. anoxia 2, hypoxia 1 vs. hypoxia 2, and oxygenated 1 vs. oxygenated 2), therefore they were considered suitable to be combined to allow the comparison between conditions (e.g., anoxia 1+2 vs. hypoxia 1+2, anoxia 1+2 vs. oxygenated 1+2, and oxygenated 1+2 vs. hypoxia 1+2). When comparing the combined 24h datasets, a significant difference was found between the contraction cycle durations of hypoxia vs. anoxia (P=0.0003), and between hypoxia vs. oxygenated (P=0.005). On the other side, no significant difference was found was found between the cycle durations of anoxia and oxygenated samples (P=0.11).

Transcriptome assembly and annotation

RNA sequencing of the 40 samples yielded a total of 1,955,077,259 reads, which resulted in ~49 million reads per sample. Basic sequencing metrics, including raw reads and library size of the transcriptomes, can be seen in Supplementary Table 1. Using SortMeRNA, we observed little ribosomal contamination (<1%) among our sequences, so we decided not to filter the raw data. Raw reads can be accessed at the Short Read Archive (SRA) under Bioproject number (*under submission*).

The reads from all 40 samples were used to construct a reference transcriptome assembly (see Table 1 for complete statistics), resulting in 316,342 assembled transcripts (N50 2,093 nt) and 128,201 ‘genes’ (i.e.,

Trinity components or ‘assembled genes’ as identified in the Trinity pipeline). The reference transcriptome fits within the expected range of size, gene number, and N50 of published sponge transcriptomes (Strehlow et al., 2023; Riesgo et al., 2014). Our BUSCO analysis recovered 97.2% of the eukaryotic conserved cassette and 94.9% of the metazoan cassette (Table 1). Therefore, the reference transcriptome was effectively complete based on BUSCO analysis (Simão et al., 2015) and was considered suitable for further analysis. Around 88% of the raw reads were mapped to the reference transcriptome per sample (Supplementary Table 1). Although 63.67% of the transcripts obtained a BLAST hit against the Swiss-Prot database, only half of these hits were with metazoan genes, and 98% of those with a metazoan hit had associated GO terms (Table 1).

Differential gene expression

A total of 5,012 genes were differentially expressed among all samples, however only 1,452 of those could be annotated as metazoan (Table 2; Figs 2 and 3). Pairwise comparisons were made between different conditions in the same time point (i.e., anoxia 1h vs. hypoxia 1h, anoxia 1h vs. oxygenated 1h, and hypoxia 1h vs. oxygenated 1h) and between the same condition in different time points (i.e., anoxia 1h vs. anoxia 6h, anoxia 1h vs. anoxia 24h, and anoxia 24h vs. anoxia 6h). Pairwise comparisons were also made between each condition and time point and the aquarium control (Table 2; Figs 2 and 3). The number of significantly differentially expressed genes in all these comparisons is summarized in Table 2. For each pairwise comparison, genes that were upregulated in one condition were consequently downregulated in the other one (i.e., within A1 vs. A6, genes upregulated in A1 were down regulated in A6 and vice-versa).

The highest number of DEGs occurred in the Anoxia 24h vs. Hypoxia 24h comparison (680 genes), followed by Oxygenated 24h vs.

Hypoxia 24h (605 genes). The lowest number of DEGs (12 genes) is from the Anoxia 1h vs. Hypoxia 1h comparison, followed by Anoxia 6h vs. Oxygenated 6h (31 genes), and Anoxia 24h vs. Oxygenated 24h (27 genes). This data highlights a pattern shown by the results, where Anoxia and Oxygenated 24h samples present similar expression profiles, which are striking different from the Hypoxia 24h samples (Table 2; Fig. 2). This pattern can also be observed in the Principal Component Analysis graph (Supplementary Fig. 8) which shows Anoxia and Oxygenated 24h samples grouped, and the Hypoxia 24h samples apart.

Functional enrichment analysis

Generally, the significantly enriched Gene Ontology (GO) terms (within Biological Process) were not related to oxidative stress, oxygen metabolism or anaerobic metabolism (Supplementary Figures 9-20). GO terms related to stress and defense such as 'response to salt stress' and 'inflammatory response' were upregulated in the 24h samples as well as in the hypoxia samples (Supplementary Figures 11 and 13). GO terms related to cell adhesion, cell fate determination and cell proliferation were upregulated in all time points and conditions tested (Supplementary Figures 9-14). To focus on certain physiological pathways, heatmaps of genes with assigned GO terms related to cell death, stress and morphogenesis were generated (Figs 4-9).

The heatmaps showing DEGs with predicted functions in regulated cell death, and GO terms associated with cell death, negative cell death regulation or both (Figs 6 and 7) showed a shift in the expression profile over time. When comparing the 1h samples, the oxygenated ones are contrasting with all others (Fig. 6). After 6h, there is no clear differentiation between the samples, but after 24h, anoxia and oxygenated present very similar expression patterns, and hypoxia is similar to the aquarium control (Fig. 6). The similarity between anoxia and oxygenated

after 24h of experimental run can also be seen in the heatmaps of genes with GO terms related to stress and oxidative stress (Fig. 4) and in the heatmap of genes related to morphogenesis (Fig. 8). When comparing the same condition in different time points, hypoxia samples seem to present more upregulated genes than oxygenated and anoxia in all three pathways analyzed (Figs 5, 7 and 9), reinforcing the distinction between anoxia and oxygenated from the hypoxia samples.

Discussion

No oxygen and high oxygen levels as equally stressful factors

Here we searched for differences in gene expression of the demosponge *Hymeniacidon heliophila* when submitted to low oxygen levels similar to those of ancient oceans of the Neoproterozoic in different time points (1h, 6h, and 24h). Our results highlighted that sponges were very tolerant to the experiments, and the similar expression profile showed by anoxia and oxygenated samples after 24h of exposure (Fig. 2) was a surprising result. Highlighting this similarity there are the few differentially expressed genes (DEGs) between 24h anoxia and oxygenated (27 genes) in contrast with the massive number of DEGs when comparing to 24h hypoxia (680 and 605 genes, respectively; Table 2). This pattern is also evident when focusing on genes related to cell death, stress, and morphogenesis (Figs 4, 6 and 8), suggesting that both anoxia and oxygenated conditions may trigger the same responses.

The natural environment of *H. heliophila* is mostly hypoxic, as they are an intertidal species adapted to endure daily air exposure which generates oxidative stress (Lysek et al., 2003; Weigel and Erwin, 2016). Specimens used in this work were collected in the Araça Bay (SP, Brazil), a mangrove area with hypoxic waters due to eutrophication and reduced water circulation (Teodoro et al., 2011). Moreover, studies have

demonstrated that pumping sponges may present a constant internal suboxic environment (Lavy et al., 2016). Additionally, even though sponges are aerobic organisms, high oxygen levels are known for generating reactive oxygen species (ROS) that can induce oxidative damage (Hewitt and Degnan, 2022). Considering that, *H. heliophila* is probably better adapted to hypoxia, therefore, the similar expression profiles of anoxic and oxygenated samples are an indicative that both conditions are stressful. Supporting this, Gunda and Janapala (2009) demonstrated that the demosponge *Haliclona pigmentifera* has a higher survival rate under hypoxia than under anoxia and normoxia environments. Similarly, Bozdag et al. (2021) showed via mathematical modeling that anoxic and oxygenated conditions produce the same relative fitness in organisms larger than a given size. These evidences agree with the hypothesis that both the total absence and the abundance of oxygen can be equally stressful for sponges.

The contraction behavior observed in the 24h experiments is another piece of evidence pointing to the similar effects that anoxia and oxygenated conditions can have on sponges. The average contraction cycle duration was significantly different between hypoxia vs. anoxia and hypoxia vs. oxygenated (Fig. 1). However, no significant differences were found between anoxia and oxygenated contraction cycle durations (Fig. 1). Anoxia and oxygenated samples had more contractions than the hypoxia ones, and this behavior of increasing the pumping rate is a mechanism sponges use to aerate its body, trying to increase oxygen and nutrients supply (Hoffmann et al., 2008; Maldonado et al., 2012). Therefore, the higher number of contractions and shorter contraction durations in anoxia and oxygenated samples could be a sign of oxidative stress as it seems to be a strategy to increase ventilation (Micaroni et al., 2022).

Early animals' oxygen sensing mechanisms

At the cellular level, when oxygen levels are low, most animals have an evolutionarily conserved pathway for maintaining oxygen homeostasis that triggers physiological changes in gene expression (Semenza, 2007). This oxygen sensing pathway is mediated by the transcription factor known as the hypoxia-inducible factor (HIF; Kaelin and Ratcliffe, 2008). However, recent studies demonstrated that key components of the HIF pathway are absent in sponges and ctenophores (Mills et al., 2018; Belato et al., 2023), which are the two candidate clades to be sister to all other animals (Pisani et al., 2015; King and Rokas, 2017; Simion et al., 2017; Whelan et al., 2017). These results suggest that the last common ancestor of metazoans lacked a functional HIF pathway as well (Mills et al., 2018; Belato et al., 2023). Our data is consistent with these studies, as we did not find HIF related genes in our transcriptomes.

Even though sponges and ctenophores lack oxygen sensing mechanisms related to HIF, they most likely detect cellular oxygen using other mechanisms. Mitochondrial cytochrome C oxidase is inhibited by low oxygen levels causing a disbalance in the redox state that generates reactive oxygen species (ROS) in the cells (Chandel and Schumacker, 2000). Cytochrome C can also be inhibited by hydrogen sulfide (H_2S), a toxic compound that accumulates in the cells when oxygen is low (Powell and Somero, 1986; Cooper and Brown, 2008; Olson, 2015). H_2S is removed by several O_2-dependent reactions which may act as a cellular oxygen sensing mechanism (Olson, 2015; Mills et al., 2018). Here we found several genes related to the sulfide-removal pathway differentially expressed. Catalase, a well-known sulfide-reductase (Olson et al., 2017) was 4 times more expressed in hypoxia 24h than in oxygenated and anoxia (Figs 4 and 5), and peptide methionine sulfoxide reductase was upregulated in anoxia 1h (Fig. 4). Different enzymes known to have their expression stimulated in the presence of H_2S were also upregulated in

anoxia and hypoxia samples, such as serine/threonine protein kinase, thyroid peroxidase, and phosphoenolpyruvate carboxykinase (Zhang et al., 2013; Das et al., 2015; Song et al., 2021; Zhao et al., 2022; Figs 4 and 5). Our results indicate that the sulfide-removal pathway is increased in anoxia and hypoxia conditions. As most enzymes related to the sulfide metabolism are conserved across the tree of life, being present in opisthokonts, plants, bacteria, and archaea (Olson, 2015; Mills et al., 2018; Mateos et al., 2023), the cellular detection of oxygen via sulfide is a mechanism that was most likely already present in the first animals.

Stress responses under low oxygen levels

Glycolysis is a metabolic pathway that generates ATP and NADH without the presence of oxygen and was expected to increase under hypoxia and anoxia conditions (Guillaumond et al., 2013; Nelson et al., 2013). Interestingly, some genes directly or indirectly involved in glycolysis were found differentially expressed here. Phosphoenolpyruvate carboxykinase was upregulated in anoxia and hypoxia in all time points tested (Figs 4 and 5; Yu et al., 2021). On the other hand, sorbitol dehydrogenase was upregulated in oxygenated and anoxia conditions after 24h (Fig. 4; Jeffery and Jörnvall, 1983), similar to serine/threonine protein kinase that was upregulated in one anoxia 1h and all oxygenated 1h samples (Fig. 4; Le Mellay et al., 2002). These results might indicate that glycolysis rates increased under anoxia and hypoxia conditions, providing anaerobically generated ATP.

Heat shock proteins are a well-known cellular stress response in metazoans (Lindquist and Craig, 1998; Li and Srivastava, 2003). Here, they were differentially overexpressed in hypoxia 6h and 24h, as well as in oxygenated 1h samples (Figs 6 and 7). Low oxygen is known to increase cellular antioxidative response (Weihe et al., 2010; Hu et al., 2015; Hammarlund et al., 2020; Andreyeva et al., 2021; Gostyukhina et al., 2022;

Lee et al., 2023). Here we found several genes related to antioxidant defense upregulated in hypoxia in most time points (Fig. 5), such as catalase (Nandi et al., 2019), glutamate cysteine ligase (Krejsa et al., 2010), peroxidasin (Hanmer and Mavri-Damelin, 2018), lysyl oxidase (Martínez-Revelles et al., 2017). Some genes involved in immune response mechanisms were also upregulated in hypoxia, such as NFX1-type zinc finger-containing protein (Vavassori et al., 2021) and phospholipase A2 (Sun et al., 2005), as well as ATPases, which are responsible for controlling oxidative stress and maintaining cellular homeostasis (Liu et al., 2018). However, it is worth mentioning that when looking to stress related genes, hypoxia presented a similar expression profile to the aquarium control samples (Fig. 5). This could be an indicative that those are the regular responses of sponges better adapted to hypoxic conditions (Micaroni et al., 2022).

Cell death as an indicator of stress

Before each experimental run, sponges were dissected and placed in the simulation chambers with air-sparged seawater for ~24h to minimize the handling effects on trimmed fragments. Previous work demonstrated that some sponges exhibit increased expression of genes related to cell death up to three to five days after being dissected (Riesgo et al., 2022). Additionally, apoptosis processes occurring after dissection are fundamental for regenerating injured tissues in the demosponges *Aplysina cavernicola* (Ereskovsky et al., 2020) and *Halisarca caerulea* (Kenny et al., 2018; Wu et al., 2022). Physiologically, cell death is a homeostatic mechanism that regulates and maintains the function and size of tissues and organs (He et al., 2021). However, oxidative stress can also induce apoptosis, inflammation, and histological changes (Sun et al., 2015; Wang et al., 2019; Nie et al., 2020; Jing et al., 2023).

Here we identified several genes that have been linked to cell death in sponges and other animals differentially expressed (Figs 6 and 7). When comparing different conditions in the same time points, members of the tumor necrosis factor (TNF) receptor family (Wiens and Müller, 2006), which trigger caspase activation through the action of adapter molecules in extrinsic apoptosis, were upregulated in mostly 24h oxygenated and anoxia samples (Fig. 6). However, when comparing the same condition in different time points, TNFs were also upregulated in hypoxia (Fig. 7). Ribosomal proteins, responsible for cell cycle arrest and apoptosis (Kang et al., 2021), were upregulated in oxygenated 1h samples (Fig. 6). The inflammasome component NACHT and other members of the NLR family involved in detection of cellular stress-associated molecules and initiation of inflammatory responses (Yuen et al., 2014) were upregulated in hypoxia after 6h and 24h (Fig. 7). Apoptosis can be considered as a biomarker for environmental stress in sponges (Wagner et al., 1998). Therefore, cell death related genes upregulated in hypoxia, as well as in 24h oxygenated and anoxia samples are suggestive of stress-mediated apoptosis responses in those conditions.

Remodeling of the aquiferous system triggered by hypoxia

Changes in the water flow and low oxygen levels can induce remodeling of the aquiferous system of sponges to improve the oxygen supply (Leys et al., 2011; Leys and Hill, 2012; Micaroni et al., 2022). Interestingly, several genes related to vertebrate blood vessel formation were found differentially expressed in our dataset (Figs 8 and 9). In vertebrates, blood vessels are formed through vasculogenesis, with the formation of endothelial cells, and angiogenesis, in which new vessels sprout from endothelial cells in preexisting vessels (Kim et al., 2011). Hypoxia is the primary physiological trigger for blood vessels formation, where vasculogenic endothelial cells activated by angiogenic signals

proliferate and migrate towards the angiogenic stimulus (Muñoz-Chápuli et al., 2004; Muñoz-Chápuli, 2011). These endothelial cells group into a new basement membrane as well as an extracellular matrix (ECM) to form a new vessel (Muñoz-Chápuli et al., 2004). Vertebrate vessels are not homologous to the aquiferous system of sponges and the real function of vertebrate blood vessels genes in the formation of the aquiferous system is unknown. However, such genes may have an ancestral role in the formation of tubular structures to canalize fluids in animals as well as similar hypoxia–related triggering mechanisms (Riesgo et al., 2022).

In our experiments, essential genes to the formation of blood vessels, such as P-selectin and E-selectin were upregulated in anoxia and oxygenated 24h samples (Figs 8 and 9; Koch et al., 1995; Hayashi et al., 2000; André, 2004). Some of the most important vertebrate stimulator of vessels formation are the endothelial growth factors (VEGF and EGF; Breier and Risau, 1996; Amin et al., 2008; Kılıçaslan et al., 2013) and ephrin and its ligands (Wang et al., 2010), which were all upregulated in anoxia and oxygenated 24h samples (Fig. 9). The formation of vertebrate blood vessels involves the reorganization of the extracellular matrix (ECM) and cell adhesion (Bischoff, 1997; Bou-Gharios et al., 2004). Here, genes involved in these two processes, such as integrin, fibulin, cadherin, neogenin, and hemicentin were upregulated in some anoxia and/or oxygenated 24h samples (Fig. 9; Cole et al., 2007; Vestweber, 2008; Yanagisawa et al., 2009; Saharinen and Ivaska, 2015; Yao et al., 2020; Welcker et al., 2021). The fact that genes involved in the formation of blood vessels are upregulated in anoxia and oxygenated conditions after 24h of exposure is suggestive of increased morphogenesis processes in such stressful situations.

The physiological adaptations of early animals

The early animals that lived in the Neoproterozoic Era had to endure severe daily redox fluctuations and even possible nocturnal anoxia (Krause et al., 2022; Hammarlund et al., *in press*). These oxygen fluctuations could be physiologically stressful, and the early animals needed to have mechanisms to cope with this challenging environmental setting (Hammarlund et al., *in press*). The ability to sense oxygen levels and shift from aerobic to anaerobic cell metabolism must have been essential traits to those organisms (Semenza, 2007; Hammarlund et al., 2020). Our results support the hypothesis that even though the HIF pathway was most likely absent in the first metazoans (Mills et al., 2018; Belato et al., 2023), they probably could sense oxygen levels via the sulfide metabolism pathway. We also confirmed that sponges can shift to the anaerobically production of ATP under oxidative stress conditions, a metabolic adaptation predicted to ancient metazoans (Hammarlund et al., 2020, *in press*). Here we corroborate the fact that sponge morphology and body plan can be modulated by the environment to a certain extent (Leys et al., 2011; Leys and Hill, 2012; Micaroni et al., 2022). The phenotypic ability to remodeling their internal channels in response to environmental changes could represent an advantageous adaptation that may have been beneficial to early animals. The similar stress responses generated by anoxic and oxygenated conditions in sponges suggest that the tolerance to hypoxia is probably an ancient inheritance from their early ancestors (Fago and Jensen, 2015).

First metazoans most likely were adapted to tolerate low environmental oxygen levels, and probably had several mechanisms to survive the Neoproterozoic redox fluctuations, such as the ones observed in modern sponges (Mills et al., 2018; Strehlow et al., 2023; Hammarlund et al., *in press*). The striking difference in the hypoxia expression profile when compared to anoxia and oxygenated indicate a better adaptation to

low oxygen conditions in sponges. Our results showing overexpression of genes related to glycolysis, sulfide-removal metabolism and morphogenesis under oxidative stress are suggestive of an ancestral role of these mechanisms in ancient metazoans. Here we provide another piece of evidence towards the increasingly strong hypothesis of the independent evolution of oxygen and animal life (Cole et al., 2020). Our findings enlighten the physiological adaptations that may have allowed early animals functional and competitive advantages during their evolution.

Acknowledgments

This study was supported by FAPESP (Fundação de Amparo à Pesquisa do Estado de São Paulo – Brazil) thematic project (2016/06114-6), coordinated by R.I.T. A fellowship to E.M.C.-P. was provided by FAPESP (2018/20268-1). F.A.B. was funded by CNPq and FAPESP (2019/18051-7 and 2021/14115-0). A JP grant (2015/50164-5) was provided by FAPESP to F.D.B. A.C.M. was funded by CNPq (307832/2022-8). Use of Digital Research Alliance of Canada computational resources at University of Alberta is acknowledged. F.A.B. would like to thank the valuable help of Dr. Ana Riesgo and Dr. Warren Gallin during her internship at the University of Alberta, as well as the support of Dr. Brian J. Haas on the Trinity GitHub forum. F.A.B. and E.M.C.-P. would like to thank Rodrigo Adrian de Oliveira Abans (*in memoriam*) for his work in the design of the 3D printed chambers. This is a contribution of NP Bio-Mar USP.

Table 1 – Statistics of the assembled reference transcriptome and details on the completeness of the reference transcriptome using BUSCO values. Abbreviations: N, number; nt, nucleotides; GO, gene ontology; SP, Swiss-Prot database; GC, guanine-cytosine.

General stats		
Total transcripts	316,342	
Total trinity 'genes'	128,201	
Total length (nt)	462,698,816	
Median contig length	828	
GC content	44.26%	
N50	2,093	
Transcripts with blast hit (SP-all domains)	201,418 (63.67%)	
Transcripts with blast hit (SP-metazoa only)	100,957 (31.91%)	
Transcripts with GO term (SP-metazoa only)	99,357 (31.41%)	
Completeness	**BUSCO Eukaryota (255)**	**BUSCO Metazoa (954)**
Complete	97.2%	94.9%
Partial	1.6%	1.4%
Missing	1.2%	3.7%
Duplication	94.5%	93%

Table 2 – Number of significantly differentially expressed genes (DEGs) among each pairwise comparison analyzed. The number of metazoan annotated genes is shown in parentheses. For each pairwise comparison, genes that were upregulated in one condition were consequently downregulated in the other one (i.e., within A1 vs. A6, genes upregulated in A1 were down regulated in A6 and vice-versa). Abbreviations: A, anoxia; H, hypoxia; O, oxygenated; 1, 1 hour; 6, 6 hours; 24, 24 hours; CA, aquarium control; UP, upregulated.

Anoxia	A1 vs. A6		A1 vs. A24		A24 vs. A6	
	UP in A1	UP in A6	UP in A1	UP in A24	UP in A24	UP in A6
	172 (81)	173 (62)	81 (25)	237 (71)	275 (85)	91 (19)
Hypoxia	H1 vs. H6		H1 vs. H24		H24 vs. H6	
	UP in H1	UP in H6	UP in H1	UP in H24	UP in H24	UP in H6
	18 (8)	178 (73)	56 (16)	242 (64)	33 (18)	224 (84)
Oxygenated	O1 vs. O6		O1 vs. O24		O24 vs. O6	
	UP in O1	UP in O6	UP in O1	UP in O24	UP in O24	UP in O6
	426 (91)	67 (14)	51 (16)	35 (13)	265 (42)	36 (7)
1 hour	A1 vs. H1		A1 vs. O1		H1 vs. O1	
	UP in A1	UP in H1	UP in A1	UP in O1	UP in H1	UP in O1
	6 (2)	6 (3)	79 (30)	372 (83)	19 (5)	300 (78)
6 hours	A6 vs. H6		A6 vs. O6		H6 vs. O6	
	UP in A6	UP in H6	UP in A6	UP in O6	UP in H6	UP in O6
	35 (6)	102 (23)	26 (13)	5 (1)	111 (24)	10 (4)
24 hours	A24 vs. H24		A24 vs. O24		H24 vs. O24	
	UP in A24	UP in H24	UP in A24	UP in O24	UP in H24	UP in O24
	504 (162)	176 (43)	24 (12)	13 (4)	84 (24)	521 (134)
Aquarium Control	A1 vs. CA		A6 vs. CA		A24 vs. CA	
	UP in A1	UP in CA	UP in A6	UP in CA	UP in A24	UP in CA
	99 (44)	34 (32)	135 (40)	176 (46)	271 (56)	32 (7)
	CA vs. H1		CA vs. H6		CA vs. H24	
	UP in CA	UP in H1	UP in CA	UP in H6	UP in CA	UP in H24
	62 (36)	102 (32)	63 (22)	210 (48)	250 (85)	351 (65)
	CA vs. O1		CA vs. O6		CA vs. O24	
	UP in CA	UP in O1	UP in CA	UP in O6	UP in CA	UP in O24
	76 (24)	525 (136)	18 (5)	29 (10)	42 (10)	299 (63)

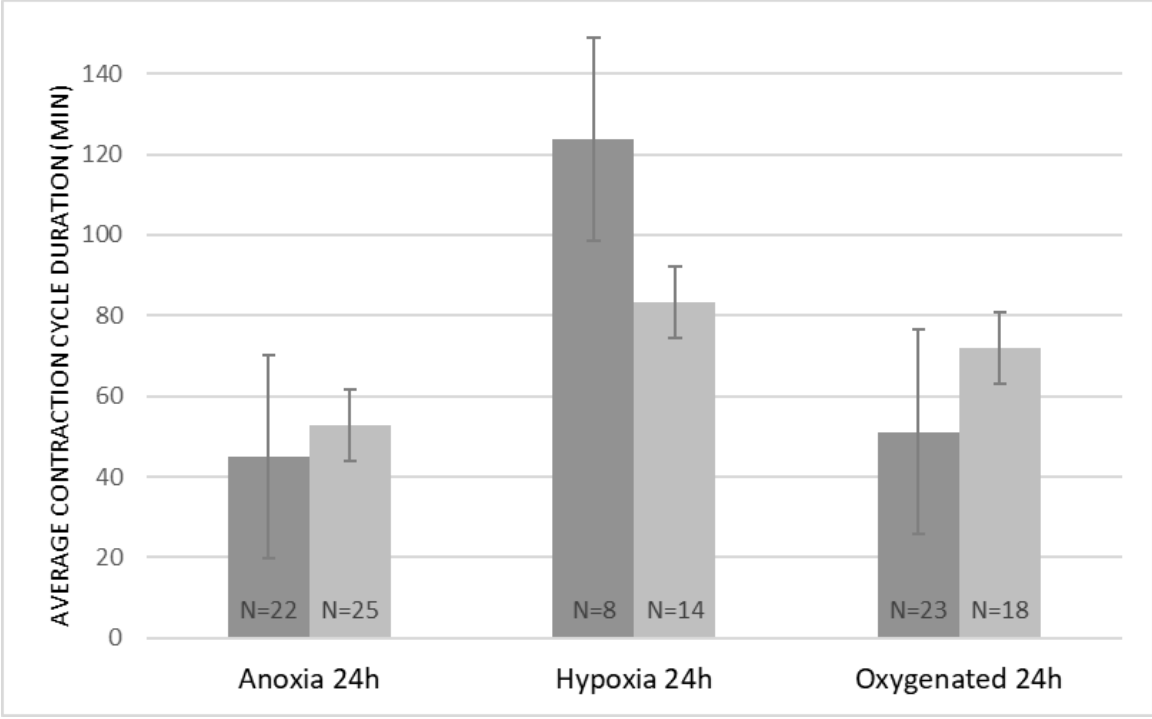

Figure 1 – Comparison of average contraction cycle duration of two Anoxia 24h samples (45.04 min, N=22; 52.88 min, N=25), two Hypoxia 24h samples (123.75 min, N=8; 83.21 min, N=14), and two Oxygenated 24h samples (51.13 min, N=23; 71.94 min, N=18). N represents the number of contraction cycles observed over 24h. Error bars represent standard error. Contraction cycle durations differ significantly between hypoxia vs. anoxia (P=0.0003) and hypoxia vs. oxygenated (P=0.005), but there is no significant difference in cycle durations between anoxia and oxygenated (P=0.11). Samples used to generate the graph were EA23/A24_3 and EA24/A24_4 for Anoxia 24h (Supplementary Figure 2), EH40/H24_4 and EH33/H24_1 for Hypoxia 24h (Supplementary Figure 3), and EO18/O24_4 and EO14/O24_3 for Oxygenated 24h (Supplementary Figure 4).

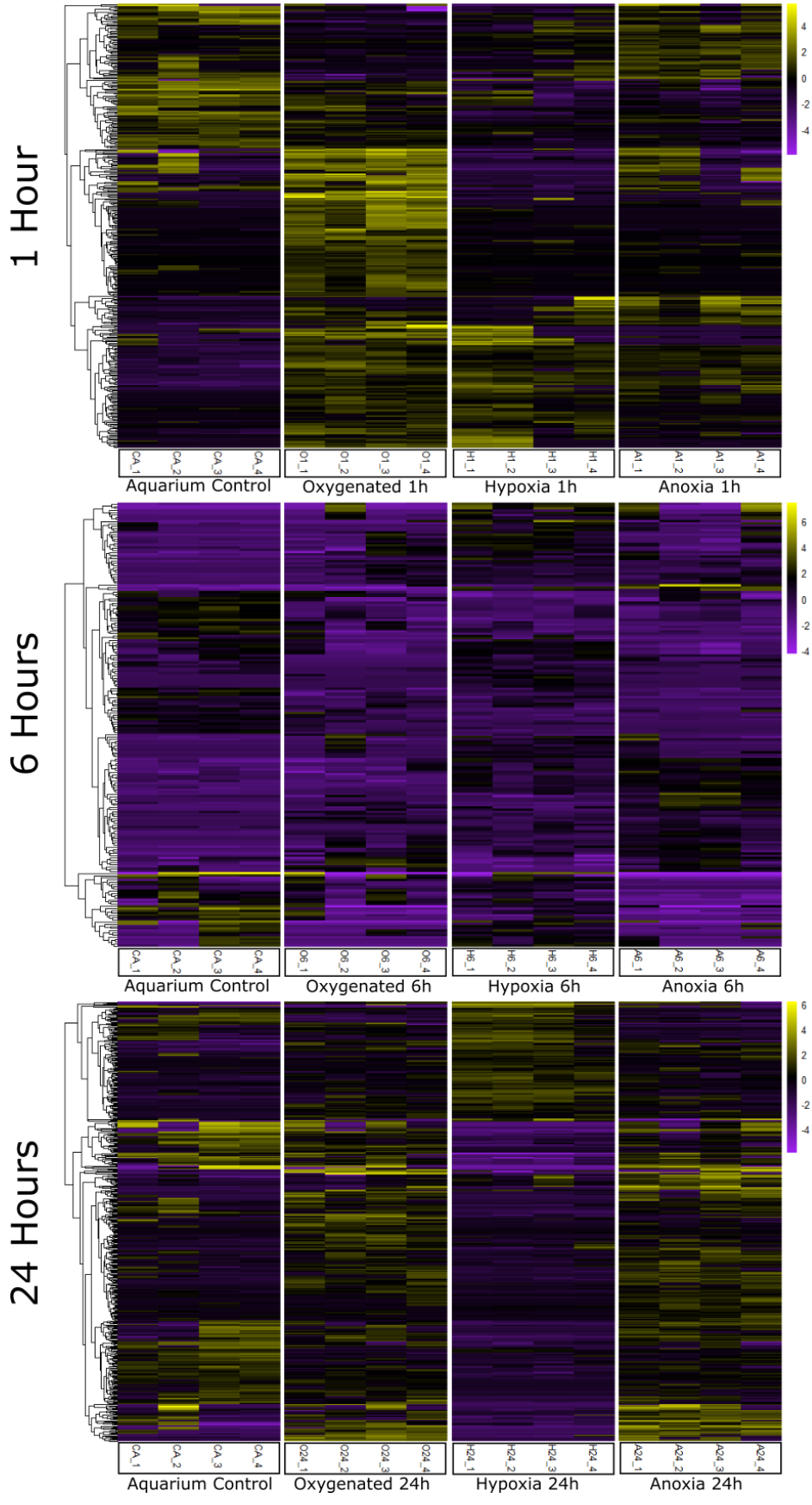

Figure 2 – Heatmap showing differential gene expression when comparing different conditions (oxygenated, hypoxia and anoxia) in the same time point. Yellow and purple intensities indicate differentially overexpressed and underexpressed genes, respectively. Abbreviations: A, anoxia; H, hypoxia; O, oxygenated; 1, 1 hour; 6, 6 hours; 24, 24 hours; CA, aquarium control.

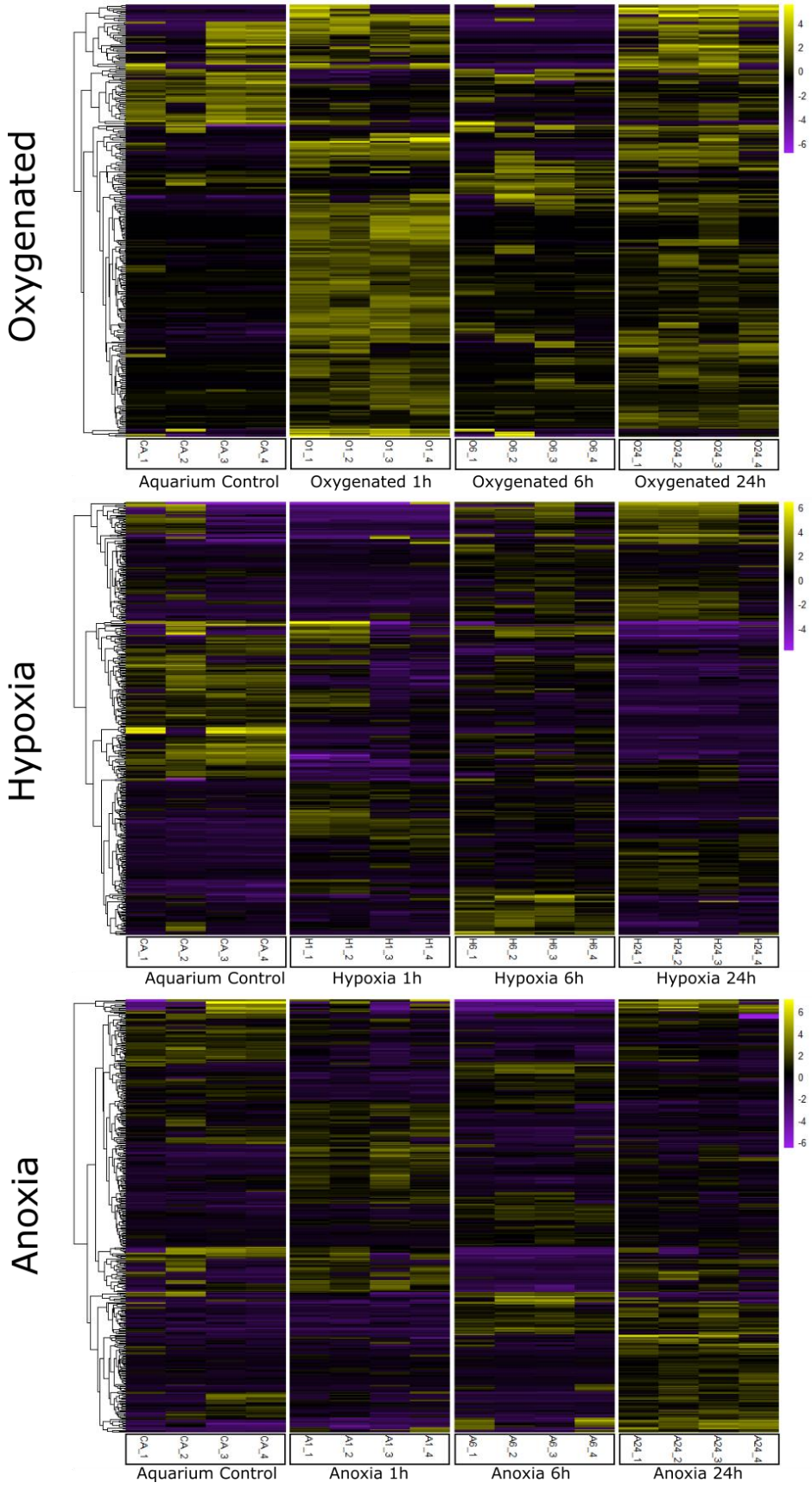

Figure 3 – Heatmap showing differential gene expression when comparing the same condition in different time points (1h, 6h and 24h). Yellow and purple intensities indicate differentially overexpressed and underexpressed genes, respectively. Abbreviations: A, anoxia; H, hypoxia; O, oxygenated; 1, 1 hour; 6, 6 hours; 24, 24 hours; CA, aquarium control.

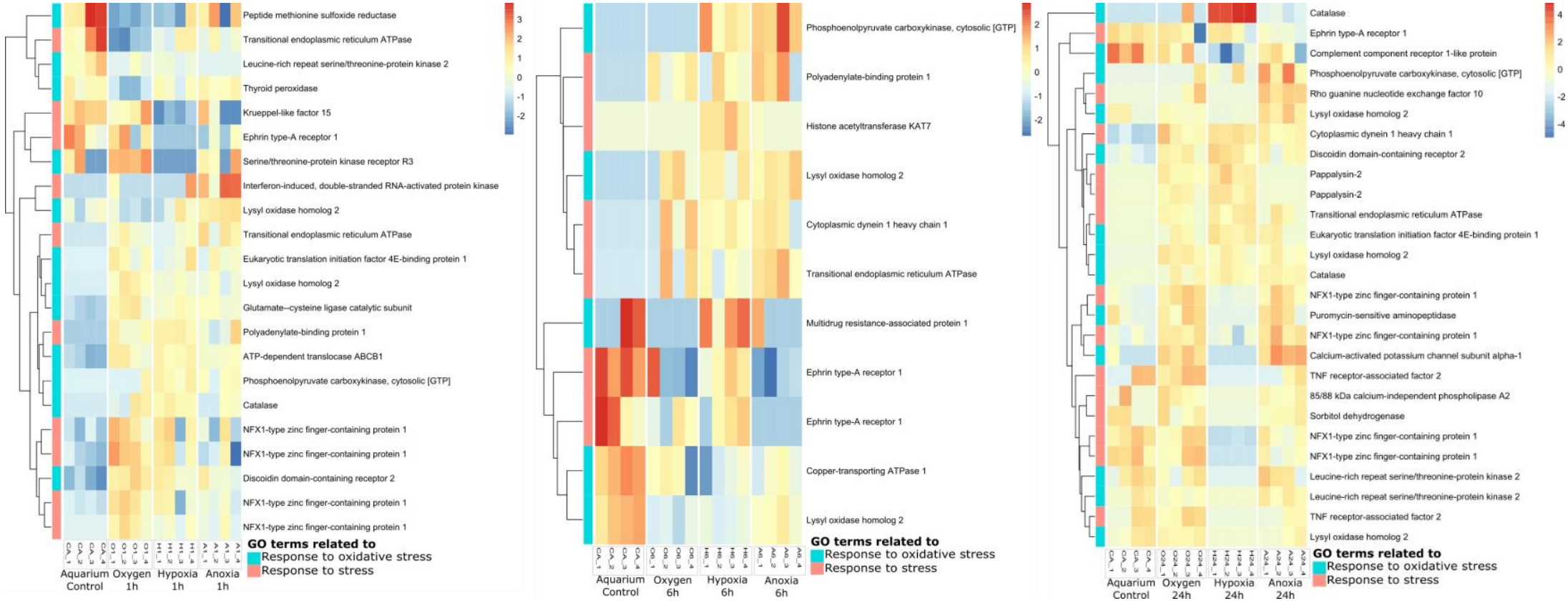

Figure 4 – Differentially expressed stress-related genes sorted by different conditions in the same time point. Heatmap showing differentially expressed genes with predicted functions in stress, and GO terms associated with response to oxidative stress (blue), and response to general stress (pink). Left panel shows 1h samples in the three conditions tested (oxygenated, hypoxia and anoxia) as well as the aquarium control. Middle panel shows 6h samples in the three conditions and the aquarium control. Right panel shows 24h samples in the three conditions as well as the aquarium control samples. Abbreviations: A, anoxia; H, hypoxia; O, oxygenated; 1, 1 hour; 6, 6 hours; 24, 24 hours; CA, aquarium control.

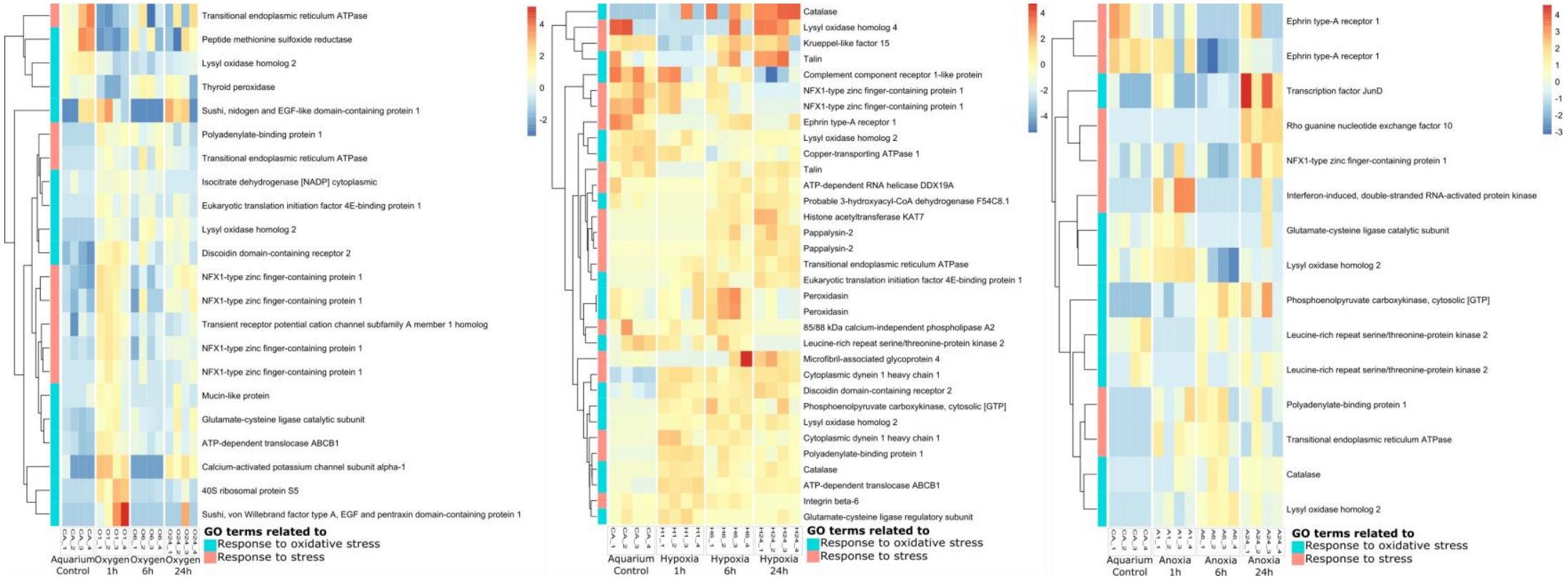

Figure 5 – Differentially expressed stress-related genes sorted by the same condition in different time points. Heatmap showing differentially expressed genes with predicted functions in stress, and GO terms associated with response to oxidative stress (blue), and response to general stress (pink). Left panel shows oxygenated samples in the three time points tested (1h, 6h, and 24h) as well as the aquarium control. Middle panel shows hypoxia samples in the three time points and the aquarium control. Right panel shows anoxia samples in the three times as well as the aquarium control samples. Abbreviations: A, anoxia; H, hypoxia; O, oxygenated; 1, 1 hour; 6, 6 hours; 24, 24 hours; CA, aquarium control.

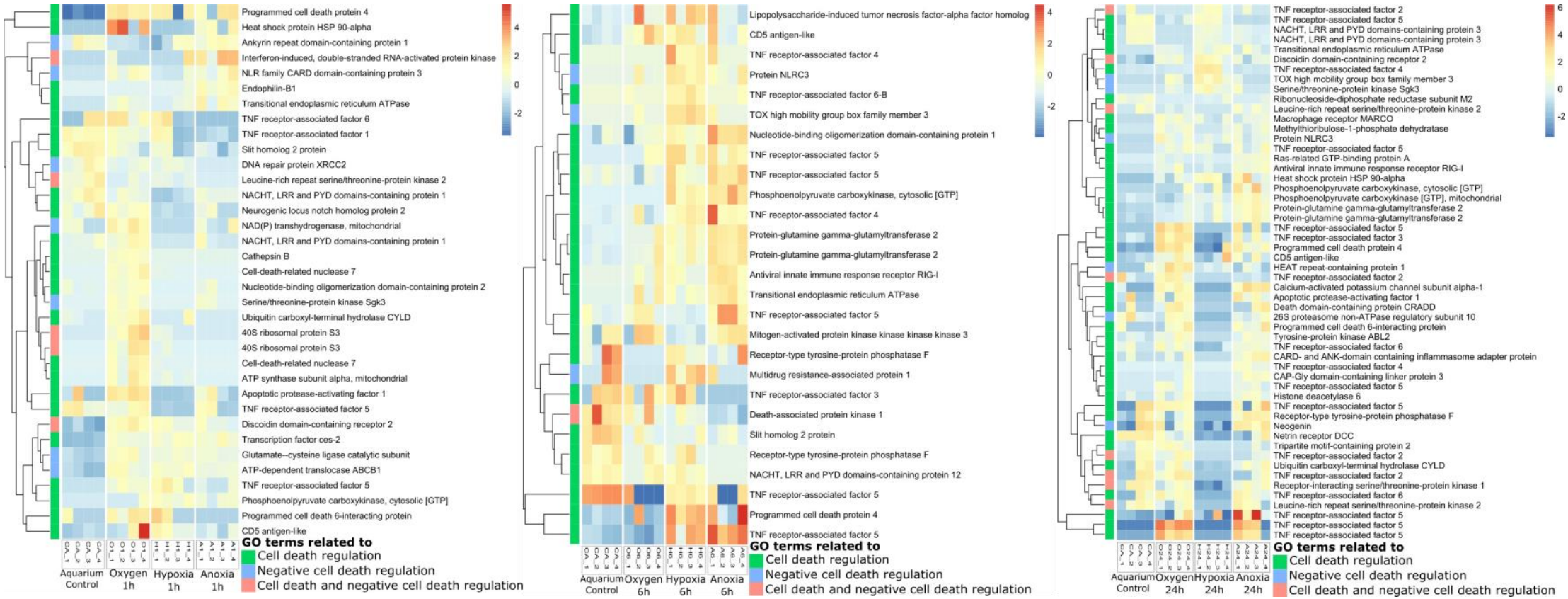

Figure 6 – Differentially expressed cell death-related genes sorted by different conditions in the same time point. Heatmap showing differentially expressed genes with predicted functions in regulated cell death, and GO terms associated with cell death (green), its negative regulation (blue), or both (pink). Left panel shows 1h samples in the three conditions tested (oxygenated, hypoxia and anoxia) as well as the aquarium control. Middle panel shows 6h samples in the three conditions and the aquarium control. Right panel shows 24h samples in the three conditions as well as the aquarium control samples. Abbreviations: A, anoxia; H, hypoxia; O, oxygenated; 1, 1 hour; 6, 6 hours; 24, 24 hours; CA, aquarium control.

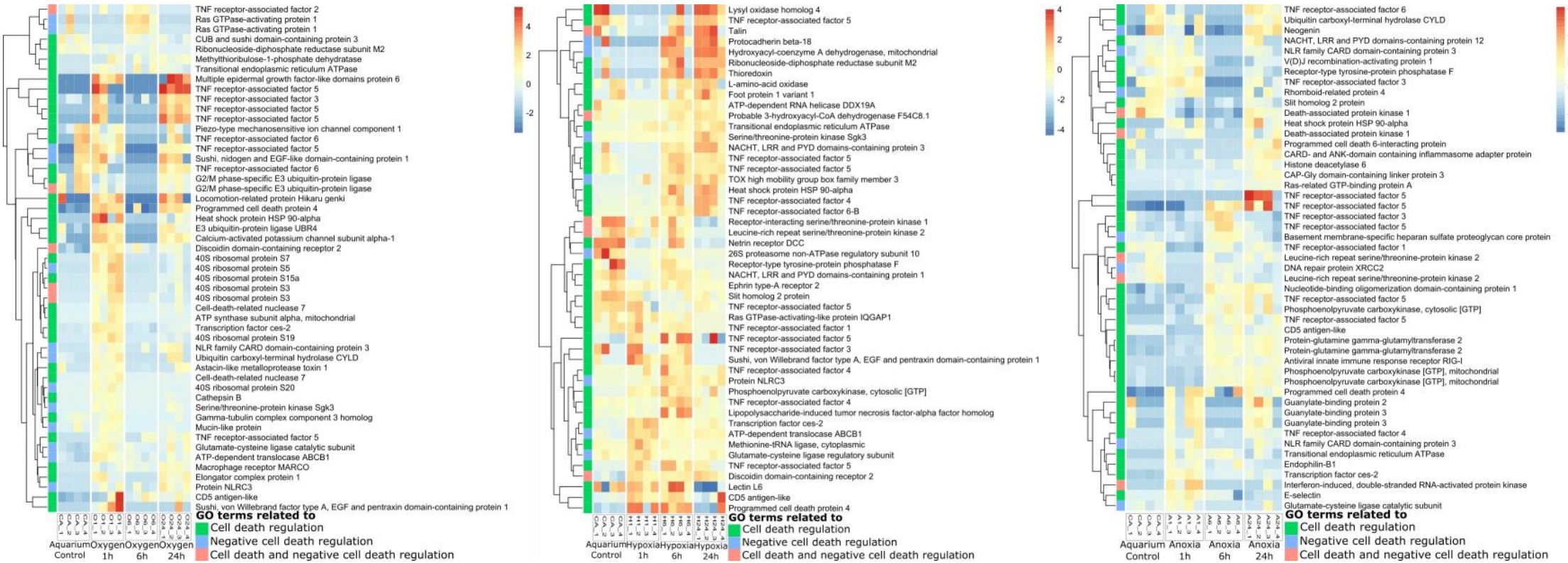

Figure 7 – Differentially expressed cell death-related genes sorted by the same condition in different time points. Heatmap showing differentially expressed genes with predicted functions in regulated cell death, and GO terms associated with cell death (green), its negative regulation (blue), or both (pink). Left panel shows oxygenated samples in the three time points tested (1h, 6h, and 24h) as well as the aquarium control. Middle panel shows hypoxia samples in the three time points and the aquarium control. Right panel shows anoxia samples in the three times as well as the aquarium control samples. Abbreviations: A, anoxia; H, hypoxia; O, oxygenated; 1, 1 hour; 6, 6 hours; 24, 24 hours; CA, aquarium control.

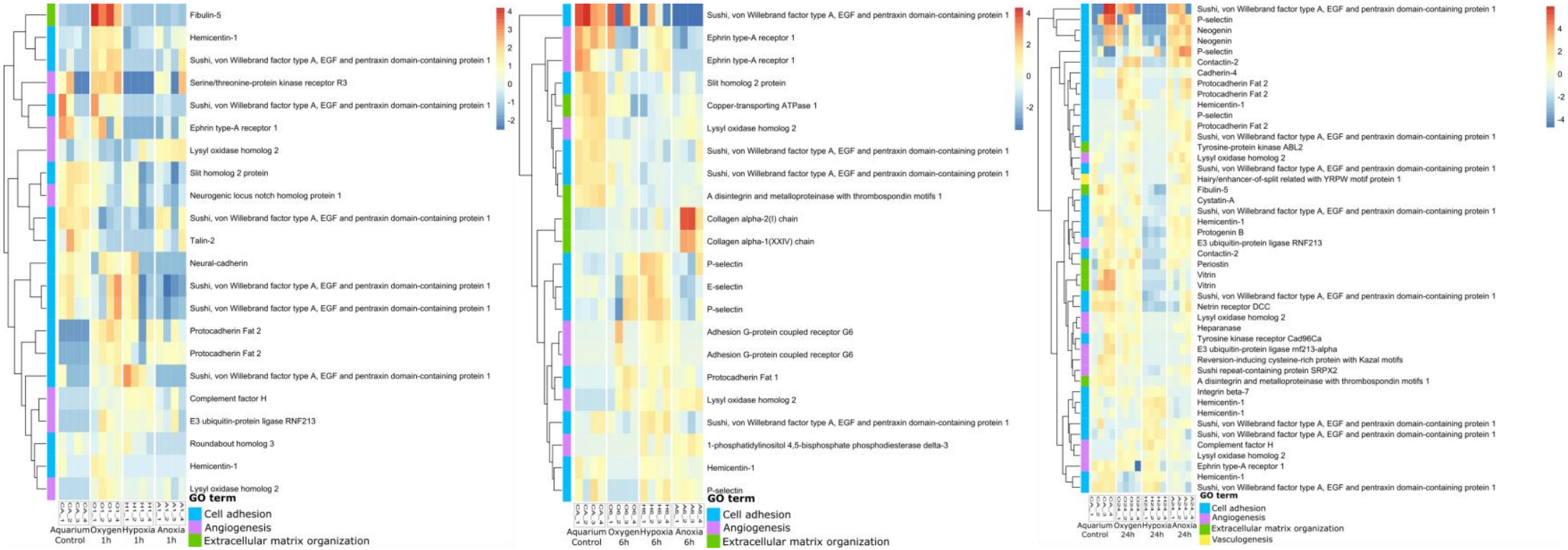

Figure 8 – Differentially expressed genes related to angiogenesis/vasculogenesis and extracellular matrix (ECM) organization sorted by different conditions in the same time point. Heatmap showing differentially expressed genes with predicted functions and GO terms associated with cell adhesion (blue), angiogenesis (purple), ECM organization (green), and vasculogenesis (yellow). Left panel shows 1h samples in the three conditions tested (oxygenated, hypoxia and anoxia) as well as the aquarium control. Middle panel shows 6h samples in the three conditions and the aquarium control. Right panel shows 24h samples in the three conditions as well as the aquarium control samples. Abbreviations: A, anoxia; H, hypoxia; O, oxygenated; 1, 1 hour; 6, 6 hours; 24, 24 hours; CA, aquarium control.

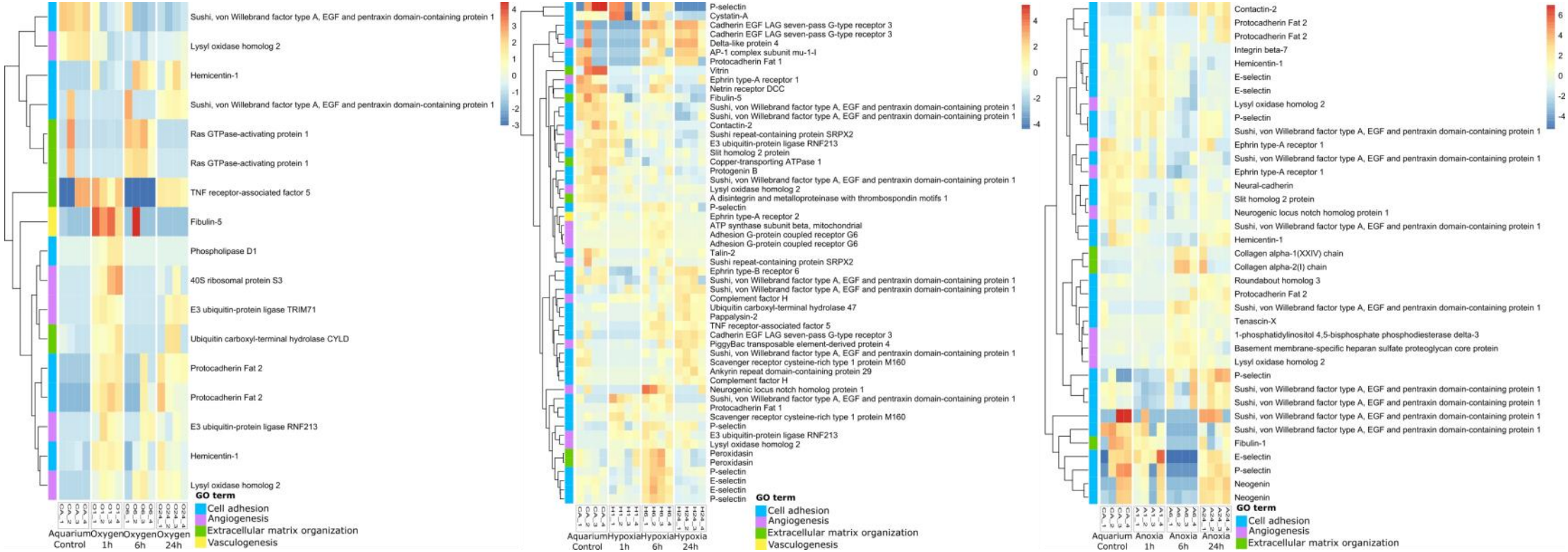

Figure 9 – Differentially expressed genes related to angiogenesis/vasculogenesis and extracellular matrix (ECM) organization sorted by the same condition in different time points. Heatmap showing differentially expressed genes with predicted functions and GO terms associated with cell adhesion (blue), angiogenesis (purple), ECM organization (green), and vasculogenesis (yellow). Left panel shows oxygenated samples in the three time points tested (1h, 6h, and 24h) as well as the aquarium control. Middle panel shows hypoxia samples in the three time points and the aquarium control. Right panel shows anoxia samples in the three times as well as the aquarium control samples. Abbreviations: A, anoxia; H, hypoxia; O, oxygenated; 1, 1 hour; 6, 6 hours; 24, 24 hours; CA, aquarium control.

References

Abràmoff, M. D., Magalhães, P. J., & Ram, S. J. (2004). Image processing with ImageJ. *Biophotonics international*, *11*(7), 36–42.

Altschul, S. F., Gish, W., Miller, W., Myers, E. W., & Lipman, D. J. (1990). Basic local alignment search tool. *Journal of molecular biology*, *215*(3), 403–410.

Amin, D. N., Bielenberg, D. R., Lifshits, E., Heymach, J. V., & Klagsbrun, M. (2008). Targeting EGFR activity in blood vessels is sufficient to inhibit tumor growth and is accompanied by an increase in VEGFR–2 dependence in tumor endothelial cells. *Microvascular research*, *76*(1), 15–22.

André, P. (2004). P-selectin in haemostasis. *British journal of haematology*, *126*(3), 298–306.

Andreyeva, A. Y., Gostyukhina, O. L., Kladchenko, E. S., Vodiasova, E. A., & Chelebieva, E. S. (2021). Acute hypoxic exposure: effect on hemocyte functional parameters and antioxidant potential in gills of the pacific oyster, *Crassostrea gigas*. *Marine Environmental Research*, *169*, 1–8.

Andrews, S. (2010). FastQC: a quality control tool for high throughput sequence data. http://www.bioinformatics.babraham.ac.uk/projects/fastqc/. Accessed 29 September 2022.

Antcliffe, J. B., Callow, R. H. T., & Brasier, M. D. (2014). Giving the early fossil record of sponges a squeeze. *Biological Reviews*, *89*(4), 972–1004.

Belato, F. A., Mello, B., Coates, C. J., Halanych, K. M., Brown, F. D., Morandini, A. C., de Moraes Leme, J., Trindade, R. I. F., & Costa-Paiva, E. M. (2023). Divergence time estimates for the hypoxia-inducible factor-1 alpha (HIF1α) reveal an ancient emergence of animals in low-oxygen environments. *Geobiology*, *22*(1), 1–14.

Bell, J. J., & Barnes, D. K. A. (2000). A sponge diversity centre within a marine `island'. In M. B. Jones, J. M. N. Azevedo, A. I. Neto, A. C. Costa, & A. M. F. Martins (Eds.), *Island, Ocean and Deep–Sea Biology* (pp. 55–64). Springer Netherlands.

Berkner, L. V., & Marshall, L. C. (1965). On the Origin and Rise of Oxygen Concentration in the Earth's Atmosphere. *Journal of the Atmospheric Sciences*, *22*(3), 225–261.

Bischoff, J. (1997). Cell adhesion and angiogenesis. *The Journal of clinical investigation*, *99*(3), 373–376.

Bou-Gharios, G., Ponticos, M., Rajkumar, V., & Abraham, D. (2004). Extra-cellular matrix in vascular networks. *Cell proliferation*, *37*(3), 207–220.

Bozdag, G. O., Libby, E., Pineau, R., Reinhard, C. T., & Ratcliff, W. C. (2021). Oxygen suppression of macroscopic multicellularity. *Nature communications*, *12*(1), 1–10.

Brain, C. K., Prave, A. R., Hoffmann, K.–H., Fallick, A. E., Botha, A., Herd, D. A., Sturrock, C., Young, I., Condon, D. J., & Allison, S. G. (2012). The first animals: ca. 760–million–year–old sponge–like fossils from Namibia. *South African Journal of Science*, *108*(1), 1–8.

Breier, G., & Risau, W. (1996). The role of vascular endothelial growth factor in blood vessel formation. *Trends in cell biology*, *6*(12), 454–456.

Brochier–Armanet, C., Talla, E., & Gribaldo, S. (2009). The multiple evolutionary histories of dioxygen reductases: Implications for the origin and evolution of aerobic respiration. *Molecular Biology and Evolution*, *26*(2), 285–297.

Bryant, D. M., Johnson, K., DiTommaso, T., Tickle, T., Couger, M. B., Payzin–Dogru, D., Lee, T. J., Leigh, N. D., Kuo, T.–H., Davis, F. G., Bateman, J., Bryant, S., Guzikowski, A. R., Tsai, S. L., Coyne, S., Ye, W. W., Freeman, R. M., Peshkin, L., Tabin, C. J., Regev, A., Haas, B. J., & Whited, J. L. (2017). A tissue–mapped axolotl de novo transcriptome enables identification of limb regeneration factors. *Cell reports*, *18*(3), 762–776.

Camacho, C., Coulouris, G., Avagyan, V., Ma, N., Papadopoulos, J., Bealer, K., & Madden, T. L. (2009). BLAST+: architecture and applications. *BMC bioinformatics*, *10*, 1–9.

Catling, D. C., Glein, C. R., Zahnle, K. J., & McKay, C. P. (2005). Why O 2 Is Required by Complex Life on Habitable Planets and the Concept of Planetary "Oxygenation Time." *Astrobiology*, *5*(3), 415–438.

Chandel, N. S., & Schumacker, P. T. (2000). Cellular oxygen sensing by mitochondria: old questions, new insight. *Journal of applied physiology*, *88*(5), 1880–1889.

Cloud, P. E. (1968). Atmospheric and hydrospheric evolution on the primitive Earth. *Science*, *160*(3829), 729–736.

Cloud, P. E. (1969). Pre–Paleozoic sediments and their significance for organic geochemistry. In Mangum, C. P. (Ed.), *Organic Geochemistry* (pp. 727–736). Springer Berlin Heidelberg.

Cole, S. J., Bradford, D., & Cooper, H. M. (2007). Neogenin: A multi–functional receptor regulating diverse developmental processes. *The international journal of biochemistry & cell biology*, *39*(9), 1569–1575.

Cole, D. B., Mills, D. B., Erwin, D. H., Sperling, E. A., Porter, S. M., Reinhard, C. T., & Planavsky, N. J. (2020). On the co-evolution of surface oxygen levels and animals. *Geobiology*, *18*(3), 260–281.

Cooper, C. E., & Brown, G. C. (2008). The inhibition of mitochondrial cytochrome oxidase by the gases carbon monoxide, nitric oxide, hydrogen cyanide and hydrogen sulfide: chemical mechanism and physiological significance. *Journal of bioenergetics and biomembranes*, *40*, 533–539.

Cunningham, J. A., Liu, A. G., Bengtson, S., & Donoghue, P. C. J. (2017). The origin of animals: Can molecular clocks and the fossil record be reconciled?. *BioEssays*, *39*(1), 1–12.

Das, A., Samidurai, A., Hoke, N. N., Kukreja, R. C., & Salloum, F. N. (2015). Hydrogen sulfide mediates the cardioprotective effects of gene therapy with PKG–Iα. *Basic Research in Cardiology*, *110*, 1–12.

Dohrmann, M., & Wörheide, G. (2017). Dating early animal evolution using phylogenomic data. *Scientific Reports*, *7*(1), 1–6.

dos Reis, M., Thawornwattana, Y., Angelis, K., Telford, M. J., Donoghue, P. C. J., & Yang, Z. (2015). Uncertainty in the timing of origin of animals and the limits of precision in molecular timescales. *Current Biology*, *25*(22), 2939–2950.

Droser, M. L., Tarhan, L. G., & Gehling, J. G. (2017). The rise of animals in a changing environment: global ecological innovation in the late Ediacaran. *Annual Review of Earth and Planetary Sciences*, *45*(July), 593–617.

Ereskovsky, A. V., Tokina, D. B., Saidov, D. M., Baghdiguian, S., Le Goff, E., & Lavrov, A. I. (2020). Transdifferentiation and mesenchymal-to-epithelial transition during regeneration in Demospongiae (Porifera). *Journal of Experimental Zoology Part B: Molecular and Developmental Evolution*, *334*(1), 37–58.

Erwin, D. H., Laflamme, M., Tweedt, S. M., Sperling, E. A., Pisani, D., & Peterson, K. J. (2011). The Cambrian conundrum: Early divergence and later ecological success in the early history of animals. *Science*, *334*(6059), 1091–1097.

Fago, A., & Jensen, F. B. (2015). Hypoxia tolerance, nitric oxide, and nitrite: lessons from extreme animals. *Physiology*, *30*(2), 116–126.

Fenchel, T., & Finlay, B. J. (1995). *Ecology and Evolution in Anoxic Worlds*. Oxford University Press.

Finn, R. D., Clements, J., & Eddy, S. R. (2011). HMMER web server: interactive sequence similarity searching. *Nucleic acids research*, *39*(suppl_2), W29–W37.

Gene Ontology Consortium. (2004). The Gene Ontology (GO) database and informatics resource. *Nucleic Acids Research*, *32*(Suppl. 1), D258–D261.

Gostyukhina, O. L., Andreyeva, A. Y., Chelebieva, E. S., Vodiasova, E. A., Lantushenko, A. O., & Kladchenko, E. S. (2022). Adaptive potential of the Mediterranean mussel *Mytilus galloprovincialis* to short–term environmental hypoxia. *Fish & Shellfish Immunology*, *131*, 654–661.

Grabherr, M. G., Haas, B. J., Yassour, M., Levin, J. Z., Thompson, D. A., Amit, I., Adiconis, X., Fan, L., Raychowdhury, R., Zeng, Q., Chen, Z., Mauceli, E., Hacohen, N., Gnirke, A., Rhind, N., di Palma, F., Birren, B. W., Nusbaum, C., Lindblad–Toh, K., Friedman, N., Regev, A. (2011). Full–length transcriptome assembly from RNA–Seq data without a reference genome. *Nature Biotechnology*, *29*(7), 644–652.

Grego, M., Riedel, B., Stachowitsch, M., & De Troch, M. (2014). Meiofauna winners and losers of coastal hypoxia: Case study harpacticoid copepods. *Biogeosciences*, *11*(2), 281–292.

Grimes, C. J., Petersen, L. H., & Schulze, A. (2021). Differential gene expression indicates modulated responses to chronic and intermittent hypoxia in corallivorous fireworms (*Hermodice carunculata*). *Scientific Reports*, *11*(1), 1–13.

Guillaumond, F., Leca, J., Olivares, O., Lavaut, M. N., Vidal, N., Berthezène, P., Dusetti, N. J., Loncle, C., Calvo, E., Turrini, O., Iovanna, J. L., Tomasini, R., & Vasseur, S. (2013). Strengthened glycolysis under hypoxia supports tumor symbiosis and hexosamine biosynthesis in pancreatic adenocarcinoma. *Proceedings of the National Academy of Sciences*, *110*(10), 3919–3924.

Gunda, V. G., & Janapala, V. R. (2009). Effects of dissolved oxygen levels on survival and growth in vitro of *Haliclona pigmentifera* (Demospongiae). *Cell and tissue research*, *337*(3), 527–535.

Haas, B. J., Papanicolaou, A., Yassour, M., Grabherr, M., Blood, P. D., Bowden, J., Couger, M. B., Eccles, D., Li, B., Lieber, M., MacManes, M. D., Ott, M., Orvis, J., Pochet, N., Strozzi, F., Weeks, N., Westerman, R., William, T., Dewey, C. N., Henschel, R., LeDuc, R. D., Friedman, N., & Regev, A. (2013). De novo transcript sequence reconstruction from RNA–seq using the Trinity platform for reference generation and analysis. *Nature protocols*, *8*(8), 1494–1512.

Hammarlund, E., Bukkuri, A., Norling, M., Posth, N., Carroll, C., Baratchart, E., Amend, S., Gatenby, R., Pienta, K., Brown, J., Peters, S., & Hancke, K. (*in press*). Benthic daily oxygen variability and stress as drivers for animal diversification in the Cambrian. *Nature Ecology and Evolution.*

Hammarlund, E. U., Flashman, E., Mohlin, S., & Licausi, F. (2020). Oxygen–sensing mechanisms across eukaryotic kingdoms and their roles in complex multicellularity. *Science*, *370*(6515), 1–13.

Hanmer, K. L., & Mavri–Damelin, D. (2018). Peroxidasin is a novel target of the redox–sensitive transcription factor Nrf2. *Gene*, *674*, 104–114.

Hayashi, S. I., Watanabe, N., Nakazawa, K., Suzuki, J., Tsushima, K., Tamatani, T., Sakamoto, S., & Isobe, M. (2000). Roles of P–selectin in inflammation, neointimal formation, and vascular remodeling in balloon–injured rat carotid arteries. *Circulation*, *102*(14), 1710–1717.

He, H., Huang, J., Wu, S., Jiang, S., Liang, L., Liu, Y., Liu, W., Xie, L., Tao, Y., Jiang, Y., & Cong, L. (2021). The roles of GTPase–activating proteins in regulated cell death and tumor immunity. *Journal of Hematology & Oncology*, *14*, 1–15.

Hewitt, O. H., & Degnan, S. M. (2022). Distribution and diversity of ROS–generating enzymes across the animal kingdom, with a focus on sponges (Porifera). *BMC biology*, *20*(1), 212.

Hoffmann, F., Røy, H., Bayer, K., Hentschel, U., Pfannkuchen, M., Brümmer, F., & De Beer, D. (2008). Oxygen dynamics and transport in the Mediterranean sponge *Aplysina aerophoba*. *Marine biology*, *153*, 1257–1264.

Hu, M., Wu, F., Yuan, M., Li, Q., Gu, Y., Wang, Y., & Liu, Q. (2015). Antioxidant responses of triangle sail mussel *Hyriopsis cumingii* exposed to harmful algae *Microcystis aeruginosa* and hypoxia. *Chemosphere*, *139*, 541–549.

Jeffery, J., & Jörnvall, H. (1983). Enzyme relationships in a sorbitol pathway that bypasses glycolysis and pentose phosphates in glucose metabolism. *Proceedings of the National Academy of Sciences*, *80*(4), 901–905.

Jing, H., Liu, Z., Wu, B., Tu, K., Liu, Z., Sun, X., & Zhou, L. (2023). Physiological and molecular responses to hypoxia stress in Manila clam *Ruditapes philippinarum*. *Aquatic Toxicology*, *257*, 1–11.

Kaelin, W. G., & Ratcliffe, P. J. (2008). Oxygen sensing by metazoans: the central role of the HIF hydroxylase pathway. *Molecular cell*, *30*(4), 393–402.

Kanehisa, M., Furumichi, M., Tanabe, M., Sato, Y., & Morishima, K. (2017). KEGG: new perspectives on genomes, pathways, diseases and drugs. *Nucleic acids research*, *45*(D1), D353–D361.

Kang, J., Brajanovski, N., Chan, K. T., Xuan, J., Pearson, R. B., & Sanij, E. (2021). Ribosomal proteins and human diseases: molecular mechanisms and targeted therapy. *Signal Transduction and Targeted Therapy*, *6*(1), 323.

Keeling, R. F., Körtzinger, A., & Gruber, N. (2010). Ocean deoxygenation in a warming world. *Annual review of marine science*, *2*, 199–229.

Kenny, N. J., de Goeij, J. M., de Bakker, D. M., Whalen, C. G., Berezikov, E., & Riesgo, A. (2018). Towards the identification of ancestrally shared regenerative mechanisms across the Metazoa: a transcriptomic case study in the demosponge *Halisarca caerulea*. *Marine genomics*, *37*, 135–147.

Kılıçaslan, S. M. S., Cevher, Ş. C., & Peker, E. G. G. (2013). Ultrastructural changes in blood vessels in epidermal growth factor treated experimental cutaneous wound model. *Pathology–Research and Practice*, *209*(11), 710–715.

Kim, J., Oh, W. J., Gaiano, N., Yoshida, Y., & Gu, C. (2011). Semaphorin 3E–Plexin–D1 signaling regulates VEGF function in developmental angiogenesis via a feedback mechanism. *Genes & development*, *25*(13), 1399–1411.

King, N., & Rokas, A. (2017). Embracing uncertainty in reconstructing early animal evolution. *Current Biology*, *27*(19), R1081–R1088.

Knoll, A. H., & Carroll, S. B. (1999). Early animal evolution: emerging views from comparative biology and geology. *Science*, *284*(5423), 2129–2137.

Koch, A. E., Halloran, M. M., Haskell, C. J., Shah, M. R., & Polverini, P. J. (1995). Angiogenesis mediated by soluble forms of E–selectin and vascular cell adhesion molecule–1. *Nature*, *376*(6540), 517–519.

Kolde, R. (2015). Package 'pheatmap'. *R package*, *1*(7), 1–8.

Kopylova, E., Noé, L., & Touzet, H. (2012). SortMeRNA: fast and accurate filtering of ribosomal RNAs in metatranscriptomic data. *Bioinformatics*, *28*(24), 3211–3217.

Krause, A. J., Mills, B. J., Merdith, A. S., Lenton, T. M., & Poulton, S. W. (2022). Extreme variability in atmospheric oxygen levels in the late Precambrian. *Science advances*, *8*(41), 1–10.

Krejsa, C. M., Franklin, C. C., White, C. C., Ledbetter, J. A., Schieven, G. L., & Kavanagh, T. J. (2010). Rapid activation of glutamate cysteine ligase following oxidative stress. *Journal of Biological Chemistry*, *285*(21), 16116–16124.

Langmead, B., & Salzberg, S. L. (2012). Fast gapped–read alignment with Bowtie 2. *Nature methods*, *9*(4), 357–359.

Lavy, A., Keren, R., Yahel, G., & Ilan, M. (2016). Intermittent hypoxia and prolonged suboxia measured in situ in a marine sponge. *Frontiers in Marine Science*, *3*, 1–11.

Le Mellay, V., Houben, R., Troppmair, J., Hagemann, C., Mazurek, S., Frey, U., Beigel, J., Weber, C., Benz, R., Eigenbrodt, E., & Rapp, U. R. (2002). Regulation of glycolysis by Raf protein serine/threonine kinases. *Advances in enzyme regulation*, *42*, 317–332.

Lee, Y., Byeon, E., Kim, D. H., Maszczyk, P., Wang, M., Wu, R. S. S., Jeung, H.–D., Hwang, U.–K., & Lee, J. S. (2023). Hypoxia in aquatic invertebrates: Occurrence and phenotypic and molecular responses. *Aquatic Toxicology*, *263*, 1–19.

Lenton, T. M., & Daines, S. J. (2017). Biogeochemical transformations in the history of the ocean. *Annual Review of Marine Science*, *9*(1), 31–58.

Leys, S. P., & Hill, A. (2012). The physiology and molecular biology of sponge tissues. *Advances in marine biology*, *62*, 1–56.

Leys, S. P., & Kahn, A. S. (2018). Oxygen and the energetic requirements of the first multicellular animals. *Integrative and Comparative Biology*, *58*(4), 666–676.

Leys, S. P., Yahel, G., Reidenbach, M. A., Tunnicliffe, V., Shavit, U., & Reiswig, H. M. (2011). The sponge pump: the role of current induced flow in the design of the sponge body plan. *PloS one*, *6*(12), 1–17.

Li, B., & Dewey, C. N. (2011). RSEM: accurate transcript quantification from RNA–Seq data with or without a reference genome. *BMC bioinformatics*, *12*, 1–16.

Li, Z., & Srivastava, P. (2003). Heat-shock proteins. *Current protocols in immunology*, *58*(1), 1–6.

Lindquist, S., & Craig, E. A. (1988). The heat–shock proteins. *Annual review of genetics*, *22*(1), 631–677.

Liu, J., Lilly, M. N., & Shapiro, J. I. (2018). Targeting Na/K–ATPase signaling: a new approach to control oxidative stress. *Current pharmaceutical design*, *24*(3), 359–364.

Love, G. D., Grosjean, E., Stalvies, C., Fike, D. A., Grotzinger, J. P., Bradley, A. S., Kelly, A. E., Bhatia, M., Meredith, W., Snape, C. E., Bowring, S. A., Condon, D. J., & Summons, R. E. (2009). Fossil steroids record the appearance of Demospongiae during the Cryogenian period. *Nature*, *457*(7230), 718–721.

Lucey, N. M., Collins, M., & Collin, R. (2020). Oxygen–mediated plasticity confers hypoxia tolerance in a corallivorous polychaete. *Ecology and Evolution*, *10*(3), 1145–1157.

Lysek, N., Kinscherf, R., Claus, R., & Lindel, T. (2003). L–5–Hydroxytryptophan: Antioxidant and Anti–Apoptotic Principle of the Intertidal Sponge *Hymeniacidon heliophila*. *Zeitschrift für Naturforschung C*, *58*(7–8), 568–572.

Maldonado, M., Ribes, M., & van Duyl, F. C. (2012). Nutrient fluxes through sponges: biology, budgets, and ecological implications. *Advances in marine biology*, *62*, 113–182.

Martínez–Revelles, S., García–Redondo, A. B., Avendaño, M. S., Varona, S., Palao, T., Orriols, M., Roque, F. R., Fortuño, A., Touyz, R. M., Martínez–González, J., Salaices, M., Rodríguez, C., & Briones, A. M. (2017). Lysyl oxidase induces vascular oxidative stress and contributes to arterial stiffness and abnormal elastin structure in hypertension: role of p38MAPK. *Antioxidants & redox signaling*, *27*(7), 379–397.

Mateos, K., Chappell, G., Klos, A., Le, B., Boden, J., Stüeken, E., & Anderson, R. (2023). The evolution and spread of sulfur cycling enzymes reflect the redox state of the early Earth. *Science Advances*, *9*(27), 1–11.

Micaroni, V., Strano, F., McAllen, R., Woods, L., Turner, J., Harman, L., & Bell, J. J. (2022). Adaptive strategies of sponges to deoxygenated oceans. *Global Change Biology*, *28*(6), 1972–1989.

Mills, D. B., & Canfield, D. E. (2014). Oxygen and animal evolution: Did a rise of atmospheric oxygen "trigger" the origin of animals? *BioEssays*, *36*(12), 1145–1155.

Mills, D. B., Francis, W. R., Vargas, S., Larsen, M., Elemans, C. P., Canfield, D. E., & Wörheide, G. (2018). The last common ancestor of animals lacked the HIF pathway and respired in low–oxygen environments. *Elife*, *7*, 1–17.

Mills, D. B., Ward, L. M., Jones, C. A., Sweeten, B., Forth, M., Treusch, A. H., & Canfield, D. E. (2014). Oxygen requirements of the earliest animals. *Proceedings of the National Academy of Sciences*, *111*(11), 4168–4172.

Mentel, M., Martin, W. (2008). Energy metabolism among eukaryotic anaerobes in light of Proterozoic ocean chemistry. *Philosophical Transactions of the Royal Society B: Biological Sciences*, *363*(1504), 2717–2729.

Mentel, M., Tielens, A. G. M., & Martin, W. F. (2016). Animals, anoxic environments, and reasons to go deep. *BMC Biology*, *14*(1), 1–3.

Mosch, T., Sommer, S., Dengler, M., Noffke, A., Bohlen, L., Pfannkuche, O., Liebetrau, V., & Wallmann, K. (2012). Factors influencing the distribution of epibenthic megafauna across the Peruvian oxygen minimum zone. *Deep Sea Research Part I: Oceanographic Research Papers*, *68*, 123–135.

Müller, M., Mentel, M., van Hellemond, J. J., Henze, K., Woehle, C., Gould, S. B., Yu, R.–Y., van der Giezen, M., Tielens, A. G. M., & Martin, W. F. (2012). Biochemistry and Evolution of Anaerobic Energy Metabolism in Eukaryotes. *Microbiology and Molecular Biology Reviews*, *76*(2), 444–495.

Muñoz–Chápuli, R. (2011). Evolution of angiogenesis. *International Journal of Developmental Biology*, *55*(4–5), 345–351.

Muñoz–Chápuli, R., Quesada, A. R., & Angel Medina, M. (2004). Angiogenesis and signal transduction in endothelial cells. *Cellular and Molecular Life Sciences CMLS*, *61*, 2224–2243.

Nandi, A., Yan, L. J., Jana, C. K., & Das, N. (2019). Role of catalase in oxidative stress–and age–associated degenerative diseases. *Oxidative medicine and cellular longevity*, *2019*, 1–20.

Narbonne, G. M. (2005). The Ediacara Biota: Neoproterozoic Origin of Animals and Their Ecosystems. *Annual Review of Earth and Planetary Sciences*, *33*(1), 421–442.

Nelson, D. L., Lehninger, A. L., & Cox, M. M. (2013). *Lehninger principles of biochemistry* (6th Ed). New York, H. Freeman.

Nickel, M. (2004). Kinetics and rhythm of body contractions in the sponge Tethya wilhelma (Porifera: Demospongiae). *Journal of Experimental Biology*, *207*(26), 4515–4524.

Nie, H., Wang, H., Jiang, K., & Yan, X. (2020). Transcriptome analysis reveals differential immune related genes expression in Ruditapes philippinarum under hypoxia stress: potential HIF and NF–κB crosstalk in immune responses in clam. *BMC genomics*, *21*(1), 1–16.

Nishimura, O., Hara, Y., & Kuraku, S. (2017). gVolante for standardizing completeness assessment of genome and transcriptome assemblies. *Bioinformatics*, *33*(22), 3635-3637.

Nursall, J. R. (1959). Oxygen as a prerequisite to the origin of the Metazoa. *Nature, 183*(4669), 1170–1172.

Olson, K. R. (2015). Hydrogen sulfide as an oxygen sensor. *Antioxidants & redox signaling*, *22*(5), 377–397.

Olson, K. R., Gao, Y., DeLeon, E. R., Arif, M., Arif, F., Arora, N., & Straub, K. D. (2017). Catalase as a sulfide–sulfur oxido–reductase: An ancient (and modern?) regulator of reactive sulfur species (RSS). *Redox biology*, *12*, 325–339.

Parris, D. J., Ganesh, S., Edgcomb, V. P., DeLong, E. F., & Stewart, F. J. (2014). Microbial eukaryote diversity in the marine oxygen minimum zone off northern Chile. *Frontiers in Microbiology*, *5*(1), 1–11.

Petersen, T. N., Brunak, S., von Heijne, G., & Nielsen, H. (2011). SignalP 4.0: discriminating signal peptides from transmembrane regions. *Nature Methods, 8*(10), 785–786.

Pisani, D., Pett, W., Dohrmann, M., Feuda, R., Rota–Stabelli, O., Philippe, H., Lartillot, N., & Wörheide, G. (2015). Genomic data do not support comb jellies as the sister group to all other animals. *Proceedings of the National Academy of Sciences*, *112*(50), 15402–15407.

Powell, M. A., & Somero, G. N. (1986). Hydrogen sulfide oxidation is coupled to oxidative phosphorylation in mitochondria of *Solemya reidi*. *Science*, *233*(4763), 563–566.

Pu, J. P., Bowring, S. A., Ramezani, J., Myrow, P., Raub, T. D., Landing, E., Mills, A., Hodgin, E., & Macdonald, F. A. (2016). Dodging snowballs: Geochronology of the Gaskiers glaciation and the first appearance of the Ediacaran biota. *Geology*, *44*(11), 955–958.

Purcell, J. E., Breitburg, D. L., Decker, M. B., Graham, W. M., Youngbluth, M. J., & Raskoff, K. A. (2001). Pelagic cnidarians and ctenophores in low dissolved oxygen environments: A review. In N. N. Rabalais & R. E. Turner (Eds.), *Coastal Hypoxia: Consequences for Living Resources and Ecosystems* (pp. 77–100). American Geophysical Union.

Reinhard, C. T., Planavsky, N. J., Olson, S. L., Lyons, T. W., & Erwin, D. H. (2016). Earth's oxygen cycle and the evolution of animal life. *Proceedings of the National Academy of Sciences*, *113*(32), 8933–8938.

Reiswig, H. M., & Miller, T. L. (1998). Freshwater Sponge Gemmules Survive Months of Anoxia. *Invertebrate Biology*, *117*(1), 1–8.

Riesgo, A., Farrar, N., Windsor, P. J., Giribet, G., & Leys, S. P. (2014). The analysis of eight transcriptomes from all poriferan classes reveals surprising genetic complexity in sponges. *Molecular biology and evolution*, *31*(5), 1102–1120.

Riesgo, A., Santodomingo, N., Koutsouveli, V., Kumala, L., Leger, M. M., Leys, S. P., & Funch, P. (2022). Molecular machineries of ciliogenesis, cell survival, and vasculogenesis are differentially expressed during regeneration in explants of the demosponge Halichondria panicea. *BMC genomics*, *23*(1), 1–17.

Robinson, M. D., McCarthy, D. J., & Smyth, G. K. (2010). edgeR: a Bioconductor package for differential expression analysis of digital gene expression data. *Bioinformatics*, *26*(1), 139–140.

Runnegar, B. (1982). Oxygen requirements, biology and phylogenetic significance of the late Precambrian worm Dickinsonia, and the evolution of the burrowing habit. *Alcheringa: An Australasian Journal of Palaeontology*, *6*(3), 223–239.

Saharinen, P., & Ivaska, J. (2015). Blocking integrin inactivation as an anti-angiogenic therapy. *The EMBO journal*, *34*(10), 1293–1295.

Sahoo, S. K., Planavsky, N. J., Kendall, B., Wang, X., Shi, X., Scott, C., Anbar, A. D., Lyons, T. W., & Jiang, G. (2012). Ocean oxygenation in the wake of the Marinoan glaciation. *Nature*, *489*(7417), 546–549.

Semenza, G. L. (2007). Life with oxygen. *Science*, *318*(5847), 62–64.

Simão, F. A., Waterhouse, R. M., Ioannidis, P., Kriventseva, E. V., & Zdobnov, E. M. (2015). BUSCO: assessing genome assembly and annotation completeness with single–copy orthologs. *Bioinformatics*, *31*(19), 3210–3212.

Simion, P., Philippe, H., Baurain, D., Jager, M., Richter, D. J., Di Franco, A., Roure, B., Satoh, N., Quéinnec, É., Ereskovsky, A., Lapébie, P., Corre, E., Delsuc, F., King, N., Wörheide, G., & Manuel, M. (2017). A large and consistent phylogenomic dataset supports sponges as the sister group to all other animals. *Current biology*, *27*(7), 958–967.

Song, N., Wang, W., Wang, Y., Guan, Y., Xu, S., & Guo, M. Y. (2021). Hydrogen sulfide of air induces macrophage extracellular traps to aggravate inflammatory injury via the regulation of miR–15b–5p on MAPK and insulin signals in trachea of chickens. *Science of The Total Environment*, *771*, 1–11.

Sperling, E. A., Halverson, G. P., Knoll, A. H., Macdonald, F. A., & Johnston, D. T. (2013). A basin redox transect at the dawn of animal life. *Earth and Planetary Science Letters*, *371–372*, 143–155.

Sperling, E. A., Wolock, C. J., Morgan, A. S., Gill, B. C., Kunzmann, M., Halverson, G. P., Macdonald, F. A., Knoll, A. H., & Johnston, D. T. (2015). Statistical analysis of iron geochemical data suggests limited late Proterozoic oxygenation. *Nature*, *523*(7561), 451–454.

Strehlow, B. W., Schuster, A., Francis, W. R., Eckford–Soper, L., Kraft, B., McAllen, R., Nielsen, R., Mandrup, S., & Canfield, D. E. (2023). Transcriptomic responses of sponge holobionts to in situ, seasonal anoxia and hypoxia. *bioRxiv*, 1–36.

Suarez, P. A., & Leys, S. P. (2022). The sponge pump as a morphological character in the fossil record. *Paleobiology*, *48*(3), 446-461.

Sun, G. Y., Xu, J., Jensen, M. D., Yu, S., Wood, W. G., González, F. A., Simonyi, A., Sun, A. Y., & Weisman, G. A. (2005). Phospholipase A 2 in astrocytes: responses to oxidative stress, inflammation, and G protein–coupled receptor agonists. *Molecular neurobiology*, *31*, 27–41.

Sun, S., Xuan, F., Fu, H., Zhu, J., Ge, X., & Gu, Z. (2015). Transciptomic and histological analysis of hepatopancreas, muscle and gill tissues of oriental river

prawn (*Macrobrachium nipponense*) in response to chronic hypoxia. *BMC genomics*, *16*(1), 1–13.
Supek, F., Bošnjak, M., Škunca, N., & Šmuc, T. (2011). REVIGO summarizes and visualizes long lists of gene ontology terms. *PloS one*, *6*(7), 1–9.
Sussarellu, R., Fabioux, C., Le Moullac, G., Fleury, E., & Moraga, D. (2010). Transcriptomic response of the Pacific oyster Crassostrea gigas to hypoxia. *Marine Genomics*, *3*(3), 133–143.
Teodoro, A. C., Duleba, W., & Gubitoso, S. (2011). Estudo multidisciplinar (geoquímica e associações de foraminíferos) para caracterizar e avaliar intervenções antrópicas na Baía do Araçá, Canal de São Sebastião, SP. *Geologia USP. Série Científica*, *11*(1), 113–136.
Tomar, S. (2006). Converting video formats with FFmpeg. *Linux journal*, *2006*(146), 10.
Tostevin, R., & Mills, B. J. W. (2020). Reconciling proxy records and models of Earth's oxygenation during the Neoproterozoic and Palaeozoic. *Interface Focus*, *10*(4), 1–13.
Troch, M., Roelofs, M., Riedel, B., & Grego, M. (2013). Structural and functional responses of harpacticoid copepods to anoxia in the Northern Adriatic: an experimental approach. *Biogeosciences*, *10*(6), 4259–4272.
Vavassori, S., Chou, J., Faletti, L. E., Haunerdinger, V., Opitz, L., Joset, P., Fraser, C. J., Prader, S., Gao, X., Schuch, L. A., Wagner, M., Hoefele, J., Maccari, M. E., Zhu, Y., Elakis, G., Gabbett, M. T., Forstner, M., Omran, H., Kaiser, T., Kessler, C., Olbrich, H., Frosk, P., Almutairi, A., Platt, C., Elkins, M., Weeks, S., Rubin, T., Planas, R., Marchetti, T., Koovely, D., Klämbt, V., Soliman, N. A., von Hardenberg, S., Klemann, C., Baumann, U., Lenz, D., Klein–Franke, A., Schwemmle, M., Huber, M., Sturm, E., Hartleif, S., Häffner, K., Gimpel, C., Brotschi, B., Laube, G., Güngör, T., Buckley, M., Kottke, R., Staufner, C., Hildebrandt, F., Reu–Hofer, S., Moll, S., Weber, A., Kaur, H., Ehl, S., Hiller, S., Geha, R., Roscioli, T., Griese, M., & Pachlopnik Schmid, J. (2021). Multisystem inflammation and susceptibility to viral infections in human ZNFX1 deficiency. *Journal of Allergy and Clinical Immunology*, *148*(2), 381–393.
Vestweber, D. (2008). VE–cadherin: the major endothelial adhesion molecule controlling cellular junctions and blood vessel formation. *Arteriosclerosis, thrombosis, and vascular biology*, *28*(2), 223–232.
Wagner, C., Steffen, R., Koziol, C., Batel, R., Lacorn, M., Steinhart, H., Simat, T., & Müller, W. E. G. (1998). Apoptosis in marine sponges: a biomarker for environmental stress (cadmium and bacteria). *Marine Biology*, *131*, 411–421.
Wang, Y., Nakayama, M., Pitulescu, M. E., Schmidt, T. S., Bochenek, M. L., Sakakibara, A., Adams, S., Davy, A., Deutsch, U., Lüthi, U., Berberis, A., Benjamin, L. E., Mäkinen, T., Nobes, C. D., & Adams, R. H. (2010). Ephrin–B2 controls VEGF–induced angiogenesis and lymphangiogenesis. *Nature*, *465*(7297), 483–486.
Wang, P., Xing, C., Wang, J., Su, Y., & Mao, Y. (2019). Evolutionary adaptation analysis of immune defense and hypoxia tolerance in two closely related Marsupenaeus species based on comparative transcriptomics. *Fish & shellfish immunology*, *92*, 861–870.
Weigel, B. L., & Erwin, P. M. (2016). Intraspecific variation in microbial symbiont communities of the sun sponge, *Hymeniacidon heliophila*, from intertidal and subtidal habitats. *Applied and Environmental Microbiology*, *82*(2), 650–658.

Weihe, E., Kriews, M., & Abele, D. (2010). Differences in heavy metal concentrations and in the response of the antioxidant system to hypoxia and air exposure in the Antarctic limpet *Nacella concinna*. *Marine environmental research*, *69*(3), 127–135.

Welcker, D., Stein, C., Feitosa, N. M., Armistead, J., Zhang, J. L., Lütke, S., Kleinridders, A., Brüning, J. C., Eming, S. A., Sengle, G., Niehoff, A., Bloch, W., & Hammerschmidt, M. (2021). Hemicentin–1 is an essential extracellular matrix component of the dermal–epidermal and myotendinous junctions. *Scientific Reports*, *11*(1), 17926.

Whelan, N. V., Kocot, K. M., Moroz, T. P., Mukherjee, K., Williams, P., Paulay, G., Moroz, L. L., & Halanych, K. M. (2017). Ctenophore relationships and their placement as the sister group to all other animals. *Nature ecology & evolution*, *1*(11), 1737–1746.

Wiens, M., & Müller, W. E. (2006). Cell death in Porifera: molecular players in the game of apoptotic cell death in living fossils. *Canadian journal of zoology*, *84*(2), 307–321.

Wood, R., Liu, A. G., Bowyer, F., Wilby, P. R., Dunn, F. S., Kenchington, C. G., Cuthill, J. F. H., Mitchell, E. G., & Penny, A. (2019). Integrated records of environmental change and evolution challenge the Cambrian Explosion. *Nature Ecology and Evolution*, *3*(4), 528–538.

Wu, Y. C., Franzenburg, S., Ribes, M., & Pita, L. (2022). Wounding response in Porifera (sponges) activates ancestral signaling cascades involved in animal healing, regeneration, and cancer. *Scientific Reports*, *12*(1), 1–13.

Yanagisawa, H., Schluterman, M. K., & Brekken, R. A. (2009). Fibulin–5, an integrin–binding matricellular protein: its function in development and disease. *Journal of cell communication and signaling*, *3*, 337–347.

Yao, L. L., Hu, J. X., Li, Q., Lee, D., Ren, X., Zhang, J. S., Sun, D., Zhang, H., Wang, Y., Mei, L., & Xiong, W. C. (2020). Astrocytic neogenin/netrin–1 pathway promotes blood vessel homeostasis and function in mouse cortex. *The Journal of clinical investigation*, *130*(12), 6490–6509.

Yin, Z., Zhu, M., Davidson, E. H., Bottjer, D. J., Zhao, F., & Tafforeau, P. (2015). Sponge grade body fossil with cellular resolution dating 60 Myr before the Cambrian. *Proceedings of the National Academy of Sciences*, *112*(12), E1453–E1460.

Young, M. D., Wakefield, M. J., Smyth, G. K., & Oshlack, A. (2012). goseq: Gene Ontology testing for RNA–seq datasets. *R Bioconductor*, *8*, 1–25.

Yu, S., Meng, S., Xiang, M., & Ma, H. (2021). Phosphoenolpyruvate carboxykinase in cell metabolism: Roles and mechanisms beyond gluconeogenesis. *Molecular metabolism*, *53*, 1–12.

Yuen, B., Bayes, J. M., & Degnan, S. M. (2014). The characterization of sponge NLRs provides insight into the origin and evolution of this innate immune gene family in animals. *Molecular Biology and Evolution*, *31*(1), 106–120.

Zhang, F., Xiao, S., Kendall, B., Romaniello, S. J., Cui, H., Meyer, M., Gilleaudeau, G. J., Kaufman, A. J., & Anbar, A. D. (2018). Extensive marine anoxia during the terminal Ediacaran Period. *Science Advances*, *4*(6), 1–11.

Zhang, L., Yang, G., Untereiner, A., Ju, Y., Wu, L., & Wang, R. (2013). Hydrogen sulfide impairs glucose utilization and increases gluconeogenesis in hepatocytes. *Endocrinology*, *154*(1), 114–126.

Zhao, X., Cao, Y., Jin, H., Wang, X., Zhang, L., Zhang, Y., Yu, Y., Huang, Y., Gao, Y., & Zhang, J. (2022). Hydrogen sulfide promotes thyroid hormone synthesis and secretion by upregulating sirtuin–1. *Frontiers in Pharmacology, 13*, 1–11.

Supplementary table 1 – Sequencing metrics for each sample, including number of raw reads, effective library size after normalization performed by Trinity, and alignment rate against the reference assembled transcriptome Abbreviations: A, anoxia; H, hypoxia; O, oxygenated; 1, 1 hour; 6, 6 hours; 24, 24 hours; CA, aquarium control.

Sample	Label	Number of raw reads	Alignment rate against reference transcriptome	Effective library size
CA_1	CA14	42,455,019	89.10%	1,035,413.7
CA_2	CA17	47,519,853	87.95%	856,948.2
CA_3	CA18	55,898,878	88.79%	1,019,878.4
CA_4	CA19	44,357,548	88.84%	980,953.8
O1_1	EO01	42,256,249	87.71%	914,947.8
O1_2	EO04	43,791,519	88.89%	877,436.0
O1_3	EO15	54,007,231	89.19%	955,005.2
O1_4	EO16	51,628,686	88.99%	909,597.7
O6_1	EO30	48,859,270	89.52%	917,924.6
O6_2	EO31	46,529,113	89.72%	998,827.1
O6_3	EO33	57,495,450	89.26%	1,039,315.2
O6_4	EO36	46,974,471	89.77%	994,559.3
O24_1	EO12	44,022,117	89.09%	979,211.9
O24_2	EO13	51,413,873	88.95%	948,128.7
O24_3	EO14	54,189,484	89.34%	880,418.2
O24_4	EO18	43,307,265	87.25%	975,951.5
H1_1	EH01	69,154,953	89.22%	923,906.2
H1_2	EH02	39,623,478	88.74%	949,813.0
H1_3	EH39	40,450,902	88.94%	1,084,699.0
H1_4	EH41	44,616,996	88.51%	1,039,091.5
H6_1	EH52	47,923,040	88.61%	944,798.1
H6_2	EH53	53,576,765	88.79%	1,025,964.2
H6_3	EH55	45,708,716	89.33%	950,695.6
H6_4	EH56	45,477,934	89.64%	996,587.6
H24_1	EH33	51,532,621	89.54%	1,114,940.7
H24_2	EH34	51,040,095	88.58%	1,093,381.2
H24_3	EH38	43,070,073	87.29%	1,109,782.9
H24_4	EH40	41,976,062	88.96%	1,031,301.8
A1_1	EA30	42,757,830	87.34%	1,071,601.4
A1_2	EA31	51,357,564	90.33%	1,030,092.0
A1_3	EA34	44,034,930	88.96%	1,122,721.7
A1_4	EA35	44,081,438	87.95%	1,024,408.6
A6_1	EA44	45,743,591	89.87%	1,017,794.5
A6_2	EA45	53,986,582	89.90%	1,053,015.5
A6_3	EA46	56,770,435	88.61%	1,106,688.0
A6_4	EA47	47,282,774	88.54%	1,013,105.2
A24_1	EA21	70,731,181	88.35%	1,013,086.1
A24_2	EA22	50,947,366	89.07%	965,881.5
A24_3	EA23	54,352,503	88.77%	916,530.8
A24_4	EA24	44,173,404	89.21%	1,005,801.4

(A)

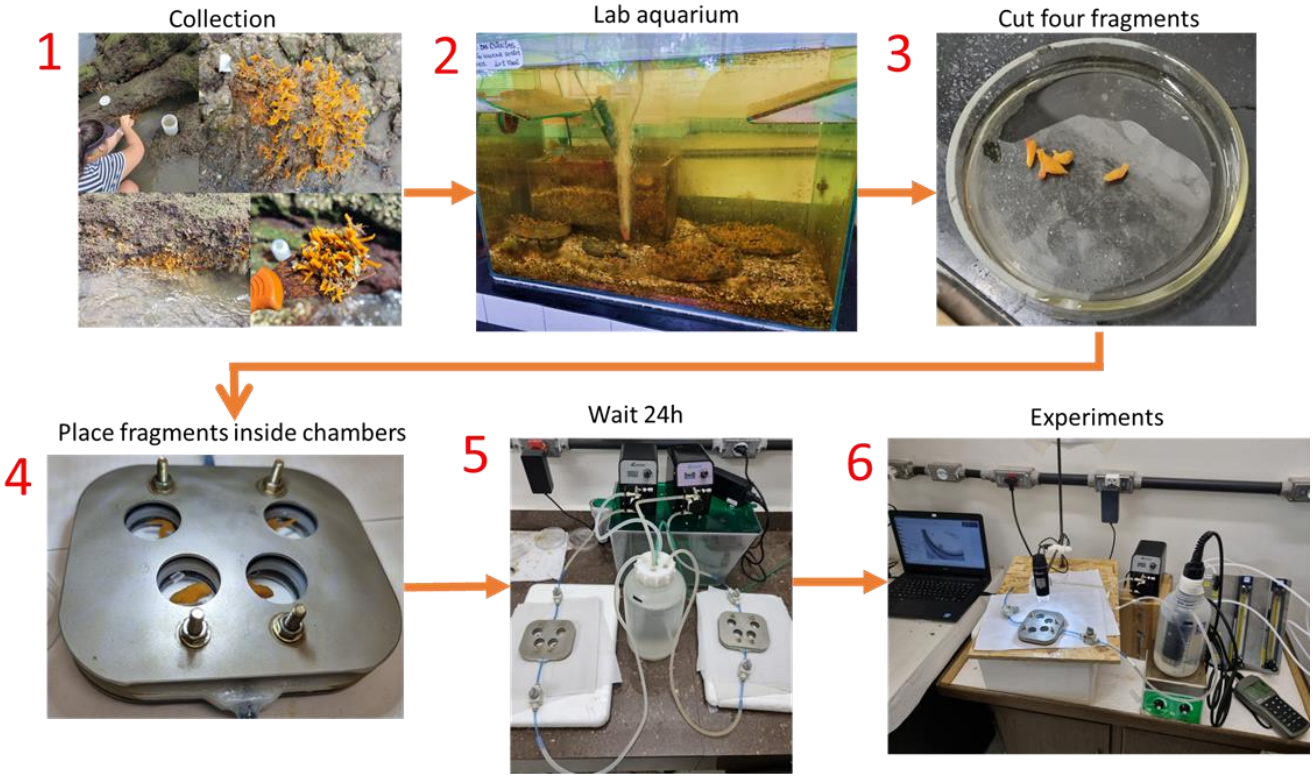

(B)

Condition	Time	Replicates
Oxygenated (>100%DO) ~8 mg/L DO	1h	4
	6h	4
	24h	4
Hypoxia (~5%DO) 0.4-0.3 mg/L DO	1h	4
	6h	4
	24h	4
Anoxia (0%DO)	1h	4
	6h	4
	24h	4
Environmental condition		4
Total samples		40

Each replicate represents a pool of 4 fragments

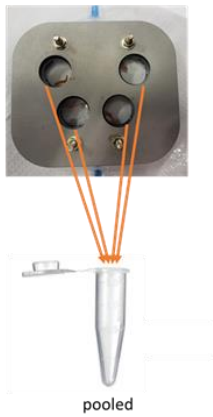

Supplementary Figure 1 – (A) Steps taken to perform the experiments. 1- Collections were made over several months. *Hymeniacidon heliophila* specimens were collected in the Araçá Bay, in São Sebastião (SP, Brazil). **2-** Specimens were taken to the lab and kept in the aquarium. **3-** For each experimental run, four small fragments were cut and **4-** placed inside each one of the four wells of the chambers. **5-** Sponges were kept inside the chambers for 24h prior to the experiments to allow them to recover. **6-** After 24h, the experimental run would start. **(B) Experimental design.** Sponges were submitted to hypoxia (5% Dissolved Oxygen (DO), 0.3 – 0.4 mg O_2 L^{-1}), anoxia (0% DO, 0 mg O_2 L^{-1}), and oxygenated (100% DO, ~8 mg O_2 L^{-1}) for three time points: 1h, 6h, and 24h. Each condition and time point tested was repeated four times to generate replicates. After each trial, the four fragments were pooled to form one sample. Four pools of samples were also frozen from specimens freshly removed from the aquarium to serve as control of the aquarium condition (environmental condition).

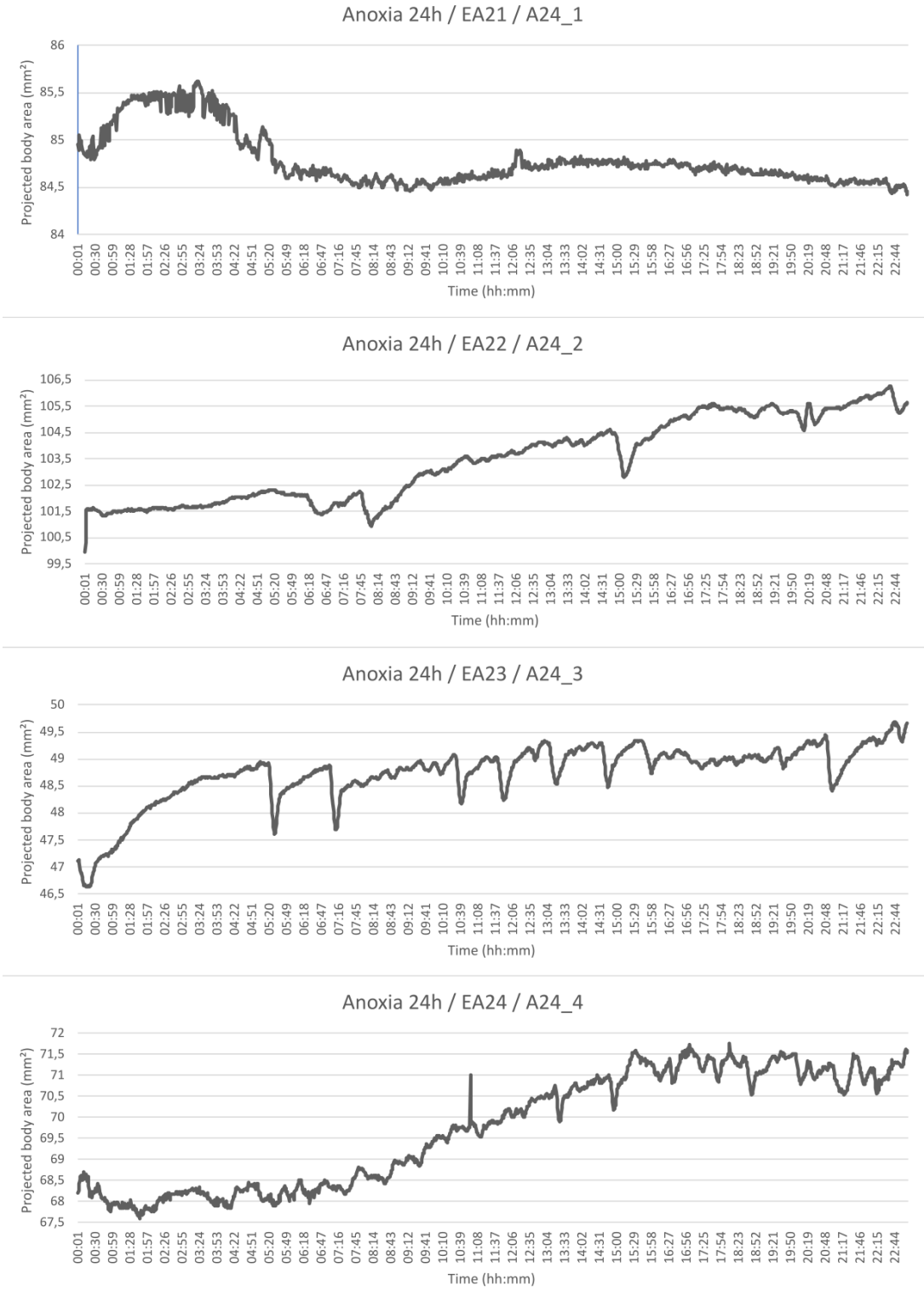

Supplementary Figure 2 – Contraction patterns of four representative sponges from each of the four anoxia 24h experiment replicates performed, representing the changes in projected areas over the experimental period of 24h. Projected area is shown in mm², and time is shown in hours and minutes (hh:mm). Above each panel is shown the condition tested, the experiment label and the RNA sample label.

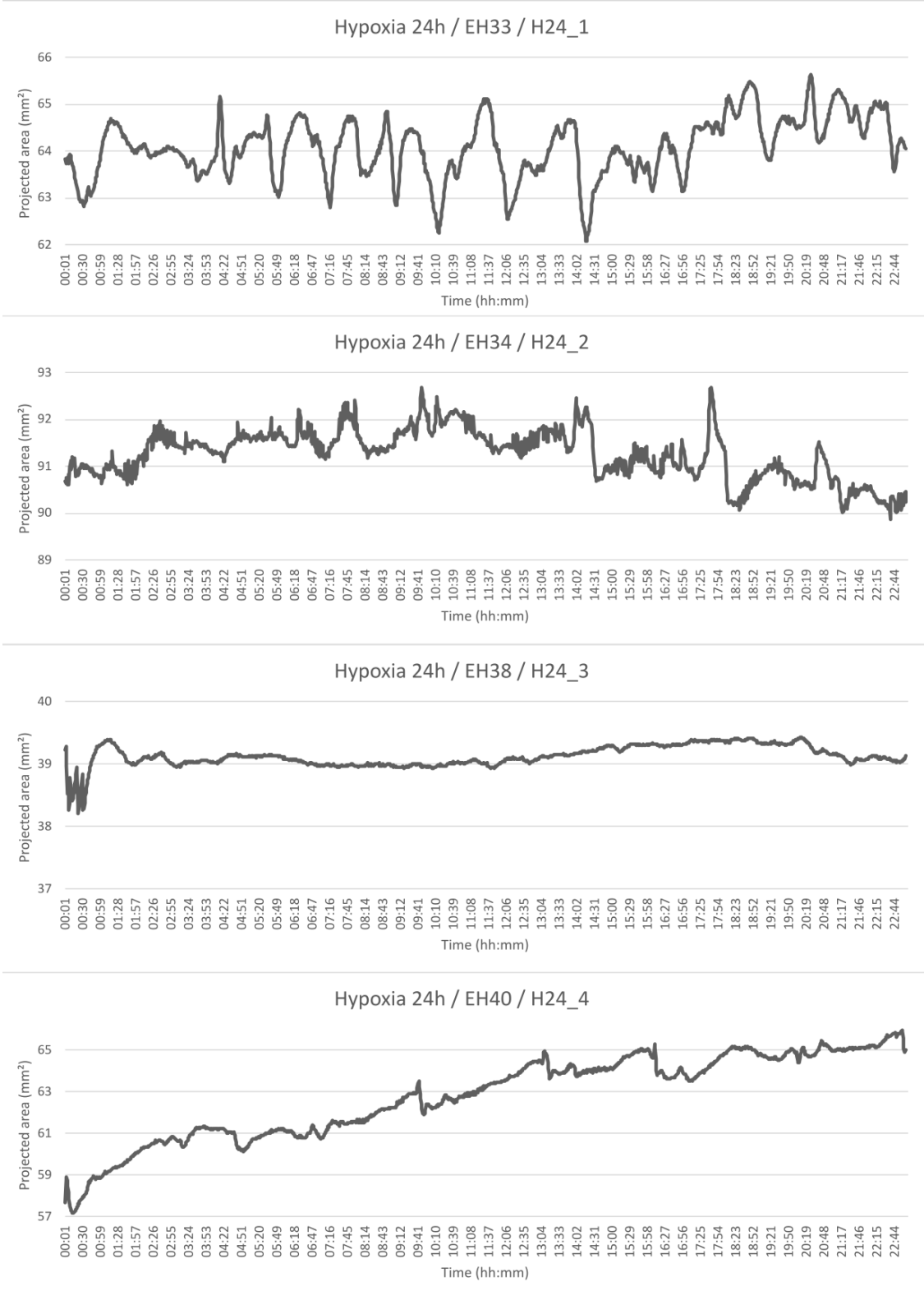

Supplementary Figure 3 – Contraction behavior of four representative sponges from each of the four hypoxia 24h experiment replicates performed, representing the changes in projected areas over the experimental period of 24h. Projected area is shown in mm², and time is shown in hours and minutes (hh:mm). Above each panel is shown the condition tested, the experiment label and the RNA sample label.

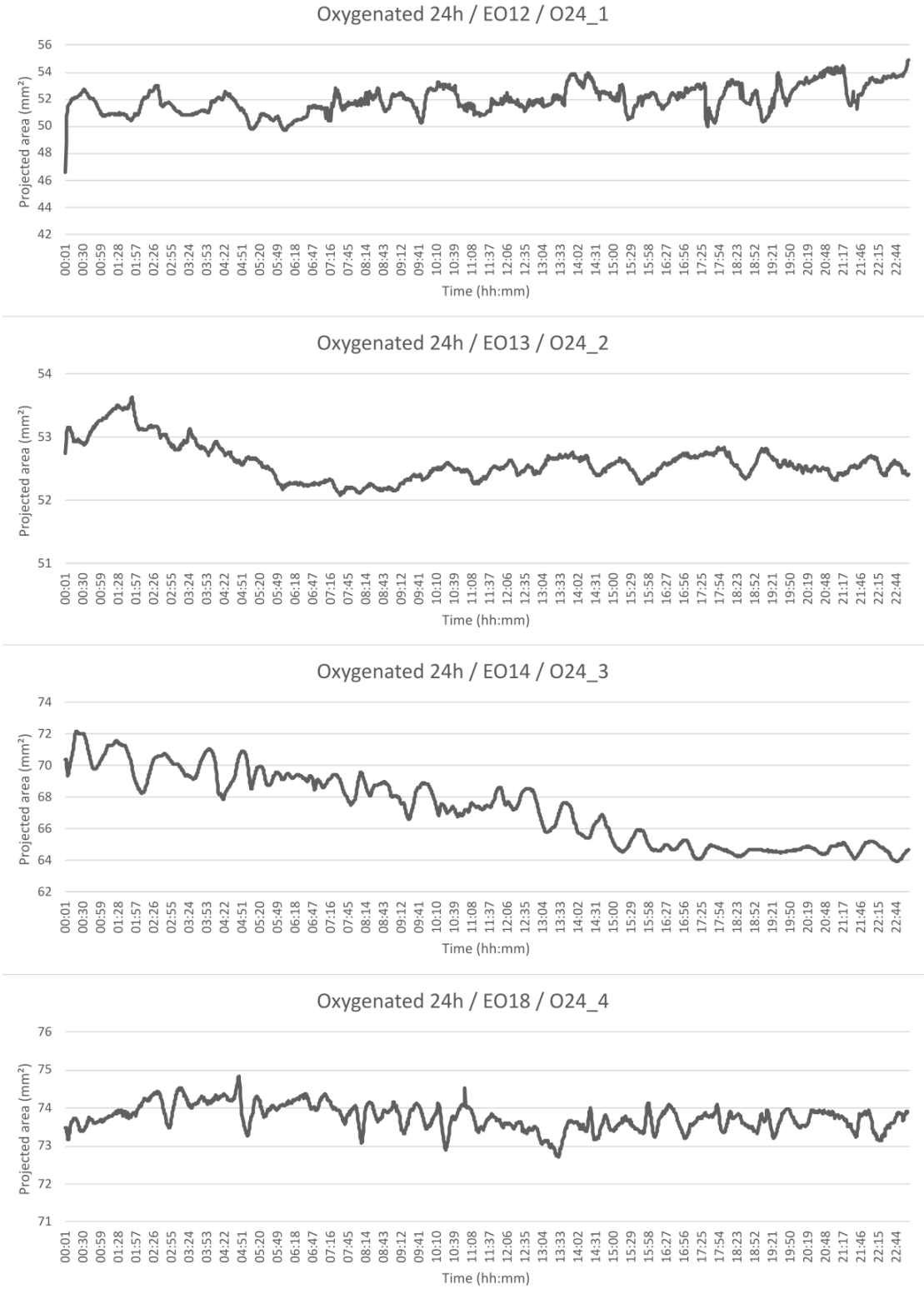

Supplementary Figure 4 – Contraction behavior of four representative sponges from each of the four oxygenated 24h experiment replicates performed, representing the changes in projected areas over the experimental period of 24h. Projected area is shown in mm², and time is shown in hours and minutes (hh:mm). Above each panel is shown the condition tested, the experiment label and the RNA sample label

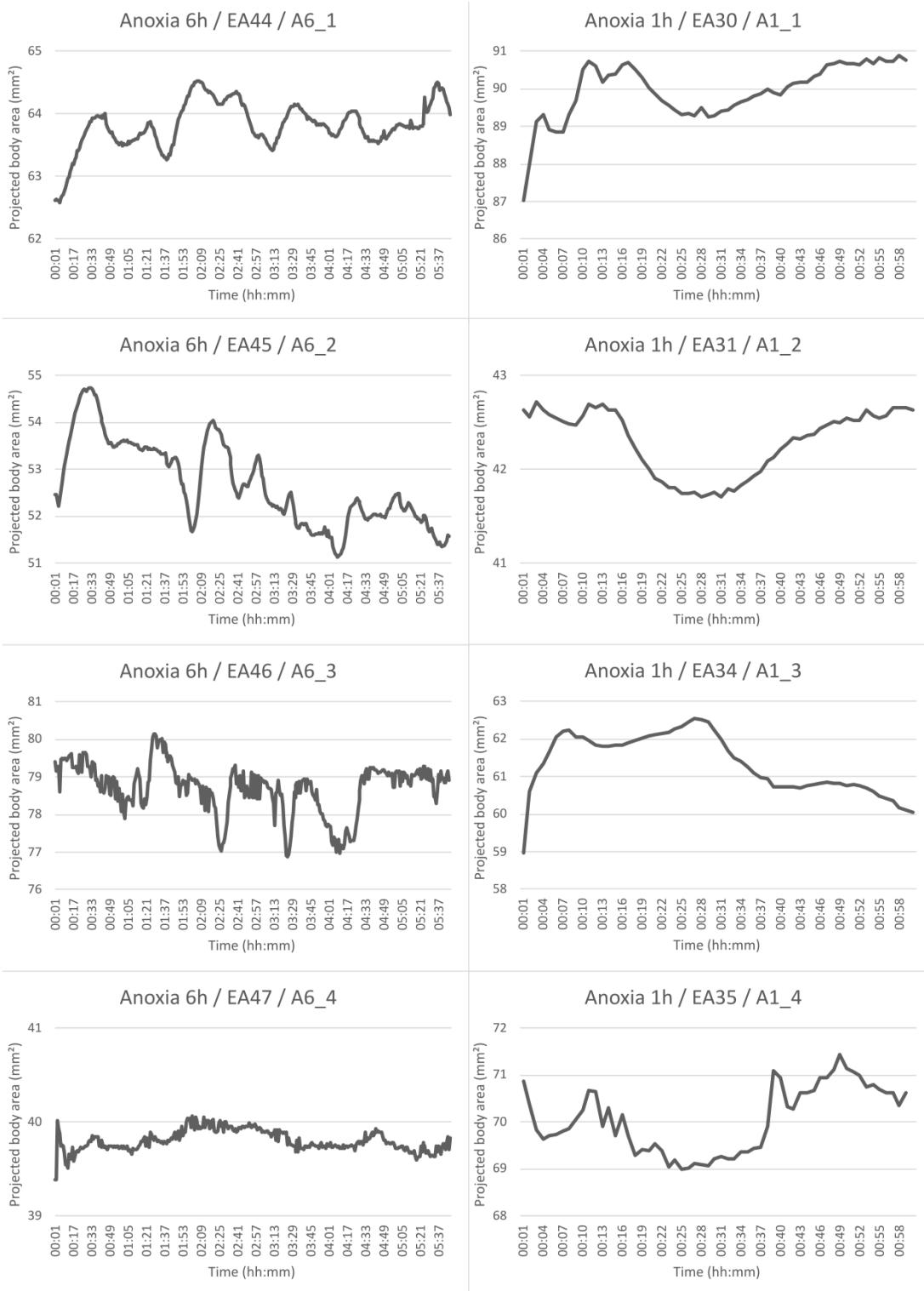

Supplementary Figure 5 – Sponges contraction behavior in anoxia. Left side panels show contraction patterns of four representative sponges from each of the four anoxia 6h experiment replicates performed. Right side panels show contraction patterns of four representative sponges from each of the four anoxia 1h experiment replicates performed.

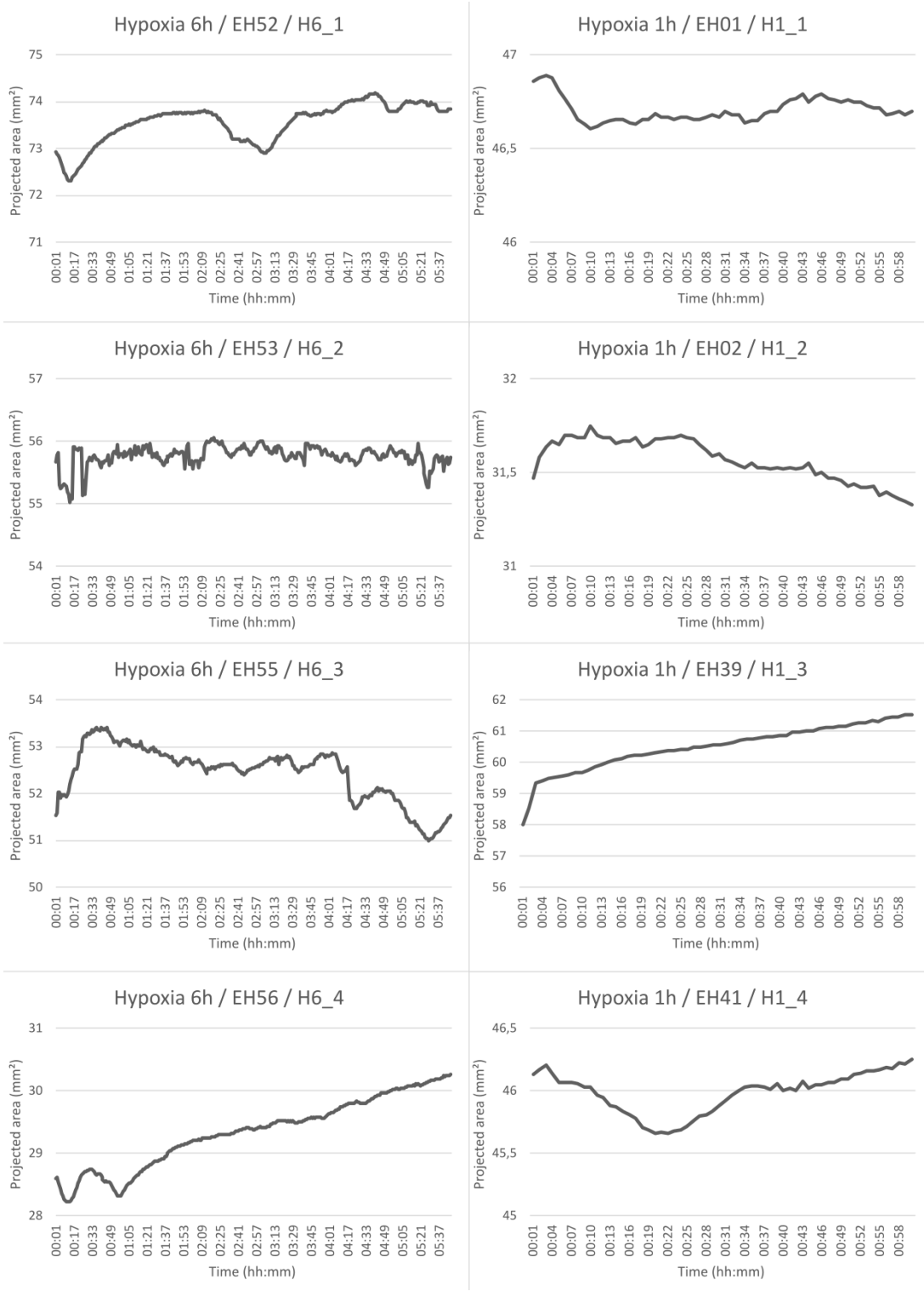

Supplementary Figure 6 – Sponges contraction behavior in hypoxia. Left side panels show contraction patterns of four representative sponges from each of the four hypoxia 6h experiment replicates performed. Right side panels show contraction patterns of four representative sponges from each of the four hypoxia 1h experiment replicates performed.

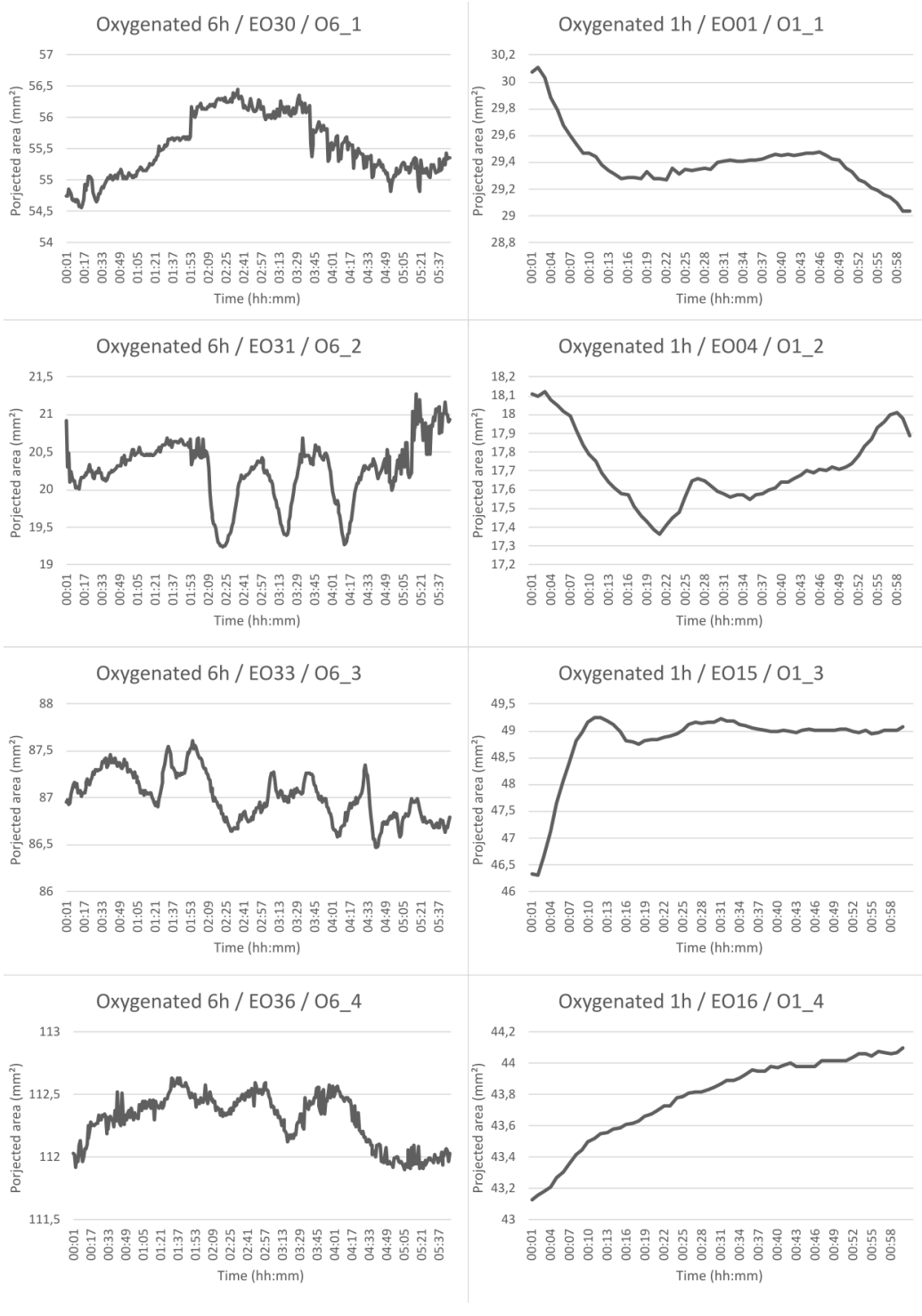

Supplementary Figure 7 – Sponges contraction behavior in oxygenated condition. Left side panels show contraction patterns of four representative sponges from each of the four oxygenated 6h experiment replicates performed. Right side panels show contraction patterns of four representative sponges from each of the four oxygenated 1h experiment replicates performed.

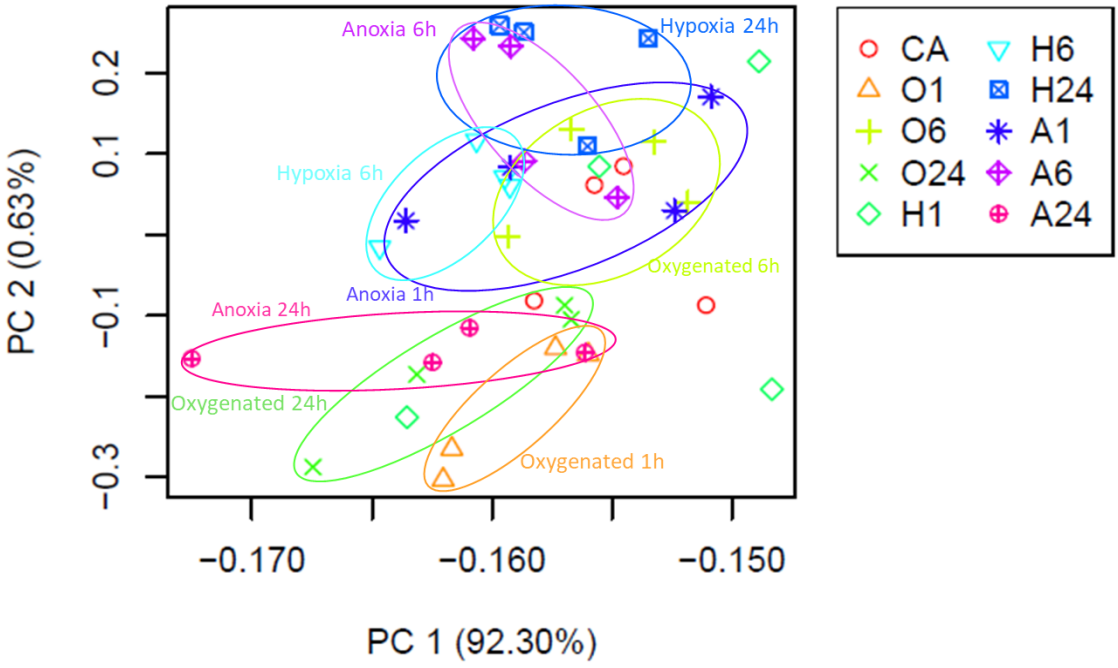

Supplementary Figure 8 – Principal Components Analysis (PCA) of the samples used in the differential expression analysis. Abbreviations: A, anoxia; H, hypoxia; O, oxygenated; 1, 1 hour; 6, 6 hours; 24, 24 hours; CA, aquarium control.

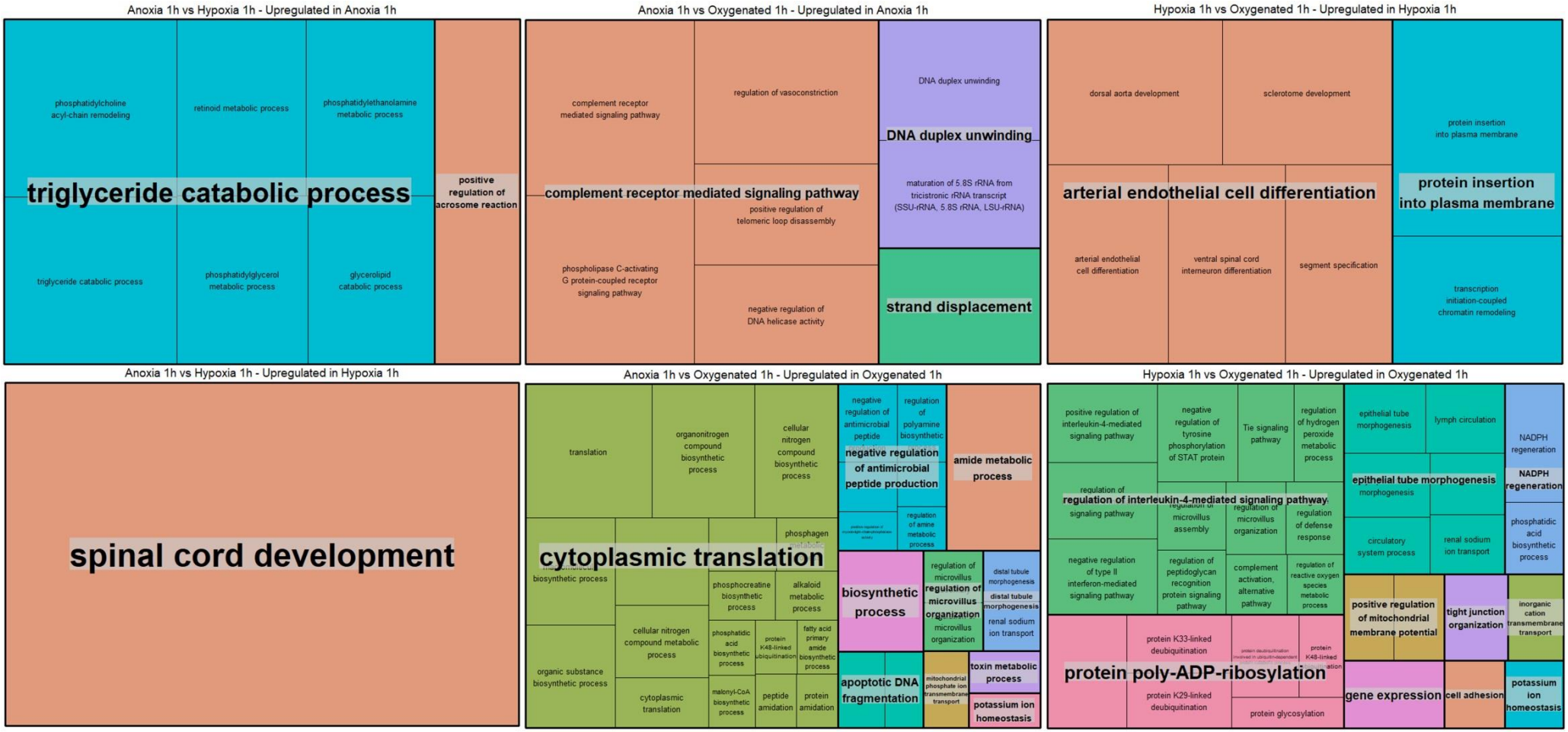

Supplementary Figure 9 – Treemaps showing the gene ontology (GO) categories (within Biological Process) associated to the differentially expressed genes in the 1 hour experiments obtained in REVIGO. Left panel shows the GO categories upregulated in the pairwise comparison between Anoxia 1h vs. Hypoxia 1h. Central panel shows the GO categories upregulated in the pairwise comparison between Anoxia 1h vs. Oxygenated 1h. Right panel shows the GO categories upregulated in the pairwise comparison between Hypoxia 1h vs. Oxygenated 1h.

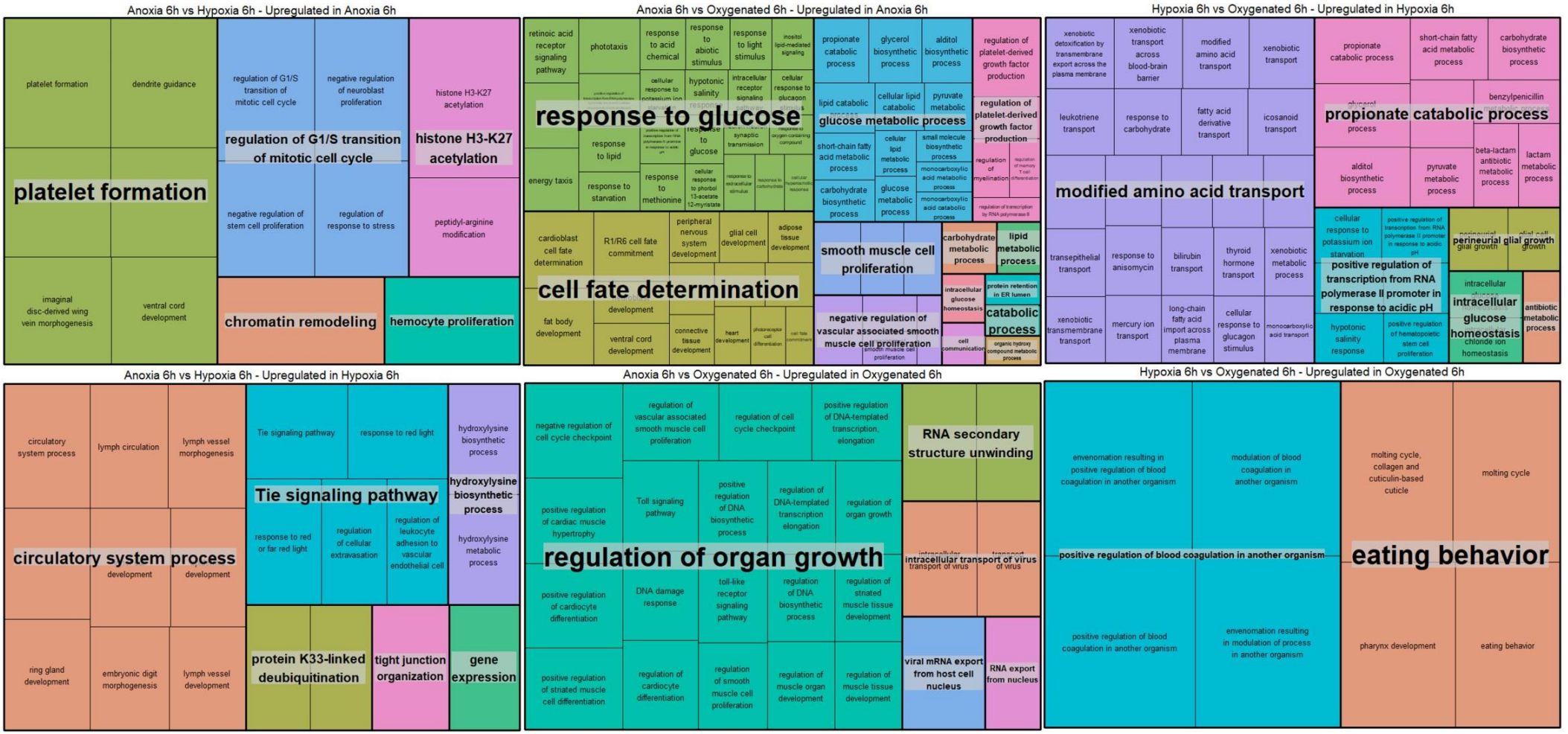

Supplementary Figure 10 – Treemaps showing the gene ontology (GO) categories (within Biological Process) associated to the differentially expressed genes in the 6 hours experiments obtained in REVIGO. Left panel shows the GO categories upregulated in the pairwise comparison between Anoxia 6h vs. Hypoxia 6h. Central panel shows the GO categories upregulated in the pairwise comparison between Anoxia 6h vs. Oxygenated 6h. Right panel shows the GO categories upregulated in the pairwise comparison between Hypoxia 6h vs. Oxygenated 6h.

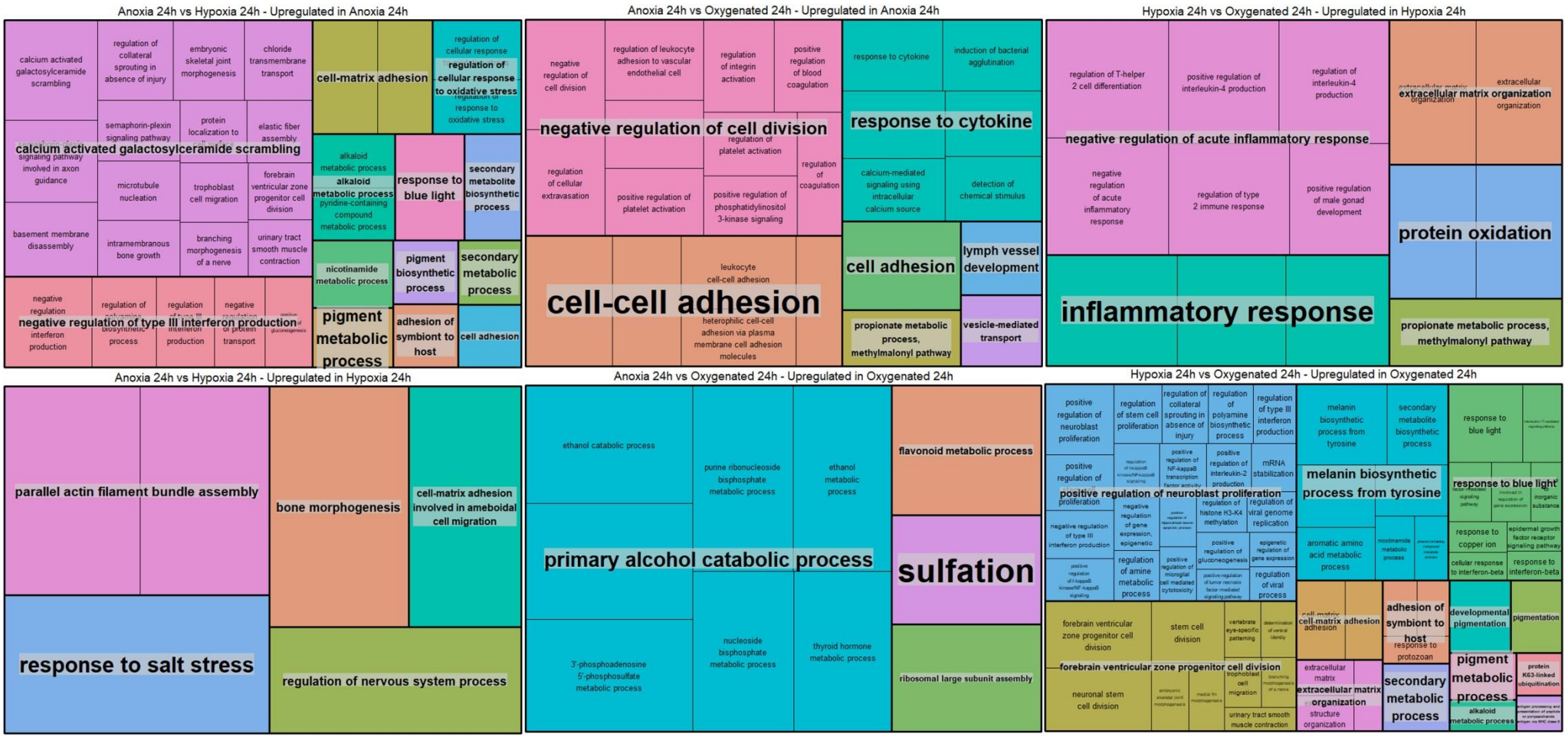

Supplementary Figure 11 – Treemaps showing the gene ontology (GO) categories (within Biological Process) associated to the differentially expressed genes in the 24 hours experiments obtained in REVIGO. Left panel shows the GO categories upregulated in the pairwise comparison between Anoxia 24h vs. Hypoxia 24h. Central panel shows the GO categories upregulated in the pairwise comparison between Anoxia 24h vs. Oxygenated 24h. Right panel shows the GO categories upregulated in the pairwise comparison between Hypoxia 24h vs. Oxygenated 24h.

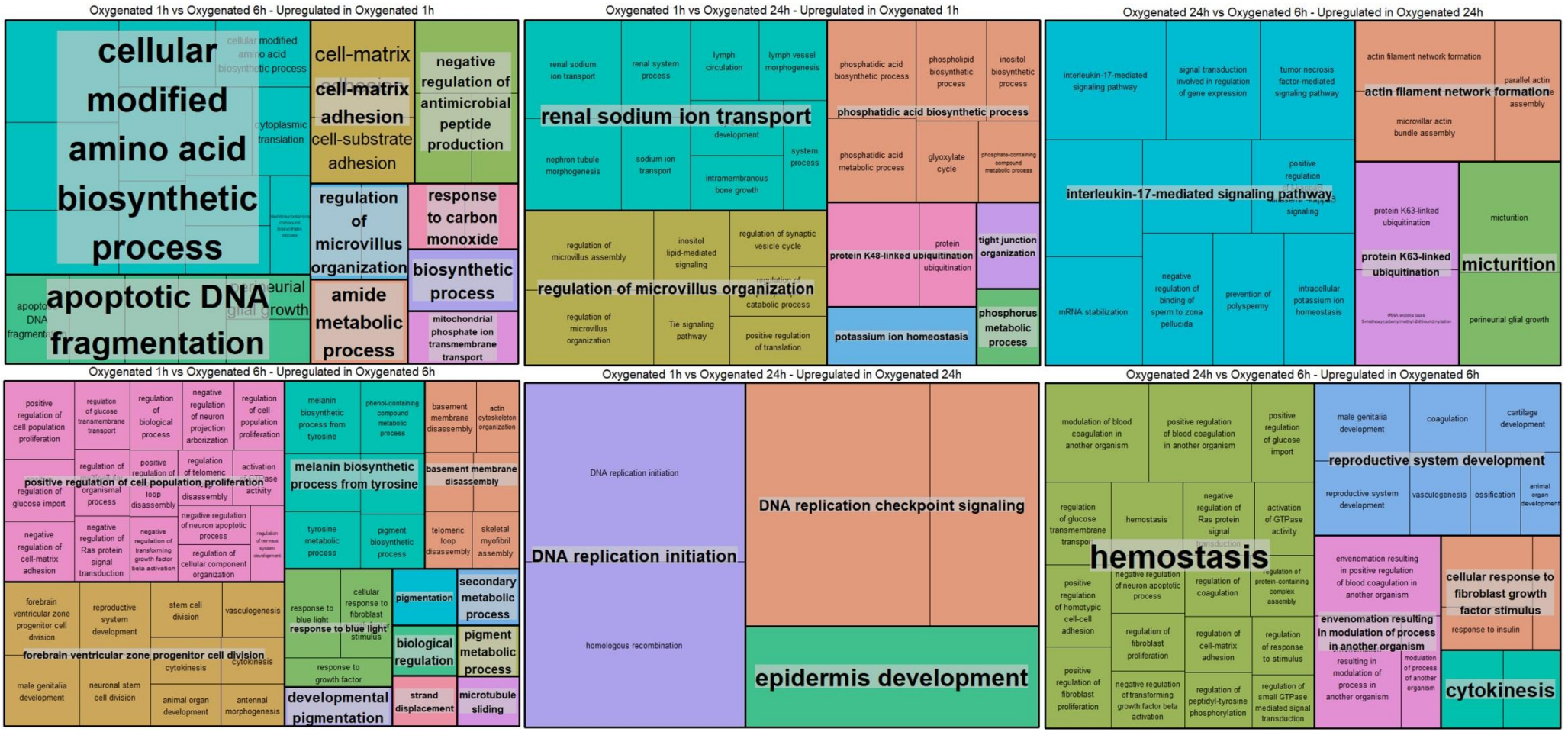

Supplementary Figure 12 – Treemaps showing the gene ontology (GO) categories (within Biological Process) associated to the differentially expressed genes in the oxygenated experiments obtained in REVIGO. Left panel shows the GO categories upregulated in the pairwise comparison between Oxygenated 1h vs. Oxygenated 6h. Central panel shows the GO categories upregulated in the pairwise comparison between Oxygenated 1h vs. Oxygenated 24h. Right panel shows the GO categories upregulated in the pairwise comparison between Oxygenated 24h vs. Oxygenated 6h.

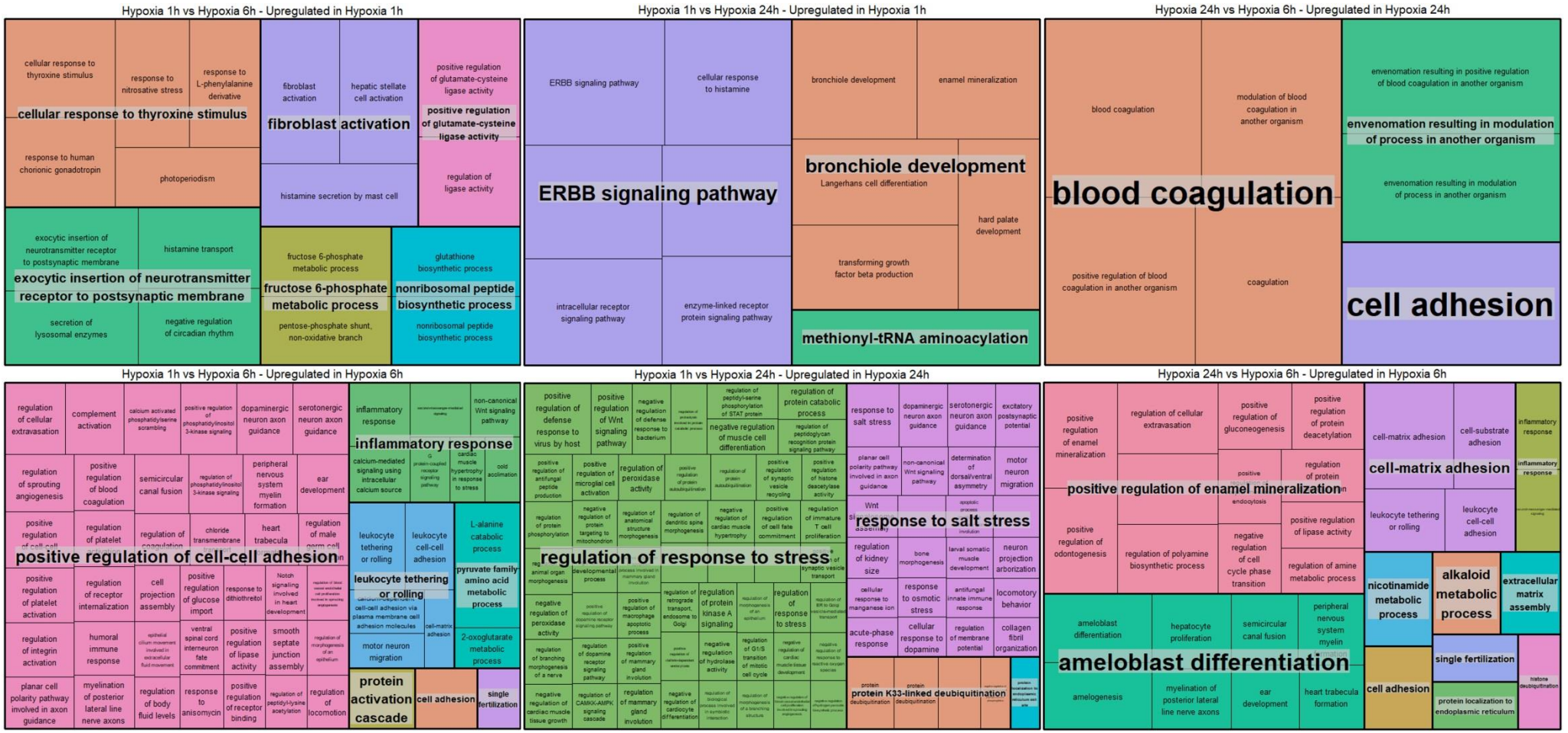

Supplementary Figure 13 – Treemaps showing the gene ontology (GO) categories (within Biological Process) associated to the differentially expressed genes in the hypoxia experiments obtained in REVIGO. Left panel shows the GO categories upregulated in the pairwise comparison between Hypoxia 1h vs. Hypoxia 6h. Central panel shows the GO categories upregulated in the pairwise comparison between Hypoxia 1h vs. Hypoxia 24h. Right panel shows the GO categories upregulated in the pairwise comparison between Hypoxia 24h vs. Hypoxia 6h.

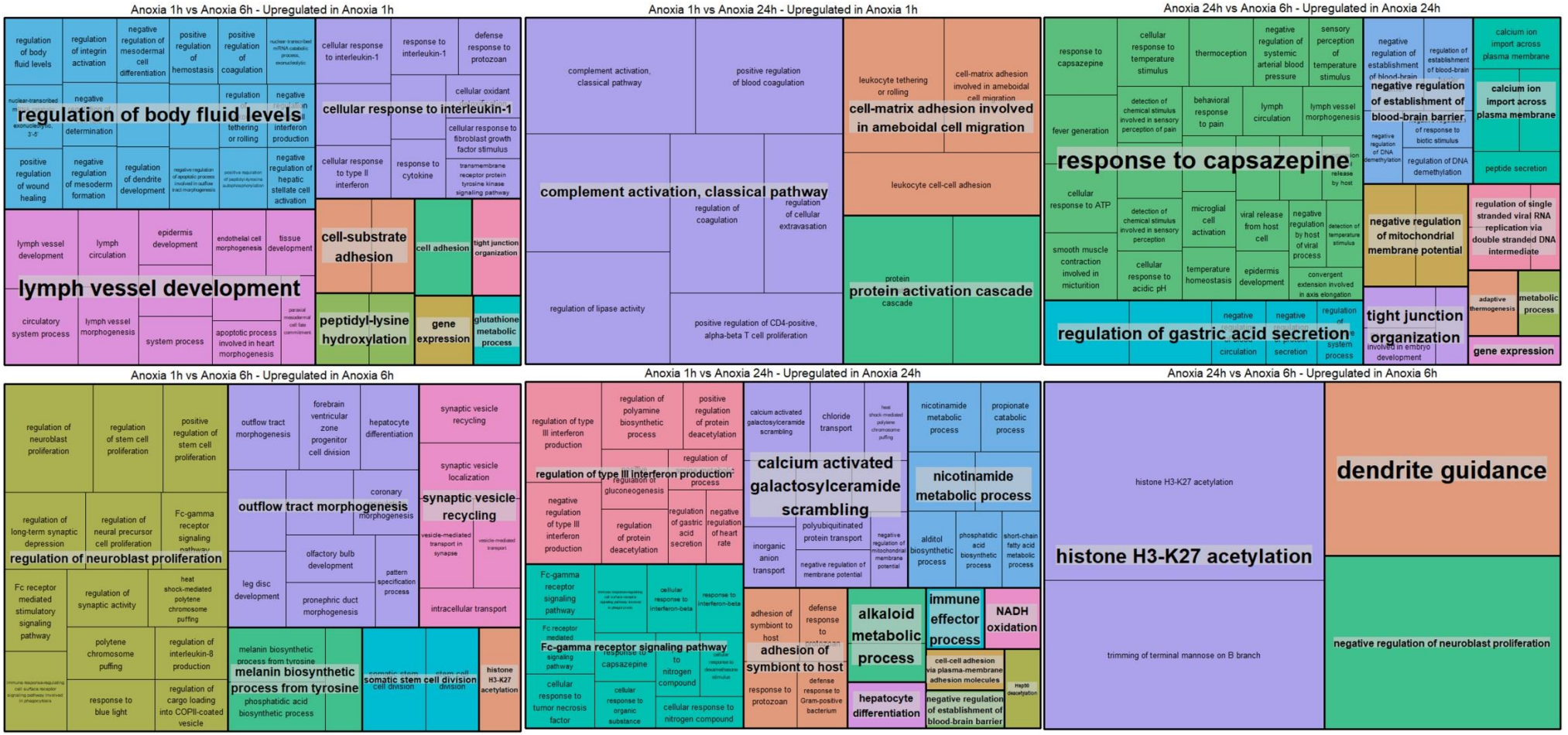

Supplementary Figure 14 – Treemaps showing the gene ontology (GO) categories (within Biological Process) associated to the differentially expressed genes in the anoxia experiments obtained in REVIGO. Left panel shows the GO categories upregulated in the pairwise comparison between Anoxia 1h vs. Anoxia 6h. Central panel shows the GO categories upregulated in the pairwise comparison between Anoxia 1h vs. Anoxia 24h. Right panel shows the GO categories upregulated in the pairwise comparison between Anoxia 24h vs. Anoxia 6h.

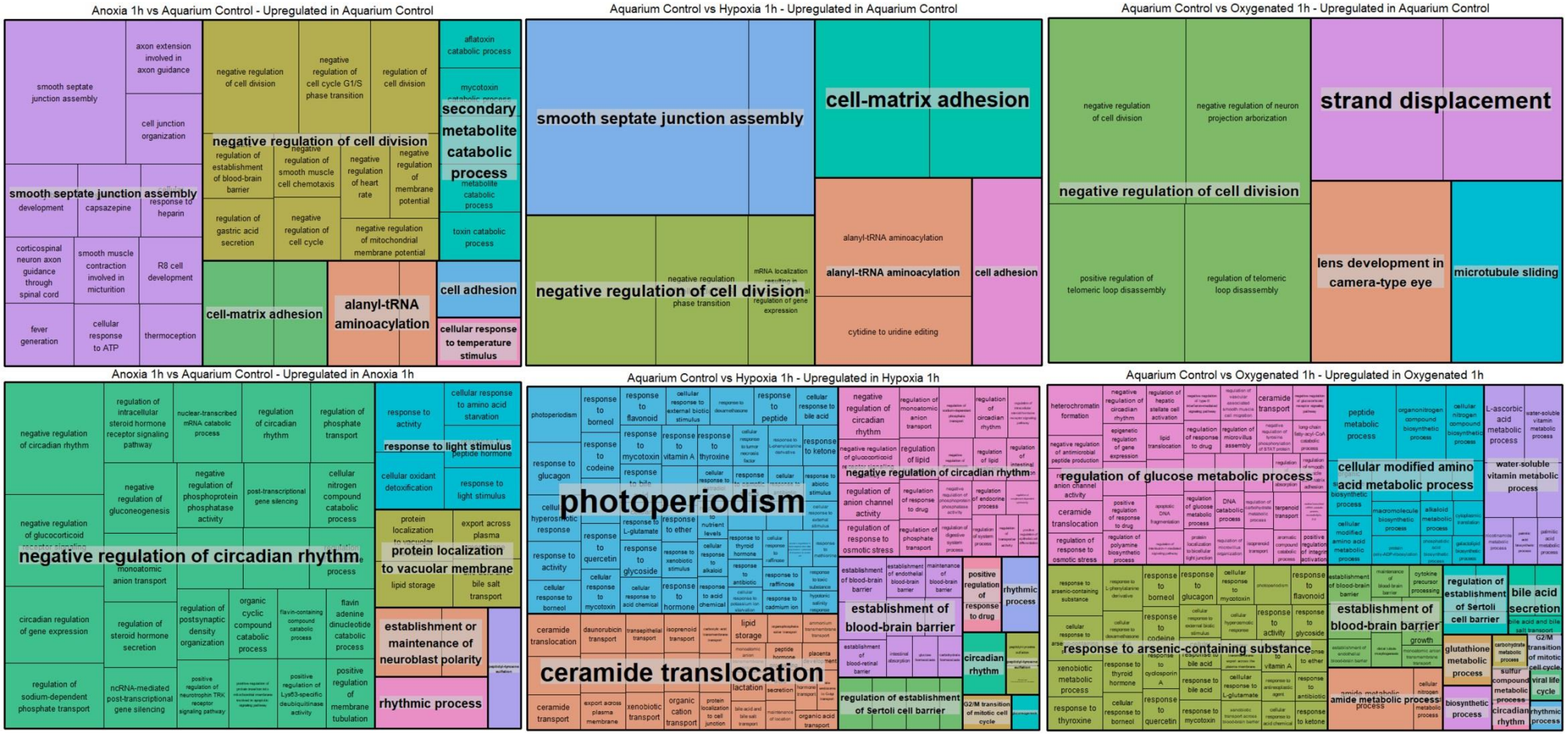

Supplementary Figure 15 – Treemaps showing the gene ontology (GO) categories (within Biological Process) associated to the differentially expressed genes in the aquarium control vs. 1h experiments obtained in REVIGO. Left panel shows the GO categories upregulated in the pairwise comparison between Anoxia 1h vs. Aquarium Control. Central panel shows the GO categories upregulated in the pairwise comparison between Aquarium Control vs. Hypoxia 1h. Right panel shows the GO categories upregulated in the pairwise comparison between Aquarium Control vs. Oxygenated 1h.

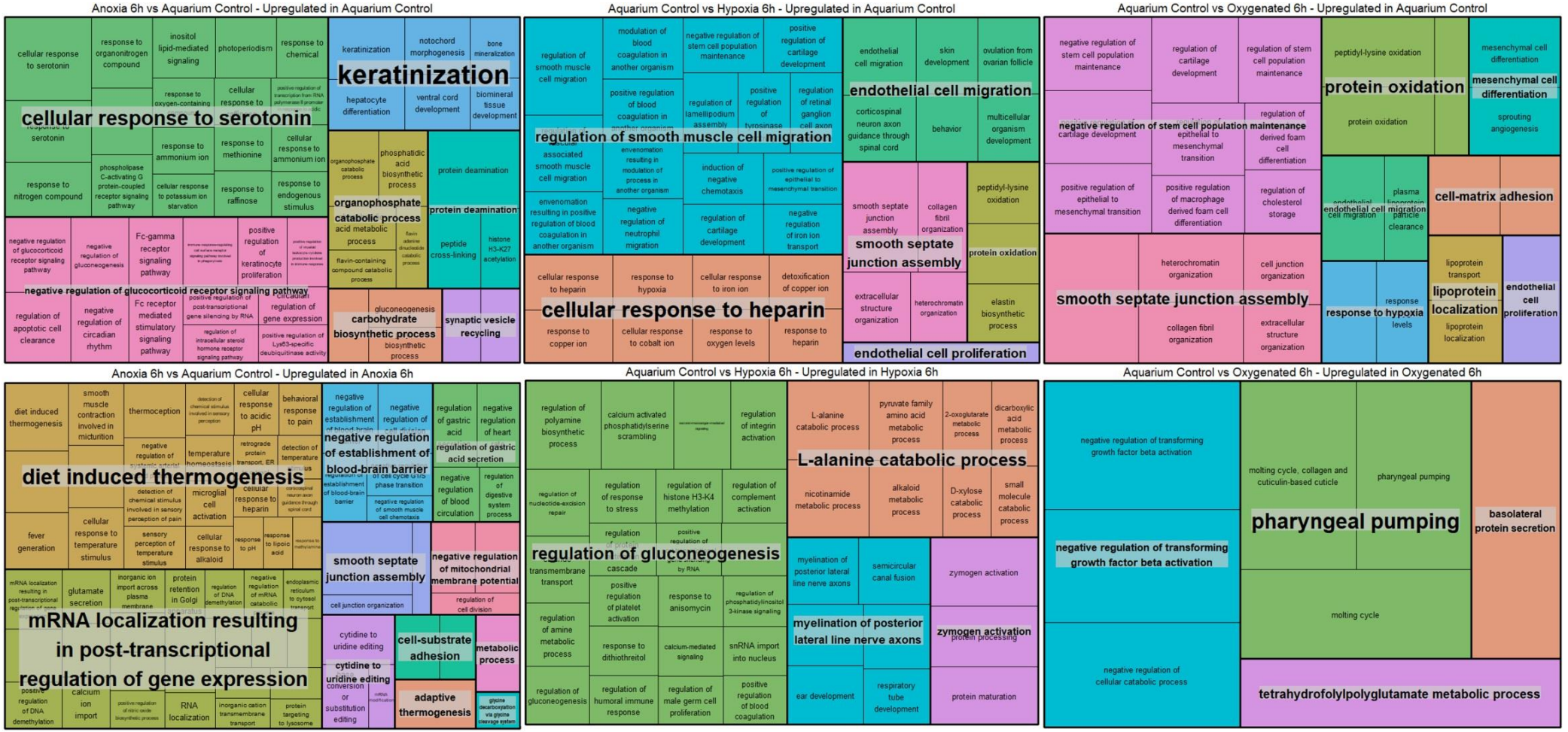

Supplementary Figure 16 – Treemaps showing the gene ontology (GO) categories (within Biological Process) associated to the differentially expressed genes in the aquarium control vs. 6h experiments obtained in REVIGO. Left panel shows the GO categories upregulated in the pairwise comparison between Anoxia 6h vs. Aquarium Control. Central panel shows the GO categories upregulated in the pairwise comparison between Aquarium Control vs. Hypoxia 6h. Right panel shows the GO categories upregulated in the pairwise comparison between Aquarium Control vs. Oxygenated 6h.

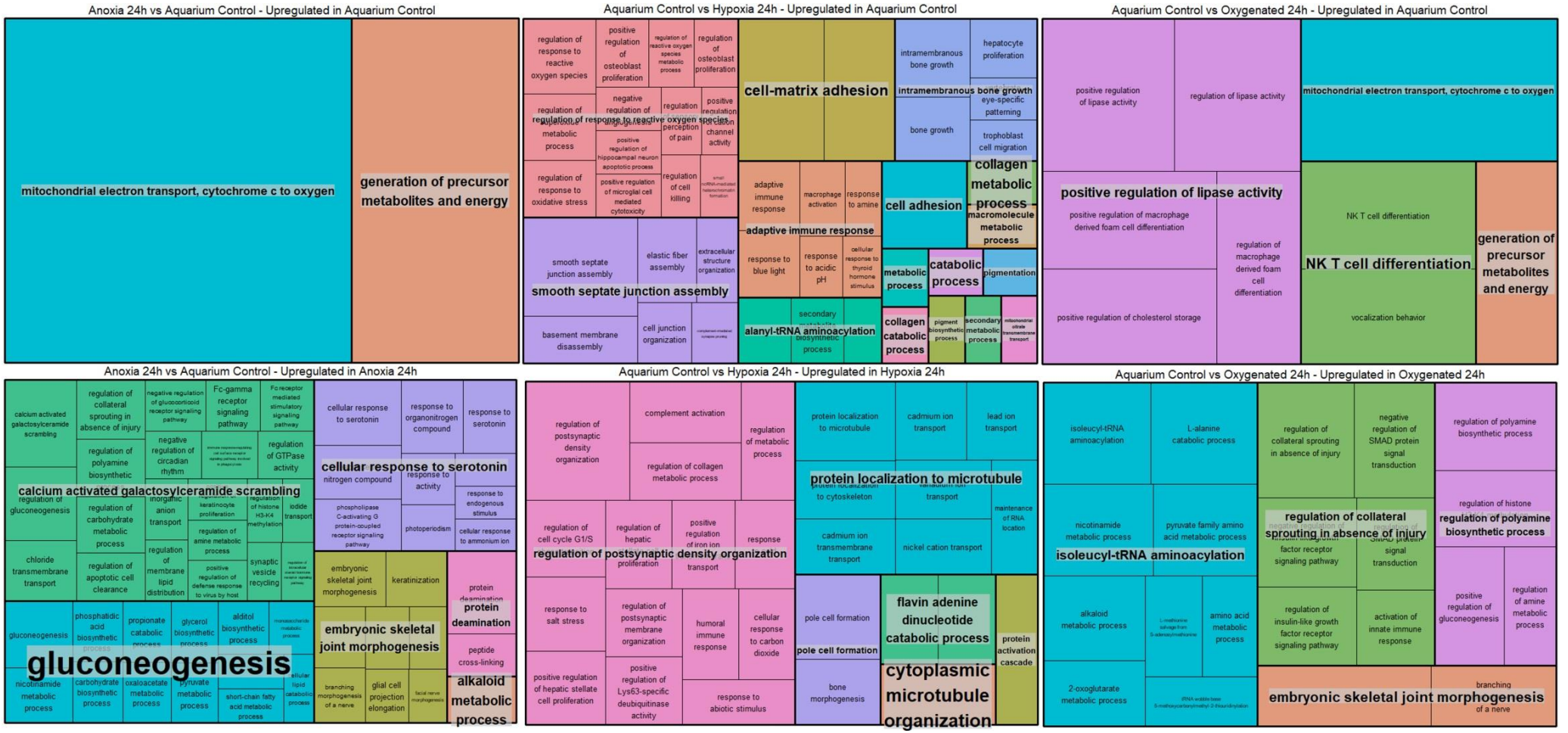

Supplementary Figure 17 – Treemaps showing the gene ontology (GO) categories (within Biological Process) associated to the differentially expressed genes in the aquarium control vs. 24h experiments obtained in REVIGO. Left panel shows the GO categories upregulated in the pairwise comparison between Anoxia 24h vs. Aquarium Control. Central panel shows the GO categories upregulated in the pairwise comparison between Aquarium Control vs. Hypoxia 24h. Right panel shows the GO categories upregulated in the pairwise comparison between Aquarium Control vs. Oxygenated 24h.

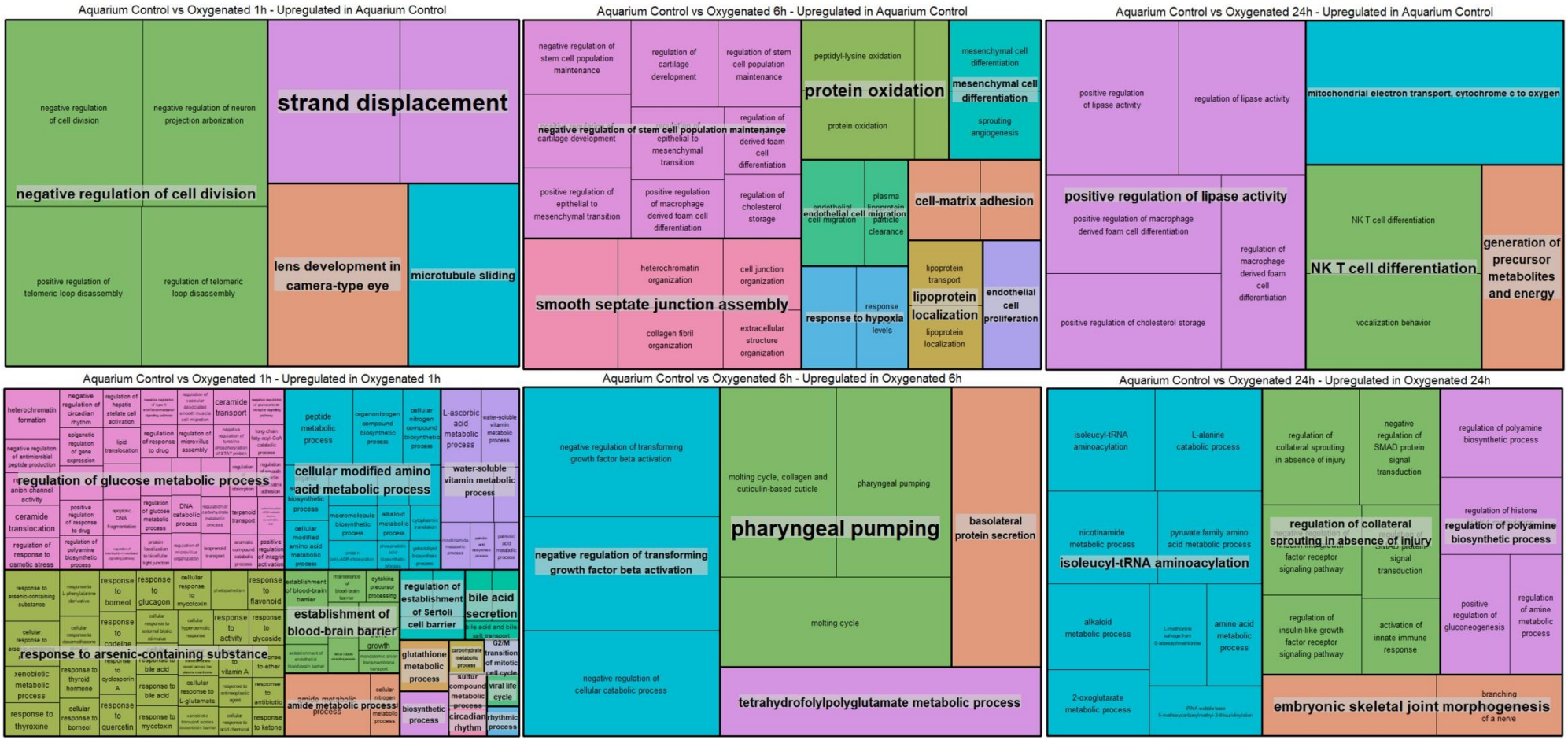

Supplementary Figure 18 – Treemaps showing the gene ontology (GO) categories (within Biological Process) associated to the differentially expressed genes in the aquarium control vs. oxygenated experiments obtained in REVIGO. Left panel shows the GO categories upregulated in the pairwise comparison between Aquarium Control vs. Oxygenated 1h. Central panel shows the GO categories upregulated in the pairwise comparison between Aquarium Control vs. Oxygenated 6h. Right panel shows the GO categories upregulated in the pairwise comparison between Aquarium Control vs. Oxygenated 24h

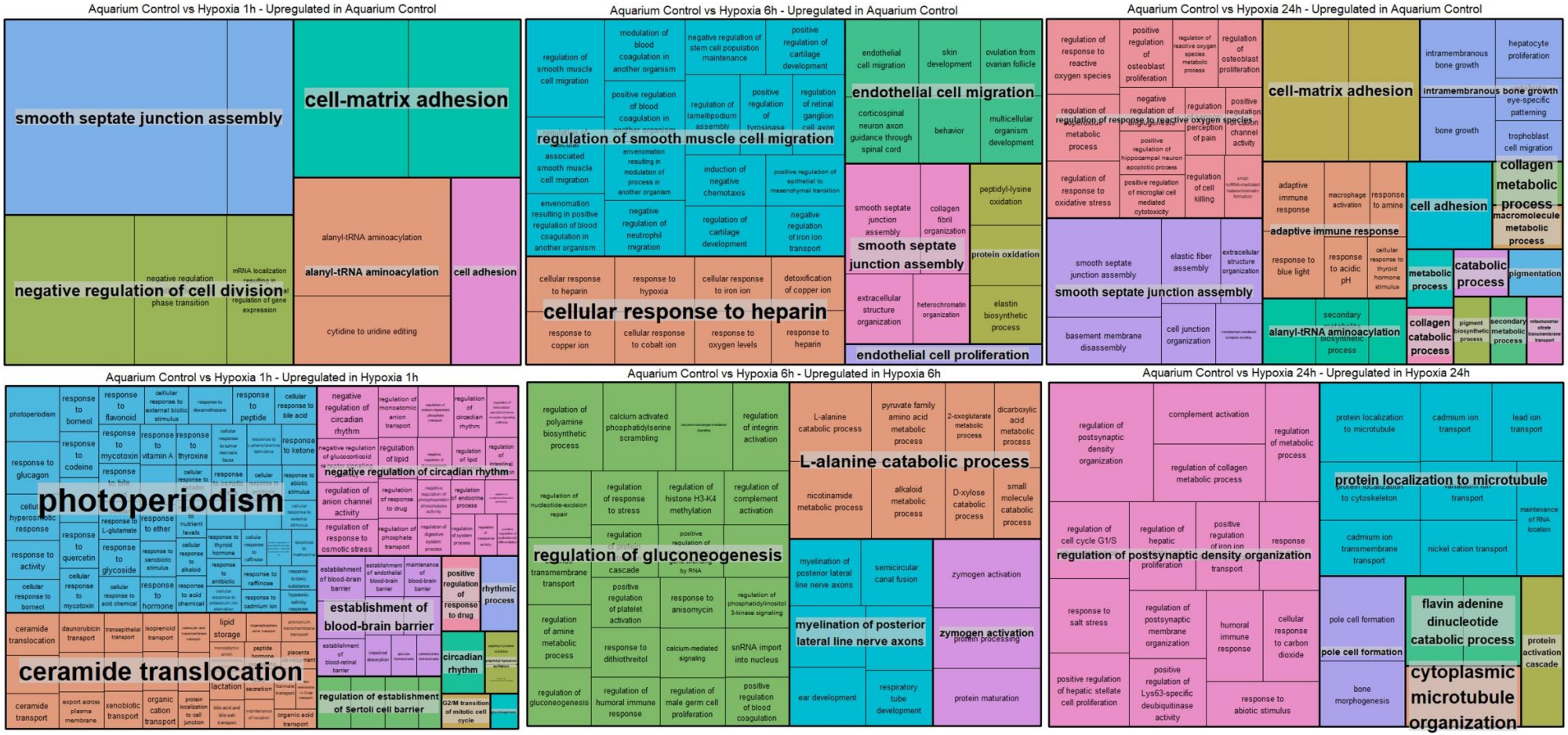

Supplementary Figure 19 – Treemaps showing the gene ontology (GO) categories (within Biological Process) associated to the differentially expressed genes in the aquarium control vs. hypoxia experiments obtained in REVIGO. Left panel shows the GO categories upregulated in the pairwise comparison between Aquarium Control vs. Hypoxia 1h. Central panel shows the GO categories upregulated in the pairwise comparison between Aquarium Control vs. Hypoxia 6h. Right panel shows the GO categories upregulated in the pairwise comparison between Aquarium Control vs. Hypoxia 24h.

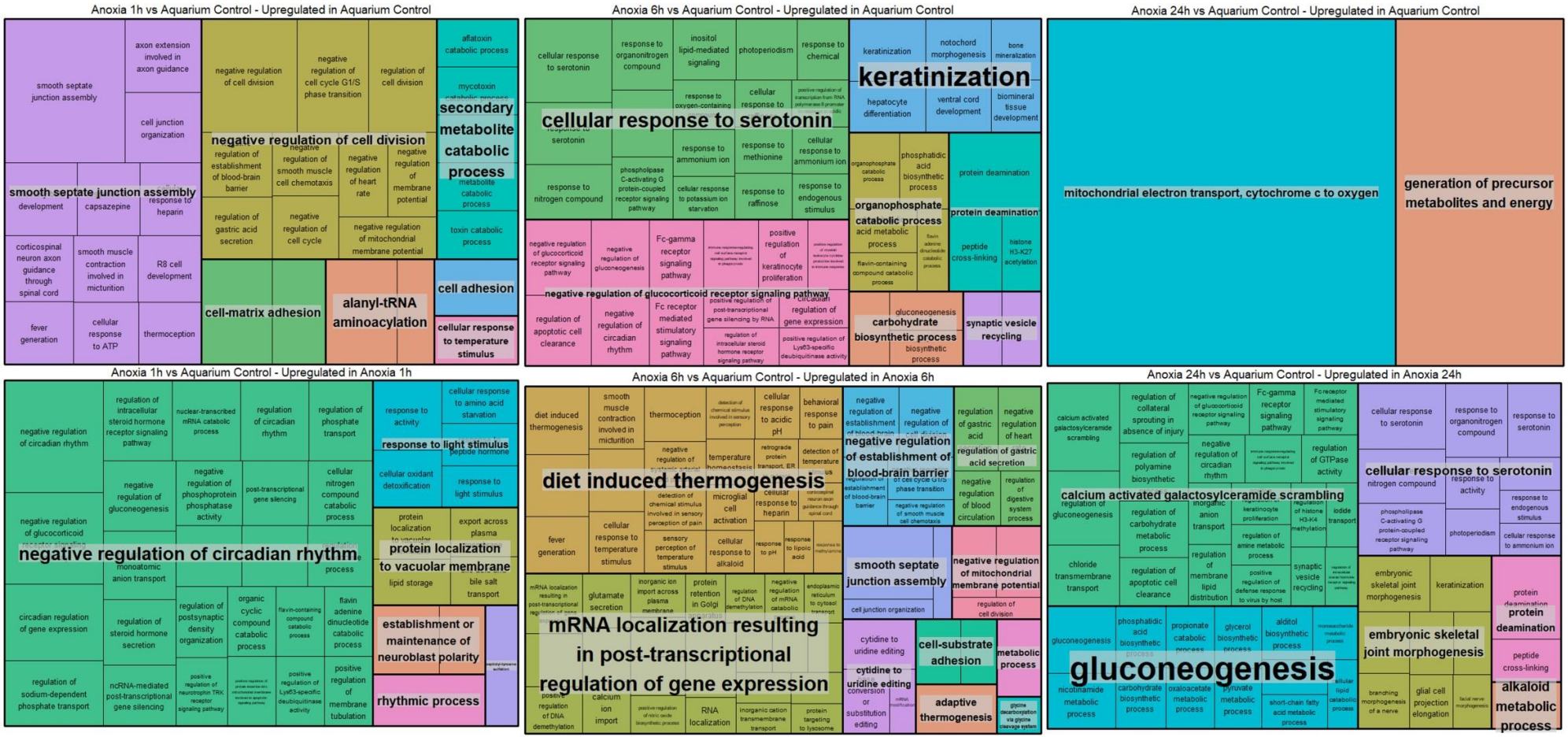

Supplementary Figure 20 – Treemaps showing the gene ontology (GO) categories (within Biological Process) associated to the differentially expressed genes in the aquarium control vs. anoxia experiments obtained in REVIGO. Left panel shows the GO categories upregulated in the pairwise comparison between Anoxia 1h vs. Aquarium Control. Central panel shows the GO categories upregulated in the pairwise comparison between Anoxia 6h vs. Aquarium Control. Right panel shows the GO categories upregulated in the pairwise comparison between Anoxia 24h vs. Aquarium Control.

Discussão Geral e Conclusões

A tese de doutorado aqui apresentada é constituída por três capítulos que utilizaram abordagens bioinformáticas e experimentais a fim de elucidar aspectos da fisiologia dos primeiros animais. Os dois primeiros capítulos abordam estudos bioinformáticos de datação molecular de genes envolvidos no metabolismo do oxigênio (O_2), e o terceiro capítulo traz um trabalho essencialmente experimental que submeteu animais modernos às condições que simulam as concentrações de O_2 no ambiente marinho do Neoproterozóico. De maneira geral, os trabalhos de datação molecular indicam um surgimento pré-Criogeniano dos metazoários, quando baixos níveis de O_2 prevaleciam nos oceanos primordiais. Os experimentos de simulação sugerem que os primeiros animais apresentavam diversas adaptações fisiológicas e moleculares às condições de hipóxia. Mesmo não possuindo mecanismos complexos de detecção dos níveis de O_2, eles provavelmente eram bem adaptados às extremas variações nas concentrações de O_2 que ocorriam durante o Neoproterozóico.

Como os animais dependem da respiração celular, a datação da evolução de proteínas relacionadas ao metabolismo oxidativo pode nos permitir estimar o tempo de divergência desses organismos. O papel crucial da enzima Isocitrato Desidrogenase (IDH) na respiração celular, regulando o fluxo metabólico do ciclo de Krebs (Mailloux et al., 2007), torna sua história evolutiva uma valiosa fonte de conhecimento para estudar a evolução dos primeiros animais e eucariotos. Para estabelecer a história evolutiva e o tempo de divergência da IDH, foram examinados dados transcriptômicos de 195 sequências de eucariotos (Bezerra et al., 2021). Empregando métodos de reconstrução filogenética e datação molecular assumindo relógio relaxado, foi demonstrado que ao menos duas duplicações gênicas ocorreram na história evolutiva da IDH, no

Mesoproterozóico. A primeira duplicação ocorreu no ancestral dos eucariotos, há ~1.967 Ma (Intervalo de Confiança (CI) 1.641–2.329 Ma), e deu origem à subunidade catalítica α. A segunda duplicação teve datação aproximada de ~1.629 Ma (CI 1.334–1.884 Ma), dando origem às subunidades reguladoras β e γ (Bezerra et al., 2021).

Corroborando os resultados que indicam uma origem muito antiga da IDH, foi demonstrado que ao menos 22 famílias de enzimas que produzem ou utilizam o O_2 surgiram em torno de 3,1 bilhões de anos, antes do Grande Evento de Oxidação (GOE; Jabłońska e Tawfik, 2021). Fato que pode ser explicado pela existência de possíveis oásis de O_2 ocupados por organismos que realizavam fotossíntese oxigenada (Olson et al., 2013). Também é argumentado que independentemente do ambiente, o O_2 molecular estava presente nas células desde o início da vida. Espécies reativas de oxigênio (ROS) produzidas abioticamente poderiam ter sido a fonte primordial de O_2 molecular (Ślesak et al., 2012). Esses resultados indicam que, ao contrário do que é pensado por muitos autores, o aumento dos níveis de O_2 atmosférico pode não ser um gatilho para novidades evolutivas (Jabłońska e Tawfik, 2021).

O surgimento da linhagem que originou as subunidades β+γ ocorreu no Mesoproterozóico (~1.629 Ma), e a datação da evolução das subunidades β (~1.249 Ma; CI 1.020–1.490 Ma) e γ (~1.532 Ma; CI 1.221–1.769 Ma) suportam um surgimento mais antigo dos animais se comparado a estudos que colocam sua origem em torno ~850 Ma (Dohrmann e Wörheide, 2017; Sperling e Stockey, 2018), antes dos registros de oxigenação oceânica difundida (Tostevin e Mills, 2020). Um período de hipóxia prolongada na evolução animal pode ter resultado em adaptações particulares para atender às demandas metabólicas de O_2 (Wood e Erwin, 2018), o que poderia explicar a tendência evolutiva de aumento da complexidade da IDH, possivelmente em resposta às mudanças ambientais

que ocorreram no Neoproterozóico. A datação molecular da história evolutiva da enzima IDH suporta a hipótese de uma diversificação de eucariotos antes do período Toniano, bem como um surgimento pré-Criogeniano dos animais em hipóxia.

Outra proteína que tem grande potencial para trazer conhecimento acerca da diversificação dos animais por meio de sua história evolutiva é o fator de transcrição induzido por hipóxia (HIF). A via metabólica mediada pela HIF é responsável por manter a homeostase do O_2 nas células animais através de mudanças adaptativas na expressão gênica (Semenza, 2007). Por conta disso, ela é considerada o regulador-mestre dos níveis de O_2 nas células (Semenza, 2007). Porém, embora os animais precisem de O_2 para sobreviver, suas demandas não são as mesmas. Sabe-se que esponjas e ctenóforos, que são os clados candidatos a serem irmãos de todos os filos animais (Whelan et al., 2015; Pisani et al., 2015; Halanych, 2016; King e Rokas, 2017), podem viver sob baixas concentrações de O_2 na natureza (Purcell et al., 2001; Levin, 2003; Thuesen et al., 2005; Mosch et al., 2012). E apesar da via HIF ser evolutivamente conservada em bilatérios, placozoários e cnidários (Loenarz et al., 2011), trabalhos recentes demonstraram que tanto esponjas quanto ctenóforos não possuem componentes-chave da via HIF (Mills et al., 2018; Belato et al., 2023). Esses dados, que foram corroborados pelos resultados apresentados nos capítulos dois e três, sugerem que o último ancestral comum animal provavelmente também não tinha uma via HIF funcional e, possivelmente, poderia manter o metabolismo aeróbico e a transcrição normal sob os baixos níveis de O_2 de seu ambiente (Mills et al., 2018; Belato et al., 2023).

No segundo capítulo desta tese, foi utilizada a mesma metodologia empregada para o estudo da IDH, datação de genes assumindo relógio molecular relaxado, com o objetivo de entender a história evolutiva da HIFa. Foi possível inferir que a linhagem gênica que deu origem à HIFa

surgiu há ~1.273 Ma (CI 957–1.621 Ma), na Era Mesoproterozóica. Essa datação corrobora a hipótese de que uma grande parte do *toolkit* gênico necessário para o desenvolvimento animal evoluiu em seus ancestrais unicelulares eucarióticos (Sebé-Pedrós et al., 2011, 2012; de Mendoza et al., 2013).

Os resultados também demonstram que pelo menos dois eventos de duplicação ocorreram ao longo da evolução da HIFa, gerando os parálogos HIF1a, HIF2a e HIF3a em vertebrados (Belato et al., 2023). As idades estimadas para os dois eventos de duplicação, há ~595 Ma (CI 550–636 Ma) e há ~558 Ma (CI 500–604 Ma), estão de acordo com as datações dos eventos de duplicação genômica que ocorreram no ancestral dos vertebrados (Panopoulou e Poustka, 2005; Kuraku et al., 2009; Sacerdot et al., 2018; Simakov et al., 2020). Assim como os resultados obtidos na datação da IDH, a história evolutiva da HIF também suporta a hipótese de um surgimento pré-Criogeniano da HIFa de animais, corroborando as estimativas de relógio molecular e dados paleontológicos que indicam um surgimento muito antigo dos animais em hipóxia (Neuweiler et al., 2009; Maloof et al., 2010; Erwin et al., 2011; Meert et al., 2011; Wallace et al., 2014; dos Reis et al., 2015; Brocks et al., 2016; Dohrmann e Wörheide, 2017).

Considerando os resultados que indicam que os primeiros animais surgiram em ambientes hipóxicos no Neoproterozóico, pouco se sabe sobre os mecanismos moleculares que eles possuíam para sobreviver nessas condições. E entender como os animais modernos respondem em nível molecular à hipóxia e anóxia pode ajudar a esclarecer a fisiologia dos primeiros metazoários. Sendo assim, no capítulo três, a esponja *Hymeniacidon heliophila* foi considerada um análogo moderno dos primeiros animais, sendo utilizada como um modelo de seus ancestrais. As esponjas foram submetidas às condições oceânicas de baixo O_2 do

Neoproterozóico em câmaras de simulação, e as variações na expressão gênica foram quantificadas. Os experimentos mostraram que após 24h, tanto a anóxia quanto a condição oxigenada desencadeiam as mesmas respostas fisiológicas e morfológicas de estresse, especialmente no caso dos genes relacionados à apoptose, que são um biomarcador de estresse em esponjas (Wagner et al., 1998). Os padrões de contração corporal das esponjas também corroboram a similaridade entre as respostas geradas pelas condições de anóxia e oxigenada. As esponjas contraíram significativamente mais vezes nessas duas condições do que quando comparadas à hipóxia após 24h. E como o aumento na taxa de contrações é um mecanismo que as esponjas usam para tentar aumentar a oxigenação do corpo (Hoffmann et al., 2008; Maldonado et al., 2012), isso sugere estresse oxidativo nos experimentos de anóxia e oxigenados. Esses resultados indicam que as esponjas estão mais bem adaptadas à condição de hipóxia (Micaroni et al., 2022).

Apesar da maioria dos metazoários possuir a via HIF como mecanismo de detecção dos níveis de O_2 nas células (Semenza, 2007), os dados aqui apresentados corroboram o fato de que as esponjas e os ctenóforos não têm uma via HIF funcional, assim como os primeiros metazoários provavelmente também não tinham (Mills et al., 2018; Belato et al., 2023). Porém, tanto os animais modernos quanto os primordiais precisariam de outros métodos para detectar as variações nos níveis de O_2, especialmente considerando que durante o Neoproterozóico as variações diárias nas condições redox eram extremas (Krause et al., 2022; Hammarlund et al., no prelo). Sabe-se que a via de remoção do sulfeto pode agir como um método de detecção dos níveis de O_2 nas células, pois o sulfeto é removido por uma série de reações dependentes do O_2 (Olson, 2015; Mills et al., 2018). As análises do capítulo três mostraram que vários genes ligados à via de remoção do sulfeto estavam diferencialmente

expressos em hipóxia e em anóxia. Especialmente a catalase, uma enzima com ação sulfeto-redutase (Olson et al., 2017), que estava superexpressa nas amostras de hipóxia após 24h. Como a maior parte das enzimas relacionadas ao metabolismo do sulfeto são evolutivamente conservadas em toda a árvore da vida (Olson, 2015; Mills et al., 2018; Mateos et al., 2023), é provável que os primeiros animais usassem essa via como método de detecção dos níveis de O_2 celular.

Para lidar com o estresse oxidativo, as esponjas apresentaram superexpressão de genes relacionados à glicólise, que é a via metabólica responsável por gerar energia na ausência do O_2 (Guillaumond et al., 2013; Nelson et al., 2013). A capacidade de detectar os níveis de O_2 e mudar do metabolismo celular aeróbico para anaeróbico provavelmente era uma característica essencial que estava presente nos primeiros animais (Semenza, 2007; Hammarlund et al., 2020). Outro mecanismo que as esponjas possuem para enfrentar baixos níveis de O_2 é a reorganização do seu sistema aquífero (Leys et al., 2011; Leys and Hill, 2012; Micaroni et al., 2022). Diversos genes ligados à formação de vasos sanguíneos em vertebrados estavam diferencialmente expressos nos experimentos, sugerindo um papel ainda desconhecido no processo de reorganização tubular das esponjas (Riesgo et al., 2022). Se os primeiros animais eram semelhantes às esponjas, a capacidade fenotípica de remodelar seus canais internos em resposta a mudanças ambientais poderia representar uma adaptação vantajosa para os primeiros animais sobreviverem em situação de hipóxia (Hammarlund et al., no prelo).

Os resultados obtidos com a datação de proteínas relacionadas ao O_2 e as análises de expressão gênica de indivíduos submetidos às condições do Neoproterozóico sugerem que os primeiros animais viviam em ambientes pouco oxigenados. A integração de diferentes metodologias, experimentais e bioinformáticas, permitiu fazer inferências não apenas

sobre o ambiente em que esses animais surgiram, mas também quais eram os mecanismos moleculares e fisiológicos que eles possuíam para sobreviver e evoluir naquelas condições. A datação muito antiga do surgimento de genes essenciais ao metabolismo aeróbico e à homeostase do O_2 celular contribuem ainda mais para a hipótese da diversificação dos animais ocorrendo antes do período Criogeniano, quando os oceanos eram predominantemente hipóxicos. Os mecanismos moleculares para lidar com o estresse oxidativo que animais modernos análogos aos primeiros metazoários apresentam também são sugestivos de adaptações que possivelmente foram herdadas de seus ancestrais. De maneira geral, os resultados aqui obtidos corroboram a possibilidade de que a evolução dos animais não exigiu níveis elevados e estáveis de O_2 ambiental. Os dados apresentados ajudam a compreender como a vida e o O_2 moldaram um ao outro desde a origem da vida, há mais de 3 bilhões de anos. Este conhecimento fundamental pode fornecer o contexto necessário para ajudar a sociedade atual a enfrentar as mudanças ambientais que vêm ocorrendo no planeta, incluindo a queda dos níveis de O_2 nos oceanos atuais.

Resumo

A relação entre o oxigênio, e o surgimento e a diversificação dos animais no Neoproterozóico é um tópico que tem sido extensamente debatido há décadas. Todos os animais conhecidos atualmente precisam de oxigênio em pelo menos uma parte de seus ciclos de vida. Portanto, a transição de um planeta anóxico para oxigenado é considerado por muitos autores como um pré-requisito para o surgimento e a expansão dos animais. No entanto, nosso entendimento sobre a correlação entre fatores ambientais e novidades evolutivas ainda é limitado. Embora seja aceito que os oceanos do Neoproterozóico eram ambientes com pouco oxigênio, pouco se sabe acerca da fisiologia dos metazoários que vivam nessas condições. Com o intuito de elucidar aspectos da fisiologia dos primeiros animais, foram utilizadas abordagens experimentais e bioinformáticas que revelaram o tempo de divergência de vias metabólicas essenciais, e possíveis adaptações fisiológicas dos animais primordiais à condição de hipóxia. A datação do surgimento de genes envolvidos no metabolismo e regulação do oxigênio, como a enzima do ciclo de Krebs, Isocitrato Desidrogenase (IDH), e o regulador celular da homeostase do oxigênio, o fator de transcrição induzido por hipóxia (HIF), sugerem um surgimento pré-Criogeniano dos animais em condições de pouco oxigênio. Tendo isso em vista, entender como os animais modernos respondem em nível molecular a baixos níveis de oxigênio também pode esclarecer aspectos da fisiologia de seus ancestrais. Para isso, a esponja *Hymeniacidon heliophila* foi usada como um análogo moderno, sendo submetida às condições oceânicas do Neoproterozóico em câmaras de simulação. A análise da expressão gênica diferencial das esponjas mostrou que tanto a condição oxigenada quanto a anóxia desencadeiam as mesmas respostas fisiológicas e moleculares de estresse, sugerindo uma melhor adaptação à hipóxia. Os resultados também sugerem que apesar dos primeiros metazoários não possuírem a via HIF como mecanismo de detecção do oxigênio, eles provavelmente utilizavam outros meios para essa função, como o metabolismo do sulfeto. A superexpressão de genes relacionados à glicólise e à reorganização do sistema aquífero sob estresse oxidativo sugere um possível papel ancestral desses mecanismos nos primeiros animais. Os resultados obtidos aqui revelam possíveis adaptações fisiológicas que podem ter sido vantajosas aos primeiros animais, e ampliam nossa compreensão acerca da relação íntima entre o oxigênio e a diversificação metazoária ao longo da evolução da vida.

Palavras-chave: hipóxia, Metazoa, evolução molecular, experimentos de simulação, Neoproterozóico, origem dos animais.

Abstract

The relationship between oxygen and the emergence and diversification of animals is a topic that has been extensively debated by scientists over the decades. All animals currently described need oxygen to survive for at least part of their life cycle. Therefore, the transition from an anoxic to an oxygenated planet is considered by many authors as a prerequisite for the emergence and diversification of animals. However, our understanding of the correlation between environmental factors and evolutionary novelties remains limited. Although it is accepted that the Neoproterozoic oceans were habitats with low dissolved oxygen levels, we know little about the respiratory physiology of early animals adapted to live in those environments. To understand the physiology of the first metazoans, experimental and bioinformatic approaches were used here and revealed the divergence time of crucial metabolic pathways, and possible physiological adaptations of early animals to hypoxic conditions. Molecular dating of genes involved in oxygen metabolism and regulation, such as the Krebs cycle enzyme, Isocitrate Dehydrogenase (IDH), and the master-regulator of oxygen homeostasis, the hypoxia-inducible factor (HIF) suggests a pre-Cryogenian emergence of animals in low-oxygen conditions. Considering that, to understand how modern animals respond to low oxygen levels can also shed light on aspects of their ancestors' physiology. To do so, the demosponge *Hymeniacidon heliophila* was considered as a modern analog and was submitted to the Neoproterozoic oceanic conditions in simulation chambers. Differential gene expression analysis showed that both oxygenated conditions and anoxia trigger the same physiological and molecular stress responses in sponges, suggesting a better adaptation to hypoxia. The results also suggest that although the first metazoans most likely did not have the HIF pathway as an oxygen-sensing mechanism, they probably used other means for that, such as the sulfide-removal pathway. The overexpression of genes related to glycolysis and the remodeling of the aquiferous system under oxidative stress suggests a possible ancestral role of these mechanisms in the first animals. Results presented here reveal possible physiological adaptations that may have been advantageous to early animals and contribute to our understanding of the intimate relationship between oxygen and metazoans diversification throughout the evolution of life.

Keywords: hypoxia, Metazoa, molecular evolution, simulation experiments, Neoproterozoic Era, origin of animals.

Referências Bibliográficas

Belato, F. A., Mello, B., Coates, C. J., Halanych, K. M., Brown, F. D., Morandini, A. C., de Moraes Leme, J., Trindade, R. I. F., & Costa-Paiva, E. M. (2023). Divergence time estimates for the hypoxia-inducible factor-1 alpha (HIF1α) reveal an ancient emergence of animals in low-oxygen environments. *Geobiology*, *22*(1), 1–14.

Bezerra, B. S., Belato, F. A., Mello, B., Brown, F., Coates, C. J., de Moraes Leme, J., Trindade, R. I. F., & Costa-Paiva, E. M. (2021). Evolution of a key enzyme of aerobic metabolism reveals Proterozoic functional subunit duplication events and an ancient origin of animals. *Scientific Reports*, *11*(1), 1–11.

Brocks, J. J., Jarrett, A. J. M., Sirantoine, E., Kenig, F., Moczydłowska, M., Porter, S., & Hope, J. (2016). Early sponges and toxic protists: possible sources of cryostane, an age diagnostic biomarker antedating Sturtian Snowball Earth. *Geobiology*, *14*(2), 129–149.

de Mendoza, A., Sebé-Pedrós, A., Sestak, M. S., Matejcic, M., Torruella, G., Domazet-Loso, T., & Ruiz-Trillo, I. (2013). Transcription factor evolution in eukaryotes and the assembly of the regulatory toolkit in multicellular lineages. *Proceedings of the National Academy of Sciences*, *110*(50), E4858–E4866.

Dohrmann, M., & Wörheide, G. (2017). Dating early animal evolution using phylogenomic data. *Scientific Reports*, *7*(1), 1–6.

dos Reis, M., Thawornwattana, Y., Angelis, K., Telford, M. J., Donoghue, P. C. J., & Yang, Z. (2015). Uncertainty in the Timing of Origin of Animals and the Limits of Precision in Molecular Timescales. *Current Biology*, *25*(22), 2939–2950.

Erwin, D. H., Laflamme, M., Tweedt, S. M., Sperling, E. A., Pisani, D., & Peterson, K. J. (2011). The Cambrian conundrum: Early divergence and later ecological success in the early history of animals. *Science*, *334*(6059), 1091–1097.

Guillaumond, F., Leca, J., Olivares, O., Lavaut, M. N., Vidal, N., Berthezène, P., Dusetti, N. J., Loncle, C., Calvo, E., Turrini, O., Iovanna, J. L., Tomasini, R., & Vasseur, S. (2013). Strengthened glycolysis under hypoxia supports tumor symbiosis and hexosamine biosynthesis in pancreatic adenocarcinoma. *Proceedings of the National Academy of Sciences*, *110*(10), 3919-3924.

Halanych, K. M. (2016). How our view of animal phylogeny was reshaped by molecular approaches: lessons learned. *Organisms Diversity and Evolution*, *16*(2), 319–328.

Hammarlund, E., Bukkuri, A., Norling, M., Posth, N., Carroll, C., Baratchart, E., Amend, S., Gatenby, R., Pienta, K., Brown, J., Peters, S., & Hancke, K. (*in press*). Benthic daily oxygen variability and stress as drivers for animal diversification in the Cambrian. *Nature Ecology and Evolution.*

Hammarlund, E. U., Flashman, E., Mohlin, S., & Licausi, F. (2020). Oxygen-sensing mechanisms across eukaryotic kingdoms and their roles in complex multicellularity. *Science*, *370*(6515), 1-13.

Hoffmann, F., Røy, H., Bayer, K., Hentschel, U., Pfannkuchen, M., Brümmer, F., & De Beer, D. (2008). Oxygen dynamics and transport in the Mediterranean sponge Aplysina aerophoba. *Marine biology*, *153*, 1257-1264.

Jabłońska, J., & Tawfik, D. S. (2021). The evolution of oxygen-utilizing enzymes suggests early biosphere oxygenation. *Nature Ecology & Evolution*, *5*(4), 442–448.

King, N., & Rokas, A. (2017). Embracing Uncertainty in Reconstructing Early Animal Evolution. *Current Biology*, *27*(19), R1081–R1088.

Krause, A. J., Mills, B. J., Merdith, A. S., Lenton, T. M., & Poulton, S. W. (2022). Extreme variability in atmospheric oxygen levels in the late Precambrian. *Science advances*, *8*(41), 1-10.

Kuraku, S., Meyer, A., & Kuratani, S. (2009). Timing of Genome Duplications Relative to the Origin of the Vertebrates: Did Cyclostomes Diverge before or after? *Molecular Biology and Evolution*, *26*(1), 47–59.

Levin, L. A. (2003). Oxygen Minimum Zone Benthos: Adaptation and Community Response to Hypoxia. *Oceanography and Marine Biology: An Annual Review*, *41*(1), 1–45.

Leys, S. P., & Hill, A. (2012). The physiology and molecular biology of sponge tissues. *Advances in marine biology*, *62*, 1-56.

Leys, S. P., Yahel, G., Reidenbach, M. A., Tunnicliffe, V., Shavit, U., & Reiswig, H. M. (2011). The sponge pump: the role of current induced flow in the design of the sponge body plan. *PloS one*, *6*(12), 1-17.

Loenarz, C., Coleman, M. L., Boleininger, A., Schierwater, B., Holland, P. W., Ratcliffe, P. J., & Schofield, C. J. (2011). The hypoxia-inducible transcription factor pathway regulates oxygen sensing in the simplest animal, Trichoplax adhaerens. *EMBO reports*, *12*(1), 63-70.

Mailloux, R. J., Bériault, R., Lemire, J., Singh, R., Chénier, D. R., Hamel, R. D., & Appanna, V. D. (2007). The Tricarboxylic Acid Cycle, an Ancient Metabolic Network with a Novel Twist. *PLOS ONE*, *2*(8), 1–10.

Maldonado, M., Ribes, M., & van Duyl, F. C. (2012). Nutrient fluxes through sponges: biology, budgets, and ecological implications. *Advances in marine biology*, *62*, 113-182.

Maloof, A. C., Rose, C. V, Beach, R., Samuels, B. M., Calmet, C. C., Erwin, D. H., Poirier, G. R., Yao, N., & Simons, F. J. (2010). Possible animal-body fossils in pre-Marinoan limestones from South Australia. *Nature Geoscience*, *3*(9), 653–659.

Mateos, K., Chappell, G., Klos, A., Le, B., Boden, J., Stüeken, E., & Anderson, R. (2023). The evolution and spread of sulfur cycling enzymes reflect the redox state of the early Earth. *Science Advances*, *9*(27), 1-11.

Meert, J. G., Gibsher, A. S., Levashova, N. M., Grice, W. C., Kamenov, G. D., & Ryabinin, A. B. (2011). Glaciation and ~770Ma Ediacara (?) Fossils from the Lesser Karatau Microcontinent, Kazakhstan. *Gondwana Research*, *19*(4), 867–880.

Micaroni, V., Strano, F., McAllen, R., Woods, L., Turner, J., Harman, L., & Bell, J. J. (2022). Adaptive strategies of sponges to deoxygenated oceans. *Global Change Biology*, *28*(6), 1972-1989.

Mills, D. B., Francis, W. R., Vargas, S., Larsen, M., Elemans, C. P., Canfield, D. E., & Wörheide, G. (2018). The last common ancestor of animals lacked the HIF pathway and respired in low-oxygen environments. *ELife*, *7*, 1-17.

Mosch, T., Sommer, S., Dengler, M., Noffke, A., Bohlen, L., Pfannkuche, O., Liebetrau, V., & Wallmann, K. (2012). Factors influencing the distribution of epibenthic megafauna across the Peruvian oxygen minimum zone. *Deep Sea Research Part I: Oceanographic Research Papers*, *68*, 123–135.

Nelson, D. L., Lehninger, A. L., & Cox, M. M. (2013). *Lehninger principles of biochemistry* (6th Ed). New York, H. Freeman.

Neuweiler, F., Turner, E. C., & Burdige, D. J. (2009). Early Neoproterozoic origin of the metazoan clade recorded in carbonate rock texture. *Geology*, *37*(5), 475–478.

Olson, K. R. (2015). Hydrogen sulfide as an oxygen sensor. *Antioxidants & redox signaling*, *22*(5), 377-397.

Olson, K. R., Gao, Y., DeLeon, E. R., Arif, M., Arif, F., Arora, N., & Straub, K. D. (2017). Catalase as a sulfide-sulfur oxido-reductase: An ancient (and modern?) regulator of reactive sulfur species (RSS). *Redox biology*, *12*, 325-339.

Olson, S. L., Kump, L. R., & Kasting, J. F. (2013). Quantifying the areal extent and dissolved oxygen concentrations of Archean oxygen oases. *Chemical Geology*, *362*, 35–43.

Panopoulou, G., & Poustka, A. J. (2005). Timing and mechanism of ancient vertebrate genome duplications - The adventure of a hypothesis. *Trends in Genetics*, *21*(10), 559–567.

Pisani, D., Pett, W., Dohrmann, M., Feuda, R., Rota-Stabelli, O., Philippe, H., Lartillot, N., & Wörheide, G. (2015). Genomic data do not support comb jellies as the sister group to all other animals. *Proceedings of the National Academy of Sciences*, *112*(50), 15402–15407.

Purcell, J. E., Breitburg, D. L., Decker, M. B., Graham, W. M., Youngbluth, M. J., & Raskoff, K. A. (2001). Pelagic cnidarians and ctenophores in low dissolved oxygen environments: A review. In N. N. Rabalais & R. E. Turner (Eds.), *Coastal Hypoxia: Consequences for Living Resources and Ecosystems* (pp. 77–100). American Geophysical Union.

Riesgo, A., Santodomingo, N., Koutsouveli, V., Kumala, L., Leger, M. M., Leys, S. P., & Funch, P. (2022). Molecular machineries of ciliogenesis, cell survival, and vasculogenesis are differentially expressed during regeneration in explants of the demosponge Halichondria panicea. *BMC genomics*, *23*(1), 1-17.

Sacerdot, C., Louis, A., Bon, C., Berthelot, C., & Roest Crollius, H. (2018). Chromosome evolution at the origin of the ancestral vertebrate genome. *Genome Biology*, *19*(1), 1–15.

Sebé-Pedrós, A., De Mendoza, A., Lang, B. F., Degnan, B. M., & Ruiz-Trillo, I. (2011). Unexpected repertoire of metazoan transcription factors in the unicellular holozoan capsaspora owczarzaki. *Molecular Biology and Evolution*, *28*(3), 1241–1254.

Sebé-Pedrós, A., Zheng, Y., Ruiz-Trillo, I., & Pan, D. (2012). Premetazoan Origin of the Hippo Signaling Pathway. *Cell Reports*, *1*(1), 13–20.

Semenza, G. L. (2007). Life with oxygen. *Science*, *318*(5847), 62-64.

Simakov, O., Marlétaz, F., Yue, J.-X., O'Connell, B., Jenkins, J., Brandt, A., Calef, R., Tung, C.-H., Huang, T.-K., Schmutz, J., Satoh, N., Yu, J.-K., Putnam, N. H., Green, R. E., & Rokhsar, D. S. (2020). Deeply conserved synteny resolves early events in vertebrate evolution. *Nature Ecology & Evolution*, *4*(6), 820–830.

Ślesak, I., Ślesak, H., & Kruk, J. (2012). Oxygen and Hydrogen Peroxide in the Early Evolution of Life on Earth: In silico Comparative Analysis of Biochemical Pathways. *Astrobiology*, *12*(8), 775–784.

Sperling, E. A., & Stockey, R. G. (2018). The Temporal and Environmental Context of Early Animal Evolution: Considering All the Ingredients of an "Explosion." *Integrative and Comparative Biology*, *58*(4), 605–622.

Thuesen, E. V, Rutherford, L. D., & Brommer, P. L. (2005). The role of aerobic metabolism and intragel oxygen in hypoxia tolerance of three ctenophores:

Pleurobrachia bachei, Bolinopsis infundibulum and Mnemiopsis leidyi. *Journal of the Marine Biological Association of the United Kingdom, 85*(3), 627–633.
Tostevin, R., & Mills, B. J. (2020). Reconciling proxy records and models of Earth's oxygenation during the Neoproterozoic and Palaeozoic. *Interface Focus, 10*(4), 1–13.
Wagner, C., Steffen, R., Koziol, C., Batel, R., Lacorn, M., Steinhart, H., Simat, T., & Müller, W. E. G. (1998). Apoptosis in marine sponges: a biomarker for environmental stress (cadmium and bacteria). *Marine Biology, 131*, 411–421.
Wallace, M. W., Hood, A. v. S., Woon, E. M. S., Hoffmann, K.-H., & Reed, C. P. (2014). Enigmatic chambered structures in Cryogenian reefs: The oldest sponge-grade organisms? *Precambrian Research, 255*, 109–123.
Whelan, N. V., Kocot, K. M., Moroz, L. L., & Halanych, K. M. (2015). Error, signal, and the placement of Ctenophora sister to all other animals. *Proceedings of the National Academy of Sciences, 112*(18), 5773–5778.
Wood, R., & Erwin, D. H. (2018). Innovation not recovery: dynamic redox promotes metazoan radiations. *Biological Reviews, 93*(2), 863–873.